Abstract

Discovering Novel Regulators of Nucleolar Form and Function

Lisa Ogawa McLean

2021

Nucleoli are dynamic nuclear condensates in eukaryotic cells that originate through ribosome biogenesis at loci that harbor the ribosomal DNA. These loci are known as nucleolar organizer regions and there are 10 in a human diploid genome. While there are 10 nucleolar organizer regions however, the number of nucleoli observed in cells is variable. Furthermore, changes in number are associated with disease, with increased numbers and size common in aggressive cancers. In the near-diploid human breast epithelial cell line, MCF10A, the most frequently observed number of nucleoli is 2-3 per cell. While ribosome biogenesis is an essential biological process that is common among all life forms, studies that elaborate on the complexities of ribosome biogenesis in higher eukaryotes, like humans, are few. In this dissertation, to identify novel regulators of ribosome biogenesis in higher eukaryotes, I used quantitative imaging of MCF10A cells to perform a high-throughput siRNA screen for proteins that, when depleted, increase the percentage of nuclei with ≥5 nucleoli. Unexpectedly, this screening approach led to the identification of proteins associated with the cell cycle. Functional analysis on a subset of hits further revealed not only proteins required for progression through S and G2/M phase, but also proteins required explicitly for the regulation of RNA polymerase I transcription and protein synthesis. Thus, results from this screen for increased nucleolar number highlight the significance of the nucleolus in human cell cycle regulation, linking RNA polymerase I transcription to cell cycle progression.

In this dissertation, I also applied this high-throughput screening approach to cancer drug discovery. Because ribosome biogenesis is essential for cell growth and is linked to the pathogenesis of cancer, targeting the nucleolus has become an attractive target for the development of novel therapies. Screening a library of ~4,000 FDA-approved drugs revealed over 100 compounds that regulate nucleolar number, with antineoplastic agents being the most common identified. Expanding the search to a library of ~25,000 novel, synthetic compounds also revealed additional regulators of nucleolar number that are structurally distinct from the FDA-approved drugs and harbor promise as putative new cancer therapies. The discoveries described herein broaden our understanding of nucleolar biology in higher eukaryotes and will provide a foundation for the development of novel and more effective therapeutics for the treatment of cancer.

Discovering Novel Regulators of Nucleolar Form and Function

A Dissertation
Presented to the Faculty of the Graduate School
of
Yale University
In Candidacy for the Degree of
Doctor of Philosophy

by
Lisa Ogawa McLean

Dissertation Director: Susan J. Baserga, M.D., Ph.D.

June 2021

Table of Contents **Page**

List of Figures and Tables **Page**

Figures for Chapter 3

Tables for Chapter 3

Figures for Chapter 4

Tables for Chapter 4

Figures for Chapter 5

Tables for Chapter 5

List of Abbreviations

Abbreviation	Meaning
rRNA	Ribosomal RNA
rDNA	Ribosomal DNA
NOR	Nucleolar organizer region
RNAPI	RNA polymerase I
Pre-rRNA	Precursor ribosomal RNA
SSU	Small subunit of the ribosome (40S)
LSU	Large subunit of the ribosome (60S)
snoRNA	Small nucleolar RNA
r-protein	Ribosomal protein
FC	Fibrillar center
DFC	Dense fibrillar component
GC	Granular component
siRNA	Small interfering RNA
ETS	External transcribed spacer
ITS	Internal transcribed spacer
Chr	Chromosome
AMD	Actinomycin D
PNB	Prenucleolar body
IDR	Intrinsically disordered region
LLPS	Liquid-liquid phase separation
mRNA	Messenger RNA
snRNA	Small nuclear RNA
5S-RNP	5S ribosomal RNA ribonucleoprotein
NOPdb	Nucleolar Proteome database
GO	Gene Ontology
NHEJ	Non-homologous end joining
BER	Base excision repair
HR	Homologous recombination
DBA	Diamond-Blackfan anemia
SDS	Shwachman-Diamond syndrome
DC	Dyskeratosis congenita
TCS	Treacher Collins syndrome
HGPS	Hutchinson-Gilford progeria syndrome
WS	Werner syndrome
CS	Cockayne syndrome
BS	Bloom syndrome
AD	Alzheimer’s disease
PD	Parkinson’s disease
MDS	Myelodysplastic syndrome
AML	Acute myeloid leukemia
RNAi	RNA interference
PE	Percent effect
NPE	Normalized percent effect

Chapter 1

Ribosome biogenesis, the nucleolus, and disease

INTRODUCTION

The nucleolus has fascinated scientists since it was first observed in the eighteenth century by bright-field microscopy. While scientists had studied this "nucleus within a nucleus" throughout the nineteenth century, these studies were largely observational and the function of this discernible nuclear body remained a mystery until the mid-1900s (Montgomery Jr., 1898; Pederson, 2011; Raška et al., 2006). An early discovery that contributed to the advancement of our current understanding of nucleolar function was that the nucleolus is associated with a specific chromosomal site (McClintock, 1934). It was not until after the discovery of the ribosome in the 1950s (Palade 1955), however, that the function of the nucleolus was finally ascertained. Here, several studies contributed to this landmark discovery, including one that found that *Xenopus* embryos lacking a nucleolus also failed to synthesize ribosomal RNA [rRNA; (Brown and Gurdon, 1964)]. Other studies concluded that RNA in the nucleolus was identical to the rRNA in the cytoplasm and hybridized specifically to repeat DNA loci within the nucleolus (Birnstiel et al., 1963; Chipchase and Birnstiel, 1963; Ritossa and Spiegelman, 1965). Thus, these discoveries and others during this same period began the decades of research that have gone towards understanding how ribosomes are synthesized within the eukaryotic nucleolus (Pederson, 2011; Raška et al., 2006). Today, it is well-established that the nucleolus is a dynamic, subnuclear compartment in which the essential process of ribosome biogenesis takes place.

Ribosome biogenesis is a modular process in which the ribosome, a megadalton cytoplasmic ribozyme, is synthesized and assembled as two distinct subunits comprised of RNA and protein. In eukaryotic organisms, the biogenesis of ribosomes initiates in

large membraneless nuclear organelles known as nucleoli (Figure 1-1). Nucleoli form around tandemly arrayed ribosomal DNA (rDNA) loci, also known as nucleolar organizer regions (NOR), upon initiation of transcription by RNA polymerase I (RNAPI) (Bersaglieri and Santoro, 2019; Grob et al., 2014; Hernandez-Verdun, 2011; McClintock, 1934; Potapova and Gerton, 2019). In mammals, the products of RNAPI transcription are precursor rRNAs (pre-rRNA) that harbor 3 of the 4 mature rRNA species (18S, 5.8S, and 28S), along with external and internal transcribed spacer sequences that are removed by numerous accessory factors (Aubert et al., 2018; Henras et al., 2015). The 18S is assembled into the small subunit of the ribosome (SSU; 40S) and the 5.8S and 28S are assembled into the large subunit of the ribosome (LSU; 60S), along with the RNA polymerase III-transcribed 5S rRNA from an extra-nucleolar locus. Additionally, pre-rRNAs undergo nucleotide modification guided by small nucleolar RNAs (snoRNA) and subunit assembly with the ~80 RNA polymerase II-transcribed SSU and LSU ribosomal proteins [r-proteins; (Bassler and Hurt, 2019; Kiss, 2002)]. As a consequence of these functions, nucleoli exhibit a tripartite substructure when observed by electron microscopy comprising a (1) fibrillar center (FC), (2) dense fibrillar component (DFC), and a (3) granular component (GC), each associated with different steps in ribosome biogenesis (Brinkley 1965; Pederson, 2011; Sugihara and Yasuzumi, 1970). Thus, while scientists have observed and studied this large and charismatic organelle for centuries, advances in microscopy and the development of molecular tools have led to a comprehensive understanding of nucleolar form and function, and continues to reveal novel complexities of ribosome biogenesis and its connection to human disease.

This dissertation will focus on several novel discoveries I have made surrounding nucleolar form and function in higher eukaryotes. The nucleolar function of ribosome biogenesis is an essential biological process that is common among all life forms and can therefore be studied in any number of model systems. As such, many of the early studies to define the process and factors involved were carried out in the single-celled budding yeast, *Saccharomyces cerevisiae* (Woolford and Baserga, 2013). While studies in *S. cerevisiae* have established a solid foundation of how ribosomes are synthesized in eukaryotic organisms, they are unable to probe any added layers of regulation that may occur in more complex, multicellular organisms, like humans. Here, I asked whether novel factors governing ribosome biogenesis could be identified by investigating regulators of nucleolar number in the human breast epithelial cell line, MCF10A. In Chapter 1, I provide the necessary background for the research presented in the remaining chapters. In Chapter 2, I report on the results from a genome-wide small interfering RNA (siRNA) screen that was carried out to identify proteins that, when depleted, cause an increase in the number of nucleoli per nucleus. In Chapter 3, I tested several proteins identified in the siRNA screen for functional roles in ribosome biogenesis. In Chapter 4, I adapted our screening approach to screen for small molecule regulators of nucleolar number and to identify putative new nucleolus-targeting drugs for the treatment of cancer. In Chapter 5, I conclude by sharing my current perspective on the field of nucleolar biology and ribosome biogenesis and suggest future research directions stemming from this dissertation. Some of the text, tables and figures that appear in this dissertation have been published in (Farley-Barnes* and Ogawa* et al., 2019; Ogawa and Baserga, 2017; Ogawa et al., 2021).

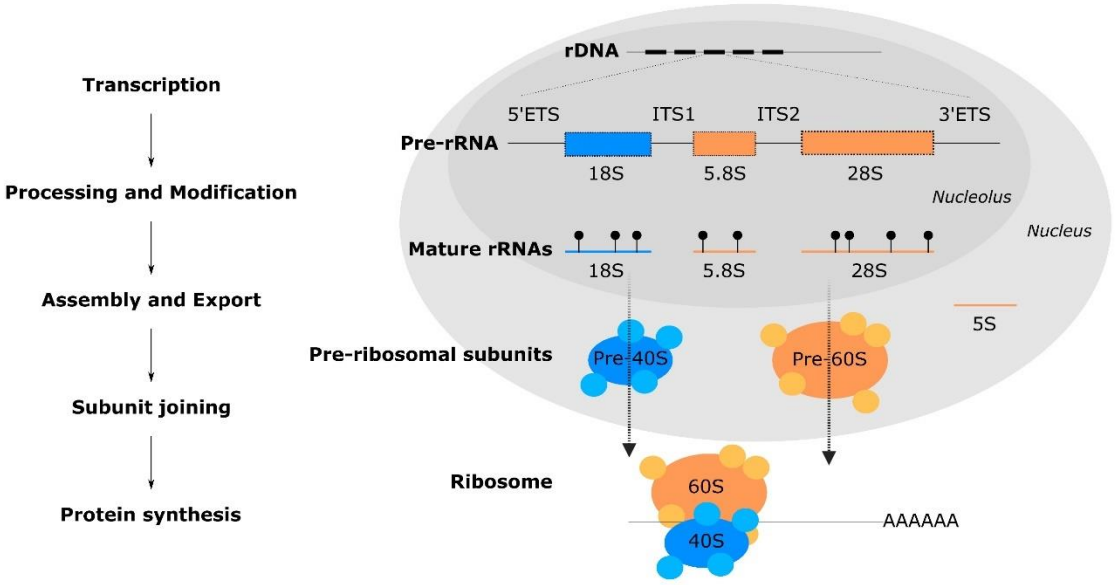

Figure 1-1. Ribosome biogenesis is a complex, stepwise and modular process that initiates in the membraneless nuclear organelle called the nucleolus. Previously published in (Ogawa and Baserga, 2017). (Left) Flow chart of the general steps of ribosome biogenesis. (Right) Simplified schematic of ribosome biogenesis. Ribosome biogenesis initiates with the transcription of the precursor-ribosomal RNA (rRNA) by RNAPI from an array of tandemly repeated rDNA loci. Following transcription, the pre-rRNA undergoes processing to release the mature rRNAs (18S; 5.8S; 28S). The 18S is assembled into the small subunit (SSU; 40S) of the ribosome, and the 5.8S and 28S are assembled into the large subunit (LSU; 60S) of the ribosome. Additionally, nucleotide modification, assembly with ribosomal proteins (r-proteins) and the 5S rRNA, and rapid nuclear export occur. Final maturation of the SSU and LSU occur in the cytoplasm, where they join on messenger RNA to perform their function in translation. Blue=SSU; Orange=LSU. Small circles=r-proteins. 5'ETS, ITS1, ITS2, and 3'ETS=transcribed spacer sequences in the precursor-rRNA. Black ball and sticks=nucleotide modifications.

Nucleolar assembly and the cell cycle

The nucleolus is a nuclear organelle "formed by the act of building a ribosome (Mélèse and Xue, 1995)." In humans, nucleoli arise from the tandemly arrayed rDNA loci that are present on the short arms (p arms) of the 5 human acrocentric chromosomes [chr 13-15, 21 and 22; (Floutsakou et al., 2013; Henderson et al., 1972). Although highly variable, approximately 300-400 copies of the ~45 kb rDNA locus are present in a human diploid cell (Gibbons et al., 2015; Gonzalez and Sylvester, 1995; McStay and Grummt, 2008; Schmickel, 1973). Interestingly, however, only around 50% of these loci are actively transcribed (Conconi et al., 1989). These sites of rDNA arrays are aptly named nucleolar organizer regions [NORs; (McClintock, 1934), and while there are 10 NORs in a human diploid cell, studies in diverse model systems reveal that the actual number of nucleoli per cell varies. Some of the variability in nucleolar number may be dependent on cell cycle stage (Anastassova-Kristeva, 1977). A more recent survey, however, in populations of asynchronized cells reveals that the average number of nucleoli also differs depending on the cell line observed (Farley et al., 2015). Indeed, while not all NORs may be competent or actively transcribed by RNAPI (Roussel et al., 1996), it is also known that nucleoli fuse and will often comprise multiple NORs (Anastassova-Kristeva, 1977; Floutsakou et al., 2013; Savino et al., 2001; van Sluis et al., 2016). Additionally, a recent study also suggests that not all acrocentric chromosomes may actually harbor rDNA (van Sluis et al., 2020). These data thus complicate the reconciliation of the number of NORs with the observed number of nucleoli. Taken together, the nucleolus is a dynamic host to the rDNA loci and embodies a complexity that is best highlighted by the coordinated remodeling of nucleoli during mitosis.

Nucleolar dynamics during mitosis

The nucleolus disassembles and reassembles every mitosis. Since Barbara McClintock first observed the disappearance of chromosomally-tethered nucleoli in late prophase and their re-emergence in telophase [Figure 1-2; (McClintock, 1934)], efforts to understand the mechanisms underlying these dynamic changes have been made. It is now well-established that the breakdown and reformation of nucleoli is a highly ordered process that establishes reservoirs of pre-rRNA and processing factors to be recruited to competent NORs following mitosis (Hernandez-Verdun, 2011). First hints that nucleolar formation did not require *de novo* transcription of the rDNA came from studies in the 1970s that observed nucleolar assembly upon mitotic exit even in the presence of the RNAPI inhibitor, actinomycin D [AMD; (Phillips and Phillips, 1973; Phillips, 1972)]. Later research elaborated on these early discoveries and observed, beginning in prophase, the ordered relocation of pre-rRNA and processing factors to the chromosome periphery that then migrates with the chromosomes during anaphase [Figure 1-2; (Gautier et al., 1992; Savino et al., 2001)]. A recent high-throughput survey to define the nucleolar proteins localized to the mitotic perichromosomal compartment identified a total of 65 such proteins (Stenström et al., 2020). Furthermore, it has recently been discovered that pre-rRNA localization to the perichromosomal compartment is dependent on the marker of proliferation, Ki67 (Hayashi et al., 2017). In telophase, nucleolar proteins at the chromosomal periphery condense to form prenucleolar bodies (PNBs) from which ribosome biogenesis factors are then recruited to the competent NORs where, with early processing factors and pre-rRNA, promote nascent nucleolar reassembly (Muro et al., 2010). Finally, in early G1, the nascent nucleoli fuse, which leads to nucleoli that are

comprised of multiple NORs, both active and inactive (Anastassova-Kristeva, 1977; Savino et al., 2001; Sullivan et al., 2001). Nucleolar disassembly and reassembly during mitosis is therefore a complex and highly ordered processes that requires the coordination of numerous factors to successfully propagate functional nucleoli from one generation of cells to the next.

Nucleolar breakdown and reassembly, however, does not occur in a vacuum and requires coordination with the cell cycle by cell cycle regulators. Beginning in prophase, activation of the CDK1-cyclin B kinase leads to the inhibition of RNAPI transcription, which coincides with the disappearance of nucleoli [Figure 1-2; (Sirri et al., 2002)]. The repression of RNAPI likely occurs in part through phosphorylation of selectivity factor 1 (SL1), which impairs association with upstream binding transcription factor (UBTF) and the formation of the RNAPI pre-initiation complex (Heix et al., 1998; Kuhn et al., 1998). RNAPI transcriptional repression is then reversed in anaphase through the inhibition of CDK1-cyclin B activity by PP1 phosphatases, which allows for nucleolar assembly to initiate by telophase (Heix et al., 1998; Sirri et al., 2000). Together, these data are consistent with the observations that nucleolar formation requires transcription by RNAPI, even though initial assembly is driven by the recruitment of early processing factors and PNBs at mitotic exit (Dousset et al., 2000). Furthermore, essential to the re-initiation of transcription is the expression of UBTF. In simple yet elegant studies using engineered pseudo- and neo-NORs, UBTF binding was shown to be required for the maintenance of competent NORs through mitosis and for the recruitment of RNAPI; however, in the absence of an rDNA array, transcription did not initiate and nucleoli did not form (Grob et al., 2014; Mais et al., 2005). The dynamic changes to the nucleolus

during mitosis are thus highly coordinated and tightly regulated by cell cycle regulators in order to ensure faithful cell duplication and viability.

While details surrounding the disassembly and reassembly of nucleoli in mitosis have been established, there is much left to be determined. In the recent survey identifying nucleolar proteins associated with the mitotic perichromosomal compartment, 65 proteins were identified, but 36 were not previously known to localize to chromosomes (Stenström et al., 2020). Furthermore, the nucleolar proteins that localize to the perichromosomal compartment are enriched in proteins with intrinsically disordered regions (IDR), and this is intriguing given that IDRs are reported drivers of nucleolar assembly through a biophysical process known as liquid-liquid phase separation [LLPS; (Hyman et al., 2014; Lafontaine et al., 2020)]. The role of LLPS in driving nucleolar organization has gained significant attention over the past decade and establishing the contribution of this biophysical process will be important to gaining a more comprehensive understanding of nucleolar form and function. Thus, while decades of research have led to significant insights into nucleolar dynamics, particularly during mitosis, many details remain to be uncovered.

Liquid-liquid phase separation in nucleolar assembly

Nucleoli are membraneless nuclear bodies that display biophysical properties associated with liquids. Currently, there is significant momentum surrounding the study of nucleolar organization as a product of the phenomenon of LLPS (Hyman et al., 2014; Lafontaine et al., 2020). This body of research initiated with a study that observed liquid droplet-like behavior of nucleoli in *Xenopus* oocytes, followed by a study that observed

purified nucleolar proteins (FBL and NPM1, respectively) with rRNA from wheatgerm form distinct liquid droplets that are immiscible when mixed and crudely mimic nucleolar organization (Brangwynne et al., 2011; Feric et al., 2016). Although *Xenopus* nucleoli are not tethered to chromosomes as in mammals, these studies and others suggest that concentration-dependent physical properties of proteins, like fluidity and surface tension, may explain higher order organization and coalescence events observed among nucleoli. More recent studies have elaborated on these initial findings in human cells with observations of coalescence in chromosomally tethered nucleoli and through the use of super resolution microscopy (Caragine et al., 2018, 2019; Yao et al., 2019). In the latter, the authors substantiate the involvement of IDRs in promoting self-association and liquid droplet formation, identifying the FBL GAR domain as necessary to promote LLPS of FBL (Yao et al., 2019). Additionally, when self-association of FBL was impaired by mutants with a truncated GAR domain, so was the localization and processing of the pre-rRNA (Yao et al., 2019). There is, however, still some skepticism surrounding the broad applicability of LLPS to explain the organization of membraneless cellular bodies, and thus the field would benefit from a set of standards for testing the hypothesis in living systems (Alberti et al., 2019; McSwiggen et al., 2019; Peng and Weber, 2019). Furthermore, because nucleoli in higher eukaryotes are tethered to multiple different chromosomes, additional factors like chromosomal movement and positioning within the nucleus are likely to also play a contributing role in nucleolar fusion and organization (Mangan and McStay, 2021; van Sluis et al., 2020). In conclusion, this new body of literature suggests that in combination with other processes, like pre-rRNA transcription

and higher-order chromosome organization, LLPS may contribute to the assembly of nucleoli.

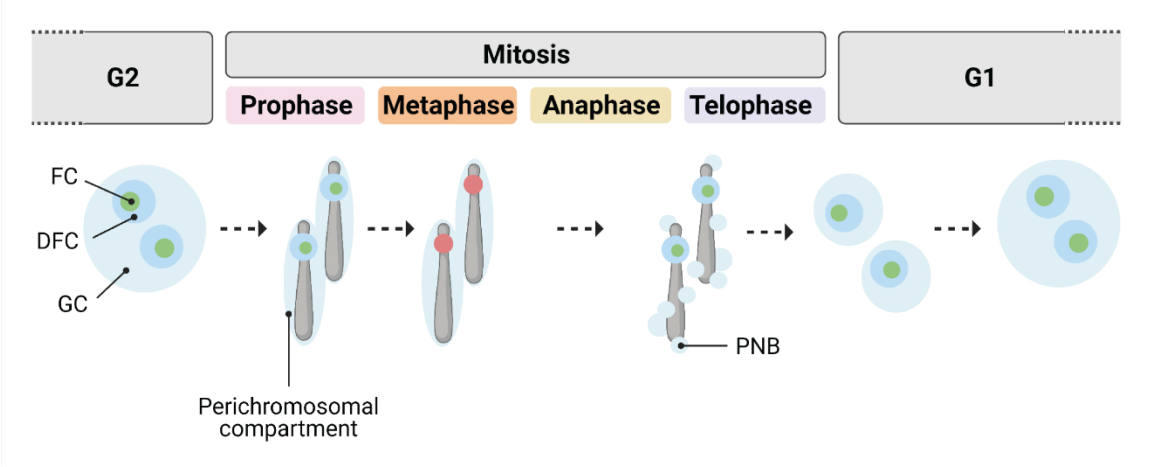

Figure 1-2. Nucleolar dynamics during mitosis. In every mitosis, the nucleolus disassembles in late prophase and reassembles in telophase. In prophase, pre-rRNA and processing factors relocate to the chromosomal periphery, also called the perichromosomal compartment. Activation of CDK1-cyclin B inhibits RNAPI transcription by metaphase (red). Inhibition of CDK1-cyclin B by PP1 phosphatases re-initiates RNAPI transcription by telophase (green). In telophase, nucleolar proteins in the perichromosomal compartment condense into prenucleolar bodies (PNB) from which ribosome biogenesis factors are recruited to the competent nucleolar organizer regions (NORs) and, with early processing factors and pre-rRNA, promote nascent nucleolar formation. In early G1, nascent nucleoli fuse to from mature nucleoli. FC=fibrillar center (green); DFC=dense fibrillar component; GC=granular component. Created with BioRender.com.

The nucleolar response to cellular stress

The nucleolus is more than just a ribosome factory. Although the primary function of the nucleolus is to synthesize ribosomes, extra-ribosomal functions have also been attributed to this organelle. These additional functions include cell cycle regulation, and the processing and maturation of mRNA, snRNA, and the RNA components of telomerase and the signal recognition particle (Boisvert et al., 2007; Pederson, 1998). However, and arguably the most striking, is that it has also been defined as a sensor of cellular stress that results in the stabilization of the tumor suppressor protein, p53. In 2003, Rubbi and Milner observed that common among all p53-inducing stressors is nucleolar disruption (Rubbi and Milner, 2003). They proceeded to define how impaired nucleolar function stabilizes p53 (Rubbi and Milner, 2003), which modulates transcriptional networks that regulate diverse cellular processes (Boutelle and Attardi, 2021). The regulatory effects of p53 stabilization include the suppression of RNAPI through direct disruption of the RNAPI pre-initiation complex (Zhai and Comai, 2000). In subsequent studies, it was identified that p53 stabilization is mediated through the interaction of the p53 E3 ubiquitin ligase, MDM2/HDM2, with the 5S ribonucleoprotein (5S-RNP), which includes unassembled r-proteins, primarily RPL5 (uL18) and RPL11 (uL5), and HEATR3 (Calviño et al., 2015; Dai and Lu, 2004; Fumagalli et al., 2009; Hannan et al., 2021; Lohrum et al., 2003; Russo and Russo, 2017). Furthermore, new research further supports that the nucleolus senses diverse cellular stresses, including stress caused by inhibition of RNA polymerases, nuclear export inhibition, and DNA damage, but not proteotoxic stress (Hannan et al., 2021). Additionally, since the discovery of the p53-mediated nucleolar stress response, several additional nucleolar

stress pathways independent of p53 have also been described (James et al., 2014). The identification of these stress response pathways has therefore positioned the nucleolus not only as essential in producing ribosomes, but also as a hub in the coordination of the cellular response to stress.

Crosstalk between the nucleolus and the DNA damage response

Discoveries made by studies employed to define the nucleolar proteome in higher eukaryotes have contributed substantially to our understanding of the nucleolar response to DNA damage. The Nucleolar Proteome Database (NOPdb3.0) is by far the most comprehensive attempt at defining a complete proteome. In its latest update, it included the identification of more than 4,500 proteins that localize to the nucleolus based on mass spectrometry of purified nucleoli from several experiments in different human cell lines (Ahmad et al., 2009; Andersen et al., 2005; Andersen et al., 2002; Leung et al., 2006; Scherl et al., 2002). Two other published proteomes include another mass spectrometry-based proteome from T-cells (Jarboui et al., 2011), and a nucleolar proteome based on immunofluorescence microscopy (Thul et al., 2017; Thul and Lindskog, 2018). One analysis of nearly 700 nucleolar proteins revealed that among the functional classes represented were not only r-proteins, RNA-binding proteins, and RNA helicases, but also cell-cycle proteins, splicing related factors, and DNA replication and DNA repair proteins (Andersen et al., 2005). I also performed an analysis of all the nucleolar proteomes and uncovered a total of 166 DNA repair proteins among the datasets using the Gene Ontology (GO) Consortium categorization for protein identification [GO:0006281; Table 1-1; Appendix I; (Ogawa and Baserga, 2017). Data from these

studies thus support a plurifunctional role for the nucleolus in higher eukaryotes and lends support to the idea of the nucleolus as a sensor of DNA damage.

Beyond the localization of DNA repair proteins to the nucleolus, several studies suggest a role for the nucleolus is the sequestration of DNA repair proteins until required for DNA repair. In support of this proposed mechanism of coordinating the DNA damage response, several studies have observed large changes in the nucleolar proteome when treated with DNA damaging agents, like AMD (Andersen et al., 2005; Andersen et al., 2002). In one study, treatment with UV and ionizing radiation revealed the mobilization of proteins associated with non-homologous end joining (NHEJ) from the nucleolus to the nucleoplasm (Moore et al., 2011). Similar observations have been made with the base excision repair (BER) enzymes APEX1 (Lirussi et al., 2012) and ALKBH2 (Li et al., 2013a), and the Werner syndrome protein [WRN; (Blander et al., 2002; Lee et al., 2015)]. It is also possible, however, that DNA repair proteins that localize to the nucleolus are not just sequestered, but actually have yet to be defined roles in ribosome biogenesis. Indeed, I explored this hypothesis and identified several DNA repair proteins with roles in ribosome biogenesis and vice versa (Ogawa and Baserga, 2017); thus, it is likely that both these explanations may be accurate. Taken together, the nucleolus is a dynamic organelle that responds to DNA damage through the redistribution of nucleolar localized proteins.

The nucleolus also responds to DNA damage through transient inhibition of RNAPI, although the precise mechanism underlying the response remains incomplete. First reported in 2007, Kruhlak and colleagues identified an ATM-mediated transcriptional repression of RNAPI upon DNA damage by ionizing radiation that also

depended on NBS1 and MDC1 (Kruhlak et al., 2007). Further, by using laser micro-irradiation the authors also observed that RNAPI repression was locally restricted to nucleoli nearest the damaged chromatin (Kruhlak et al., 2007). Since this first study there have been several additional studies that not only validated the ATM-mediated RNAPI transcriptional repression, but that also further defined the mechanisms underlying this response [Figure 1-3, A; (Calkins et al., 2013; Ciccia et al., 2014; Korsholm et al., 2019; Larsen et al., 2014; Mooser et al., 2020)]. One clear discovery from these studies is the central role that the ribosome biogenesis factor, treacle (TCOF1), plays in mediating the response. TCOF1 is not only required to recruit NBS1 and possibly the rest of the MRN complex (MRE11 and RAD50), but has also been shown to recruit TOPBP1 which is required to activate ATR for the repression of RNAPI transcription [Figure 1-3, A; (Ciccia et al., 2014; Korsholm et al., 2019; Larsen et al., 2014; Mooser et al., 2020)]. Other discoveries include in one study the observed absence of RNAPI transcriptional repression with ionizing radiation (Moore et al., 2011), and in another the global silencing of nucleoli upon micro-irradiation (Larsen et al., 2014), both in contrast to initial findings and that suggest there are nuances in the nucleolar DNA damage response that remain to be elucidated. What is certain, however, is that RNAPI transcriptional repression upon DNA damage requires ATM-mediated recruitment of NBS1 and TOPBP1 by TCOF1 that triggers RNAPI repression in an ATR-dependent manner.

DNA damage also leads to nucleolar reorganization into cap-like structures on the nucleolar periphery. Observed over half a century ago, treatment with DNA damaging agents like 4-nitroquinoline *N*-oxide and AMD led to nucleolar disruption and the formation of nucleolar “caps” (Reynolds et al., 1964; Reynolds et al., 1963). Several

decades later, recent studies on DNA damage specifically in the rDNA by the I-Ppol endonuclease have finally made progress towards defining these intriguing structures. Like DNA damage in nuclear chromatin, ATM-dependent RNAPI silencing is also observed when damage occurs in the rDNA (Franek et al., 2016; Harding et al., 2015; Kruhlak et al., 2007; van Sluis and McStay, 2015; Warmerdam et al., 2016). Interestingly, however, it was RNAPI silencing and not DNA damage specifically that led to the formation of nucleolar caps (Figure 1-3, B). This was ascertained because, remarkably, treatment with AMD at doses that inhibited RNAPI that do not cause DNA damage also led to cap formation, but that was independent of ATM (Harding et al., 2015; van Sluis and McStay, 2015). Furthermore, probing the composition of caps caused by DNA damage suggest that damaged rDNA from the nucleolar interior retreats to the caps to be repaired. This is supported by the colocalization of caps with the rDNA, FC and DFC ribosome biogenesis proteins, γH2AX, and DNA repair factors [Figure 1-3, C; (Franek et al., 2016; Harding et al., 2015; Larsen et al., 2014; van Sluis and McStay, 2015; Warmerdam et al., 2016). Taken together, these data support an ATM-dependent mechanism of RNAPI inhibition upon DNA damage in the rDNA; however, the purpose of nucleolar reorganization may differ depending on the type of damage.

It is clear from this recent body of literature that there is a substantial crosstalk between the nucleolus and the DNA damage response. Questions, however, still remain including why the DNA damage response includes repression of RNAPI. For damage in the nucleolar chromatin it may be an adaptation to preserve genome integrity. As the most highly transcribed region in the human genome, repression of transcription during DNA repair would limit collision between transcription and repair machinery (Lindstrom

et al., 2018). Furthermore, as a highly repetitive region, prevention of double strand breaks is important to limit homologous recombination (HR)-mediated gain or loss of rDNA repeats, which has been associated with human disease (Lindstrom et al., 2018; Warmerdam and Wolthuis, 2019). In the nuclear chromatin, repression of RNAPI may represent a mechanism to coordinate DNA repair with cellular growth or with the p53 nucleolar-mediated stress response if damage is too severe, given that ribosome biogenesis is an energetically costly process (Antoniali et al., 2014; Hannan et al., 2021; Kruhlak et al., 2007; Warner et al., 2001).

Another outstanding question is, "What is the primary mode of DNA repair in the nucleolar chromatin?." A few well-supported studies have arrived at conflicting conclusions regarding the predominant pathway for repair. In one study, HR-mediated repair was concluded (van Sluis and McStay, 2015), whereas in two others, NHEJ was shown as the primary mode of repair in the rDNA (Harding et al., 2015; Warmerdam et al., 2016), with HR actually delaying repair and leading to the loss of rDNA repeats (Warmerdam et al., 2016). Taken together, the nucleolus is highly responsive to cellular DNA damage and occupies a central role coordinating the DNA damage response.

Table 1-1. Human nucleolar proteomes include proteins involved in DNA repair. Three databases exist on proteins that localize to the human nucleolus. Within each database, a subset of proteins are classified as DNA repair proteins based on Gene Ontology (GO) Consortium categorization (GO: 0006281).

	NOPdb (Ahmad et al., 2009; Leung et al., 2006)	T-cell nucleolar proteome (Jarboui et al., 2011)	Human Protein Atlas subcellular proteome (Thul et al., 2017; Thul and Lindskog, 2018)
Total proteins	2717	872	1153
DNA repair proteins	136	38	40
DNA repair proteins with a yeast ortholog	89	30	23

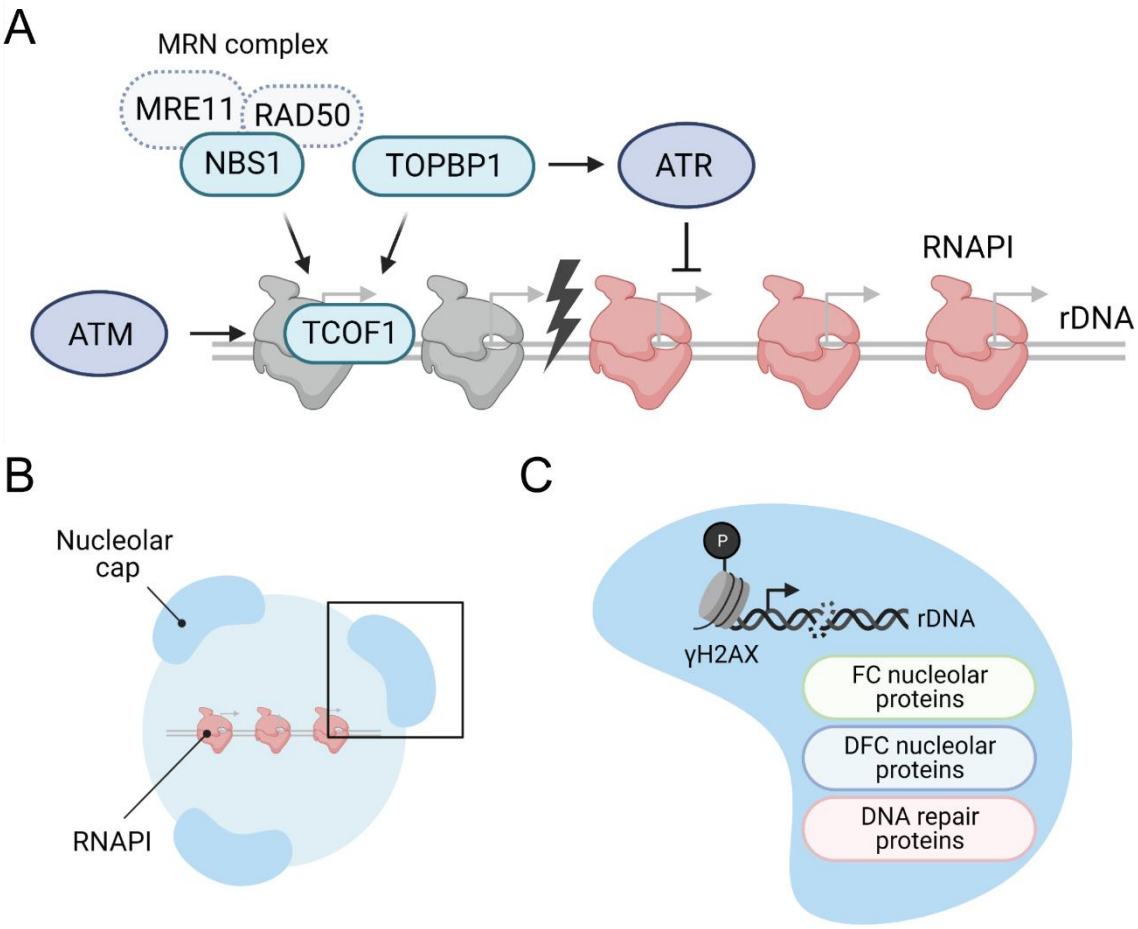

Figure 1-3. Nucleolar response to DNA damage. The nucleolus is a cellular stress sensor that responds to DNA damage. DNA damage in the nucleolar and nuclear chromatin both result in the transient inhibition of RNAPI and the formation of nucleolar caps. Created with BioRender.com.

(A) Model of ATM- and ATR- dependent inhibition of RNAPI upon DNA damage. ATM-dependent TCOF1 recruitment of NBS1 and TOPBP1 results in the ATR-dependent silencing of RNAPI in the nucleolus. TCOF1 may recruit the entire MRN complex (MRE11-RAD50-NBS1). Black lightning bolt=DNA damage. Grey=RNAPI; Red=silenced RNAPI.

(B) Nucleolar caps. The nucleolar stress response results in the transient inhibition of RNAPI. When RNAPI is silenced, dense nucleolar caps form on the nucleolar periphery. The boxed nucleolar cap is defined in C.

(C) Nucleolar cap composition. When DNA damage, specifically double strand breaks, occur in the rDNA, RNAPI is silenced and nucleolar caps are formed. The caps comprise individual nucleolar organizer regions (NORs), γH2AX (a marker of DNA damage), nucleolar proteins from the fibrillar center (FC) and dense fibrillar component (DFC), and DNA repair proteins.

Ribosome biogenesis and disease

Nucleolar dysfunction is associated with a wide range of diseases. Because the nucleolus is essential for growth and the cellular response to stress, it is not surprising that dysfunction may contribute to disease. Today, a large body of evidence implicates nucleolar dysfunction in a subset of congenital disorders, known as the ribosomopathies. The nucleolus, however, has also been linked to aging, including neurodegenerative diseases, and the pathogenesis of cancer. Gaining a broader understanding of the connection of the nucleolus and ribosome biogenesis to disease will serve to improve our ability to develop more targeted and effective therapeutics. While research has amassed in understanding the connection of the nucleolus to disease, many questions remain to be answered.

Ribosomopathies

The ribosomopathies are a diverse subset of congenital disorders caused by mutations in genes associated with ribosome biogenesis. While all ribosomopathies share defects in ribosome production, not all are caused by defects at the same step in the process (Farley-Barnes* and Ogawa* et al., 2019). Perhaps the most studied of the ribosomopathies are the bone marrow failure syndromes, including Diamond-Blackfan anemia (DBA), Shwachman-Diamond syndrome (SDS), and Dyskeratosis Congenita (DC), which can be caused defects in ribosome assembly (Ellis and Gleizes, 2011; Ruggero and Shimamura, 2014; Warren, 2018). The association of ribosome biogenesis with bone marrow failure was first identified in DBA (Draptchinskaia et al., 1999). DBA can be caused by mutations in one of at least 19 r-proteins, however, the most common

mutation among DBA patients is in RPS19 (Aspesi and Ellis, 2019). The consequence of these mutations is r-protein haploinsufficieny, which results in a reduction in the concentration of mature cytoplasmic ribosomes (Khajuria et al., 2018). Another well-studied ribosomopathy is the mandibulofacial dysostosis Treacher Collins syndrome (TCS). In most cases TCS is caused by mutations in TCOF1, however, it has also been identified in patients with mutations in RNAPI subunits, POLR1B, POLR1C and POLR1D (Bowman et al., 2012; Dauwerse et al., 2011; Sanchez et al., 2020; Splendore et al., 2000; Teber et al., 2004). A related disorder, acrofacial dysostosis, Cincinnati type, has also been identified and is caused by mutations in POLR1A (Weaver et al., 2015). TCOF1 is a multifunctional protein with roles in pre-rRNA transcription, modification, and the nucleolar response to DNA damage (Gonzales et al., 2005; Larsen et al., 2014; Mooser et al., 2020; Valdez et al., 2004). However, because RNAPI subunits share the pathophysiology of TCS, it is likely that a reduction in pre-rRNA levels observed with TCS is the causative mechanism. Among the ribosomopathies, mutations have been identified in factors required not only for ribosome assembly and transcription, but also in pre-rRNA processing (Farley-Barnes* and Ogawa* et al., 2019; Warren, 2018). There are currently at least 21 suspected and defined ribosomopathies (Farley-Barnes* and Ogawa* et al., 2019; Warren, 2018), and new ribosomopathies continue to be discovered.

One of the most fascinating aspects of the ribosomopathies is the tissue specific clinical manifestations of the diseases. While tissue-specificity in disease is not unique to the ribosomopathies (Hekselman and Yeger-Lotem, 2020), the diversity of unique tissue types effected by defective ribosome biogenesis has intrigued scientists. At this time, the clinical manifestations of the ribosomopathies range from bone marrow failure and

craniofacial abnormalities to intellectual disability and cardiac deficiencies [Figure 1-4; (Danilova and Gazda, 2015; Farley-Barnes* and Ogawa* et al., 2019; Warren, 2018)]. Interestingly, however, a unifying feature of several ribosomopathies are defects in the tissues that arise from the neural crest cell lineage (Trainor and Merrill, 2014; Watt and Trainor, 2014). Neural crest cells are migratory progenitor cells that arise during early embryonic development and differentiate into several unique cell types including those that derive the skeletal structures of the face, heart, glia, peripheral nervous system, skin, and teeth [Figure 1-4 (Trainor and Merrill, 2014; Watt and Trainor, 2014)]. In fact, many ribosomopathies manifest with defects in craniofacial morphology (TCS; DBA; acrofacial dysostosis, Cincinnati type), and studies on TCS in animal models have implicated p53-mediated apoptosis of the neural crest cells in the development of the craniofacial phenotype (Bowen and Attardi, 2019; Rinon et al., 2011). Furthermore, p53 inhibition, remarkably, rescues the observed craniofacial defects, linking the nucleolar-mediated p53 stress response to the clinical manifestation of the disease (Calo et al., 2018; Jones et al., 2008; Watt et al., 2018). Ribosomopathies, however, also manifest with defects in unrelated tissues, including the liver [North American Indian childhood cirrhosis; (Freed et al., 2012)], bone marrow [DBA; SDS; DC; (Ellis and Gleizes, 2011; Ruggero and Shimamura, 2014; Warren, 2018)], spleen [isolated congenital asplenia; (Bolze et al., 2013)], and brain [ANE syndrome, RPS23 ribosomopathy; Figure 1-4; (Nousbeck et al., 2008; Paolini et al., 2017)]. While there is some evidence for the role of p53 in the pathogenesis of some of these ribosomopathies, it is not implicated in all of them. The underlying mechanisms for many of the ribosomopathies therefore remain to

be thoroughly defined, and further research in animal models on the consequences of mutations in ribosome biogenesis factors will be revealing.

How tissue specific defects arise from dysfunction in a ubiquitous process has drawn significant recent attention. Beyond the role of p53 and the nucleolar stress response, other leading hypotheses have emerged to describe the mechanisms underlying tissue specificity in the ribosomopathies (Farley-Barnes* and Ogawa* et al., 2019). One hypothesis is based on the concept of ribosome heterogeneity or "specialized ribosomes," and a second hypothesis is based on cellular ribosome concentration. The ribosome concentration hypothesis suggests that reduced production of ribosomes leads to increased competition among mRNA for the ribosomes that are available (Lodish, 1974; Mills and Green, 2017). As a consequence, a subset of proteins may not be synthesized at a capacity required for the normal function of a specific tissue. The most notable example associated with this hypothesis is with the pathogenesis of DBA and the erythroid specific transcription factor GATA1. GATA1 is required for erythroid cell development, and decreased levels of GATA1 protein have been observed in DBA patients (Khajuria et al., 2018; Ludwig et al., 2014). Confounding, however, is that it could then be hypothesized that mutations in all r-proteins could lead to bone marrow failure; however, this is not observed. The ribosome heterogeneity hypothesis, on the other hand, suggests that unique pools of ribosomes exist in different tissues that may differentially translate subsets of mRNAs (Genuth and Barna, 2018). This hypothesis echoes most closely the idea regarding tissue-specific diseases in general that a causal mutation in a protein disrupts interactions of that protein with a tissue specific network (Hekselman and Yeger-

Lotem, 2020). In the case of ribosome heterogeneity this would be exemplified by the differential expression of r-proteins that interact with and/or recruit a specific subset of mRNAs (Genuth and Barna, 2018; Shi et al., 2017). It is important to note that these proposed mechanisms are not likely to be mutually exclusive. Both of these hypotheses, however, are limited in the evidentiary support for the proposed mechanisms and therefore require further substantiation (Farley-Barnes* and Ogawa* et al., 2019). Advances in technologies and further research aimed at exploring these hypotheses in specific disease model systems will be essential to defining the pathogenesis of the tissue specific manifestation of ribosomopathies.

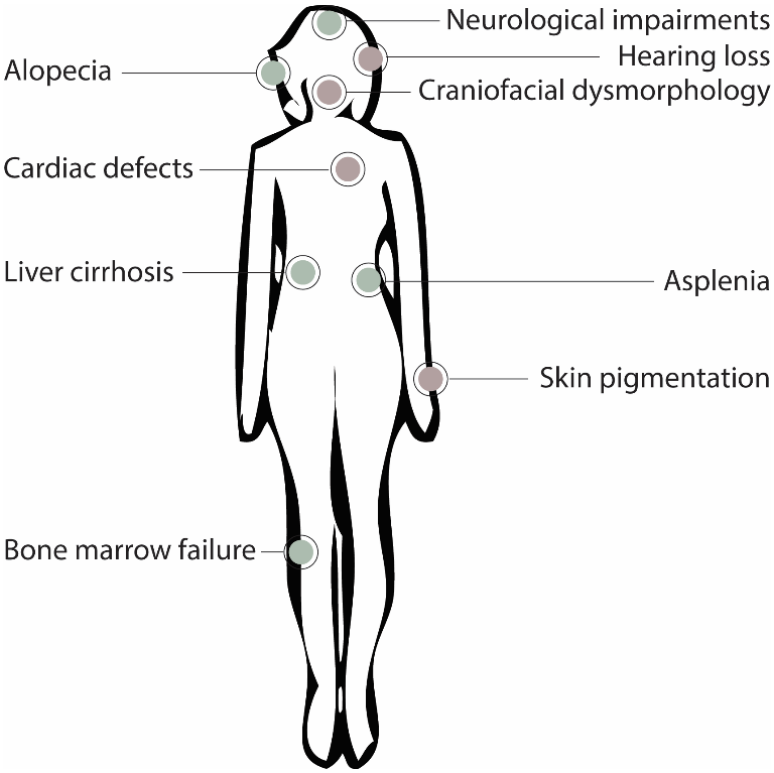

Figure 1-4. Tissue specific clinical manifestation of ribosomopathies. Ribosomopathies are a diverse subset of congenital disorders that arise from defects in ribosome biogenesis. A unifying feature of several ribosomopathies are defects in the tissues that arise from the neural crest cell lineage (green), including hearing loss, craniofacial dysmorphology (TCS; DBA; acrofacial dysostosis, Cincinnati type), cardiac defects, and alterations in skin pigmentation. Ribosomopathies also manifest with defects in unrelated tissues (red), including neurological impairments (ANE syndrome; RPS23 ribosomopathy), alopecia, liver cirrhosis (North American Indian childhood cirrhosis), asplenia (isolated congenital asplenia), and bone marrow failure (DBA; SDS; DC). Only the ribosomopathies discussed are included in the parenthesis. Previously published in (Farley-Barnes* and Ogawa* et al., 2019)

Aging and related diseases

Research on longevity, premature aging disorders, and neurodegeneration support a connection between aging and the nucleolus. Understanding the molecular basis for aging has long interested scientists, yet the link between the nucleolus and aging is a more recent development in the history of aging research. Some of the earliest studies linking the nucleolus to aging began with experiments in yeast mother cells that found a requirement for the histone deacetylase, Sir2, in maintaining genome stability at rDNA loci. Additionally, loss-of-function mutants had a shorter lifespan and gain-of-function mutants had a longer lifespan (Gottlieb and Esposito, 1989; Guarente, 1997; Sinclair and Guarente, 1997). Today, genome instability in the rDNA is still one of the leading hypotheses for why we age (Ganley and Kobayashi, 2014; Tiku and Antebi, 2018; Turi et al., 2019). A recent study on mammalian SIRT7 has validated a role for sirtuins in maintaining rDNA heterochromatin, connecting rDNA genome stability to lifespan (Etchegaray and Mostoslavsky, 2018; Paredes et al., 2018). Mammalian SIRT1 has also been reported to regulate RNAPI transcription and rDNA stability and is a leading target in the development of anti-aging therapeutics, which include resveratrol and other synthetic agonists (Murayama et al., 2008; Stacchiotti et al., 2018; Zhou et al., 2009). Several lines of evidence thus support a link between rDNA genome stability and aging.

Nucleolar form and function have also been linked to aging. In a recent study, smaller nucleolar size predicted longer lifespan in a *C. elegans* model of longevity, mediated by ncl-1 [TRIM2/Brat; (Tiku et al., 2017)]. This observation also extended to models of longevity in fly, mouse and humans, and included a concomitant observed decrease in ribosome biogenesis (Tiku et al., 2017). Reduced nucleolar activity as a

hallmark of longevity is consistent with other areas of research like the targeting of mTOR (mechanistic/mammalian target of rapamycin) to treat age-related diseases. mTOR is a kinase central to growth regulation, and inhibition is known to decrease ribosome biogenesis and translation (Tee, 2018; Walters and Cox, 2018). Also consistent with this view is the observation that the rDNA in aged mice, canids, and humans show increased CpG methylation (Wang and Lemos, 2019). This may suggest not only decreased nucleolar activity, but also perhaps a compensatory mechanism to increase rDNA genome stability as we age. In this same study, however, it was also observed that under paradigms associated with longevity (e.g. calorie restriction), methylation was decreased (Wang and Lemos, 2019). One possible explanation is that decreased methylation does not necessarily suggest increased nucleolar activity or genome instability. It is also possible, however, that methylation may be secondary to another cause for aging that is reversed in models of longevity. Taken together, the link between aging and nucleolar form and function is not yet well defined.

Premature aging disorders further complicate the link between aging and the nucleolus. Hutchinson-Gilford progeria syndrome (HGPS) is a premature aging disorder caused by mutant lamin A/C. Intriguingly, however, a recent study on fibroblasts from HGPS patients has revealed increased nucleolar size and function that also demonstrated increases in rDNA transcription and translation (Buchwalter and Hetzer, 2017). In contrast, Werner syndrome (WS), Cockayne syndrome (CS), and Bloom syndrome (BS), are premature aging disorders caused by mutations in DNA repair proteins that exhibit decreased nucleolar activity (Karikkineth et al., 2017; Mukherjee et al., 2018). Studies on the proteins implicated in these syndromes have all revealed that impaired function yields

decreased RNAPI transcription (Bradsher et al., 2002; Grierson et al., 2012; Hannan et al., 2013; Lebedev et al., 2008; Lutomska et al., 2008; Okur et al., 2020; Shiratori et al., 2002). Interestingly, WS models, like HGPS, exhibit disruption in the nuclear lamina, including the nuclear pores and lamin B1 (Li et al., 2013b), and lamin B2 has been shown to regulate nucleolar morphology and function (Sen Gupta and Sengupta, 2017) that together may suggest a broader link among the nuclear membrane, the nucleolus, and aging. Despite the discordance between HGPS and the other premature aging disorders, there remains a link underlying premature aging and the nucleolus.

Neurodegenerative diseases share similar nucleolar dysfunction when compared to the premature aging disorders. Several lines of evidence have led to the proposal that nucleolar form and function are linked to the pathogenesis of neurodegenerative diseases (Herrmann and Parlato, 2018; Hetman and Pietrzak, 2012; Parlato and Bierhoff, 2015; Parlato and Kreiner, 2013; Parlato and Liss, 2014; Sia et al., 2016). In Alzheimer's disease (AD), observations include reduced nucleolar size (Donmez-Altuntas et al., 2005; Mann et al., 1988), hypermethylation of the rDNA promoter (Pietrzak et al., 2011), increased rRNA oxidation (Ding et al., 2006; Honda et al., 2005), and decreased ribosome activity (Ding et al., 2005; Hernandez-Ortega et al., 2016; Langstrom et al., 1989). In Parkinson's disease (PD), nucleolar disruption has also been observed (Parlato and Liss, 2014). In mouse models of PD, RNAPI transcription is decreased, as was mouse lifespan (Evsyukov et al., 2017). In another study, when the RNAPI transcription factor, RRN3/TIF-1A, is depleted in mouse dopaminergic neurons, p53-dependent apoptosis and PD-like symptoms are exhibited (Rieker et al., 2011). This result in particular is intriguing given that these data suggest a link between the nucleolar stress

response and neurodegeneration that echoes that mechanism underlying craniofacial defects among a subset of ribosomopathies. Defects in ribosome recycling have also been shown to have impacts on nucleolar function and are also implicated in aging and neurodegeneration (Ishimura et al., 2014; Sudmant et al., 2018). Together, these data suggest that reduced nucleolar function underlies neurodegenerative diseases. A recent study, however, has reported that children heterozygous for a gain-of-function mutation in the RNAPI transcription factor, UBTF, also exhibit neurodegeneration, which contradicts this conclusion, yet may be consistent with increased nucleolar activity causing increased rDNA genome instability (Edvardson et al., 2017). Taken together, a link between the nucleolus and neurodegeneration is evident (Figure 1-5); however, informational gaps remain as they do with the association of the nucleolus with aging in general, suggesting that there is much left to be discovered.

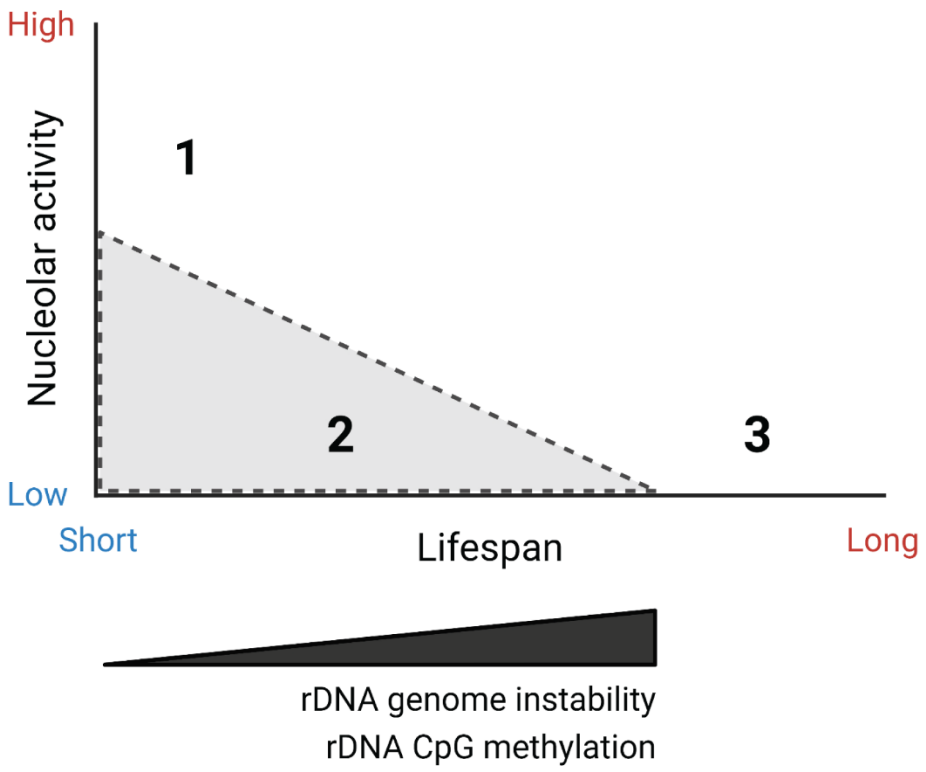

Figure 1-5. A working model for the association between the nucleolus and aging. Genome instability and CpG methylation at the tandemly arrayed rDNA loci increase as we age. Evidence also suggests that reduced nucleolar activity is associated with aging. The grey dashed triangle represents normal aging. The numbers 1-3 represent specific diseases and are placed relative on the plot relative to normal aging. 1= Hutchinson-Gilford progeria syndrome (HGPS) and UBTF-associated childhood neurodegeneration; 2=Werner syndrome, Cockayne syndrome, Bloom syndrome, Alzheimer's disease, and Parkinson's disease; 3=Models of longevity; mTOR inhibition. Created with BioRender.com.

The nucleolus and cancer

Changes in nucleolar morphology have long been associated with cancer. For over a century, cancer pathologists have observed changes in nucleolar size and number in diverse tumor types, and concluded that tumors with larger and more numerous nucleoli predicted a worse prognosis for the patients (Derenzini et al., 2009; Penzo et al., 2019; Pianese, 1896). The association of the nucleolus with cancer is not surprising given that the nucleolus drives growth and cellular proliferation. Indeed, ribosome biogenesis is a highly energy-consuming process and as such is tightly regulated, and most often at the first step in the process, transcription (Drygin et al., 2010; Warner et al., 2001). Furthermore, retrospective studies on the molecular mechanisms underlying common chemotherapeutic agents revealed that several drugs in fact target stages of ribosome biogenesis, not only at the site of RNAPI transcription, but also at stages of pre-rRNA processing (Burger et al., 2010; Quin et al., 2014). Drugs developed specifically to target RNAPI transcription have since proven promising both preclinically and in clinical trials for solid tumors and hematological malignancies. CX-3543 (quarfloxin) and CX-5461 have revealed few adverse events and stable disease in some trial participants (Drygin et al., 2011; Drygin et al., 2009; Drygin et al., 2008; Haddach et al., 2012; Hilton et al., 2020; Khot et al., 2019; Papadopoulos et al., 2007; Sanij et al., 2020; Xu et al., 2017b). BMH-21 is yet another novel RNAPI inhibitor that is currently in preclinical development and which has shown promising antineoplastic properties in mouse xenograft models of melanoma and drug-resistant prostate cancer (Colis et al., 2014; Low et al., 2019). Taken together, nucleolar form and function are linked to pathogenesis of cancer and is a promising target in the development of novel cancer therapeutics.

Ribosomopathies are also comorbid with a predisposition to cancer. Observations in patients with ribosomopathies also suggest a link between nucleolar function and cancer pathogenesis (Ruggero and Pandolfi, 2003). This is best defined by observations among those with the classic bone marrow failure syndromes (DBA, SDS, and DC), however, it is also observed among patients with 5q minus syndrome and cartilage hair hypoplasia (Aspesi and Ellis, 2019; Ruggero and Pandolfi, 2003). In SDS, patients show an increased risk for developing myelodysplastic syndrome (MDS) and acute myeloid leukemia (AML). In 90% of cases, SDS is caused by mutations in the ribosome assembly factor SBDS, which is important in the final maturation steps of the 60S subunit by releasing EIF6 (Warren, 2018). While ribosomopathies can often be categorized as diseases of hypo-proliferation, for example of the erythroid cells in the bone marrow, cancer as a disease of hyper-proliferation presents a paradox (Dameshek, 1967). Several mechanisms have been proposed to explain the increased risk for cancer among patients with ribosomopathies. One of the most compelling proposals is that patients acquire secondary mutations to compensate for the reduced capacity to synthesize ribosomes. In a study of SDS patients undergoing bone marrow transplants for MDS, mutations in known oncogenes were observed, 19% of which were in p53 suggesting a selective pressure to bypass the nucleolar stress response (Lindsley et al., 2017). Acquired mutations have also been observed in a small longitudinal study on SDS patients, which revealed either duplicated SBDS or deleted EIF6 to presumably overcome ribosomal deficiencies (Pressato et al., 2015). Intriguingly, among these patients, none were reported to have developed MDS or AML yet (Pressato et al., 2015). Overcoming ribosome deficiencies through p53 inactivation may in fact be a common mechanism underlying the

predisposition for cancer. In most cases where r-proteins are mutated, mutations in p53 are also observed (Ajore et al., 2017). Thus, there is a clear connection between the nucleolus and cancer and further studies aimed at validating and elaborating the mechanisms underlying the elevated cancer risk among ribosomopathy patients will be informative for better understanding the molecular basis for the link.

Finally, genome instability at the rDNA loci, in addition to being associated with aging, has also been implicated in cancer. As highly transcribed and repetitive sites, the rDNA repeats are not only susceptible to DNA damage, but also increased rates of recombination during repair that can result in the gain or loss of repeats (Lindstrom et al., 2018). Interestingly, it has been observed that rearrangements at the rDNA loci are common among tumors from lung and colorectal cancer patients (Stults et al., 2009). A larger, more comprehensive survey of cancers supported these data by revealing that rDNA copy number is in fact reduced in tumors relative to adjacent normal tissue from the same patient (Xu et al., 2017a). At first, this is counterintuitive as fewer copies might suggest a decreased proliferative capacity. However, concomitant increases in copy number of the extra-nucleolar 5S rRNA locus were also observed, as were p53 inactivating mutations and increased proliferative capacity (Xu et al., 2017a). Experiments in yeast complement these data, revealing that strains with low rDNA copy number exhibit an increased proportion of active to inactive rDNA repeats and increased rates of pre-rRNA synthesis (Ide et al., 2010). While the mechanisms underlying rDNA gene alterations in cancer remain unclear, genome instability at rDNA loci may have a selective advantage in cancer. The existence of endogenous sensors that detect and maintain rDNA copy number have been proposed, but evidence in higher eukaryotes is

limited (Nelson et al., 2019; Salim et al., 2017). While many aspects remain to be defined, targeting the multifaceted link between the nucleolus and cancer holds promise for the development of novel and more effective cancer therapeutics.

Chapter 2

Genome-wide RNAi screen for increased nucleolar number reveals regulators of cell cycle progression

INTRODUCTION

Ribosome biogenesis is an essential biological process shared among all living organisms (Ebersberger et al., 2014). As such, for several decades, this conserved process in eukaryotes has been largely defined by its study in the genetically tractable single-celled eukaryote, *Saccharomyces cerevisiae* (Woolford and Baserga, 2013). Humans, however, are multi-cellular organisms with innumerable differences including a more complex regulation of growth control (Miller, 2012). Furthermore, while a diploid *S. cerevisiae* cell maintains two nucleolar organizing regions and ~150 rDNA loci (Kobayashi et al., 1998), the diploid human genome harbors 10 nucleolar organizing regions and ~200-600 rDNA loci (Henderson et al., 1972; Parks et al., 2018; Stults et al., 2008). Thus, due to this increased complexity and the growing evidence linking nucleolar dysfunction to human congenital diseases (Farley-Barnes* and Ogawa* et al., 2019; Narla and Ebert, 2010; Warren, 2018), cancer (Bursac et al., 2020; Penzo et al., 2019; Ruggero, 2012; Sulima et al., 2019), viral infections (Jarboui et al., 2012; Rawlinson et al., 2018), and aging (Hetman and Pietrzak, 2012; Tiku and Antebi, 2018), it has become imperative to study the intricacies of ribosome biogenesis in higher eukaryotes to better understand how defects lead to the development of disease.

To this end, advances in technologies and high-throughput screening approaches have led multiple laboratories to mount screening campaigns to explore ribosome biogenesis in higher eukaryotes. A candidate screening approach using small interfering RNAs (siRNA) targeting nucleolar proteins in HeLa cells, for instance, classified regulators of pre-rRNA processing, identifying a large proportion either with different functions from the corresponding yeast ortholog or no known yeast ortholog (Tafforeau

et al., 2013). The former observation was independently supported by an siRNA screen for ribosomal subunit maturation factors that identified a novel role for exportin 5 (XPO5) in the nuclear export of pre-60S subunits in vertebrates (Wild et al., 2010). Genome-wide screens quantifying changes in nucleolar size in *S. cerevisiae* and *Drosophila melanogaster* identified the loss of the RNA polymerase I regulatory function of the histone information regulator (HIR) complex in higher eukaryotes (Neumuller et al., 2013). Furthermore, in a genome-wide screen in HeLa cells for 40S ribosomal subunit maturation factors, 302 proteins were identified, several of which were novel factors that are not present in yeast (Badertscher et al., 2015). Results from these pioneering studies thus not only support divergent roles for proteins in ribosome biogenesis that are conserved from yeast to humans, but also support the hypothesis that a subset of proteins unique to higher eukaryotes play important functional roles in the regulation of ribosome biogenesis.

Among the early screening campaigns to identify unique regulators of ribosome biogenesis in higher eukaryotes, we performed a screen identifying proteins that regulate nucleolar number. This screening approach was based on the prior observation that depletion of ribosome biogenesis factors, UTP4 and NOL11, decreased nucleolar number from 2-3 per nucleus to one (Freed et al., 2012). Kat McCann and the Yale Center for Molecular Discovery executed the genome-wide siRNA screen in the near-diploid MCF10A human breast epithelial cell line for proteins involved in the regulation of nucleolar number, and Katherine Farley-Barnes defined a high confidence set of 139 hits that, when depleted, decreased nucleolar number in cells to one per nucleus (Farley-Barnes et al., 2018). Remarkably, a large proportion of the hits had no previously defined

role in ribosome biogenesis and yet investigation on a subset of these proteins revealed varied ribosome biogenesis deficits upon depletion, ranging from RNAPI transcriptional silencing to aberrant pre-rRNA processing and decreased protein synthesis. Furthermore, the majority of hits do not have a known ortholog in yeast, strengthening support for the hypothesis that there exist unique regulators of ribosome biogenesis in higher eukaryotes. Our screening for regulators of nucleolar number was therefore a viable approach for uncovering novel human ribosome biogenesis factors.

In addition to identifying proteins that decreased nucleolar number when depleted, our screen also uncovered proteins that increased nucleolar number. I report on my analyses of the results from this side of the screen, where I defined 113 high confidence hits that, when depleted, caused an increase in the percentage of cells with ≥5 nucleoli. I also performed a range of bioinformatic analyses on the screen hits, and with the Yale Center for Molecular Discovery, performed screen validation and cell cycle profiling. The results from these analyses reveal the identity of a unique subset of proteins in the human proteome, the majority of which have no known ortholog in *S. cerevisiae*, that are required for the maintenance of typical nucleolar numbers in the MCF10A human breast epithelial cell line.

RESULTS

siRNA screen for increased nucleolar number revealed 113 hits

A genome-wide, high-content siRNA screen was performed by Kathleen L. McCann, in collaboration with the Yale Center for Molecular Discovery, to identify novel protein regulators of ribosome biogenesis in higher eukaryotes (Figure 2-1). To

achieve this objective, the expression of 18,107 genes was targeted in the human breast epithelial cell line, MCF10A, by pools of 4 individual siRNAs in order to identify proteins whose depletion caused an increase in the percentage of cells with ≥5 nucleoli (Figure 2-1, A). Nucleoli were identified based on immunofluorescent staining with a monoclonal antibody to the abundant nucleolar protein fibrillarin [72B9 (Reimer et al., 1987)], and cells were identified using the DNA stain, Hoechst. A pipeline in CellProfiler (Carpenter et al., 2006; McQuin et al., 2018) was developed by the Yale Center for Molecular Discovery to perform the unbiased enumeration of nucleoli. The average number of nucleoli per nucleus was quantified from 3 fields of view for each gene target and normalized to the average of the 16 negative and 16 positive control wells (3 fields of view each) included on the same plate. The negative control was siRISC-free and set to a 0 percent effect (PE) and the positive control was siKIF11 and set to a 100 PE. The result of this screen was therefore a calculated normalized percent effect (NPE) for each gene target that was used to identify screen hits.

This screen for increased nucleolar number revealed 113 high-confidence hits. Initially, hits were identified as genes with an NPE ≥ mean + 3 standard deviations (SD), which revealed 186 hits, including the positive control KIF11 (Figure 2-1, B). I filtered this list to identify a high confidence set of hits by first discarding 38 hits that were not expressed in MCF10A cells. This was determined based on a transcriptome analysis I performed in Partek Flow with RNA collected by Katherine Farley-Barnes from MCF10A cells treated with a non-targeting (NT) control pool of siRNAs (n=3; FPKM>0; GEO accession no. GSE154764). I then filtered the list by viability, discarding hits with a viability of <5% relative to the calculated average viability of the 16 siRISC-free control

wells on the same plate. This filter was included to ensure that an adequate number of cells were used to determine the NPE. This step resulted in the elimination of 35 hits, leaving 113 hits that I identified as high-confidence hits that, when depleted, cause an increase in the percentage of cells with ≥5 nucleoli per nucleus (Appendix II).

Screen performance based on statistical measures was strong. The Z-prime factor was calculated for each screening plate to monitor screen performance (n=58; Figure 2-1, C). The Z-prime factor is a statistical measure of the separation between the negative and positive controls. A Z-prime =1 indicates an ideal screening assay, whereas a Z-prime <0 indicates significant overlap between the controls and an unusable assay. While an excellent screening assay is often defined as one with a Z-prime >0.5, Z-prime factors between 0 and 0.5 are still acceptable for the positive identification of hits. The average Z-prime for the screen was strong at 0.41, with a Z-prime for all plates >0. Additionally, the mean signal to background ratio (S/B) was also monitored throughout the screen (Figure 2-1, D). The average S/B for the screen was 10.29. Viability across all gene targets was variable, ranging from 0.41-160.16, and also highly variable among the hits, ranging from 0.80-73.70 prior to filtering, but all with a viability of <100% (Figure 2-1, E). A representative subset of images and NPE from the scree are shown (Figure 2-2, A), including the frequency distribution of nucleoli per nucleus, which shows a flattening and rightward shift in the distribution from 2-3 nucleoli per nucleus to ≥5 (Figure 2-2, B).

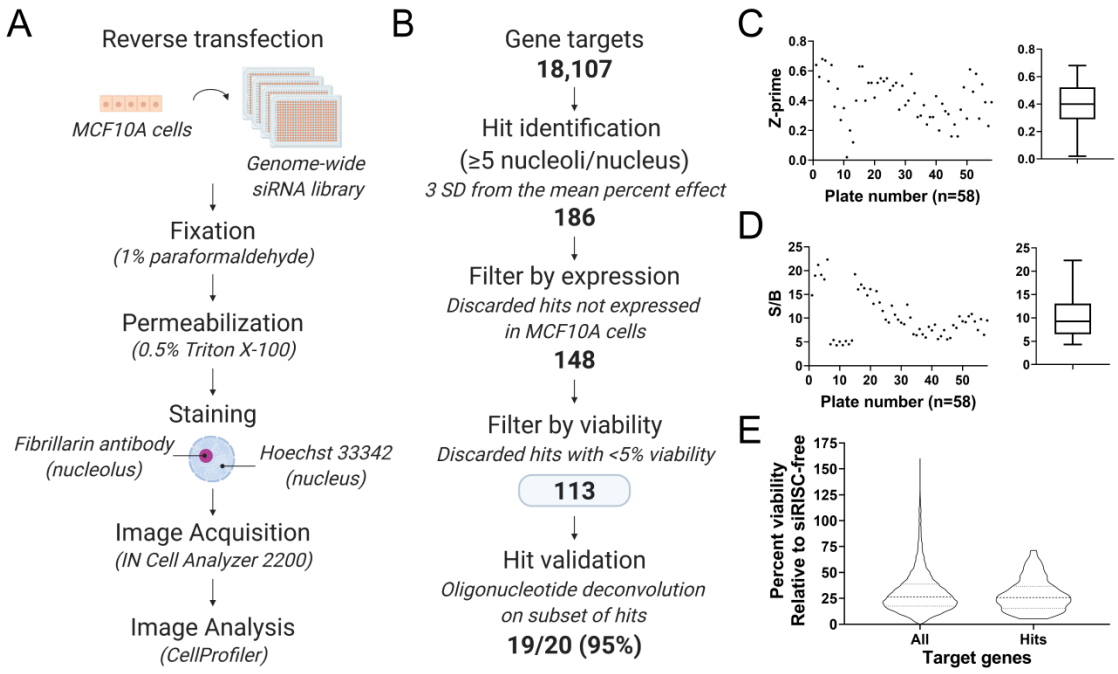

Figure 2-1. High-content, genome-wide siRNA screen in human MCF10A cells revealed 113 hits that increase the percentage of nuclei with ≥5 nucleoli. Previously published in (Ogawa et al., 2021).

(A) Screen workflow. MCF10A cells were reverse transfected into 384-well plates containing the siGENOME SMARTpool siRNA genome library (Horizon Discovery). After 72 hours, cells were fixed, permeabilized, and stained with an antibody to the nucleolar protein fibrillarin and Hoechst dye to stain the nucleus. Cell images were collected on an IN Cell Analyzer 2200 widefield, multicolor, fluorescent microscope and nucleolar number quantified using a pipeline in CellProfiler (Carpenter et al., 2006; McQuin et al., 2018).

(B) Screen analysis workflow. 18,107 genes were screened, and hits were identified based on a cut-off of ≥3 SD from the mean percent effect (PE) normalized to the positive

(siKIF11, 100 PE) and negative (siRISC-free, 0 PE) controls. Viability relative to siRISC-free negative control was quantified based on Hoechst-stained nuclei, and hits were then discarded if not expressed in MCF10A cells and if viability was <5%. 113 high confidence hits remained and of those we validated a subset (n=19/20; 95%) by oligonucleotide deconvolution, where the siRNAs in the pools are re-tested individually to ensure that the observed increase in nucleolar number is driven by more than one siRNA.

(C) Z-prime statistic by plate (left) and as a minimum to maximum box and whiskers plot (right) indicated a strong, screenable phenotype with an average Z-prime of 0.41 and a Z-prime on all plates of >0.

(D) Signal-to-background (S/B) ratio by plate (left) and as a minimum to maximum box and whiskers plot (right) indicated a strong S/B with an average S/B of 10.29.

(E) Violin plot of the percent viability of all target genes and the 113 hits relative to siRISC-free. A and B were created with BioRender.com.

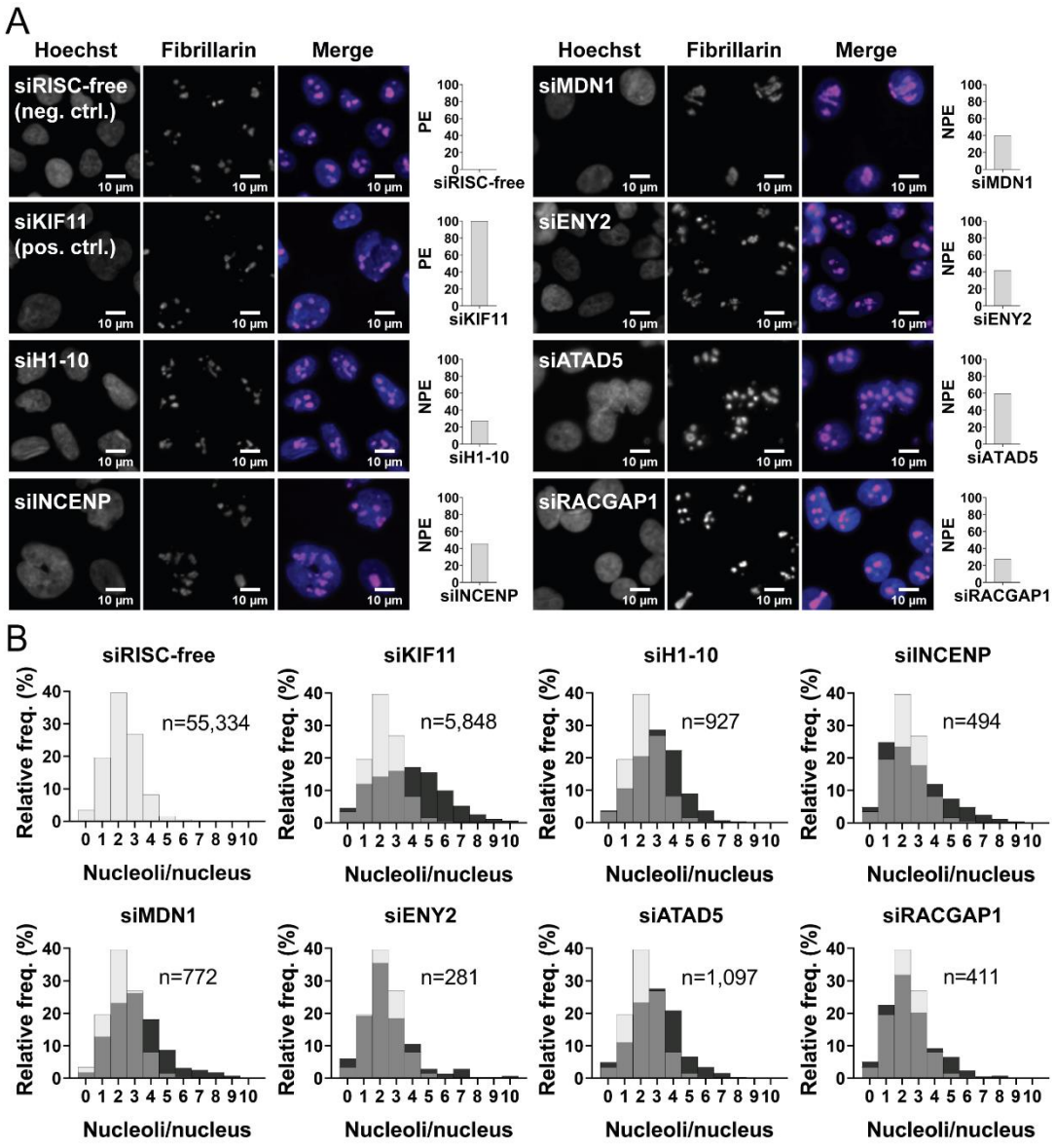

Figure 2-2. Representative hits showing an increase in nuclei with ≥5 nucleoli. Previously published in (Ogawa et al., 2021).

(A) Representative images of hits from the screen and the normalized percent effects (NPE). Shown are a selection of nuclei (100x100 µM) stained with Hoechst 33342 (blue) and an antibody to the nucleolar protein fibrillarin [72B9 (Reimer et al., 1987); pink] from the negative control (siRISC-free, 0 PE), positive control (siKIF11, PE), and representative screen hits (siH1-10, siINCENP, siMDN1, siENY2, siATAD5, and

siRACGAP1) enlarged 3-fold using bicubic interpolation from a single field of view (left), and a bar graph of the NPE (right).

(B) Histograms of the relative frequency of nucleoli per nucleus and the number of nuclei quantified are shown for the controls and representative hits in A. Relative to siRISC-free (gray bars), among the hits (and KIF11; black bars) there is a clear decrease in nuclei with 2-3 nucleoli and an increase in nuclei with ≥5 nucleoli (gray bars=overlap between siRISC-free and hit). Histograms for siRISC-free and siKIF11 are representative and were generated from the images collected from a single screening plate (Plate 1; 16 wells; 48 fields of view). Histograms for each hit were made from the images collected from their respective well and plate in the screen (3 fields of view). The x-axis was limited to 10 nucleoli per nucleus to aid in visualization; protein depletion conditions with nuclei with >10 nucleoli include siRISC-free (n=3), siKIF11 (n=36), siH1-10 (n=1), siINCENP (n=2), siMDN1 (n=3), siENY2 (n=4), and siRACGAP1 (n=2).

Bioinformatic analysis reveals a unique subset of proteins

To gain insight into the subset of proteins uncovered by this screen, I performed a range of bioinformatic analyses aimed at determining the degree of conservation, biological functions, and cellular localization of the 113 high confidence hits. Because the primary goal of this screen was to identify novel regulators of ribosome biogenesis in higher eukaryotes, I first identified the proportion of hits that are conserved to the yeast, *Saccharomyces cerevisiae*. To achieve this objective, I manually curated information from the published literature and two data mining tools. Using e!Ensembl's BioMart tool (Kinsella et al., 2011), I identified 22/113 hits with yeast orthologs. Using the *Saccharomyces* Genome Database's YeastMine tool (Balakrishnan et al., 2012), I identified 26/113 hits with yeast orthologs. Manual curation of these data resulted in the identification of 39/113 hits with yeast orthologs (Table 2-1; Appendix II). This analysis suggests that while one-third of the hits identified are conserved to yeast, two-thirds are regulators of nucleolar number that are unique to higher eukaryotes.

Table 2-1. One-third (39/113) of the hits identified by increased nucleolar number in MCF10A cells are conserved to the yeast, *Saccharomyces cerevisiae*. For a subset of hits, more than one gene name is listed for the yeast ortholog due to a lack of consensus in the literature. The ≥5 nucleoli/nucleus normalized percent effect (NPE) and percent viability from the screen are also included.

Screen hit (HGNC)	Yeast ortholog	≥5 nucleoli/nucleus NPE	Percent viability
KIF11	Cin8/Kip1	68.75	19.00
CDCA8	Nbl1	66.59	12.91
CMPK2	Cdc8	64.91	17.38
ATAD5	Elg1	59.75	27.67
SKP1	Skp1	57.64	13.00
MAN1A1	Mnl2	46.40	35.63
INCENP	Sli15	45.64	18.92
ENY2	Sus1	41.93	6.02
CUL1	Cdc53	41.61	36.50
MDN1	Rea1	39.82	29.07
ZDHHC17	Akr1/2	39.45	53.42
PMM2	Sec53	37.35	23.22
XRCC5	Yku80	35.61	42.14
RRM1	Rnr1/3	35.33	9.46
SMG5	Ebs1/Est1	31.03	27.66
RFC1	Rfc1	30.18	46.61
MCM6	Mcm6	29.60	54.59
OSBP2	Hes1/Kes1	29.58	14.65
TARS2	Mst1	28.66	36.20
ABCE1	Rli1	28.57	25.65
RIMS3	Tcb3	27.82	10.82
H1-10	Hho1	27.78	31.61
RACGAP1	Bem2/Rga1/2/Rgd1	27.62	15.60
STK24	Kic1/Pbs2	27.53	13.92

SLC2A12	Stl1	27.49	71.34
NGRN	Rrg9	27.47	25.68
LUC7L	Luc7	27.15	25.86
YIPF7	Yip1	27.11	5.29
WRAP53	Swt21	27.10	9.48
DYNC1H1	Dyn1	26.87	19.67
FGD4	Cdc24/Rom1/2	26.65	28.85
TOPBP1	Dpb11	26.37	10.58
SMAP2	Glo3/Gts1	26.24	33.90
OXNAD1	Aim33/Pga3	26.16	60.29
MARCH9	Ssm4	26.06	68.46
MPV17L2	Mpv17	25.65	13.92
NFYB	Hap3	25.50	41.60
MASTL	Pkh3/Rim15	25.41	32.46
NLRC5	Gip3/Her1	25.12	46.44

To determine the biological functions associated with the 113 high confidence hits from the screen, I performed analyses using two distinct software packages with unique algorithms to determine statistical enrichment. First, I performed a Gene Ontology (GO) over-representation analysis using PANTHER (Mi et al., 2017). This analysis revealed enrichment of 80 overlapping GO-Slim categories associated with biological process ($p<0.05$). The top 19 enriched categories, defined as a $\log_2$ fold enrichment >3.33, were largely associated with DNA replication and mitosis, including Regulation of exit from mitosis (GO:0007096), DNA double-strand break processing (GO:0000729), Mitotic sister chromatid cohesion (GO:0007064), and Non-recombinational repair (GO:0000726), among others (Figure 2-3, A).

Second, I performed the Molecular and Cellular Function core analysis in the Ingenuity Pathway Analysis software (IPA, Qiagen). Results from this analysis revealed 23 molecular and cellular functions significantly associated with the 113 hits ($-\log_{10}$ $p>1.3$; Table 2-2). The top functions revealed by this analysis, defined by the highest $-\log_{10}$ p-value, were Cell Cycle, Cellular Assembly and Organization, and DNA Replication, Recombination, and Repair (Figure 2-3, B). However, an analysis of these three top categories in the STRING Consortium database of protein-protein interactions, revealed a large degree of overlap among the categories and interconnectedness among the hits (Figure 2-3, C). Taken together, both these analyses of biological function revealed that the screen uncovered a unique subset of proteins largely associated with cell cycle-related processes, particularly in S and M phase, that are also required for the regulation of nucleolar number.

Finally, I determined the cellular localization of the 113 high confidence hits uncovered by this screen. Specifically, I was interested in determining what proportion of the hits localize to the nucleolus, because I hypothesize that depletion of a nucleolar protein would cause changes to nucleolar form. To determine whether a hit localizes to the nucleolus, I utilized 3 nucleolar proteomes, including 2 generated by mass spectrometry (Ahmad et al., 2009; Jarboui et al., 2011; Leung et al., 2006), and 1 inferred by immunofluorescence confocal microscopy (Thul et al., 2017). If the hit was present in at least 1 of the 3 proteomes, I identified it as a nucleolar protein. Based on this analysis, 23/113 (20.4%) hits were identified as nucleolar (Figure 2-3, D; Appendix II). When compared to estimates of the total number of nucleolar proteins in the human proteome (4-14%; Figure 2-3, D), this analysis suggests that our hits are enriched in nucleolar proteins. Thus, despite the lack of association with ribosome biogenesis categories in the analysis of biological function, the hits are enriched for nucleolar proteins suggesting the discovery of a unique subset of proteins required for the regulation of nucleolar number and the putative discovery of novel proteins required for the regulation of nucleolar function.

The enrichment in nucleolar proteins further led to me ask whether the 113 high confidence hits are proteins required for the liquid-liquid phase separation (LLPS) behavior reported to drive nucleolar formation. Proteins with intrinsically disordered regions (IDRs) are thought to be key drivers of LLPS (Lafontaine et al., 2020); thus, I looked for the hits from this screen in the DisProt database of proteins with IDRs (Hatos et al., 2020). Intriguingly, only 4/113 hits contain IDRs (HYPK, MICA, SMG5, and XRCC5). This analysis suggests that while the hits are enriched in nucleolar proteins, the

majority are not proteins likely to contribute to the LLPS behavior associated with nucleolar formation; and furthermore, LLPS may not be the key driver in the determination of increased nucleolar number.

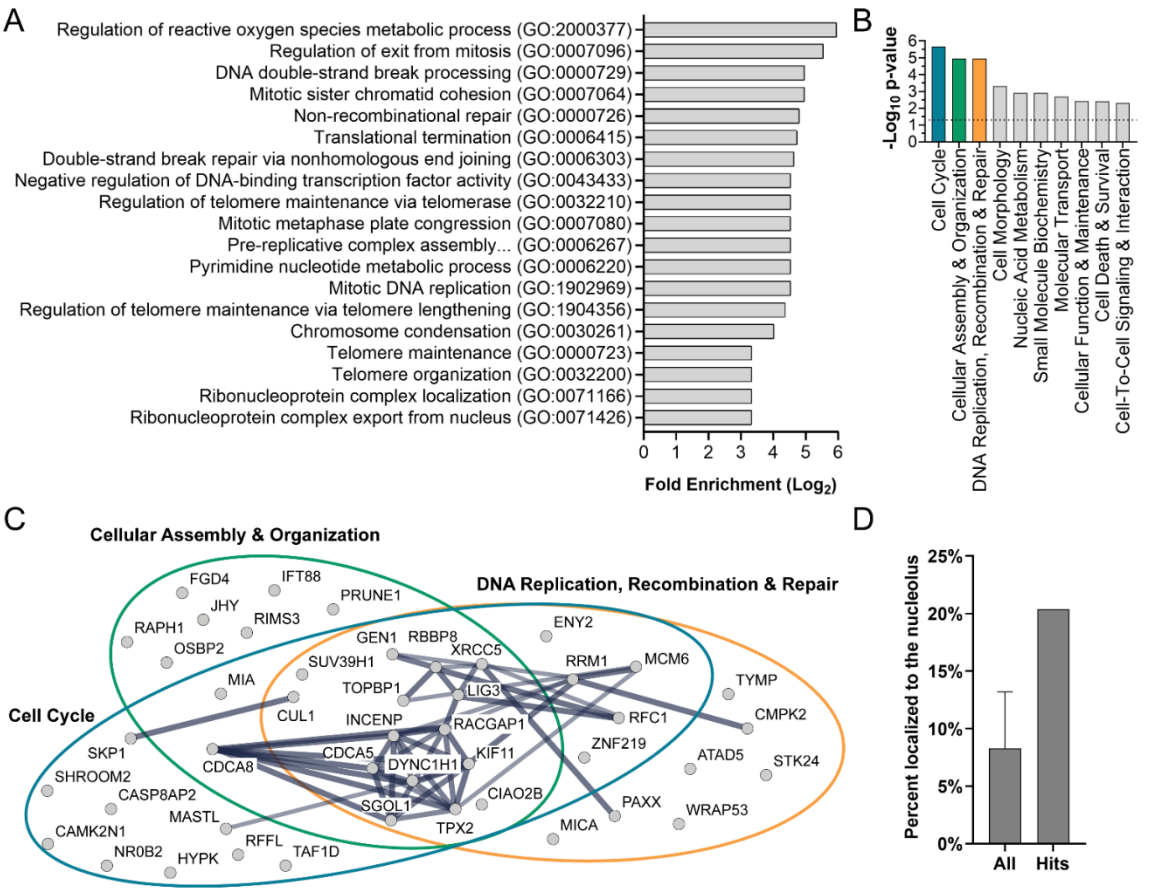

Figure 2-3. Bioinformatic analysis of the 113 hits reveals a unique set of proteins required for maintaining normal nucleolar number. Previously published in (Ogawa et al., 2021).

(A) Gene Ontology (GO) over-representation analysis using PANTHER is shown as a bar graph of the top enriched GO-Slim categories associated with biological process (Log2 fold enrichment >3.33; Binomial test, Bonferroni correction, $p<0.05$). Processes associated with mitosis [e.g. Regulation of exit from mitosis (GO:0007096) and Mitotic sister chromatid cohesion (GO:0007064)], and DNA replication and repair [e.g. DNA double-strand break processing (GO:0000729) and Non-recombinational repair (GO:0000726)] are common among the top enriched categories, but processes associated with ribosome biogenesis are strikingly absent.

(B) Molecular and Cellular Function analysis in Ingenuity Pathway Analysis (IPA; Qiagen) is shown as a bar graph of the top 10 molecular and cellular functions associated with the 113 hits using the Fisher's Exact Test scoring method in IPA ($p<0.05$). Top associated functions include Cell Cycle (n=31), Cellular Assembly and Organization (n=24), and DNA Replication, Recombination, and Repair (n=27). Colored bars are associated with the colored circles in C. All significantly associated categories and genes are listed in Table 2-2.

(C) Interaction networks of the hits in the top 3 categories in B are shown as STRING high confidence (≥0.700 interaction score) interaction networks and reveal a large degree of overlap among the categories and interconnectedness among the hits. The heavier weighted lines represent the highest degree of confidence (≥0.900 interaction score).

(D) Nucleolar proteins are enriched among the 113 hits. The percent of proteins in the human proteome (left) and of the hits (right) that localize to the nucleolus are shown as a bar graph. 20.4% of hits localize to the nucleolus, whereas the total number of nucleolar proteins in the human proteome ranges from 4.4-13.8%. These estimates were based on 3 published datasets (Ahmad et al., 2009; Jarboui et al., 2011; Leung et al., 2006; Thul et al., 2017), and a total number of proteins equal to 19,670 based on (Thul et al., 2017). In our calculation based on NOPdb, we used 2,717 proteins as the number of nucleolar proteins based on the last available dataset accessed on 01/22/2009. All=mean ± SD.

Table 2-2. Molecular and Cellular Function core analysis in the Ingenuity Pathway Analysis software (IPA; Qiagen) revealed a significant association of the 113 hits with 23 categories. The screen hits included in each category are listed.

Category	$-\log_{10}$ p-value	# of hits	Screen hits (HGNC)
Cell cycle	5.66	31	CAMK2N1, CASP8AP2, CDCA5, CDCA8, CIAO2B, CUL1, DYNC1H1, ENY2, GEN1, HYPK, INCENP, KIF11, LIG3, MASTL, MCM6, MIA, NR0B2, RACGAP1, RBBP8, RFC1, RFFL, RRM1, SGO1, SHROOM2, SKP1, SUV39H1, TAF1D, TOPBP1, TPX2, XRCC5, ZNF219
Cellular Assembly and Organization	4.95	24	CDCA5, CDCA8, CIAO2B, CUL1, DYNC1H1, FGD4, GEN1, IFT88, INCENP, JHY, KIF11, LIG3, MIA, OSBP2, PRUNE1, RACGAP1, RAPH1, RBBP8, RIMS3, SGO1, SUV39H1, TOPBP1, TPX2, XRCC5
DNA Replication, Recombination, and Repair	4.95	27	ATAD5, CDCA5, CIAO2B, CMPK2, CUL1, DYNC1H1, ENY2, GEN1, INCENP, KIF11, LIG3, MCM6, MICA, PAXX, RACGAP1, RBBP8, RFC1,

			RRM1, SGO1, STK24, SUV39H1, TOPBP1, TPX2, TYMP, WRAP53, XRCC5, ZNF219
Cell Morphology	3.32	16	CTF1, FGD4, IFT88, KIF11, LDB1, OSBP2, RACGAP1, RAPH1, RBBP8, RIMS3, SMAD5, SUV39H1, TOPBP1, TPX2, TYMP, XRCC5
Nucleic Acid	2.91	4	CMPK2, PMM2, RRM1, TYMP
Small Molecule Biochemistry	2.91	13	CMPK2, DYNC1H1, GLYATL2, HSD11B2, KMT2C, NAT2, NR0B2, OSBP2, PMM2, RAPH1, RRM1, SUV39H1, TYMP
Molecular Transport	2.69	6	KMT2C, NR0B2, RACGAP1, RAPH1,
Cellular Function and Maintenance	2.42	17	CDCA5, DYNC1H1, FGD4, IFT88, JHY, KIF11, MIA, PRUNE1, RAPH1,
Cell Death and Survival	2.42	36	ABCE1, AGR2, ASIC1, ATAD5, CASP8AP2, CCN4, CDCA5, CTF1, CUL1, DYNC1H1, FGD4, HSD11B2, HYPK, IFT88, INCENP, KIF11, LIG3, MDN1, MIA, MICA, NR0B2, OSBP2, PAXX, RACGAP1, RFC1, RRM1, SHC3, SHROOM2, SMAD5, STK24,

			SUV39H1, TM2D1, TOPBP1, TPX2, TYMP, XRCC5
Cell-To-Cell	2.32	5	ASIC1, GTF2IRD1, HSD11B2, IFT88,
Cellular Compromise	2.32	9	ASIC1, CTF1, CUL1, DYNC1H1,
Cellular Development	2.32	15	CCN4, CDCA5, CTF1, CUL1, EBF3, IFT88, MIA, OSBP2, PRUNE1, RAPH1, RFC1, RIMS3, SMAD5, STK24, SUV39H1
Cellular Growth and Proliferation	2.32	16	CCN4, CDCA5, CTF1, CUL1, EBF3, HSD11B2, IFT88, LDB1, MIA, OSBP2, PRUNE1, RAPH1, RFC1, RIMS3, SMAD5, SUV39H1
Cellular Movement	2.32	5	CCN4, FGD4, IFT88, INCENP, MIA
Cellular Response to	2.32	2	PAXX, XRCC5
Drug Metabolism	2.32	3	CMPK2, HSD11B2, NAT2
Lipid Metabolism	2.32	7	DYNC1H1, GLYATL2, HSD11B2,
Amino Acid	2.02	2	GLYATL2, SUV39H1
Carbohydrate	2.02	2	PMM2, RAPH1
Gene Expression	2.02	3	LIG3, NR0B2, SUV39H1
Post-Translational	2.02	4	FGD4, GLYATL2, MAP4K5, SUV39H1
Vitamin and Mineral	1.84	1	NR0B2
Cell Signaling	1.70	2	FGD4, MAP4K5

Screen validation supports approach and the identification of unique subset of proteins

Following initial evaluation of screen performance and hit analysis, I sought to validate the screen due to the known potential for siRNAs to bind unintended targets. While nucleolar enrichment served as primary evidence for the validity of the screening approach, in addition I performed oligonucleotide deconvolution on a subset of hits in collaboration with the Yale Center for Molecular Discovery. Oligonucleotide deconvolution is a common approach to siRNA screen validation, where the siRNAs in the pools against each target are tested individually in the primary screening assay (Sigoillot and King, 2011). I subjectively selected a representative subset of the high confidence hits to include in the validation assay (20/113, or ~20% of the hits; Table 2-3), including mitosis and DNA replication factors, nucleolar and non-nucleolar proteins, and proteins with putative RNA binding domains. Results revealed that 19/20 hits validated based on at least 2 of the 4 individual siRNAs in the original pools yielding an increase in percentage of cells with ≥5 nucleoli per nucleus (Z-prime=0.61; NPE≥15; Table 2-4). These data suggested a 95% validation rate, which supported the screen results and the unique subset of proteins identified by this approach.

I also compared the proteins uncovered by the screen to other published screens of nucleolar form and function. I compared the 113 high confidence hits to screens in *S. cerevisiae* (Neumuller et al., 2013), *D. melanogaster* (Neumuller et al., 2013), and in human cell lines (Badertscher et al., 2015; Tafforeau et al., 2013; Wild et al., 2010), to identify the degree of overlap among the hits and different screening approaches. Intriguingly, this analysis revealed minimal overlap between this screen for increased nucleolar number and other approaches (<2%; Table 2-5). Notably, however, in the

genome-wide screens for changes to nucleolar size or fragmentation in *S. cerevisiae* and *D. melanogaster* (Neumuller et al., 2013), our positive control and hit KIF11/Cin8/Klp61f was identified in both datasets. Furthermore, in *S. cerevisiae*, an enrichment for mitotic spindle assembly proteins was uncovered (Neumuller et al., 2013), consistent with the discovery of mitosis-associated factors in this screen. Thus, while there was a low degree of overlap among the hits, this analysis revealed a putative conserved link between the nucleolar regulation and mitosis.

The 113 high confidence hits were also compared to screens in human cell lines. I compared the hits to 3 screens performed in HeLa cells that aimed to identify novel factors required for ribosome biogenesis in humans. Two screens utilized fluorescently-tagged ribosomal proteins to identify proteins required for ribosomal subunit export (Badertscher et al., 2015; Wild et al., 2010), and the third used northern blots to identify proteins required for pre-rRNA processing (Tafforeau et al., 2013). Here, only 6 hits overlapped with the high confidence hits, including ABCE1, MDN1, DYNC1H1, CDCA8, SUV39H1, and TOPBP1 (Table 2-5). DYNC1H1 and CDCA8 both have reported roles in mitosis (Gassmann et al., 2004; Raaijmakers and Medema, 2014; Sampath et al., 2004); whereas ABCE1, MDN1, SUV39H1, and TOPBP1 have all been previously reported to be required for ribosome biogenesis and/or ribosome function (Bassler et al., 2010; Galani et al., 2004; Mooser et al., 2020; Murayama et al., 2008; Pisarev et al., 2010; Sokka et al., 2015; Young et al., 2015). Possible explanations for the lack of significant overlap include species (*S cerevisiae* vs. human) and cell line differences (MCF10A vs. HeLa), as well as differences in scale (genome-wide vs. candidate approach) and the screening assay itself (nucleolar number vs. fluorescent r-

protein retention). Finally, the hits were also completely non-overlapping with the hits from the parallel screen for decreased nucleolar number (Farley-Barnes et al., 2018). Taken together, this unique screening approach for increased nucleolar number led to the discovery of a distinct subset of proteins required to maintain the typical nucleolar form.

Table 2-3. High-confidence screen hits validated by oligonucleotide deconvolution. 20 hits were selected for validation by oligonucleotide deconvolution. The 14 hits selected for further analysis have the HGNC symbol in bold. Nucleolar localization (Y/N) and a brief description of each hit are included.

Protein name	HGNC Symbol	Aliases	Validated (Y/N)	Nucleolar (Y/N)	Description
ATP Binding Cassette Subfamily E Member 1	ABCE1	RNASEL1, RNASELI, RNS4I	Y	Y	Inhibits endoribonuclease activity through inhibition of RNase L. Also a ribosome recycling factor.
ATPase family AAA domain containing 5	**ATAD5**	C17orf41, ELG1, FRAG1	Y	N	DNA replication factor C-like complex subunit.
Cell division cycle associated 8	**CDCA8**	Borealin, BOR,	Y	Y	Mitotic chromosomal passenger

		DasraB, Nbl1p			complex member.
Dynein Cytoplasmic 1 Heavy Chain 1	DYNC1H1	DNECL, DNCL, DNCH1	Y	Y	Microtubule-activated molecular motor. Mitotic spindle assembly and metaphase plate congression factor.
ENY2 transcription and export complex 2 subunit	**ENY2**	Sus1	Y	N	Transcriptional co-activator through association with the SAGA complex and others.
Cytosolic Iron-Sulfur Assembly Component 2B	CIAO2B	FAM96B	Y	N	Mediates incorporation of Fe/S proteins.

					Component of mitotic spindle-associated MMXD complex.
Family with sequence similarity 98 member A	**FAM98A**		Y	N	Regulator of arginine methyltransferase, PRMT1, and contains a putative RNA-binding domain.
H1 histone family member X	**H1-10**	H1FX	Y	Y	H1 linker histone.
Inner centromere protein	**INCENP**		Y	Y	Mitotic chromosomal passenger complex member.

Inka box actin regulator 1	**INKA1**	FAM212 A, C3orf54	Y	N	PAK4 (P21 activated kinase) inhibitor.
Kinectin 1	KTN1		Y	N	Binds kinesins and elongation factor-delta in endoplasmic reticulum.
LUC7-like	LUC7L	Luc7	Y	N	Putative RNA-binding protein similar to yeast Luc7p subunit of the U1 snRNP splicing complex.
Midasin AAA ATPase 1	**MDN1**	Rea1	Y	Y	Large ribosomal subunit maturation factor.

Rac GTPase Activating Protein 1	**RACGAP1**		Y	N	Mitotic centralspindlin complex member.
Replication factor C subunit 1	**RFC1**		Y	Y	DNA replication factor C complex subunit.
Serine/threonine kinase 24	**STK24**	MST-3	Y	Y	GCK-3 family kinase involved in MAPK signaling.
TPX2 microtubule nucleation factor	**TPX2**		Y	Y	Mitotic spindle assembly factor and activator of Aurora A kinase signaling.

Cellular communication network factor 4	**CCN4**	Wisp1	Y	N	Wnt1-inducible signaling pathway protein.
WD repeat containing antisense to TP53	**WRAP53**	WDR79, Tcab1	Y	N	Telomerase holoenzyme member.
X-ray repair cross-complementing protein 5	XRCC5	Ku80	N`	Y	Non-homologous end joining (NHEJ) DNA repair factor.

Table 2-4. Oligonucleotide deconvolution of 20 screen hits supports validity of the screen approach and the identification of a unique subset of proteins. Listed are the 4 individual siRNAs for each hit, the mean percent effect (PE) of 3 wells, standard deviation (SD) of 3 wells, the mean normalized percent effect (NPE) relative to the negative (siRISC-free) and positive controls (siKIF11 pool), and whether the mean NPE was ≥15. If at least 2/4 individual siRNAs yielded a mean NPE≥15, the hit was considered validated.

Hit (siRNA)	Mean PE	SD (PE)	Mean NPE	≥15 Mean NPE (Y/N)
siRISC-free	4.45	0.98	0.00	
siKIF11 (pool)	44.23	4.13	100.00	
siKIF11				
siKIF11-05	40.25	1.27	116.70	Y
siKIF11-06	51.64	3.09	118.62	Y
siKIF11-07	34.19	3.93	74.75	Y
siKIF11-08	50.88	1.27	116.70	Y
siATAD5				
siATAD5-01	26.57	1.51	55.60	Y
siATAD5-02	11.01	0.39	16.49	Y
siATAD5-03	14.40	1.39	25.01	Y
siATAD5-04	13.44	5.39	22.60	Y
siCCN4				

siCCN4-01	11.55	0.45	17.85	Y
siCCN4-02	11.81	1.38	18.51	Y
siCCN4-03	13.95	0.31	23.89	Y
siCCN4-17	21.20	2.96	42.10	Y
siCDCA8				
siCDCA8-01	37.14	1.82	82.17	Y
siCDCA8-02	28.40	1.02	60.19	Y
siCDCA8-03	13.76	1.04	23.40	Y
siCDCA8-04	22.11	0.55	44.40	Y
siENY2				
siENY2-01	10.67	1.70	15.62	Y
siENY2-02	16.01	0.21	29.06	Y
siENY2-03	14.25	1.59	24.64	Y
siENY2-04	11.03	1.41	16.54	Y
siINCENP				
siINCENP-01	29.64	1.48	63.31	Y
siINCENP-02	47.36	4.27	107.86	Y
siINCENP-03	38.02	4.75	84.39	Y
siINCENP-04	30.33	0.53	65.05	Y
siRACGAP1				
siRACGAP1-01	24.96	2.42	51.56	Y
siRACGAP1-02	18.03	3.41	34.13	Y
siRACGAP1-03	30.90	1.33	66.49	Y

siRACGAP1-04	27.69	2.63	58.42	Y
siTPX2				
siTPX2-01	19.90	4.89	38.82	Y
siTPX2-02	45.26	2.08	102.59	Y
siTPX2-03	19.99	1.01	39.05	Y
siTPX2-04	17.00	0.77	31.55	Y
siABCE1				
siABCE1-01	24.62	2.43	50.71	Y
siABCE1-02	13.45	0.98	22.63	Y
siABCE1-04	14.92	2.27	26.31	Y
siABCE1-17	8.37	1.08	9.86	N
siDYNC1H1				
siDYNC1H1-01	13.36	0.73	22.40	Y
siDYNC1H1-02	14.36	1.14	24.91	Y
siDYNC1H1-03	35.99	3.39	79.29	Y
siDYNC1H1-04	8.05	1.42	9.05	N
siCIAO2B				
siCIAO2B-01	14.16	0.51	24.41	Y
siCIAO2B-03	7.48	0.72	7.62	N
siCIAO2B-04	10.61	0.13	15.48	Y
siCIAO2B-18	14.87	1.84	26.18	Y
siFAM98A				
siFAM98A-01	13.77	2.40	23.43	Y

siFAM98A-02	16.63	2.65	30.61	Y
siFAM98A-03	4.01	0.28	-1.10	N
siFAM98A-04	19.51	2.30	37.85	Y
siH1-10				
siH1-10-01	12.40	1.06	19.98	Y
siH1-10-02	19.69	1.57	38.30	Y
siH1-10-03	11.17	1.69	16.89	Y
siH1-10-04	8.55	1.76	10.30	N
siINKA1				
siINKA1-01	36.83	2.22	81.39	Y
siINKA1-02	9.41	0.93	12.47	N
siINKA1-03	11.47	0.79	17.64	Y
siINKA1-04	32.87	1.73	71.44	Y
siKTN1				
siKTN1-17	21.11	1.03	41.87	Y
siKTN1-18	21.96	1.71	44.02	Y
siKTN1-19	6.29	0.58	4.61	N
siKTN1-20	11.18	0.80	16.93	Y
siWRAP53				
siWRAP53-19	5.60	0.11	2.90	N
siWRAP53-20	15.64	1.69	28.11	Y
siWRAP53-21	11.79	1.90	18.45	Y
siWRAP53-22	19.78	1.31	38.53	Y

siLUC7L				
siLUC7L-01	18.85	3.88	36.19	Y
siLUC7L-02	7.11	1.19	6.67	N
siLUC7L-03	7.57	0.44	7.84	N
siLUC7L-04	13.21	0.27	22.01	Y
siMDN1				
siMDN1-03	10.91	0.66	16.23	Y
siMDN1-17	8.77	1.43	10.86	N
siMDN1-18	8.00	0.41	8.92	N
siMDN1-19	15.60	0.96	28.03	Y
siRFC1				
siRFC1-01	9.35	0.98	12.31	N
siRFC1-02	10.73	0.82	15.79	Y
siRFC1-03	12.80	1.63	20.99	Y
siRFC1-04	4.69	0.43	0.60	N
siSTK24				
siSTK24-05	7.25	0.96	7.04	N
siSTK24-21	5.17	0.56	1.81	N
siSTK24-22	11.48	0.98	17.66	Y
siSTK24-23	16.34	1.21	29.89	Y
siXRCC5				
siXRCC5-01	7.67	1.02	8.08	N
siXRCC5-02	7.19	0.71	6.89	N

siXRCC5-03	3.85	0.32	-1.50	N
siXRCC5-04	3.38	0.46	-2.68	N

Table 2-5. Overlap of high confidence screen hits with proteins identified in other screens for regulators of ribosome biogenesis reveals a unique subset of proteins. The 113 high confidence hits were compared to the hit lists from screens in human cell lines (Badertscher et al., 2015; Tafforeau et al., 2013; Wild et al., 2010), *S. cerevisiae* (Neumuller et al., 2013), and *D. melanogaster* (Neumuller et al., 2013) as indicated. Indicated in parentheses are the number of overlapping hits compared to the total number of hits identified by the screening approach. Gene names of the overlapping hits are listed.

Neumüller *et al.* *S. cerevisiae* (4/388)	Neumüller *et al.* *D. melanogaster* (6/757)	Wild *et al.* HeLa cells (2/153)	Badertscher *et al.* HeLa cells (2/300)	Tafforeau *et al.* HeLa cells (4/286)
KIF11/Cin8	IFT88/nompB	ABCE1	ABCE1	CDCA8
PMM2/Sec53	INCENP	MDN1	DYNC1H1	MDN1
SKP1/Skp1	KIF11/Klp61f			SUV39H1
YIPF7/Yip1	LIG3			TOPBP1
	MAN1A1/alpha-Man-I			
	RAP2C/Rap2I			

Nuclear area is significantly larger in nuclei with ≥5 nucleoli

Observations of images from the screen, like those shown in Figure 2-2, A, suggest that the nuclei of screen hits with ≥5 nucleoli may be larger than the nuclei in the siRISC-free control. To test whether nuclei are larger, using the images collected for the subset of hits analyzed in the screen validation, I used CellProfiler to classify nuclei by nucleolar number (0-4 vs. ≥5) and quantify the nuclear area of the Hoechst stain. My analysis revealed that the nuclear area of nuclei ≥5 nucleoli are significantly larger than nuclei with 0-4 nucleoli (n=3 or 6; $q<0.01$; Figure 2-4, A and B; Table 2-6). Interestingly, however, this result is observed not only when screen hits are depleted, but also in the negative control cells. There is some variability in the nuclear size increase among some hits; notably, depletion of CDCA8 and INCENP resulted in a ≥2-fold increase in the nuclear area of nuclei with ≥5 nucleoli compared to siRISC-free and a majority of the screen hits (Figure 2-4, B). These proteins are known mitotic inhibitors and thus suggests that this increase may be driven by a failure in cell division. As a result, and in addition to the bioinformatic analyses revealing significant association of screen hits with the cell cycle, these data suggest that cell cycle profiling is warranted to address whether failed cell cycle progression, specifically in mitosis, is a unifying feature of cells treated with these siRNAs.

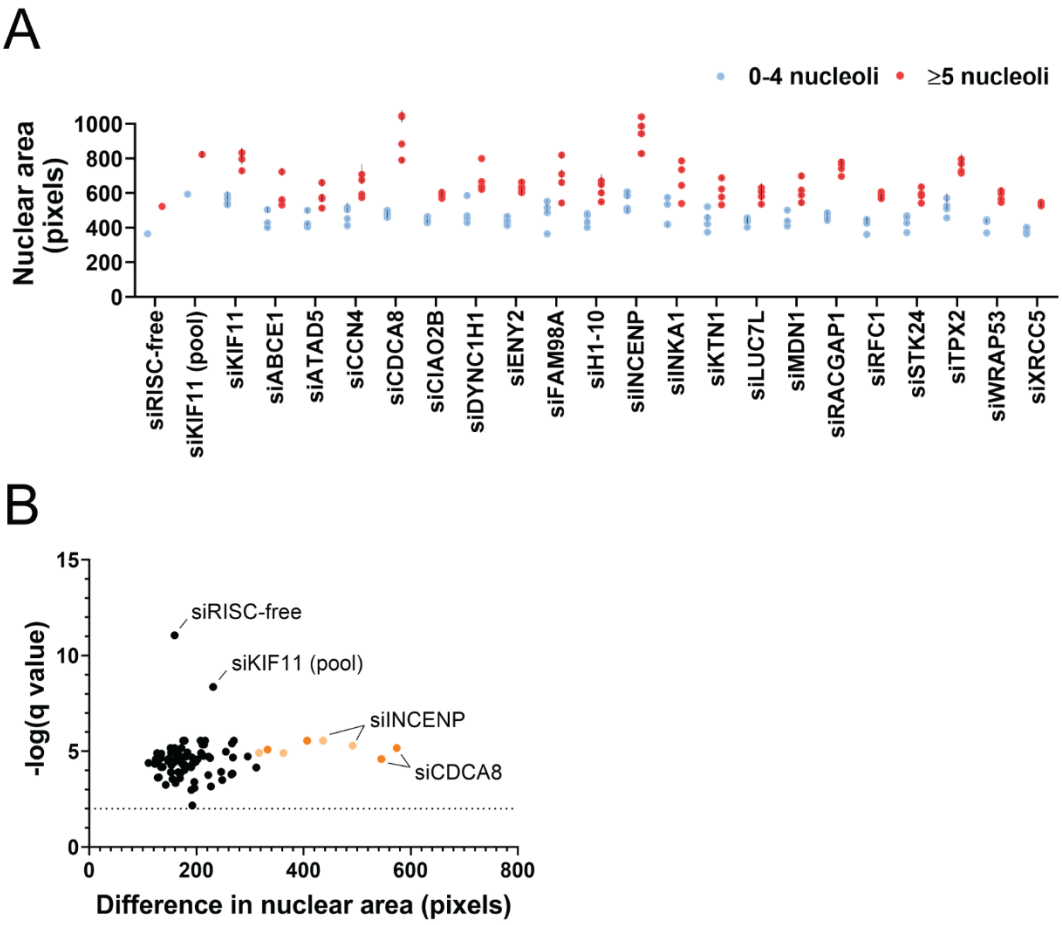

Figure 2-4. Nuclear area is significantly greater in nuclei with ≥5 nucleoli. Previously published in (Ogawa et al., 2021).

(A) Nuclear area is greater in nuclei with ≥5 nucleoli, including in the siRISC-free treatment. Nuclear area was quantified in pixels using analysis of the Hoechst-stained images collected for screen validation by oligonucleotide deconvolution. Three (3) replicates were analyzed for each screen hit depletion and 6 replicates were analyzed in this analysis for the controls, siRISC-free and siKIF11 (pool). Blue dots=nuclei with 0-4 nucleoli. Red dots=nuclei with ≥5 nucleoli. Each dot represents the mean ± SD of an individual siRNA (SD=black vertical line). For each blue dot there is a corresponding red dot (Table 2-6).

(B) Volcano plot of the statistical analysis of the data in A reveals that in all depletion conditions, including siRISC-free, nuclei with ≥5 nucleoli are significantly larger that nuclei with 0-4 nucleoli. Unpaired t-tests were performed, and significance was determined based on a False Discovery Rate approach using the two-stage step-up method of Benjamini, Krieger and Yekutieli (n=3 or 6; q<0.01/-log q-value>2; Table 2-6). The x-axis represents the difference in nuclear area between nuclei with 0-4 nucleoli and ≥5 nucleoli. The purple dots=individual siRNAs with the greatest difference between the two categories. Light orange dots=siINCENP individual siRNAs. Dark orange dots=siCDCA8 individual siRNAs.

Table 2-6. Nuclear area analysis of screen hit depletions comparing nuclei with 0-4 nucleoli to nuclei with ≥5 nucleoli. For each screen hit depletion, nuclei were classified as either nuclei with 0-4 nucleoli or ≥5 nucleoli and the average nuclear area was calculated (n=3 for hits; n=6 for controls). Significance was determined by unpaired t-tests and based on a False Discovery Rate approach using the two-stage step-up method of Benjamini, Krieger and Yekutieli (n=3 or 6; q<0.01/-log q-value>2). siRISC-free=negative control. siKIF11 (pool)=screen positive control.

Screen Hit (siRNA HGNC, -last 2 digits of product number)	Nuclear area 0-4 nucleoli (mean ± SD)	Nuclear area ≥5 nucleoli (mean ± SD)	Significance (q-value)
siRISC-free	206.4 ± 2.9	365.7 ± 6.5	q<0.0001
siKIF11 (pool)	435.8 ± 10.1	666.9 ± 18.1	q<0.0001
siKIF11 -05	382.2 ± 10.4	572.5 ± 14.5	q<0.0001
siKIF11 -06	374.9 ± 11.9	640.1 ± 29.5	q<0.001
siKIF11 -07	409.2 ± 16.8	676.5 ± 26.3	q<0.001
siKIF11 -08	430.4 ± 22.1	678.7 ± 28.5	q<0.001
siABCE1 -01	345.6 ± 15.5	567.6 ± 22.4	q<0.001
siABCE1 -02	244.4 ± 3.5	403.3 ± 6.5	q<0.0001
siABCE1 -04	270.8 ± 4.6	404.7 ± 11.5	q<0.0001

siABCE1 -17	243.8 ± 6.0	374.3 ± 3.7	q<0.0001
siATAD5 -01	342.5 ± 11.0	503.6 ± 23.5	q<0.001
siATAD5 -02	245.6 ± 3.2	356.4 ± 8.2	q<0.0001
siATAD5 -03	264.5 ± 7.1	411.7 ± 8.2	q<0.0001
siATAD5 -04	262.2 ± 5.9	417.5 ± 21.0	q<0.001
siCCN4 -01	254.2 ± 6.1	437.5 ± 5.7	q<0.0001
siCCN4 -02	359.6 ± 30.2	551.9 ± 57.1	q<0.01
siCCN4 -03	294.4 ± 6.8	417.0 ± 7.5	q<0.0001
siCCN4 -17	347.8 ± 7.6	519.7 ± 11.3	q<0.0001
siCDCA8 -01	318.2 ± 21.5	892.2 ± 1.5	q<0.0001
siCDCA8 -02	342.4 ± 5.0	887.7 ± 36.1	q<0.0001
siCDCA8 -03	301.8 ± 3.9	634.8 ± 12.7	q<0.0001
siCDCA8 -04	322.3 ± 8.6	728.9 ± 4.6	q<0.0001
siCIAO2B -01	286.0 ± 5.4	412.7 ± 3.2	q<0.0001
siCIAO2B -03	277.8 ± 9.4	446.7 ± 21.1	q<0.001
siCIAO2B -04	270.5 ± 1.9	445.7 ± 4.1	q<0.0001
siCIAO2B -18	305.7 ± 4.4	433.4 ± 16.5	q<0.001

siDYNC1H1 -01	311.5 ± 2.3	464.9 ± 13.1	q<0.0001
siDYNC1H1 -02	296.8 ± 2.4	511.1 ± 6.1	q<0.0001
siDYNC1H1 -03	427.8 ± 2.6	644.3 ± 4.9	q<0.0001
siDYNC1H1 -04	271.8 ± 5.5	483.0 ± 3.6	q<0.0001
siENY2 -01	284.6 ± 3.5	507.5 ± 12.6	q<0.0001
siENY2 -02	254.6 ± 5.3	446.6 ± 15.3	q<0.0001
siENY2 -03	272.8 ± 1.8	464.5 ± 11.5	q<0.0001
siENY2 -04	307.5 ± 6.2	479.5 ± 1.7	q<0.0001
siFAM98A -01	395.4 ± 5.7	663.7 ± 15.4	q<0.0001
siFAM98A -02	357.8 ± 24.9	554.2 ± 27.6	q<0.001
siFAM98A -03	206.6 ± 3.9	386.6 ± 9.8	q<0.0001
siFAM98A -04	329.4 ± 4.2	505.3 ± 14.8	q<0.0001
siH1-10 -01	274.9 ± 10.2	444.9 ± 16.8	q<0.001
siH1-10 -02	313.8 ± 4.2	493.6 ± 9.2	q<0.0001
siH1-10 -03	244.2 ± 4.9	392.5 ± 8.5	q<0.0001
siH1-10 -04	323.7 ± 6.4	514.4 ± 37.9	q<0.01
siINCENP -01	340.5 ± 9.4	832.2 ± 13.0	q<0.0001

siINCENP -02	426.7 ± 14.7	788.9 ± 10.0	q<0.0001
siINCENP -03	449.7 ± 8.8	886.4 ± 6.5	q<0.0001
siINCENP -04	355.5 ± 6.2	672.4 ± 13.8	q<0.0001
siINKA1 -01	417.5 ± 7.3	630.3 ± 9.4	q<0.0001
siINKA1 -02	262.5 ± 3.4	488.3 ± 13.9	q<0.0001
siINKA1 -03	258.9 ± 8.2	382.9 ± 1.4	q<0.0001
siINKA1 -04	377.2 ± 5.9	579.2 ± 12.5	q<0.0001
siKTN1 -17	301.1 ± 16.8	467.2 ± 7.8	q<0.001
siKTN1 -18	364.0 ± 3.1	532.1 ± 11.4	q<0.0001
siKTN1 -19	216.3 ± 3.0	375.5 ± 5.0	q<0.0001
siKTN1 -20	262.9 ± 3.8	420.5 ± 11.7	q<0.0001
siLUC7L -01	299.1 ± 8.4	451.4 ± 14.6	q<0.001
siLUC7L -02	278.5 ± 12.5	474.4 ± 27.6	q<0.001
siLUC7L -03	245.2 ± 3.2	379.3 ± 7.9	q<0.0001
siLUC7L -04	281.2 ± 12.3	424.0 ± 21.0	q<0.001
siMDN1 -03	251.2 ± 3.0	388.2 ± 12.3	q<0.0001
siMDN1 -17	343.7 ± 4.7	542.5 ± 14.4	q<0.0001

siMDN1 -18	280.5 ± 6.2	460.7 ± 8.9	q<0.0001
siMDN1 -19	279.3 ± 2.5	431.6 ± 10.9	q<0.0001
siRACGAP1 -01	318.7 ± 3.5	585.2 ± 6.8	q<0.0001
siRACGAP1 -02	285.1 ± 9.7	540.0 ± 5.5	q<0.0001
siRACGAP1 -03	328.5 ± 10.5	624.4 ± 13.5	q<0.0001
siRACGAP1 -04	300.5 ± 9.1	612.2 ± 28.2	q<0.0001
siRFC1 -01	268.2 ± 5.5	431.4 ± 6.8	q<0.0001
siRFC1 -02	288.4 ± 5.9	450.9 ± 3.2	q<0.0001
siRFC1 -03	288.9 ± 11.5	418.6 ± 12.7	q<0.001
siRFC1 -04	203.3 ± 1.5	412.1 ± 10.0	q<0.0001
siSTK24 -05	302.4 ± 4.7	479.9 ± 14.3	q<0.0001
siSTK24 -21	214.0 ± 0.8	385.5 ± 10.9	q<0.0001
siSTK24 -22	269.5 ± 3.2	427.1 ± 11.2	q<0.0001
siSTK24 -23	311.2 ± 3.1	439.1 ± 9.7	q<0.0001
siTPX2 -01	413.9 ± 25.9	641.0 ± 31.6	q<0.001
siTPX2 -02	367.8 ± 11.9	613.8 ± 24.1	q<0.001
siTPX2 -03	352.0 ± 4.8	559.8 ± 0.6	q<0.0001

siTPX2 -04	299.9 ± 2.2	570.1 ± 5.9	q<0.0001
siWRAP53 -19	211.7 ± 1.4	389.8 ± 4.1	q<0.0001
siWRAP53 -20	276.9 ± 2.9	407.9 ± 7.7	q<0.0001
siWRAP53 -21	279.4 ± 5.5	457.2 ± 17.4	q<0.0001
siWRAP53 -22	288.0 ± 1.8	440.0 ± 5.4	q<0.0001
siXRCC5 -01	243.6 ± 5.8	378.0 ± 3.6	q<0.0001
siXRCC5 -02	238.6 ± 1.1	389.1 ± 10.2	q<0.0001
siXRCC5 -03	218.0 ± 2.9	370.8 ± 6.5	q<0.0001
siXRCC5 -04	204.7 ± 2.2	370.7 ± 7.4	q<0.0001

Cell cycle analysis reveals proteins required for progression through S and G2/M phase

To evaluate whether failed cell cycle progression upon depletion of screen hits is a unifying theme, I used high-content image analysis of the Hoechst-stained nuclei as previously reported (Chan et al., 2013; Gomes et al., 2018; Roukos et al., 2015; Roukos et al., 2013). Using the images collected for screen validation by oligonucleotide deconvolution (Table 2-3), the integrated intensity of the Hoechst stain for each nucleus was quantified and log2 values were plotted as histograms for each of the 4 individual siRNAs from the 20 hits. Cell cycle phases were normalized to the siRISC-free 2N and 4N peaks as described in (Chan et al., 2013). I concluded cell cycle accumulation conservatively when depletion of at least 2 of 4 individual siRNAs resulted in a significant ≥2-fold decrease or increase in the percent of nuclei in a phase relative to siRISC-free ($q<0.01$). As expected, depletion of KIF11, a mitotic kinesin, resulted in an accumulation of cells in G2/M phase (Figure 2-5; Appendix III). However, depletion of only 2/20 hits caused an accumulation of cells in G2/M (INCENP and TPX2), with an additional 6/20 hits yielding a significant increase in >4N DNA content (ABCE1, CDCA8, DYNC1H1, ENY2, INKA1, and RACGAP1; Figure 2-5; Appendix III). Mitosis-associated factors, CDCA8, INCENP, and RACGAP1, yielded the greatest accumulation of nuclei with >4N DNA content (>10% nuclei), while the increase among the other hits was more modest (<10% nuclei).

Cell cycle data were confirmed by at least a 50% increase in at least 1 of 2 replicates in a separate cell cycle profiling experiment where the hits in bold in Table 2-3 were depleted using the siRNA pools (Table 2-7). Furthermore, cell cycle results are consistent with a post hoc analysis of the screen images that I performed to evaluate how

our CellProfiler pipeline segmented atypical nuclei and nucleoli. I observed annular and semi-annular nuclei among some hits (e.g. siINCENP), which are indicative of late mitotic defects, that were counted both as one and more than one nucleus potentially skewing estimates of nucleolar number [Figure 2-6; (Verstraeten et al., 2011)]. I also observed "stretched" nucleoli, reminiscent of anaphase bridges and mitotic defects [e.g. siMDN1; (Daniloski et al., 2019)], that in some cases could lead to an over-estimate of nucleolar number (Figure 2-7). Regardless, while defects in G2/M phase progression and cytokinesis failures were present among the hits tested, they were not observed in all cases.

Other aspects of the cell cycle were also affected to varying degrees. In addition to hits that, when depleted, caused an accumulation of cells in G2/M phase, our analysis also revealed that depletion of 8/20 hits caused a significant accumulation of cells in S phase ($q<0.01$; CIAO2B, DYNC1H1, ENY2, FAM98A, LUC7L, RFC1, STK24, and WRAP53; Figure 2-5; Appendix III). Interestingly, 2 of these (DYNC1H1 and ENY2) were hits that also led to a significant increase in nuclei with >4N DNA content, suggesting that defects in S phase progression may also contribute to failures in cell division. Furthermore, 4 hits (CDCA8, INCENP, RACGAP1, and TPX2) resulted in a significant decrease in nuclei in G0/G1 phase and correlate with the hits that resulted in an accumulation of cells in either G2/M or with a >4N DNA content ($q<0.01$). Finally, depletion of 6/20 hits (ATAD5, CCN4, H1-10, KTN1, MDN1, and XRCC5) showed no change in cell cycle distribution based on our designated threshold, although significant minor differences were observed that may be meaningful (Figure 2-5; Appendix III). Finally, when considering whether an individual siRNA treatment that caused a

significant cell cycle accumulation also resulted in an increase in the ≥5 nucleoli per nucleus NPE, there are instances where a change in cell cycle distribution is observed, but no concomitant increase in nucleolar number is observed (CIAO2B, DYNC1H1, INKA1, LUC7L, MDN1, RFC1, STK24 and XRCC5; Figure 2-5; Appendix III). Taken together, our cell cycle analysis using DNA content suggests that despite an increase in the nuclear area of nuclei with ≥5 nucleoli, failures in G2/M phase progression and cytokinesis may only in some cases explain the increased numbers of nucleoli that I observe, and the contribution of other mechanisms may be in part responsible.

To further investigate the link between the cell cycle and ≥5 nucleoli per nucleus NPE, I asked whether the occurrence of the ≥5 nucleoli per nucleus phenotype correlated with an individual phase of the cell cycle. Interestingly, when I restricted our analysis of nucleolar number by cell cycle phase and calculated the ≥5 nucleoli per nucleus NPE for each of the 20 hits, I found that the median NPE of the 4 individual siRNAs is greater when considering cells in the G2/M phase of the cell cycle (19/20; Figure 2-8; Table 2-8). The one exception was XRCC5, which was also the only hit that did not pass our initial validation. In addition, only when considering cells in the G2/M phase is there an observable difference in PE between siRISC-free and siKIF11 (Z-prime=0.47). The Z-prime statistics were negative for both cells in G0/G1 phase (Z-prime=-0.08) and S phase (Z-prime=-0.12), suggesting no significant distinction between the negative and positive controls. Furthermore, it has been reported that nuclear volume scales with cellular volume, which gradually increases through the cell cycle (Cantwell and Nurse, 2019; Jorgensen et al., 2007; Maeshima et al., 2011; Neumann and Nurse, 2007); therefore, these data are consistent with our observation that nuclei with ≥5 nucleoli are

significantly larger (Figure 2-4, A and B). Taken together, while these data suggest that some hits are required for S and G2/M phase progression, in most cases it is likely the cells specifically in G2/M phase that are driving the increase in the percentage of nuclei with ≥5 nucleoli observed.

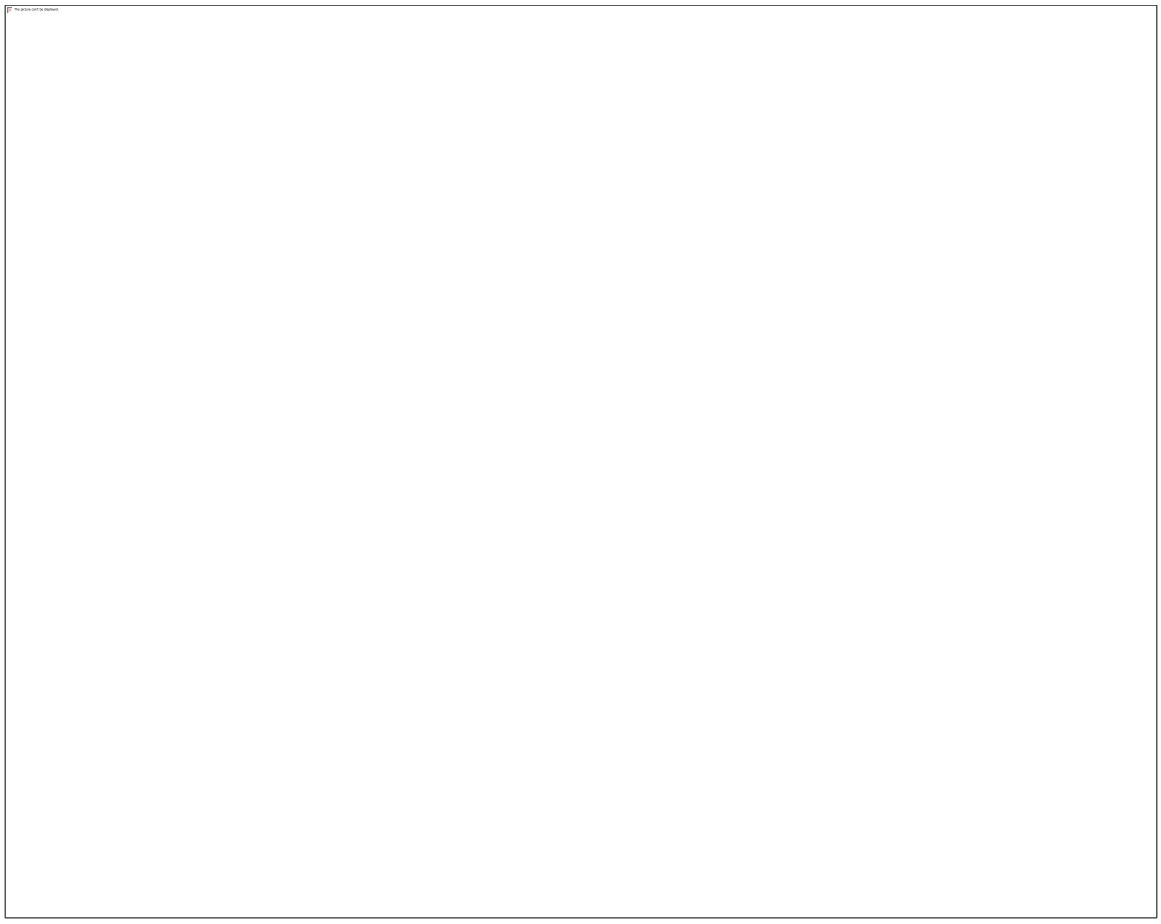

Figure 2-5. Cell cycle analysis reveals that hits are required for progression through either S or G2/M phase. Representative histograms of DNA content by quantification of Hoechst 33342 log2 integrated intensity. The log2 integrated intensities of nuclei in the negative, siRISC-free, control (sum of 48 replicates; n=498,155 nuclei) were plotted and the G0/G1 peak set to 1.0 (red lines and text) and G2/M peak set to 2.0 (blue lines and text), and all other depletion conditions were then normalized to siRISC-free. Phases were assigned based on (Chan et al., 2013), with G2/M phase including late G2 nuclei; G0/G1=0.75-1.25; S=1.25-1.75; G2/M=1.75-2.25 and 2.25-2.50; >4N=>2.50. Depletion of the positive control, siKIF11 (pool) resulted in the expected accumulation of cells in G2/M phase and a subset of cells with a >4N DNA content (sum of 48 replicates; n=93,027 nuclei). Cell cycle profiling reveals that several hits are required for

progression through either S or G2/M phase. Representative histograms for screen hits are shown as a sum of the 3 replicates, yet each replicate for every depletion condition was characterized individually to perform statistical testing (Appendix III). Significance was determined by unpaired t-tests relative to siRISC-free and a False Discovery Rate approach using the two-stage step-up method of Benjamini, Krieger and Yekutieli (n=3 or 48; $q<0.01$=*; $q<0.001$=**; $q<0.0001$=***; Appendix III). Cell cycle defects were concluded based on a conservative threshold of whether treatment with ≥2 of 4 individual siRNAs resulted in a ≥2-fold significant increase or decrease in the percent of nuclei in a phase relative to siRISC-free. Each hit is listed below one of four representative histograms for the statistically significant cell cycle defects identified. Previously published in (Ogawa et al., 2021).

Table 2-7. Cell cycle profiling of screen hits in bold in Table 2-3 by pooled depletion validate hits with G2/M phase defects. Mock and siNT were included as negative controls. siKIF11 was included as a positive control. Shown are the number of nuclei assayed and the percent nuclei in each cell cycle phase for each of two replicates (1/23/20 and 1/27/20).

Hits	Number of cells analyzed		% G0/G1		% S		% G2/M		% >4N	
	Rep 1	Rep 2	Rep 1	Rep 2	Rep 1	Rep 2	Rep 1	Rep 2	Rep 1	Rep 2
Mock	20288	11735	37.5	37.1	20.6	20.6	20.9	28.2	4.28	3.86
siNT	15299	7768	44.4	44.7	18.2	17.3	13.2	18.8	1.95	2.1
siUTP4	13842	6025	46.7	47.6	12.5	11.3	9.6	14.1	1.2	2.6
siKIF11	3685	1943	**21.1**	**22.3**	**32.4**	16.0	**29.2**	**42.8**	1.7	**6.7**
siINCENP	1927	765	**29.9**	38.2	24.7	14.9	**25.7**	18.2	**3.5**	**3.5**
siCDCA8	1287	648	**20.6**	**19.4**	27.0	18.8	**29.2**	**29.8**	**10.6**	**17.4**
siRACGAP1	3839	1531	**30.7**	**26.1**	17.8	12.9	**24.8**	**28.2**	**11.4**	**17.6**
siINKA1	2340	1099	38.1	**32.8**	24.0	19.1	**22.3**	26.0	1.0	**3.2**
siTPX2	1168	590	**24.1**	**29.8**	**31.8**	19.0	**23.2**	26.3	1.5	3.1
siFAM98A	3331	1469	50.3	52.5	15.8	12.7	8.6	9.6	0.7	1.0
siWRAP53	5781	1943	45.3	40.1	14.8	12.8	9.2	12.1	1.0	2.0
siATAD5	6352	1749	47.1	41.0	16.9	13.0	9.7	13.7	0.9	1.9
siCCN4	3763	1215	48.8	47.2	10.9	10.9	5.7	11.3	0.3	1.5
siENY2	5378	2208	49.7	42.8	15.0	12.3	7.2	11.4	0.6	2.3
siH1-10	3490	1268	49.7	48.1	8.2	12.2	3.9	9.6	0.4	3.1
siRFC1	3728	1337	44.8	**37.5**	20.8	22.6	11.3	17.0	0.4	2.1
siMDN1	5064	2038	53.3	56.8	9.0	7.1	4.8	6.9	0.2	0.5
siSTK24	4179	1385	50.9	53.1	10.6	8.2	4.5	5.0	0.5	0.6

Figure 2-6. Atypical annular and semi-annular nuclei were counted both as one and more than one nucleus, potentially skewing estimates of nucleolar number per nucleus. In a subset of screen images where atypical nuclei were observed, CellProfiler pipeline segmentation of annular and semi-annular nuclei revealed inconsistent nuclear identification. Annular nuclei were sometimes segmented as a single nucleus, whereas semi-annular nuclei were sometimes segmented as more than one nucleus. Each colored spot represents a single segmented nucleus. In the merge, blue=Hoechst (nuclei) and pink=fibrillarin (nucleoli). Normal nuclei shown were from siRISC-free and atypical nuclei shown were from siINCENP. Previously published in (Ogawa et al., 2021).

Figure 2-7. Atypical “stretched” nucleoli in some cases led to an overestimate of nucleolar number per nucleus. In a subset of screen images where atypical nucleoli were observed, CellProfiler pipeline segmentation of “stretched” nucleoli were sometimes incorrectly identified as multiple nucleoli. Each colored spot represents a single segmented nucleolus. In the merge, blue=Hoechst (nuclei) and pink=fibrillarin (nucleoli). Normal nucleoli shown were from siRISC-free and atypical nucleoli shown were from siMDN1. Previously published in (Ogawa et al., 2021).

Figure 2-8. The observed increase in nucleolar number (NPE) is greater when restricting analysis to cells in G2/M phase. ≥5 nucleoli per nucleus NPE is greater when restricting the analysis of nucleolar number to cells in G2/M phase. We restricted our analysis of the ≥5 nucleoli per nucleus NPE for each of the 20 hits based on cell cycle phase. Only when considering nuclei in G2/M phase was there a statistical separation between siRISC-free and siKIF11 (Z-prime=0.47). The NPE for each individual siRNA are depicted as dots. The bars show the median NPE + interquartile range for the 4 individual siRNAs for each hit, for all nuclei (gray) and nuclei in G2/M phase only (blue). Previously published in (Ogawa et al., 2021).

Table 2-8. ≥5 nucleoli per nucleus normalized percent effect (NPE) is greater when considering cells in G2/M phase only. NPE for each siRNA in the pool of 4 comparing NPE for all cells to cells in G2/M only.

Hits	All cells				G2/M cells			
	1	2	3	4	1	2	3	4
siKIF11	89.98	118.62	74.75	116.70	104.40	130.50	111.60	133.20
siINCENP	63.31	107.86	84.39	65.05	103.10	119.60	106.60	85.90
siCDCA8	82.17	60.19	23.40	44.40	116.70	90.80	41.80	74.10
siRACGAP1	51.56	34.13	66.49	58.42	73.40	58.90	89.90	71.90
siINKA1	81.39	12.47	17.64	71.44	91.90	18.70	48.80	91.60
siTPX2	38.82	102.59	39.05	31.55	44.60	125.30	91.20	64.60
siKTN1	41.87	44.02	4.61	16.93	81.80	51.40	14.90	31.90
siFAM98A	23.43	30.61	-1.10	37.85	47.70	51.00	-2.20	64.00
siABCE1	50.71	22.63	26.31	9.86	68.80	37.60	60.00	16.50
siDYNC1H1	22.40	24.91	79.29	9.05	25.70	41.80	104.80	20.90
siWRAP53	2.90	28.11	18.45	38.53	7.50	53.00	35.60	74.90
siATAD5	55.60	16.49	25.01	22.60	80.00	30.30	40.90	23.70
siCCN4	17.85	18.51	23.89	42.10	53.00	30.50	32.30	63.10
siENY2	15.62	29.06	24.64	16.54	32.70	38.70	49.70	44.00
siCIAO2B	24.41	7.62	15.48	26.18	55.40	24.40	28.10	64.20
siH1-10	19.98	38.30	16.89	10.30	26.20	48.60	32.10	37.80
siLUC7L	36.19	6.67	7.84	22.01	43.50	18.50	29.50	46.80
siRFC1	12.31	15.79	20.99	0.60	13.60	20.00	26.80	3.50
siMDN1	16.23	10.86	8.92	28.03	50.30	30.80	21.50	53.00
siSTK24	7.04	1.81	17.66	29.89	23.10	7.50	35.80	54.50
siXRCC5	8.08	6.89	-1.50	-2.68	17.10	11.20	-8.10	-5.90

Inhibition of DNA replication and mitosis increase nucleolar number

Cell cycle analysis revealed that depletion of a subset of screen hits resulted in failures in progression through S and G2/M phase of the cell cycle. I therefore asked whether inhibition of DNA replication and mitosis by small molecule inhibitors is sufficient to cause increased nucleolar numbers (Weiss et al., 2007). Small molecules tested included tubulin inhibitors (nocodazole and paclitaxel), aurora kinase A and B inhibitors [MK-5108 and hesperadin, respectively (de Groot et al., 2015)], topoisomerase inhibitors (etoposide and ICRF-193), a KIF11 inhibitor (ispinesib), and the DNA replication inhibitors, mitomycin C and 5-fluorouracil. MCF10A cells were incubated with low doses of the inhibitors for prolonged periods of time (24, 48, and 72 hrs) to best mimic the conditions from our siRNA screen. Following treatment, the ≥5 nucleoli per nucleus PE was quantified relative to 0.1% dimethyl sulfoxide (DMSO) treatment, which was set to a 100 PE. In this experiment, all mitosis and DNA replication inhibitors tested caused a significant >2-fold increase in the percentage of cells with ≥5 nucleoli per nucleus by the 72 hr time point (and all but 1 by the 48 hr time point; Figure 2-9). Furthermore, the PE increased with each time point. Thus, inhibition of DNA replication and mitosis cause an increase in the percentage of cells with ≥5 nucleoli and validates the connection between progression through the cell cycle and maintenance of normal nucleolar numbers.

Additionally, I also tested whether inhibition of RNAPI was sufficient to drive increased nucleolar number. This was asked, in part, due to the known nucleolar segregation that occurs upon treatment with AMD and other chemotherapeutic agents (Burger et al., 2010; Reynolds et al., 1964); but was also asked to address whether

inhibition of nucleolar function itself is enough to drive increased nucleolar numbers. RNAPI inhibitors tested included AMD, BMH-21, and CX-5461. Interestingly, both AMD and BMH-21 at most time points yielded a significant decrease in the percentage of cells with ≥5 nucleoli (Figure 2-9). Only CX-5461 at the 72 hr time point caused a significant >2-fold increase in the percentage of cells with ≥5 nucleoli, progressing from a significant decrease at 24 hrs, distinguishing it from the other two RNAPI inhibitors. This could be explained, in part, by the different mechanisms by which these inhibitors are proposed to function, with the former as DNA intercalators, and the latter as a topoisomerase inhibitor (Bruno et al., 2020). Thus, I discovered that inhibition of ribosome biogenesis through RNAPI inhibition is not sufficient to cause an increase in the percentage of cells with ≥5 nucleoli. Taken together, these data further support the role of faithful cell cycle progression through S and G2/M phase as an important component in the maintenance of normal nucleolar number.

Figure 2-9. Inhibition of mitosis and DNA replication increase the percentage of nuclei with ≥5 nucleoli. The ≥5 nucleoli per nucleus PE was quantified relative to DMSO (set to a 100 PE) in MCF10A cells treated with a panel of small molecule inhibitors of the cell cycle for 24 (light gray), 48 (dark gray), and 72 hrs (blue). A dotted line is drawn at 100 PE. M=Inhibitors of mitosis (ispinesib, nocodazole, paclitaxel, hesperadin, and MK-5108). S=Inhibitors of DNA replication (mitomycin C and 5-fluorouracil). M/S=Inhibitors of both mitosis and DNA replication (topoisomerase II inhibitors: etoposide and ICRF-193). RNAPI=Inhibitors of RNAPI transcription (AMD, BMH-21, and CX-5461). Statistical significance was calculated by unpaired t tests with the Holm-Sidak method of correction for multiple comparisons (*=$p<0.05$, **=$p<0.01$, ***=$p<0.001$; n=3). Previously published in (Ogawa et al., 2021).

DISCUSSION

Through a high-content genome-wide siRNA screen in the near-diploid MCF10A human breast epithelial cell line, I have identified a high confidence set of 113 proteins that, when depleted, cause an increase in the percentage of cells with ≥5 nucleoli. Of the 113 proteins, two-thirds are proteins without a known ortholog in *S. cerevisiae*, suggesting the identification of a subset of proteins with putative nucleolar regulatory functions that are unique to higher eukaryotes. My subsequent analyses revealed that the hits are enriched for nucleolar proteins (20%), yet not for proteins typically associated with the nucleolar function of ribosome biogenesis. While multiple factors associated with ribosome biogenesis were identified [e.g. ABCE1 (Pisarev et al., 2010; Young et al., 2015), MDN1 (Bassler et al., 2010; Galani et al., 2004), SUV39H1 (Murayama et al., 2008), and TAF1D (Gorski et al., 2007)], enrichment analyses revealed that the hits are instead significantly associated with cell cycle processes including mitosis and replication. Cell cycle profiling on a subset of hits confirmed that several, but not all, are required for progression through S and G2/M phase of the cell cycle. Thus, this screen for increased nucleolar number uncovered a subset of proteins required for the regulation of nucleolar number and suggests an interdependence between faithful cell cycle progression and the nucleolus.

The 113 hits uncovered by this screen are a unique subset of proteins when compared to other screens for regulators of nucleolar form and function. When compared to other screens for regulators of ribosome biogenesis in higher eukaryotes, the overlap among the hits was <2%. Of the hits that are shared (ABCE1, MDN1, DYNC1H1, SUV39H1, TOPBP1, and CDCA8), there is no clear underlying theme that connects

them. Differences among the model systems employed or experimental readouts evaluated however may largely explain the lack of overlap. For instance, the screens for human ribosome biogenesis factors were all performed in the aneuploid HeLa cervical cancer cell line (Badertscher et al., 2015; Tafforeau et al., 2013; Wild et al., 2010), whereas my study was performed in a near-diploid non-cancer-derived cell line, MCF10A. Each screen also utilized different experimental methodologies and readouts to establish ribosome biogenesis factors, where it is conceivable that the proteins required for the regulation of nucleolar number may be different from the proteins that regulate ribosomal subunit export. Despite minimal overlap, however, comparison of the 113 hits to the screens for changes in nucleolar size in *S. cerevisiae* and *D. melanogaster* lends support to potentially conserved links between the nucleolus and both mitosis and mannose metabolism (Neumuller et al., 2013). For instance, spindle pole body proteins required for mitotic spindle assembly were enriched in the *S. cerevisiae* dataset, and spindle assembly factor, KIF11/Cin8/Klp61f, specifically was present in both datasets as well as in my screen (a hit and the positive control). Also shared among the datasets and my screen are the mannose-associated proteins PMM2/Sec53 identified in *S. cerevisiae* and MAN1A1/alpha-Man-I identified in *D. melanogaster*, which suggests a novel putative role for glycoprotein biosynthesis in the regulation of nucleolar form and function. Finally, and perhaps most intriguing, is that I also observed no overlap among the hits and over-represented GO categories (Fold enrichment ≥ 5, $p<0.05$) when compared to our hits for decreased nucleolar number (Farley-Barnes et al., 2018). These results suggest that the mechanisms underlying the regulation of nucleolar number are likely distinct depending on whether the number has increased or decreased. The 113 hits

identified by my screen for increased nucleolar number are therefore unique compared to proteins uncovered by other screens for ribosome biogenesis factors and may serve to broaden our understanding of the regulation of nucleolar form and function in higher eukaryotes.

Among the discoveries uncovered by my screen are the diverse subset of proteins that support a connection between the nucleolus and mitosis. Bioinformatic analyses revealed that the hits are enriched for cell cycle-associated proteins, including proteins required for mitosis. Cell cycle profiling supported the role for a subset of the hits in progression through G2/M phase. Included among the mitosis-associated hits are proteins required for mitotic spindle assembly, including KIF11, RACGAP1, and TPX2, as well as the aurora B kinase (AURKB)-associated proteins, CDCA8 and INCENP (Uehara et al., 2013). In addition, sister chromatid cohesion proteins (CDCA5 and SGOL1) and mitosis-associated cell cycle regulators [CUL1, SKP1, and MASTL; (Nakayama and Nakayama, 2006)] were also identified. There has long been an appreciation for the role of the nucleolus in cell cycle regulation, including in the nucleolar sequestration of proteins required for cell cycle progression (Boisvert et al., 2007; Visintin and Amon, 2000). It is also well known that the nucleolus undergoes dynamic remodeling as a consequence of the cell cycle, exemplified by cyclin-dependent kinase 1 (CDK1)-mediated silencing of RNAPI and the disassembly and reformation of nucleoli in mitosis (Hernandez-Verdun, 2011). Furthermore, a novel complex of ribosome biogenesis factors required for RNAPI transcription was recently implicated in the regulation of mitotic entry, chromatid cohesion, and spindle assembly through AURKB (Fujimura et al., 2020). Taken together, these data strengthen the support for significant crosstalk between

the nucleolus and the cell cycle. Thus, my screen revealed a unique subset of proteins that both regulate nucleolar number and mitosis and raises the question of whether they also regulate nucleolar function through RNAPI transcription.

The results from my screen also support a connection between the nucleolus and DNA replication. Bioinformatic analyses revealed that the hits are also enriched for proteins required for DNA replication, recombination, and repair. Cell cycle profiling again supported the role for a subset of hits in the progression through S phase. Included among these hits are two proteins, ATAD5 and RFC1, that form heteromeric replication factor complexes that are required for the loading and unloading of the DNA clamp and processivity factor, PCNA. In eukaryotic genomes, the rDNA loci are the most highly transcribed loci and conflict between the transcription and replication machinery can lead to genome instability at replication forks (Lindstrom et al., 2018). Furthermore, replication stress, particularly at fragile site loci like the rDNA, has been associated with defects in mitosis including increased DNA bridges in anaphase, chromosome breakage, and cancer (Chan et al., 2009; Franchitto, 2013; Stults et al., 2009; Warmerdam and Wolthuis, 2019). As a result, mechanisms have evolved to ensure replication fidelity, including evidence for transient silencing of RNAPI in response to DNA damage (Ciccia et al., 2014; Kruhlak et al., 2007; Larsen et al., 2014; Larsen and Stucki, 2016). Thus, the hits from this screen may represent additional mechanisms by which the fidelity of the rDNA loci are maintained through S phase, which may be through regulation of RNAPI transcription. Taken together, these data also support an interdependency between the nucleolus and DNA replication that has important consequences for cell cycle progression.

Testing small molecule compounds for their impact on nucleolar number further supports the association between S and G2/M phase progression and increased nucleolar number. I found that prolonged inhibition of mitosis and DNA replication with several different inhibitors led to significant increases in the percentage of cells with ≥5 nucleoli per nucleus. Furthermore, duration of treatment was an important factor in driving the PE, as we observed little to no effect at 24 hrs and the greatest effect at 72 hrs. The drugs tested included the KIF11 inhibitor, ispinesib, which independently validated the role for KIF11 in the regulation of nucleolar number. Also tested was the AURKB-selective inhibitor, hesperadin, and inhibitors of topoisomerases known to aid in the resolution of DNA in both anaphase (Daniloski et al., 2019; Gemble et al., 2020) and during replication (Vesela et al., 2017). Interestingly, however, prolonged inhibition of nucleolar function with the RNAPI inhibitors, BMH-21 and AMD, did not cause an increase in the percentage of nuclei with ≥5 nucleoli. These results suggest that disruption of nucleolar function alone is not sufficient to cause increased nucleolar numbers; although, actinomycin D and BMH-21 both cause nucleolar segregation by 3 hr (Peltonen et al., 2014; Reynolds et al., 1964), which might appear as an increase in number, and thus we may be missing the effect by looking at longer time points. Taken together, these data validate the role of faithful cell cycle progression in maintaining typical numbers of nucleoli per cell.

Screening for increased nucleolar number in MCF10A cells was thus a novel screening approach that led to the identification of 113 high confidence proteins. Included among the hits were a large proportion that do not have a known ortholog in *S. cerevisiae*, supporting the hypothesis that higher eukaryotes may harbor additional

regulatory mechanisms over nucleolar form and function. Additionally, subsequent analyses of the 113 hits strengthens prior established links between the nucleolus and cell cycle regulation and suggests an underappreciated role for mitosis and replication factors, in particular, in nucleolar biology. While the mechanisms underlying increased nucleolar number remain unknown, we do know that increases in nucleolar number are correlated with increased RNAPI transcription and poor prognosis in cancer (Derenzini et al., 2009; Montanaro et al., 2008). Furthermore, our screen for decreased nucleolar number was successful in identifying proteins with previously undefined roles in the regulation of ribosome biogenesis; thus, I hypothesize that my hits too may be proteins that regulate nucleolar function. This unique screening approach was therefore successful in identifying a novel subset of proteins in the human proteome that are required for the maintenance of typical nucleolar numbers in human cells, and may represent proteins with fundamental roles in the regulation of nucleolar function.

MATERIALS AND METHODS

Cell lines

The human breast epithelial cell line, MCF10A (ATCC, CRL-10317), was 2D subcultured in DMEM/F-12 medium (Gibco, 1130-032) supplemented with 5% horse serum (Gibco, 16050), 10 μg/mL insulin (Sigma, I1882), 0.5 μg/mL hydrocortisone (Sigma, H0135), 100 ng/mL cholera toxin (Sigma, C8052), and 20 ng/mL epidermal growth factor (Peprotech, AF-100-15).

RNAi

For screen validation and cell cycle analysis, the individual siGENOME Set of 4 siRNAs (Horizon Discovery) for each hit were used. Unless otherwise noted, subconfluent cells (log phase) were transfected with siRNAs (20-30 nM, final concentration) using Lipofectamine RNAiMAX Transfection Reagent (ThermoFisher Scientific, 13778150) and incubated for 72 hrs prior to the experimental assays.

siRNA screen

The high-content genome-wide siRNA screen was performed as reported in (Farley-Barnes et al., 2018) by Kat McCann and the Yale Center for Molecular Discovery using the human siGENOME SMARTpool siRNA library that contained 18,107 pools of 4 siRNAs against each target. Cells were imaged on an IN Cell Analyzer 2200 (Cytiva), which is a widefield, multicolor, fluorescence microscope. 3 fields of view (20X; 665.63 μm x 665.63 μm) were acquired per well and high throughput image analysis was performed using CellProfiler (Carpenter et al., 2006; McQuin et al., 2018) to segment nucleoli based on fibrillarin staining (72B9; (Reimer et al., 1987)) and nuclei based on Hoechst 33342 staining. In this analysis, raw nucleolar number data was normalized to the 16 negative (siRISC-free; 0 PE) and 16 positive (siKIF11; 100 PE) control wells run on the same plate and averaged across the fields of view to yield a mean NPE. Screen performance was monitored by Z-prime factors and signal-to-background (S/B). Hits with ≥5 nucleoli per nucleus were identified based on a stringent cut-off of 3 standard deviations (SD) from the mean NPE yielding 186 hits, and then I filtered the hits by expression and viability to yield a subset of 113 high confidence hits.

RNA sequencing analysis

Hits were filtered by expression in MCF10A cells based on a poly(A) transcriptome analysis by RNA sequencing performed at the Yale Center for Genome Analysis (West Haven, CT; GEO accession no. GSE154764) on siNT-treated RNA collected by Katherine Farley-Barnes and analyzed using a pipeline I developed in Partek Flow (Partek Inc., St. Louis, MO). Sequencing reads were aligned to the human genome (hg19 assembly) using Bowtie 2 (v2.2.5) and quantified to the transcriptome (RefSeq 16 08 01 v2) using Cufflinks (v2.2.1) (n=3; FPKM>0). Thirty-eight (38) hits are not expressed in MCF10A cells based on this analysis and were therefore discarded.

Since my initial analysis of gene expression in MCF10A cells, however, 3 additional MCF10A RNA sequencing datasets have been deposited in Gene Expression Omnibus (GEO; NCBI). Carson J. Bryant analyzed these datasets in Partek Flow, and re-analyzed the dataset generated by our laboratory, to identify the genes expressed in MCF10A cells based on the zFPKM normalization metric developed by the Salomon laboratory (Hart et al., 2013). If the hits were expressed in any one of the 4 RNA sequencing datasets, they were considered expressed ($\log_2$ zTPM > -3). When aligned to the Ensembl annotation database (v99) Carson found that 8 of the 113 high-confidence hits that I identified are not likely expressed in MCF10A cells. These hits include FAM58A, GOLGA8EP, MARCH9, MICA, NR0B2, PRAM1, SCN2B, and YIPF7, and may represent off-target effects from the siRNA pools used to deplete them.

Screen validation by oligonucleotide deconvolution

Oligonucleotide deconvolution was performed on the 20 hits listed in Table 2-3, as well as on the positive control siKIF11, where the 4 siRNAs in each pool are re-tested individually to ensure that the observed increase in nucleolar number is driven by more than one siRNA. Three wells per individual siRNA were included in the assay to determine the mean percent effect. These data were normalized to the mean of 48 wells of the negative control, siRISC-free, and positive control, siKIF11 (pool), yielding a mean NPE for each individual siRNA. Hits were validated if the NPE was ≥15.0 in at least 2/4 individual siRNAs in the pool. This cutoff was less than the screen cutoff of NPE=25.0 based on an analysis of known LSU maturation factor, MDN1. Deconvolution of MDN1 yielded 3/4 individual siRNAs with an NPE<25.0, with one siRNA yielding an NPE=8.92; yet, all 4 siRNAs yielded pre-rRNA processing defects when analyzed by northern blot for defects in the processing of LSU pre-rRNA precursors (Figure 2-10). Thus, an NPE≥15.0 was arbitrarily selected as a cutoff to be inclusive, yet conservative.

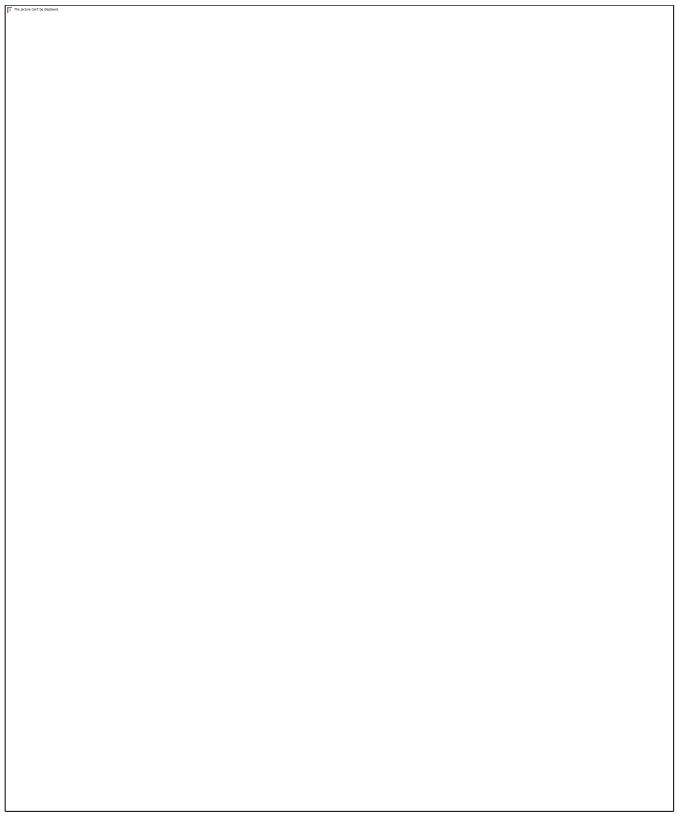

Figure 2-10. Northern blot analysis of pre-rRNA intermediates of MDN1 depletion by the pool and each individual siRNA revealed the expected large subunit (LSU) processing defect in all depletion conditions.

(A) Schematic depicting the 47S pre-rRNA and position of the probe, P4, used to detect the LSU pre-rRNA intermediates. Black arrows=cleavage sites.

(B) Northern blot (n=1) of total RNA, which revealed that depletion by the pool and each individual siRNA targeting MDN1 all yielded the accumulation of the 32/36S and 12S pre-rRNA intermediates, despite 3/4 individual siRNAs yielding an NPE less than the screen cutoff of 25.0. Mock and siNT=negative controls. 7SL RNA=loading control. Black arrows=accumulated LSU pre-rRNA intermediates.

Northern blots

Total RNA was extracted from siRNA-depleted cells using TRIzol Reagent. To assay for changes in levels of pre-rRNA intermediates, 4 μg of total RNA was run on a 1% agarose/1.25% formaldehyde gel in a 1.5M tricine/1.5M triethanolamine buffer. RNA was transferred overnight to a Hybond XL nylon membrane (GE Healthcare, RPN 303S) by capillary transfer in 10X saline-sodium citrate (SSC) transfer buffer after a brief 15 min soak in a 0.5M sodium hydroxide solution. Membranes were then exposed to UV (254 nm) to immobilize the RNA, and incubated with denatured yeast tRNA for 1 hr at 42° C and hybridized overnight at 37° C with 5' end radiolabeled oligonucleotide probes in a solution of 7.5X Denhardt's solution, 5X sodium chloride-sodium phosphate-EDTA (SSPE) buffer, and 0.1% SDS as in (Farley-Barnes et al., 2018).

Cell cycle analysis

We analyzed the images of the 20 hits collected for oligonucleotide deconvolution to evaluate cell cycle based on the integrated intensity of the Hoechst DNA stain. A histogram of the log2 integrated intensities for the negative control (siRISC-free; 48 wells) was plotted and the G1 peak set to 1.0 and G2 peak set to 2.0. Each hit depletion condition (3 wells per siRNA) was then normalized to siRISC-free, including siKIF11 as individual siRNAs (3 wells per siRNA) as well as a pool (48 wells). Cell cycle phases were defined as in (Chan et al., 2013). G0/G1 phase nuclei were defined as normalized log2 integrated intensities of 0.75-1.25, S phase nuclei were defined as 1.25-1.75, and G2/M phase nuclei were defined as 1.75-2.50, and nuclei with >4N were defined as >2.50.

Small molecule inhibition

MCF10A cells were treated with inhibitors of the cell cycle for 24, 48, and 72 hrs in triplicate. Drugs were all dissolved in dimethyl sulfoxide (DMSO) and doses were selected based on reported EC_{50} values in cell culture conditions for each drug, with final DMSO concentration=0.1%. The ≥5 nucleoli per nucleus PE was quantified by the same CellProfiler pipeline use in the initial screen and analyzed relative to the 0.1% DMSO treatment, which was set to a 100 PE. Tested inhibitors of mitosis included ispinesib (0.082 μM; Cayman Chemical, 18014), nocodazole (0.741 μM; Cayman Chemical, 13857), paclitaxel (0.0274 μM; Sigma, T7402), hesperadin (0.082 μM; Cayman Chemical, 24199), and MK-5108 (0.247 μM; Cayman Chemical, 19167). Inhibitors of DNA replication included mitomycin C (0.741 μM; Cayman Chemical, 11435) and 5-fluorouracil (0.741 μM; Sigma, F6627). Topoisomerase inhibitors included etoposide (0.741 μM; Sigma, E1383) and ICRF-193 (6.67 μM; Sigma, I4659), and inhibitors of RNAPI transcription included AMD (0.00914 μM; Sigma, A1410), BMH-21 (0.741 μM; Sigma, SML1183), and CX-5461 (0.741 μM; Cayman Chemical, 18392). Doses were selected based on doses used at prolonged time points as reported in the literature.

Statistical analyses

All statistical analyses were performed in GraphPad Prism 8.2.1 (GraphPad Software, Inc.) using the tests described in the Figure Legends.

Chapter 3

Increased nucleolar number reveals regulators of RNA polymerase I transcription

INTRODUCTION

In eukaryotic organisms, nucleoli are large, membraneless, nuclear condensates associated with the biogenesis of ribosomes. In mammalian cells, nucleoli form upon initiation of transcription by RNAPI around the tandemly arrayed rDNA loci known as NORs (Bersaglieri and Santoro, 2019; Grob et al., 2014; Hernandez-Verdun, 2011; Potapova and Gerton, 2019). The total number of nucleoli present in mammalian cells is highly variable. In the human genome there are 10 NORs located on the short arms of the 5 acrocentric chromosomes [13-15, 21, and 22; (Floutsakou et al., 2013; Henderson et al., 1972)]. Yet, high throughput resolution of nucleolar number by fluorescence microscopy in diverse cell lines reveals few cells with 10 nucleoli per nucleus, with many averaging as few as 3 nucleoli per nucleus (Farley et al., 2015). Furthermore, increased nucleolar number and size in the tumors of cancer patients are often associated with increased nucleolar activity and a poor prognosis (Derenzini et al., 2009; Montanaro et al., 2008). Dynamic remodeling of nucleolar structure, however, is not restricted to changes in nucleolar number. During mitosis the nucleolus undergoes dynamic remodeling that is exemplified by the disassembly and reformation of nucleoli in an open mitosis (Hernandez-Verdun, 2011). Furthermore, diverse cellular stress signals can cause nucleolar disruption and large changes to the nucleolar proteome (Boisvert et al., 2010; Moore et al., 2011; Rubbi and Milner, 2003). This observation has been studied most extensively in the nucleolar response to DNA damage (Kruhlak et al., 2007; Larsen et al., 2014; Larsen and Stucki, 2016), and most notably upon treatment with AMD, where RNAPI transcription is silenced and nucleolar caps are formed at the nucleolar periphery (Floutsakou et al., 2013; Reynolds et al., 1964). Thus, the nucleolus is a highly

responsive organelle that integrates signals from a vast network of cellular processes and that nucleolar form, including both number and morphology, is not fixed.

Intriguingly, the genome-wide siRNA screen for proteins that regulate nucleolar number described in Chapter 2 revealed a unique subset of proteins that are not enriched for ribosome biogenesis factors. From this screen I identified 113 hits that cause an increase in the percentage of nuclei with ≥5 nucleoli. These hits are enriched for proteins that localize to the nucleolus, as well as proteins associated with the cell cycle, including specifically mitosis and DNA replication. Furthermore, cell cycle profiling confirmed the association of a subset of proteins with S and G2/M phase progression, and several proteins were identified as yielding an accumulation of nuclei with a >4N DNA content when depleted. These data support failed cell division among a subset of the hits evaluated and lend a possible explanation for the increased number of nucleoli observed. However, there were several hits that did not reveal accumulation of nuclei with a >4N DNA content when depleted and thus a unifying rationale for the observed increase in nucleolar number remains unknown. Given that we previously identified novel ribosome biogenesis factors when screening for a decrease in nucleolar number, I asked whether proteins that, when depleted, increase nucleolar numbers also reveal novel regulators of nucleolar function?

Screening for changes in nucleolar number previously uncovered proteins with undefined roles in the regulation of ribosome biogenesis. In our prior screen for decreased nucleolar number we reported more than 100 proteins that caused a decrease in nucleolar number from 2-3 to just 1 (Farley-Barnes et al., 2018). Of these hits, further investigation on a subset revealed varied deficits in ribosome biogenesis upon depletion,

including RNAPI transcriptional repression and aberrant pre-rRNA processing. Here, based on these discoveries, I likewise tested the role of 14 validated screen hits revealed by increased nucleolar number for roles in the regulation of RNAPI transcription and pre-rRNA processing. Amber Buhagiar confirmed depletion of the selected hits by qPCR, and I performed the remaining experiments to ascertain roles in nucleolar function. The results from these experiments revealed that the majority of hits evaluated are required strictly for the regulation of RNAPI transcription and supports the hypothesis that screening for increased nucleolar number could also uncover novel regulators of nucleolar function.

RESULTS

Rationale for the selection of hits

Hits were subjectively selected to be representative of the dataset based on bioinformatic analyses described in Chapter 2 (Table 2-3, in bold). The selected hits include cell cycle-associated proteins, including those associated with mitosis and DNA replication. Proteins with and without yeast orthologs were also selected. Finally, I selected proteins that localize to the nucleolus, as well as those not reported to localized to the nucleolus.

72 hr depletion by siGENOME pools yields effective knockdown of screen hits

To test whether the screen hits are involved in the nucleolar function of ribosome biogenesis, I first sought to validate knockdown of the mRNA levels of the 14 screen hits selected for further analysis. This was performed by quantitative reverse transcription

polymerase chain reaction (qRT-PCR) by Amber Buhagiar, using RNA collected and reverse transcribed by me. Hits were depleted in MCF10A cells for 72 hrs, as they were in the screen, by siGENOME pools of 4 siRNAs. In all conditions, depletion for 72 hrs with the siRNA pools led to a significant decrease in the mRNA of the target relative to the non-targeting (NT) negative control (Figure 3-1). Depletion of UTP4 and KIF11 were also confirmed (Figure 3-1). UTP4 is a nucleolar protein required for ribosome biogenesis and the positive control in the screen that identified proteins that when depleted caused a decrease in nucleolar number (Farley-Barnes et al., 2018). KIF11 is a mitotic kinesin and the positive control in this screen for increased nucleolar number described in Chapter 2. These data suggest that this method of depletion is sufficient to knockdown the mRNAs for the 14 screen hits selected for further analysis.

Figure 3-1. 72 hr depletion using siGENOME pools yields effective mRNA knockdown of hits. Quantitative reverse transcription polymerase chain reaction (qRT-PCR) analysis confirms depletion of a subset of validated nucleolar (n=7; gray) and non-nucleolar (n=7; white) screen hits in MCF10A cells. After depletion using pools of siRNAs targeting the indicated genes, respectively, or non-targeting siRNA control (siNT), the mRNA levels were quantified relative to beta-actin mRNA expression. Relative expression values were calculated using the comparative CT method. Statistical significance for three biological replicates, each with three technical replicates, was performed using a two-tailed, unpaired t-test. All comparisons are relative to siNT ($p<0.05$=*, $p<0.01$=**, $p<0.001$=***; n=3). Data are shown as a bar graph (mean ± SD), and with each replicate shown as a dot. These data were collected, analyzed, and graphed by Amber Buhagiar, using RNA collected and reverse transcribed by me. Previously published in (Ogawa et al., 2021).

11/14 screen hits are required for RNA polymerase I transcription

To test the hypothesis that increased nucleolar number reflects changes in RNAPI transcription, I used an established dual-luciferase reporter assay system (Ghoshal et al., 2004). In this system, two plasmids are co-transfected into cells 24 hrs prior to lysis and luminescence detection. One plasmid encodes the firefly luciferase gene, in which expression is driven by the human rDNA promoter. The second plasmid is included as a transfection control and encodes the *Renilla* luciferase gene, in which expression is driven by a constitutively active cytomegalovirus promoter. MCF10A cells were depleted for 72 hrs of the 14 selected hits, as well as the NT negative control, the screen positive control, KIF11, and known ribosome biogenesis factors, UTP4 and NOL11. Cells were then lysed, and firefly luminescence was normalized to *Renilla* luminescence and plotted relative to siNT.

Strikingly, depletion of 11/14 hits significantly affect RNAPI transcription. An increase in the ratio of firefly to *Renilla* luminescence suggests increased transcription by RNAPI, whereas a decrease in the ratio of firefly to *Renilla* luminescence suggests decreased transcription by RNAPI. As expected, depletion of known RNAPI transcription co-factors, UTP4 and NOL11, decreased RNAPI transcription relative to siNT [(Freed et al., 2012); n=10; $p<0.05$; Figure 3-2], whereas mock treated cells revealed no effect. Of the 14 selected hits, depletion of only 2 caused a significant increase in RNAPI transcription (RFC1 and ATAD5; n=5 or 6; $p<0.05$); whereas depletion of 9 caused significant decreases in RNAPI transcription (H1-10, INCENP, MDN1, TPX2, ENY2, FAM98A, RACGAP1, CCN4, and WRAP53; n=5 or 6; $p<0.05$; Figure 3-2). Of these hits, INCENP, H1-10, MDN1, TPX2, and RFC1 are reported in the nucleolus suggesting

that this regulation may be direct at the rDNA loci (Appendix II). ENY2, FAM98A, RACGAP1, CCN4, WRAP53, and ATAD5, on the other hand, have not been reported in the nucleolus and thus their regulation of RNAPI may be indirect. In contrast, depletion of CDCA8, STK24, and INKA1 showed no significant impact on RNAPI transcription; however, depletion of the screen positive control KIF11 revealed an unexpected decrease in RNAPI transcription. These data suggest that increased nucleolar number is indeed reflective of impacts on nucleolar function. Furthermore, these data reveal that screening for an increase in the percentage of cells with ≥5 nucleoli per nucleus was successful in the identification of proteins required for the regulation of RNAPI transcription.

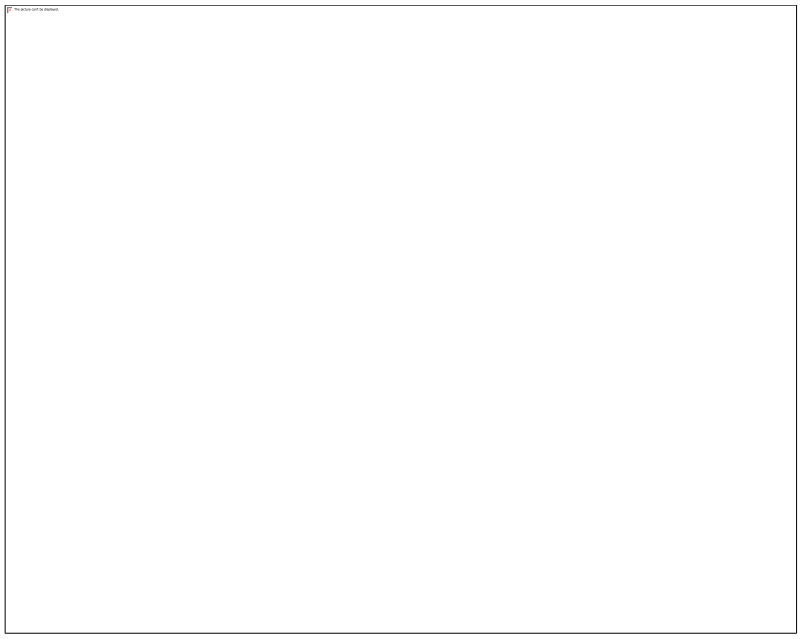

Figure 3-2. Depletion of the selected hits reveal 11/14 significantly decrease or increase RNAPI transcription. RNAPI transcription was assayed using a dual-luciferase reporter system utilizing a plasmid encoding the firefly luciferase gene, in which expression is driven by the human rDNA promoter [-410 to +314; (Ghoshal et al., 2004)]. Data were normalized to *Renilla* luciferase gene expression driven by a constitutively active cytomegalovirus promoter. Statistical significance for 5 or 6 replicates relative to siNT was calculated by two-tailed, unpaired t tests (*=$p<0.05$, **=$p<0.01$, ***=$p<0.001$; n=5 or 6). Mock=negative control; siNOL11 and siUTP4=positive controls. Data are shown as minimum to maximum box and whiskers plots, and with each replicate represented as a dot. Gray=nucleolar proteins; white=non-nucleolar proteins (Table 2-3; Appendix II). Previously published in (Ogawa et al., 2021).

1/14 screen hits are required for pre-rRNA processing

Several ribosome biogenesis factors that are required for transcription of the rDNA also have defined roles in processing the pre-rRNA (Calo et al., 2015; Farley-Barnes et al., 2018; Freed et al., 2012; Gallagher et al., 2004; Prieto and McStay, 2007). These factors include nucleolar proteins like those in the SSU subcomplex t-UTP/UTPA (Freed et al., 2012; Gallagher et al., 2004; Prieto and McStay, 2007), as well as non-nucleolar proteins including several previously identified in the screen for decreased nucleolar number (Farley-Barnes et al., 2018). To test whether the 14 selected screen hits are required for pre-rRNA processing I used northern blots to quantify steady-state levels of pre-rRNA intermediates and analyzed precursor-product relationships. Northern blots were performed using RNA from MCF10A cells depleted of each of the 14 hits, as well as UTP4 as a positive control, and hybridized to 4 previously reported oligonucleotide probes that detect different intermediates in the pre-rRNA processing pathways [(Farley-Barnes et al., 2018); Figure 3-3; Figure 3-4]. Intermediates were then quantified by phosphorimager and Ratio Analysis of Multiple Precursors profiles were plotted relative to siNT [RAMP; (Wang et al., 2014); Figure 3-5; Figure 3-6].

Interestingly, depletion of only 1/14 hits resulted in aberrant pre-rRNA processing. Overall, while depletion of the 14 selected hits led to some ratios from individual probes to be statistically significant, only depletion of the nucleolar protein MDN1 caused a more than 2-fold change in ratios of intermediates relative to siNT ($n=3$; $p<0.05$; Figure-3-4; Figure 3-5; Figure 3-6). Specifically, MDN1 depletion resulted in a significant increase in the ratios of the 12S pre-rRNA to its precursors and is an intermediate of the large ribosomal subunit (LSU) 5.8S rRNA (Figure 3-4, D; Figure 3-

5), which is consistent with the protein's reported role in LSU maturation (Bassler et al., 2010; Galani et al., 2004). As expected, RNA from mock-treated cells showed no significant difference relative to siNT (Figure 3-4; Figure 3-5), whereas UTP4 depletion caused a significant increase in the 30S+1 pre-rRNA precursor and a decrease in the 21S product ($n=3$; $p<0.05$; Figure 3-4, A-C; Figure 3-5). These results suggest that increased nucleolar number is largely not reflective of impacts on pre-rRNA processing for either nucleolar or non-nucleolar hits.

Further analysis of the northern blots also revealed a decreasing trend in the overall steady-state levels of pre-rRNA intermediates after depletion of the 14 selected hits. Individual pre-rRNA intermediates were quantified relative to the 7SL RNA component of the signal recognition particle, which was probed on all northern blots as a loading control (Figure 3-7). As expected, UTP4-depleted cells showed a significant increase in the primary transcript plus (43S-47S; PTP) and 30S+1, and decrease in the 30S and 21S pre-rRNAs, whereas mock-treated cells showed little impact on the levels of steady-state intermediates. Overall, among the 14 hits, steady-state levels trended towards a modest decrease (<2-fold) among all pre-rRNA intermediates measured, with all but 2 showing a significant decrease of at least 1 intermediate by a single probe. While these differences are small, they are consistent with the majority of selected hits causing significant decreases in RNAPI transcription (Figure 3-2). Intriguingly, the 2 that did not show a significant decrease of an intermediate (ATAD5 and RFC1) were also the only 2 hits to show a significant increase in RNAPI transcription. Taken together, analysis of pre-rRNA intermediates by northern blots revealed that screening for an increase in the percentage of cells with ≥5 nucleoli per nucleus uncovered proteins that are less likely to

be required for pre-rRNA processing and more likely to be required for the regulation of overall levels of pre-rRNA intermediates.

Figure 3-3. Pre-rRNA processing diagram labeled with the oligonucleotide probes used to detect pre-rRNA intermediates. Depletion of a subset of nucleolar (n=7) and non-nucleolar (n=7) hits in MCF10A cells were analyzed by northern blot to ask whether depletion affects steady-state levels of pre-rRNA intermediates, and whether pre-rRNA processing defects can be inferred from observed changes in precursor-product relationships. The two predominant pathways for releasing the mature ribosomal RNAs (18S, 5.8S, and 28S) from the primary 47S transcript are depicted. Cleavage sites are indicated with black triangles and are listed next to the black arrows. The 4 oligonucleotide probes used to quantify levels of the different pre-rRNA intermediates are indicated below the 47S both by colored lines and probe number (P5'ETS, P5'ITS1, P3, and P4). Previously published in (Ogawa et al., 2021).

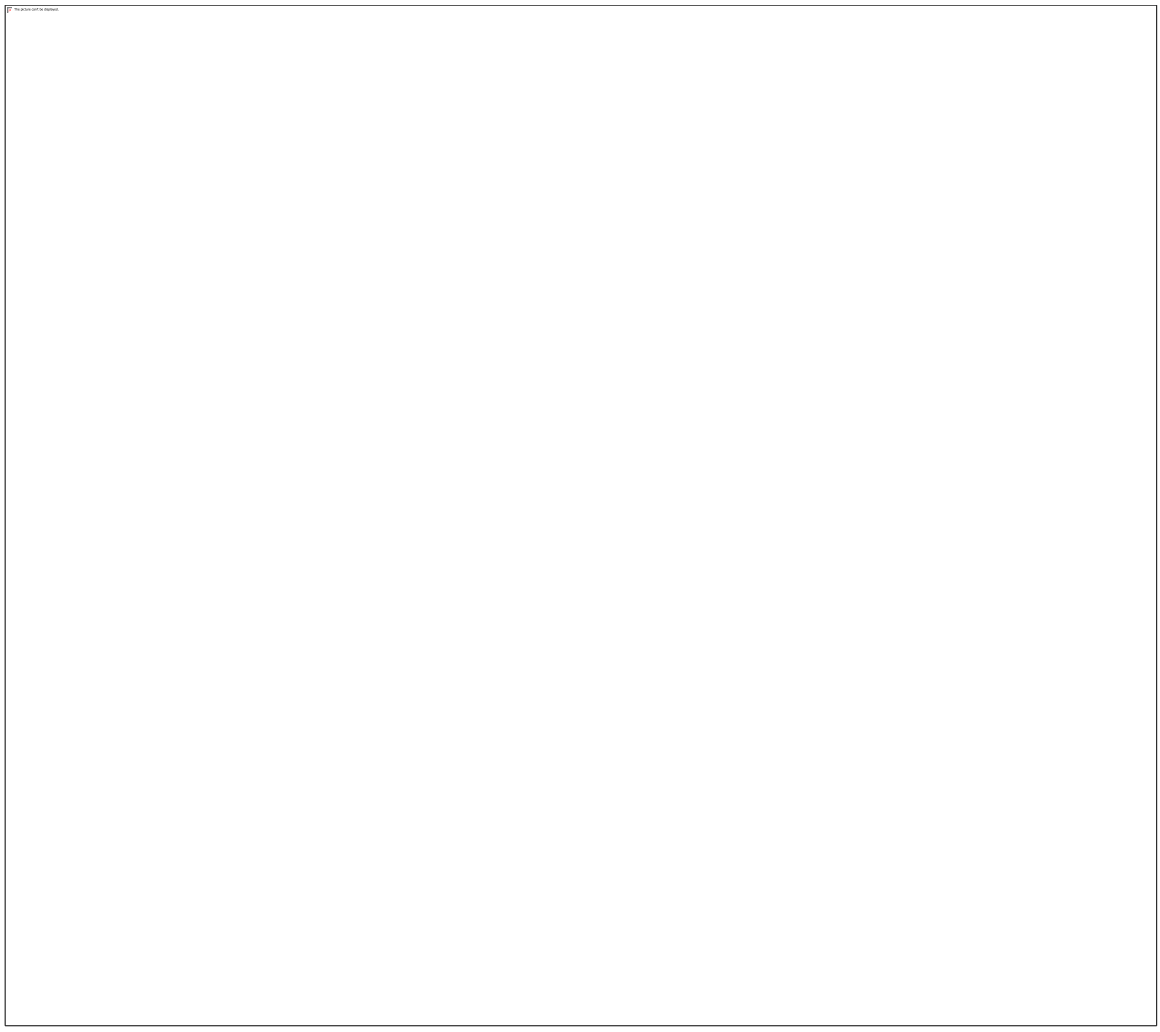

Figure 3-4. Qualitative analysis of pre-rRNA intermediates reveals no obvious pre-rRNA processing defects among the 14 selected hits. Representative northern blots are shown for each of the 4 probes, (A) P5'ETS, (B) P5'ITS1, (C) P3, and (D) P4. The 7SL RNA component of the signal recognition particle was used as a loading control. In each blot, mock and siNT=negative controls, and siUTP4=positive control. PTP=primary transcript plus or the 43S-47S pre-rRNA. Previously published in (Ogawa et al., 2021).

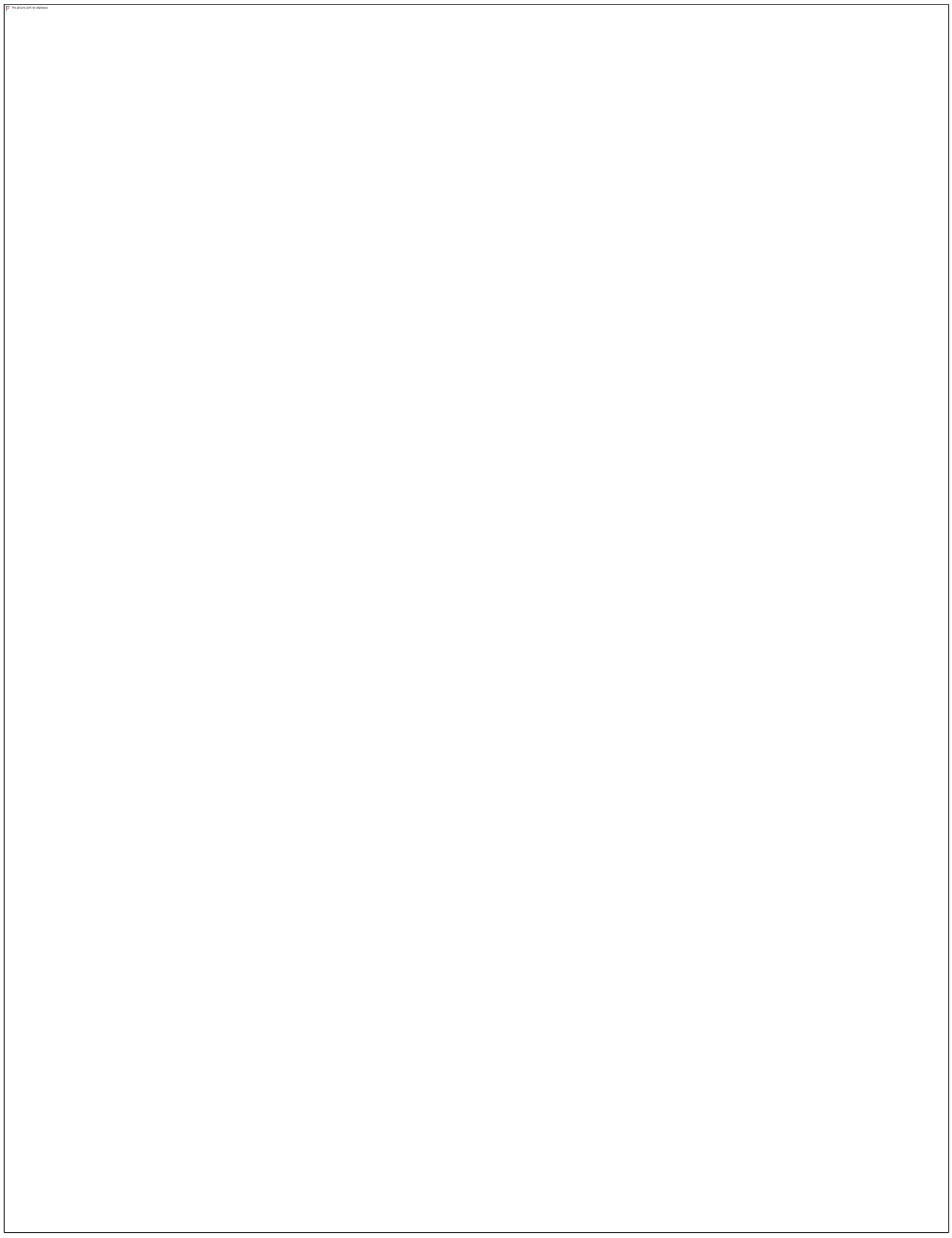

Figure 3-5. Quantitative analysis of the northern blots of total RNA from nucleolar hits reveals that MDN1-depletion significantly affects processing of the 12S pre-rRNA. Quantitative analysis of the northern blots of nucleolar hits was performed by Ratio

Analysis of Multiple Precursors (RAMP) relative to siNT (mean ± SD). Mock-treated cells and UTP4-depleted cells were included as negative and positive controls, respectively. Depletion of the screen positive control, KIF11, was also analyzed. Statistical significance was calculated for 3 replicates by unpaired t tests for each ratio with the Holm-Sidak method of correction for multiple comparisons (*=$p<0.05$, **=$p<0.01$, ***=$p<0.001$; n=3). PTP=primary transcript plus, 43S-47S. Previously published in (Ogawa et al., 2021).

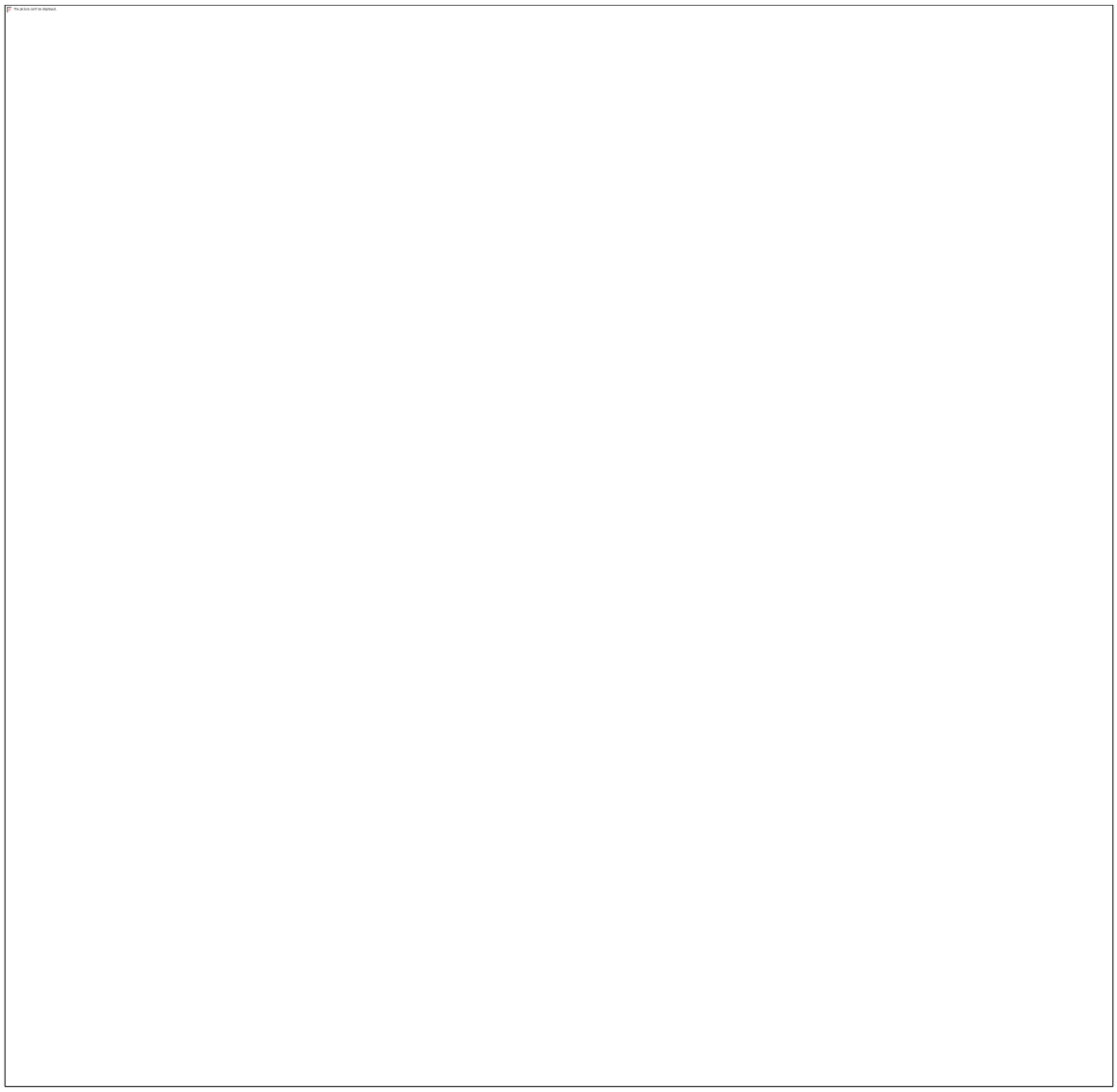

Figure 3-6. Quantitative analysis of the northern blots of total RNA from non-nucleolar hits reveals pre-rRNA processing is not impacted. Quantitative analysis of the northern blots of non-nucleolar hits was performed by Ratio Analysis of Multiple Precursors (RAMP) relative to siNT (mean ± SD). Statistical significance was calculated for 3 replicates by unpaired t tests for each ratio with the Holm-Sidak method of correction for multiple comparisons (*=$p<0.05$, **=$p<0.01$, ***=$p<0.001$; n=3). PTP=primary transcript plus, 43S-47S. Previously published in (Ogawa et al., 2021).

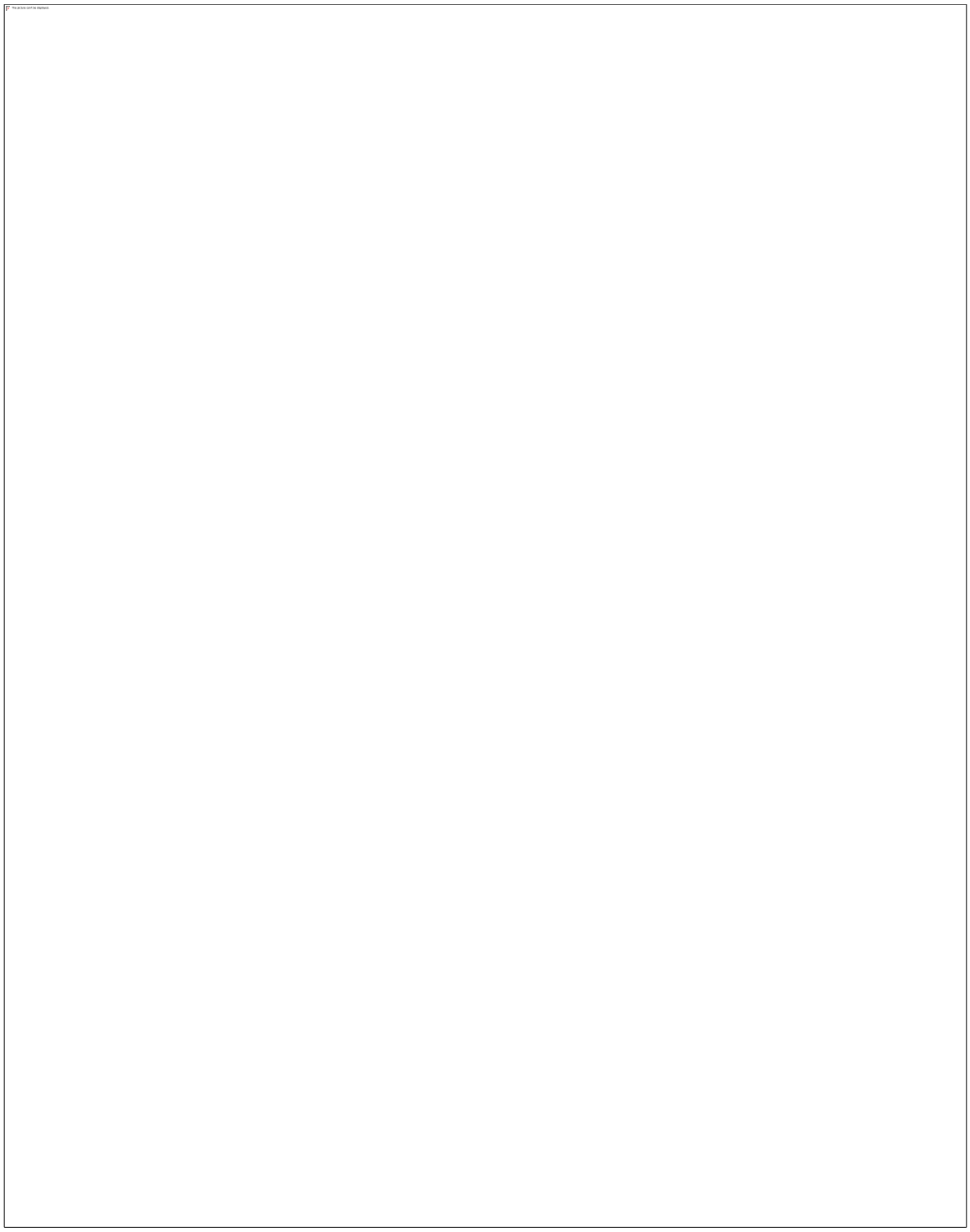

Figure 3-7. Quantitative analysis of pre-rRNA intermediates relative to the 7SL RNA loading control reveals a general trending decrease in overall levels of pre-rRNA intermediates.

Quantitative analysis of the northern blots was performed relative to the 7SL RNA component of the signal recognition particle relative to siNT (mean ± SD). Statistical significance for 3 replicates was calculated by unpaired t tests for each ratio with the Holm-Sidak method of correction for multiple comparisons (*=$p<0.05$, **=$p<0.01$, ***=$p<0.001$; n=3). PTP=primary transcript plus, 43S-47S. Previously published in (Ogawa et al., 2021).

13/14 screen hits are required for global protein synthesis

Finally, if depletion of a protein impacts ribosome biogenesis through either RNAPI transcription or pre-rRNA processing, I hypothesize that ribosome levels and translational function will also be impacted. To test whether depletion of the 14 selected screen hits impacts global protein synthesis, I used an established puromycin labeling assay of nascent peptides followed by western blot with a puromycin antibody (Kelleher et al., 2013). MCF10A cells were depleted of the 14 screen hits prior to puromycin treatment (1 μM) and protein harvest. MCF10A cells were also mock-treated and treated with siNT as negative controls, and half the concentration of puromycin (0.5 μM) and the ribosome biogenesis factor siUTP4 as positive controls.

Puromycin labeling followed by western blot revealed that depletion of 13/14 hits caused a significant decrease in global protein synthesis ($p<0.05$; Figure 3-8). As expected, mock-treated cells showed no significant difference relative to siNT, and cells treated with half the concentration of puromycin (0.5 μM) showed a decrease in global protein synthesis by half. Furthermore, as predicted, depletion of the ribosome biogenesis factor UTP4 also led to a decrease in protein synthesis. Results from this assay therefore suggest that depletion of nearly all hits tested, 13/14, cause a significant reduction in global levels of protein synthesis. Furthermore, consistent with previous reporting (Bartoli et al., 2011), depletion of the screen positive control, KIF11, also yielded a significant decrease in protein synthesis. Intriguingly, while depletion of ATAD5 and RFC1 caused an increase in the transcription of the pre-rRNA ($p<0.001$; Figure 3-2), protein synthesis was reduced ($p<0.05$; Figure 3-8). These data suggest that in the case of ATAD5 or RFC1 depletion, increased transcription does not necessarily lead to an

increase in ribosome levels and consequently ribosomal function. Additionally, INKA1, STK24, and CDCA8 were not identified as either pre-rRNA transcription or processing factors (Figure 3-2; Figure 3-5; Figure 3-6), yet depletion also resulted in a significant decrease in protein synthesis ($p<0.001$; Figure 3-8). These data suggest that these INKA1, STK24, and CDCA8 may have an as yet unidentified role in some other aspect of ribosome biogenesis, such as ribosome assembly or subunit export. Conversely, depletion of FAM98A revealed a significant decrease in RNAPI transcription by nearly 50% ($p<0.001$; Figure 3-2), but did not yield a significant impact on global protein synthesis (Figure 3-8), suggesting possible limitations in using this assay to infer functional consequences of defects in RNAPI transcription, or a downstream compensatory response that limited the impacts of FAM98A on ribosome biogenesis and ribosomal function. Thus, from these results, I conclude that screening for an increase in the percentage of nuclei with ≥5 nucleoli uncovered proteins, in most cases, required for the ribosomal function of translation.

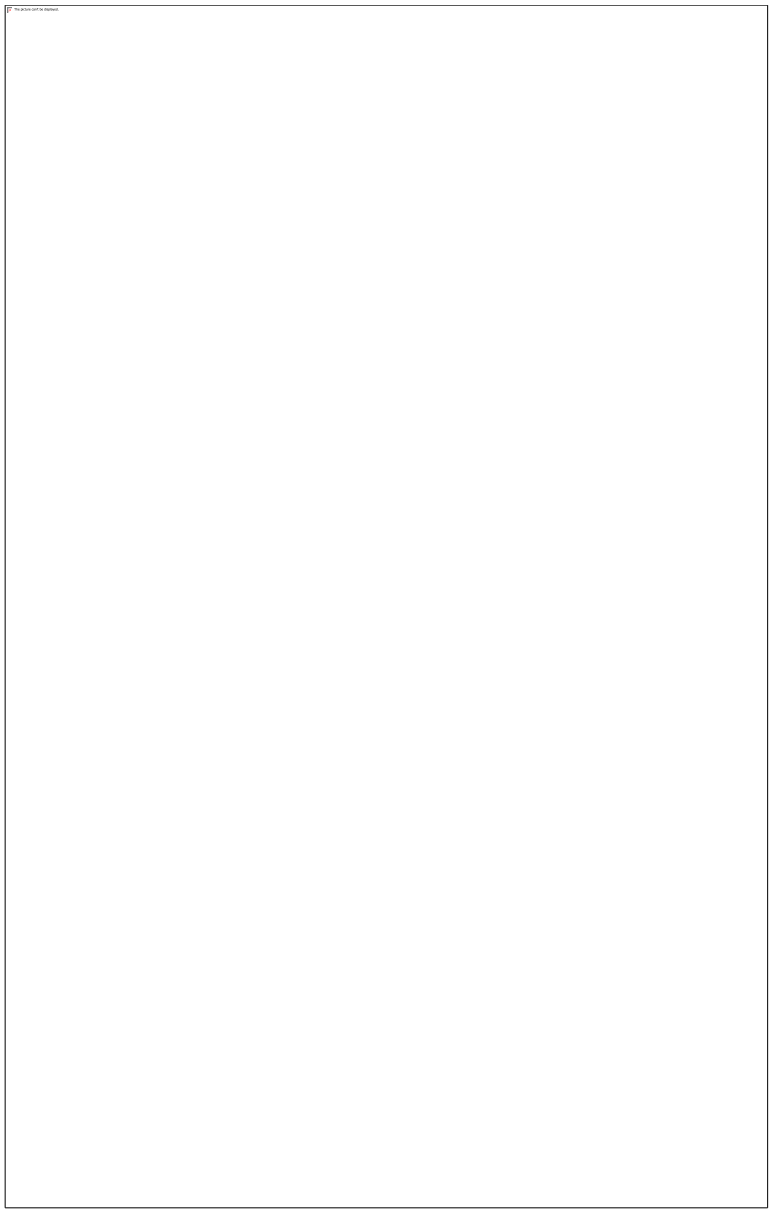

Figure 3-8. Global protein synthesis was significantly decreased upon depletion of 13/14 of the selected screen hits. Previously published in (Ogawa et al., 2021).

(A) Shown are representative western blots from the total protein harvested from hit-depleted MCF10A cells treated with 1 μM puromycin for 1h. Protein was quantified by Bradford assay and run on a 10% SDS-PAGE gel followed by western blots using an antibody to puromycin to test for puromycin incorporation into the nascent peptides. Beta-actin (ACTB)=loading control. Mock (1 μM) and siNT=negative controls. Mock

(0.5 μM)=cells treated with half the concentration of puromycin. Depletion of ribosome biogenesis factor UTP4=positive control.

(B) Quantification of results in A from 3 replicates. ImageJ was used to quantify the differences in puromycin signal intensity, normalized to the beta-actin signal intensity. Statistical significance for the 3 replicates relative to siNT was calculated by two-tailed, unpaired t tests (*=$p<0.05$, **=$p<0.01$, ***=$p<0.001$; n=3). Data are shown as a bar graph (mean ± SD), and with each replicate represented as a dot. Gray=nucleolar proteins; white=non-nucleolar proteins.

Depletion of 2/14 screen hits results in p53 stabilization

Considering that I identified defects in cell cycle progression for several of the screen hits analyzed as reported in Chapter 2, it may be possible that these defects could lead to RNAPI transcription and translation defects through TP53 (p53) repression of RNAPI (Beckerman and Prives, 2010). On the contrary, it is also possible that defects in RNAPI transcription and translation could lead to cell cycle arrest through both p53-mediated and p53-independent mechanisms through what is commonly referred to as the nucleolar stress response (James et al., 2014; Rubbi and Milner, 2003). As a result, I also evaluated levels of p53 by western blot. As expected, depletion of the known ribosome biogenesis factor, NOL11, resulted in a significant 2-fold increase in p53 levels [n=3; $p<0.05$; (Griffin et al., 2015)]. Depletion of a subset of screen hits, on the other hand, revealed that only 2/14 caused a significant increase in p53 (RFC1 and RACGAP1; n=3; $p<0.05$; Figure 3-9). These data suggest that while it is possible that p53 could be mediating the effects on RNAPI transcription that I observe when RFC1 and RACGAP1 are depleted, it is not likely mediating the effects I observe in all cases. In conclusion, screening for increased nucleolar number was successful in identifying novel regulators of ribosome biogenesis (Table 3-1).

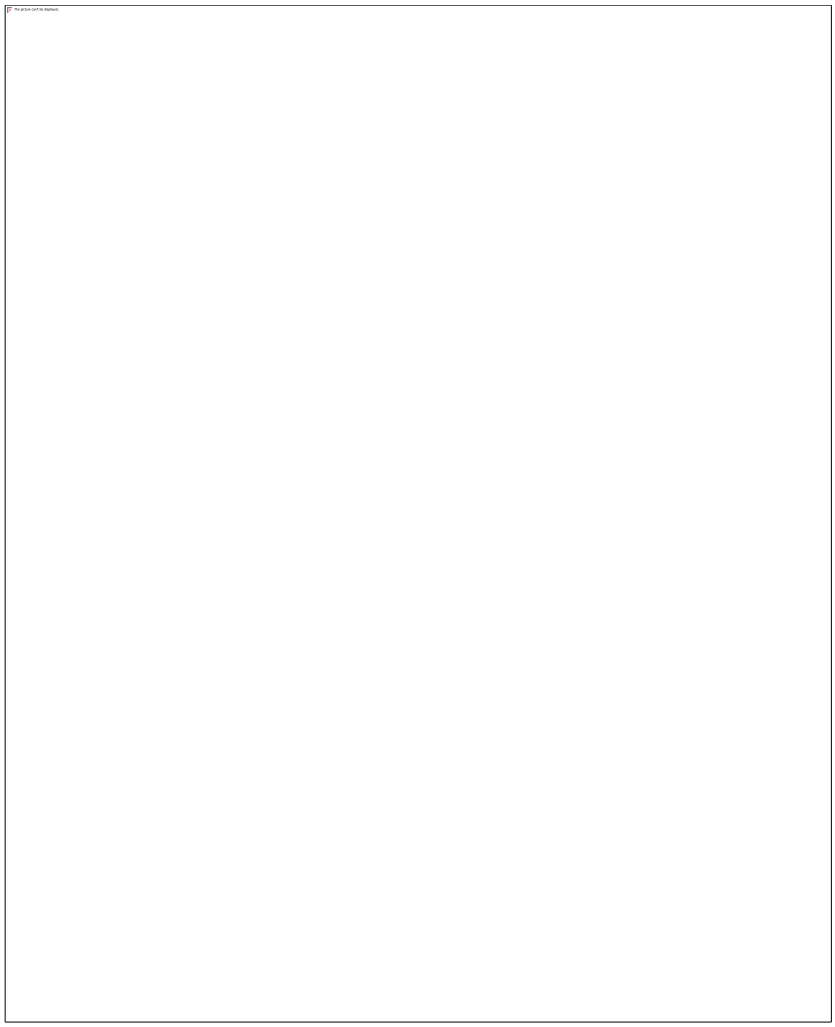

Figure 3-9. Depletion of only 2 hits results in the stabilization of the tumor suppressor protein, p53. Previously published in (Ogawa et al., 2021).

(A) Representative western blots from the total protein harvested from MCF10A cells depleted of the screen hits in Table 2-3 (in bold). Protein was quantified by Bradford assay and run on a 10% SDS-PAGE gel followed by western blots using an HRP-conjugated antibody to the tumor suppressor protein, p53 (TP53). Beta-actin (ACTB) was used as a loading control. Mock and siNT-treated cells=negative controls. siNOL11=positive control. siUTP4 was included as a known ribosome biogenesis factor,

and siKIF11 was included because it was the screen positive control and elicited a RNAPI and protein synthesis defect upon treatment.

(B) Quantification of results in A from 3 replicates. ImageJ was used to quantify the differences in p53 signal intensity, normalized to the beta-actin signal intensity. Statistical significance for the 3 replicates relative to siNT was calculated by two-tailed, unpaired t tests (*=$p<0.05$; n=3). Data are shown as a bar graph (mean ± SD), and with each replicate represented as a dot. Gray=nucleolar proteins; white=non-nucleolar proteins.

Table 3-1. Summary of discoveries associated with nucleolar function upon depletion of a subset of screen hits, and the screen positive control, KIF11. Inc=Increased, Dec=Decreased, Y=Yes, N=No, and Dash ("-")=No significant change are concluded based on statistical analysis that identified a significant difference from siNT ($p<0.05$).

Screen hit (HGNC)	RNAPI transcription (Inc/Dec)	Pre-rRNA processing defect	Global protein synthesis (Inc/Dec)	p53 stabilization
ATAD5	Inc	-	Dec	-
CDCA8	-	-	Dec	-
ENY2	Dec	-	Dec	-
FAM98A	Dec	-	-	-
H1-10	Dec	-	Dec	-
INCENP	Dec	-	Dec	-
INKA1	-	-	Dec	-
KIF11	Dec	-	Dec	-
MDN1	Dec	Y	Dec	-
RACGAP1	Dec	-	Dec	Y
RFC1	Inc	-	Dec	Y
STK24	-	-	Dec	-
TPX2	Dec	-	Dec	-
CCN4	Dec	-	Dec	-
WRAP53	Dec	-	Dec	-

DISCUSSION

A genome-wide siRNA screen for increased nucleolar number has uncovered proteins required for nucleolar function. Biochemical analyses of a subset of the 113 identified proteins revealed several required for ribosome biogenesis, including 11/14 required for RNAPI transcription and 1/14 required for pre-rRNA processing. The identified pre-rRNA processing factor (MDN1), however, also resulted in decreased RNAPI transcription, suggesting the overwhelming association of screen hits with the transcriptional regulation of the pre-ribosomal RNA. Additionally, as expected for defects in the biogenesis of ribosomes, depletion of 13/14 screen hits further resulted in decreased protein synthesis. These data are in contrast to the dataset generated when screening for a decrease in nucleolar number (Farley-Barnes et al., 2018). In the screen for proteins that cause a decrease in nucleolar number when depleted, of the hits evaluated for roles in ribosome biogenesis, the majority were associated with defects in pre-rRNA processing (16/20). Proteins required for RNAPI transcription were also uncovered (7/20); however, all but one demonstrated a concomitant pre-rRNA processing defect (Farley-Barnes et al., 2018). Taken together, these data suggest that changes in nucleolar number in MCF10A cells are indicative of a negative impact on nucleolar function. Screening for increased nucleolar number revealed a unique subset of proteins required primarily for the nucleolar function of RNAPI transcription.

Of the identified regulators of RNAPI transcription few were repressors of nucleolar activity. Cancer pathologists know that increased nucleolar number and area are associated with increased nucleolar activity and poor prognosis in cancer patients (Derenzini et al., 2009). As such, one possibility is that hits that cause an increase in

nucleolar number when depleted will also reveal increased RNAPI transcription. In this analysis, however, only 2/14 screen hits evaluated resulted in an increase in RNAPI transcription upon depletion (RFC1 and ATAD5), suggesting roles as repressors. In support of this finding, RFC1 has previously been reported to repress rDNA transcription in *S. cerevisiae* (Smith et al., 1999), and in plants (Liu et al., 2010). Furthermore, both proteins are large subunits of heteropentameric protein complexes that share subunits, RFC2-5, and associate with proliferating cell nuclear antigen (PCNA) during DNA replication. The majority of hits tested were thus promoters of rDNA transcription. Of the 14 hits tested, 9 caused a decrease in RNAPI transcription upon depletion, as well as the screen positive control, KIF11. In all, each screen hit that caused defects in RNAPI transcription upon depletion, with the exception of FAM98A, which also resulted in decreased protein synthesis. Thus, while increased nucleolar number and size are commonly associated with cancer and increased growth and proliferation, our screen for increased nucleolar number identified primarily promoters of RNAPI transcription.

The p53-mediated nucleolar stress response is not likely to be the only root cause of the observed reduction in RNAPI transcription. The tumor suppressor protein, p53 (TP53), is a well-documented cellular stress sensor that suppresses oncogenic activity through its regulation of transcription, which leads to cell cycle arrest and apoptosis (Mantovani et al., 2019). Mutations in p53 are some of the most commonly observed in human cancer (Kandoth et al., 2013). While the most widely reported gene targets of p53 include genes transcribed by RNA polymerase II (Allen et al., 2014; Kim et al., 2011), p53 has also been reported to directly inhibit RNAPI (Zhai and Comai, 2000). Furthermore, the stabilization of p53 is mediated by the nucleolus and scales with the

degree of cellular stress, with greater stress eliciting higher levels of p53 and vice versa (Rubbi and Milner, 2003). Thus, the inhibition of RNAPI transcription I observe upon depletion of a subset of screen hits can be a cause or consequence of p53 stabilization. Intriguingly, however, while MCF10A cells maintain wild-type p53 (Merlo et al., 1995) inhibition of RNAPI is concomitant only with increased levels of p53 after depletion of 2/14 proteins (siRFC1 and siRACGAP1). These data suggest that not only is the RNAPI transcriptional inhibition I observe not likely caused by p53-mediated inhibition of RNAPI, but also that the level of RNAPI transcription is not sufficient to trigger p53 stabilization. Furthermore, RFC1 depletion led to increased RNAPI transcription rather than decreased transcription counter to what would be expected with p53 stabilization, and thus further analysis is required to better understand the specific relationship between RFC1 and p53. Together, these data suggest that for 12/14 hits, the reduction in RNAPI transcription is independent of increased levels of p53, and further supports that this screen for increased nucleolar number identified novel regulators of ribosome biogenesis.

Finally, depletion of several of the novel regulators of RNAPI transcription yielded defects in cell cycle progression and cell division. Of the screen hits evaluated, depletion of KIF11 and 8/20 hits resulted in the accumulation of cells with a >4N DNA content (Chapter 2). Failures in cell division could provide an explanation for the observed increase in the percentage of nuclei with ≥5 nucleoli. However, given that several of these proteins also resulted in defects in RNAPI transcription (KIF11, ENY2, INCENP, RACGAP1, and TPX2), the cause for increased nucleolar number may not be so easily explained. Additionally, depletion of KIF11, INCENP, and TPX2 resulted in the accumulation of cells in G2/M phase and depletion of ENY2, FAM98A, RFC1, and

WRAP53 resulted in an accumulation of cells in S phase (Chapter 2). Thus, alternatively, failures in the regulation of RNAPI transcription during S or G2/M phase could lead to the increase in nucleolar number observed. While it is possible that each of the screen hits may function in ribosome biogenesis outside of S or G2/M phase, as reported previously for KIF11 in translation (Bartoli et al., 2011), the enrichment of replication and mitosis factors among the hits supports the possibility that the regulation of RNAPI specifically during S and G2/M phase is essential to maintaining nucleolar integrity. In conclusion, the functional analysis of a subset of screen hits has supported the hypothesis that screening for increased nucleolar number could also identify novel regulators of nucleolar function and has further broadened our understanding of the regulation of ribosome biogenesis in higher eukaryotes.

MATERIALS AND METHODS

Cell lines

As described in Chapter 2, the human breast epithelial cell line, MCF10A (ATCC, CRL-10317), was 2D subcultured in DMEM/F-12 medium (Gibco, 1130-032) supplemented with 5% horse serum (Gibco, 16050), 10 μg/mL insulin (Sigma, I1882), 0.5 μg/mL hydrocortisone (Sigma, H0135), 100 ng/mL cholera toxin (Sigma, C8052), and 20 ng/mL epidermal growth factor (Peprotech, AF-100-15).

RNAi

For biochemical assays on the subset of validated hits, the siGENOME SMARTpool siRNAs (Horizon Discovery) were used, except for with siNT, which was

the ON-TARGETplus Non-targeting pool (D-001810-10-20). Unless otherwise noted, subconfluent cells (log phase) were transfected with siRNAs (20-30 nM, final concentration) using Lipofectamine RNAiMAX Transfection Reagent (ThermoFisher Scientific, 13778150) and incubated for 72 hrs prior to the experimental assays.

Quantitative reverse transcription polymerase chain reaction (qRT-PCR)

Total RNA was extracted from siRNA-depleted cells using TRIzol reagent (ThermoFisher Scientific, 15596018) as per the manufacturer's instructions. After validating that A260/280 values were >1.80 and A260/230 values were >1.7, complementary DNA synthesis was performed using the iScript gDNA Clear cDNA Synthesis Kit (Bio-Rad, 172–5035) using 1 μg of total RNA and a mix of random hexamer and oligo dT primers. Previously published primers were used to test mRNA levels of ATAD5 (Bell et. al, 2011) and RFC1 (Stielow et. al, 2014). BioRad PrimePCR Assay gene-specific primers were used to test mRNA levels of the remaining hits (Bio-Rad, 10025636; UTP4, qHsaCID0021354; KIF11, qHsaCID0015908; CDCA8, qHsaCED0044566; H1-10, qHsaCED0019411; INCENP, qHsaCID0010103; MDN1, qHsaCID0006754; STK24, qHsaCID0012429; TPX2, qHsaCID0016024; ENY2, qHsaCED0003040; FAM98A, qHsaCID0010948; INKA, qHsaCED0020031; RACGAP1, qHsaCID0011308; CCN4, qHsaCED0036389; WRAP53, qHsaCID0006849). Beta-actin primers were designed in our laboratory (intron-spanning; Forward - 5' ATT GGC AAT GAG CGG TTC 3' and Reverse - 5' CGT GGA TGC CAC AGG ACT 3'). All qPCR reactions were completed using the iTaq Universal SYBR Green Supermix (Bio-Rad, 172-5121). To verify the amplification of a single PCR product, melt curves were generated for each sample. Three biological replicates, each

with three technical replicates, were measured for each of the 14 tested hits as well as siUTP4, siKIF11, and the negative non-targeting control (siNT). Amplification of the beta-actin mRNA was used as an internal control, and analysis was completed using the comparative C_T method ($\Delta\Delta C_T$).

Dual-luciferase reporter assay

Following siRNA-depletion of hits for 48 hrs, cells were transfected with 1000 ng of pHrD-IRES-Luc (Ghoshal et al., 2004) and 0.1 ng of a plasmid that constitutively expresses *Renilla* luciferase (Freed et al., 2012) using Lipofectamine 3000 Reagent (ThermoFisher Scientific, L3000015). After 72 hrs of siRNA-depletion and 24 hrs of incubation with the reporter plasmids, luminescence was detected using the Dual-Luciferase Reporter Assay System (Promega, E1910) and a GloMax 20/20 luminometer (Promega). In addition to incubation with the 1X passive lysis buffer for 15 min, MCF10A cells were scraped prior to collection for luminescence readings.

Northern blots

Total RNA was extracted from siRNA-depleted cells using TRIzol Reagent. To assay for changes in levels of pre-rRNA intermediates, 4 μg of total RNA was run on a 1% agarose/1.25% formaldehyde gel in a 1.5M tricine/1.5M triethanolamine buffer. RNA was transferred overnight to a Hybond XL nylon membrane (GE Healthcare, RPN 303S) by capillary transfer in 10X saline-sodium citrate (SSC) transfer buffer after a brief 15 min soak in a 0.5M sodium hydroxide solution. Membranes were then exposed to UV (254 nm) to immobilize the RNA, and incubated with denatured yeast tRNA for 1 hr at

42° C and hybridized overnight at 37° C with 5’ end radiolabeled oligonucleotide probes in a solution of 7.5X Denhardt’s solution, 5X sodium chloride-sodium phosphate-EDTA (SSPE) buffer, and 0.1% SDS as in (Farley-Barnes et al., 2018). The oligonucleotide probes used were the same as in (Farley-Barnes et al., 2018) and include:

5’ETS 5’ – CCTCTCCAGCGACAGGTCGCCAGAGGACAGCGTGTCAGC - 3’

5’ITS1 5’ – CCTCGCCCTCCGGGCTCCGTTAATGATC - 3’ (Sloan et al., 2013)

P3 5’ – AAGGGGTCTTTAAACCTCCGCGCCGGAACGCGCTAGGTAC - 3’

P4 5’ – CGGGAACTCGGCCCGAGCCGGCTCTCTCTTTCCCTCTCCG - 3’

7SL 5’ – TGCTCCGTTTCCGACCTGGGCCGGTTCACCCCTCCTT - 3’

Puromycin labeling assay

Following siRNA-depletion of hits for 72 hrs, cells were treated as described in (Farley-Barnes et al., 2018), with the exception that puromycin antibody (Kerafast, EQ0001) was used at a 1:500 dilution.

Western blots

Following siRNA-depletion of hits for 72 hrs, total protein was harvested by the same method used in the puromycin labeling assay described in (Farley-Barnes et al., 2018). Protein concentration was quantified by Bradford assay and 30 μg of total protein was run by SDS-PAGE on a 10% gel with a 5% stacking gel. Protein was transferred to a PVDF membrane using a Trans-Blot Turbo Transfer System (Bio-Rad) and blocked for 1 hr with 5% milk in PBST before incubating overnight with HRP-conjugated p53 antibody (Santa Cruz Biotechnology, sc-126) diluted in PBST (1:5000). Following imaging on a

ChemiDoc Imaging System (Bio-Rad), blots were stripped and re-probed for beta-actin as performed in the puromycin labeling assay and quantified using ImageJ.

Statistical analyses

All statistical analyses were performed in GraphPad Prism 8.2.1 (GraphPad Software, Inc.) using the tests described in the Figure Legends.

Chapter 4

High-throughput screen for nucleolar-targeted cancer therapies reveals small molecule regulators of nucleolar number

INTRODUCTION

Ribosome biogenesis is essential for cell growth and proliferation and is linked to cancer pathogenesis. Cancer pathologists observe larger and more numerous nucleoli in aggressive tumors (Derenzini et al., 2009), and retrospective studies found that several chemotherapeutic agents target ribosome biogenesis either directly or indirectly (Burger et al., 2010; Quin et al., 2014). While the enthusiasm was initially put towards identifying inhibitors of translation for cancer therapy (Hagner et al., 2010; Malina et al., 2012; Novac et al., 2004; Ruggero, 2013; Silvera et al., 2010), interest surrounding the development of drugs targeting ribosome biogenesis specifically has gained recent momentum (Brighenti et al., 2015; Drygin et al., 2010; Pelletier et al., 2018; Quin et al., 2014). Thus, targeting the nucleolus and ribosome biogenesis holds promising therapeutic potential.

Preclinical and clinical data support that drugs developed specifically to target RNAPI transcription hold promise in the treatment of cancer. While drugs targeting a ubiquitous cellular function may hold limited therapeutic efficacy and yield poor toxicity profiles, studies on pioneering RNAPI-selective inhibitors suggest instead that growth adaptations in cancer may actually make tumors more sensitive to the inhibition of ribosome biogenesis (Brighenti et al., 2015; Ruggero, 2012). The RNAPI inhibitor, CX-3543 (quarfloxin), may in part target rDNA-enriched G-quadruplexes (Drygin et al., 2009; Drygin et al., 2008). Phase I and II clinical trials of CX-3543 in solid tumors and blood cancer revealed no serious adverse events and resulted in stable disease through the course of the study for several participants (Papadopoulos et al., 2007). CX-5461, likewise, has shown promising preclinical and clinical data for the treatment of

hematological malignancies and DNA repair-deficient cancers (Hilton et al., 2020; Khot et al., 2019; Sanij et al., 2020; Xu et al., 2017b). CX-5461 inhibits RNAPI by disrupting the interaction between RNAPI and the transcription initiation factor, SL1 (Drygin et al., 2011). More recent studies on the mechanism, however, suggest that CX-5461 may also inhibit topoisomerase II (Bruno et al., 2020), and therefore the therapeutic benefit from its effect on RNAPI versus topoisomerase remains to be elucidated. Finally, the RNAPI inhibitor, BMH-21, a planar heterocyclic DNA intercalator, leads to the selective degradation of the large catalytic subunit of RNAPI, RPA194 (Peltonen et al., 2014). In preclinical studies, BMH-21 treatment has shown promising antiproliferative activity across a range of cancer cell lines with limited impact on normal fibroblast cells (Fu et al., 2017; Peltonen et al., 2014). Furthermore, BMH-21 also has promising antineoplastic activity in mouse xenograft models of melanoma and drug-resistant prostate cancer (Low et al., 2019; Peltonen et al., 2014). Taken together, promising preclinical and clinical research on these pioneering compounds have energized some laboratories to further explore inhibition of ribosome biogenesis for cancer drug discovery.

High-throughput screens to identify novel inhibitors of ribosome biogenesis have yielded some success in identifying promising new drug candidates. In one screen, ~150,000 compounds were screened for reduced nascent ribosome levels in the human melanoma A375 cell line (Scull et al., 2019). This primary screen was then followed by a secondary screen for compounds that specifically decrease pre-rRNA levels, which revealed 2 structurally similar compounds, RB1 and RB2, that both decreased cell viability. Furthermore, RB2 had limited impact on viability of normal, HUVEC, cells and RB2 treatment resulted in decreased colony growth in a metastatic, anchorage-

independent growth model (Scull et al., 2019). Another screen of ~700 compounds used a virtual structure-based screening approach using the yeast crystal structure of the human RNAPI ortholog (Tan and Awuah, 2019). Six compounds were identified in this virtual screen, including CX-5461 and, intriguingly, the HMG-CoA reductase inhibitor, cerivastatin sodium. Follow up using a yeast cell line engineered with the human rDNA and promoter sequence revealed that cerivastatin sodium inhibited yeast growth and also decreased proliferation when tested in human cancer cell lines (Tan and Awuah, 2019). Finally, in yet another recent high-throughput screen for inhibitors of ribosome biogenesis, ~1,000 compounds were surveyed in a yeast system detecting defects in ribosomal subunit export. Of the compounds tested, several were identified to impact either 40S or 60S export and subsequent analysis of hits revealed that many inhibit pre-rRNA processing; however, they have yet to be validated in a mammalian system (Awad et al., 2019). Thus, there has been success in screening for small molecule inhibitors of ribosome biogenesis in eukaryotes and the data suggest that the approach may be a promising opportunity for the identification of novel drugs for therapeutic development.

Previously, the Baserga lab, including myself, was successful in identifying proteins required for ribosome biogenesis by performing a high-throughput RNAi screen in the non-cancer-derived human, MCF10A, breast epithelial cell line for changes in nucleolar number [(Farley-Barnes et al., 2018); Chapter 2]. I applied this robust assay to discover putative new cancer therapeutics by screening for small molecule compounds that effect nucleolar number. I therefore performed two high-throughput screens for small molecules that regulate nucleolar number. Here, I report on the results from these two screens, which included a pilot screen of nearly 4,000 FDA-approved drugs, followed by

a screen of a curated collection of approximately 25,000 synthetic compounds selected based on exhibiting promising pharmaceutical properties. Through these screens I discovered several small molecule regulators of nucleolar number, including both compounds that decrease nucleolar number and those that increase nucleolar number. Validation screening of the hits as well as bioinformatic analyses to classify hits reveal not only several promising drug candidates, but also common molecular targets that lend insight into the regulation of nucleolar number and activity. I performed these two screens, screen validation, and the structure clustering in collaboration with the Yale Center for Molecular Discovery.

RESULTS

Identification of small molecule positive controls for high-throughput screening

To identify novel cancer therapeutics by screening for small molecule regulators of nucleolar number I needed to identify small molecule compounds that yield a strong and reproducible decrease in nucleolar number [one nucleolus per nucleus percent effect (PE)] and increase in nucleolar number (≥5 nucleoli per nucleus PE) to use as positive controls. To identify these positive controls, I tested 25 compounds with different mechanisms of action at eight different concentrations (20 μM-9.14 nM, 3-fold dilutions), three different time points (24, 48, and 72 hrs), and two cell seeding densities (1,000 and 2,000 cells/well; Table 4-1). I curated the list of compounds with Katherine Farley-Barnes and Cecelia Harold, and I performed the high-throughput screen and data analysis in collaboration with the Yale Center for Molecular Discovery. Nucleoli were identified based on immunofluorescent staining with a monoclonal antibody to the abundant

nucleolar protein fibrillarin [72B9 (Reimer et al., 1987)], and cells were identified using the DNA stain, Hoechst. Nucleolar number was quantified using CellProfiler as described in (Farley-Barnes et al., 2018), and the one nucleolus PE and ≥5 nucleoli PE were both quantified relative to the negative control (0.1% DMSO; DMSO=100 PE). The seeding density of 2,000 cells per well and a 48 hr incubation led to several promising candidates with adequate viability (Appendix IV). As a result, we selected several with which to perform follow-up testing in order to identify the best candidates with which to move forward with as positive controls for the screen.

To identify positive controls from among the candidates in this small screen, we selected compounds that yielded a high PE for each phenotype (one nucleolus and ≥5 nucleoli) to re-screen for reproducibility. The Z-prime statistic is the best measure of a strong and reproducible control as it reports the separation between the distributions of the positive and negative controls. As described in Chapter 2, a Z-prime =1 indicates an ideal screening assay, whereas a Z-prime <0 indicates overlap between the controls and a noisy assay. While in high-throughput screening a Z-prime ≥0.5 is desired, Z-prime values <0.5 may still identify positive hits. I selected two compounds for each phenotype to re-screen at several different concentrations at a seeding density of 2,000 cells per well and an incubation time of 48 hr and calculated the Z-prime statistic for each condition. These compounds included RNAPI inhibitors, BMH-21 and CX-5461, for the one nucleolus per nucleus phenotype, and mitomycin C and topotecan for the ≥5 nucleoli per nucleus phenotype. Interestingly, based on the results from this experiment, BMH-21 (1 and 1.5 μM) and mitomycin C (14 μM) both yielded promising Z-prime values (Z-prime ≥0.5) for decreased nucleolar number (Table 4-2). This was intriguing given that

mitomycin C had originally been selected as a putative positive control for increased nucleolar number and suggests a possible relationship between the two unique phenotypes. With regards to the ≥5 nucleoli per nucleus phenotype neither of the selected compounds yielded Z-prime values ≥0.5; however, mitomycin C at 250 nM did yield a positive Z-prime value (Z'=0.11; Table 4-3). Based on these data, BMH-21 (1 μM) and mitomycin C (250 nM) were selected as the two positive controls for our screen.

Table 4-1. Candidate compounds screened in positive control search for a high-throughput screen to identify small molecule regulators of nucleolar number. The twenty-five (25) compounds selected harbored a wide range of mechanisms of action and reported effects on the nucleolus or nucleolar proteins.

Compound	Catalog no.	Mechanism of action	Rationale
5-Fluorouracil	F6627 (Sigma-Aldrich)	Thymidylate synthase inhibitor	Reported to effect late pre-rRNA processing (Burger and Eick, 2013)
Actinomycin D	A1410 (Sigma-Aldrich)	DNA intercalator	RNA polymerase inhibitor; causes nucleolar disruption (Reynolds et al., 1964)
Amperozide	sc-203512 (Santa Cruz Biotechnology)	5-HT receptor agonist	Treated cells may show one nucleolus phenotype (Gustafsdottir et al., 2013)
BMH-21	SML1183 (Sigma-Aldrich)	DNA intercalator; RNAPI inhibitor	RNAPI inhibitor (Peltonen et al., 2014)
C646	328968-36-1 (Cayman Chemical)	UBTF acetylation inhibitor	UBTF is an RNAPI transcription co-factor (McStay and Grummt, 2008; Sanij and Hannan, 2009)

CDK9 Inhibitor II	238811 (Sigma-Aldrich)	CDK9 inhibitor	Preclinical blood cancer drug and putative rRNA processing inhibitor (Burger et al., 2013; Yin et al., 2014)
Cisplatin	C2210000 (Sigma-Aldrich)	Platinum-containing chemotherapeutic	Breast cancer therapeutic; Binds the ribosome (Melnikov et al., 2016)
CX-5461	1138549-36-6 (Cayman Chemical)	RNAPI inhibitor; Topoisomerase inhibitor (Bruno et al., 2020)	RNAPI inhibitor (Drygin et al., 2011; Haddach et al., 2012)
Doxorubicin		Topoisomerase inhibitor	Breast cancer therapeutic; Inhibits RNAPI transcription (Burger et al., 2010)
Etoposide	E1383 (Sigma-Aldrich)	Topoisomerase inhibitor	Treated cells show large, flat nucleoli (Gustafsdottir et al., 2013)
Fenbendazole	F5396 (Sigma-Aldrich)	Tubulin modulator	Reported effect on nucleolar morphology (Gustafsdottir et al., 2013)
Flavopiridol	131740-09-5 (Cayman Chemical)	CDK1 inhibitor	CDK1 activity is required for RNAPI silencing during mitosis (Hernandez-Verdun, 2011)

Hesperadin	422513-13-1 (Cayman Chemical)	Aurora B kinase-selective inhibitor	Aurora B kinase interacting proteins were hits in siRNA screen for increased nucleolar number (Chapter 2)
Ispinesib	336113-53-2 (Cayman Chemical)	KIF11 inhibitor	KIF11 inhibition by siRNA yields an increase in nucleolar number (Chapter 2)
IWP-2	I0536 (Sigma-Aldrich)	WNT inhibitor	Wnt proteins regulate ribosome biogenesis (Pfister and Kuhl, 2018)
LY411575	209984-57-6 (Cayman Chemical)	Gamma-secretase inhibitor	Notch pathway implicated in breast cancer progression (Kontomanolis et al., 2018)
Metarrestin	AOB1384 (Aobious)	Peri-nucleolar compartment inhibitor	Inhibits RNAPI transcription (Frankowski et al., 2018)
Metformin	PHR1084 (Sigma-Aldrich)	mTOR inhibitor	mTOR regulates ribosome biogenesis (Mayer and Grummt, 2006)
Mitomycin C	50-07-7 (Cayman Chemical)	DNA crosslinker	Inhibits rRNA synthesis (Snodgrass et al., 2010)

Paclitaxel	T7402 (Sigma-Aldrich)	Microtubule depolymerization inhibitor	Breast cancer therapeutic; Mitosis inhibitor; siRNA screen for increased nucleolar number revealed enrichment of mitosis factors (Chapter 2)
SBE 13	SML0012 (Sigma-Aldrich)	PLK1 inhibitor	Mitosis inhibitor; siRNA screen for increased nucleolar number revealed enrichment of mitosis factors (Chapter 2)
Temsirolimus	PZ0020 (Sigma-Aldrich)	mTOR inhibitor	mTOR regulates ribosome biogenesis (Mayer and Grummt, 2006)
Topotecan	119413-54-6 (Cayman Chemical)	Topoisomerase inhibitor	Topoisomerase inhibitors have reported effects on ribosome biogenesis (Burger et al., 2010)
Trichostatin A	T8552 (Sigma-Aldrich)	HDAC inhibitor	UBTF RNA polymerase I transcription co-factor is a substrate (Pelletier et al., 2000)
XAV939	X3004 (Sigma-Aldrich)	WNT inhibitor	Wnt proteins regulated ribosome biogenesis (Pfister and Kuhl, 2018)

Table 4-2. Screen statistics for re-screened one nucleolus per nucleus candidates. Compound, concentration tested (μM), coefficient of variation (CV), signal-to-background (S/B), and Z-prime value are reported. A Z-prime >0.5 is desired for high-throughput screening, although Z-prime values between 0 and 0.5 are still acceptable for the positive identification of hits. Compounds at concentrations that led to a viability of <10% are not reported. Compound and concentration selected as the positive control is in bold.

Compound	Concentration (μM)	Coefficient of Variation (%)	Signal-to-Background (S/B)	Z-prime
BMH-21	2.2	14.3	3.3	0.24
BMH-21	1.5	5.7	3.7	0.64
BMH-21	**1.0**	**7.0**	**3.5**	**0.57**
BMH-21	0.75	6.3	3.5	0.59
BMH-21	0.375	7.1	2.3	0.37
CX-5461	20	8.5	2.5	0.36
Mitomycin C	14	5.4	4.1	0.67
Mitomycin C	7	8.0	3.2	0.49
Mitomycin C	3.5	8.1	2.4	0.33

Table 4-3. Screen statistics for re-screened ≥5 nucleoli per nucleus candidates. Compound, concentration tested (μM), coefficient of variation, signal-to-background (S/B), and Z-prime values are reported. A Z-prime >0.5 is desired for high-throughput screening, although Z-prime values <0.5 may still identify positive hits. Compounds at concentrations that led to a viability of <10% are not reported. Compound and concentration selected as the positive control is in bold.

Compound	Concentration (μM)	Coefficient of Variation (%)	Signal-to-Background (S/B)	Z-prime
Mitomycin C	0.5	16.7	2.4	-0.3
Mitomycin C	**0.25**	**10.7**	**2.6**	**0.11**
Mitomycin C	0.125	11.3	2.3	-0.05
Topotecan	0.018	9.4	2.2	-0.02

Pilot screen of FDA-approved drugs revealed 140 compounds

To identify new cancer therapeutics by screening for small molecule regulators of nucleolar number, I first performed a pilot screen of FDA-approved compounds to test whether any proven small molecule drugs impact nucleolar number. I screened 3,923 compounds maintained in 3 different drug libraries curated by the Yale Center for Molecular Discovery. MCF10A cells were seeded at a density of 2,000 cells per well and 24 hrs later cells were treated for 48 hrs with compounds at a final concentration of 10 μM. Nucleolar number was quantified by CellProfiler as reported in (Farley-Barnes et al., 2018), and the one nucleolus PE and ≥5 nucleoli PE were both quantified and normalized to the average of the 12 negative (0.1% DMSO; PE=0) and 12 positive (1 μM BMH-21 or 0.25 μM mitomycin C; PE=100) control replicates included on each screening plate. The calculated normalized percent effect (NPE) values were then used to identify hits in the screen.

The screen for compounds that cause a decrease in nucleolar number was robust and revealed 110 active compounds. Statistical monitoring of the 13 screening plates revealed a mean S/B of 3.09 (range, 2.91 to 3.26) and mean Z-prime value of 0.56 (range, 0.40 to 0.68), suggesting good signal and separation of the two controls (Figure 4-1, A). Based on a conservative threshold of ≥3 standard deviations (SD) from the median NPE, compounds that yielded a one nucleolus NPE ≥53.2 were considered a hit. This yielded a hit rate of 2.8%, or 110 compounds, with a mean percent viability of 10.9% relative to DMSO (range, 0.5 to 33.6; Figure 4-1, B-D; Appendix V). Of the 110 hits, several were identified multiple times due to overlap in the compound libraries (Table 4-4). As a

result, 83 unique compounds were identified to cause a decrease in nucleolar number and suggests the identification of several putative new regulators of nucleolar function.

In contrast, the screen for compounds that cause an increase in nucleolar number was not as robust. Statistical monitoring of the 13 screening plates revealed a mean S/B of 1.88 (range, 1.56 to 2.28) and mean Z-prime value of -0.56 (range, -1.05 to -0.20). Negative Z-prime values suggest overlap among the percent effect distributions of the controls; however, the means of the controls were separated with only slight overlap of the distributions (Figure 4-2, A), and therefore I proceeded with caution. I identified hits based on the same conservative threshold of ≥3 SD from the median NPE (NPE ≥108.3), which yielded a NPE greater than the positive control. Based on this threshold, 30 hits were identified to cause an increase in the percentage of nuclei with ≥5 nucleoli (hit rate=0.8%) with a mean percent viability relative to DMSO among the hits of 35.7% (range, 0.8 to 99.2; Figure 4-2, B-D; Appendix VI). While some of these hits may be false positives, they are good candidates for re-screening to identify a better positive control.

The pilot screen to identify small molecule regulators of nucleolar number was therefore effective in identifying 140 compounds that either decrease or increase nucleolar number. While the screen for decreased nucleolar number was more robust with favorable and reproducible Z-prime values among the screening plates, the screen for increased nucleolar number may still hold promise and revealed 30 hits with an NPE>100. Interestingly, mebendazole was a hit in both screens (Appendix V; Appendix VI). Comparisons to prior screens for inhibitors of ribosome biogenesis revealed several overlapping hits (Table 4-5). These data support to my results, but also suggest that the

Baserga lab's unique screening approach may reveal a broader range of regulators of nucleolar function than the previously reported screens. While promising, these data necessitate further analysis and validation, including repeat testing, dose-response curves to identify EC50 concentrations, and testing in cancer versus normal cell lines to identify the extent to which hits share any common targets and whether they harbor any anti-cancer potential.

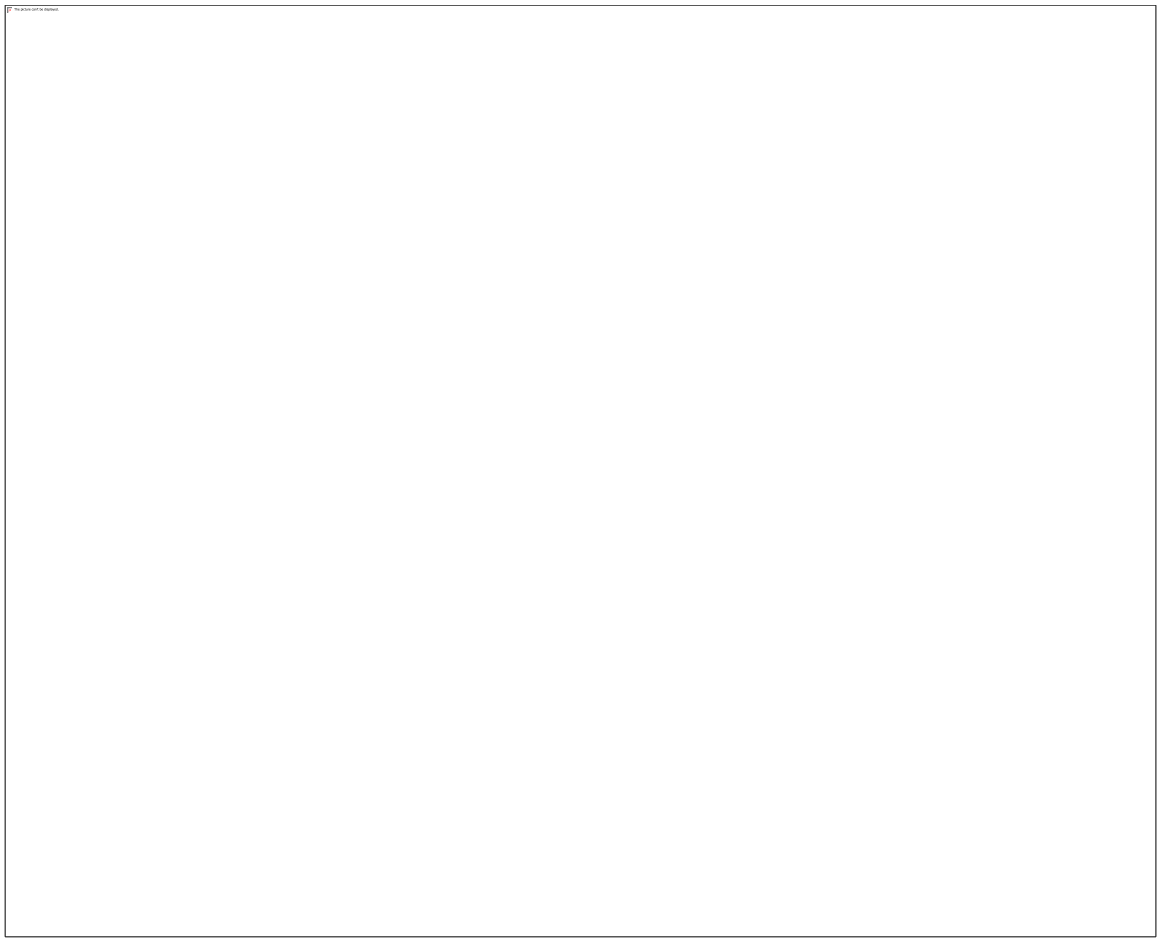

Figure 4-1. High-throughput screen of FDA-approved drugs revealed 110 compounds (2.8%) that caused a decreased in nucleolar number.

(A) Frequency distribution of the one nucleolus phenotype mean percent effect (PE) of the negative and positive control treatments included on each screening plate (n=13). DMSO=negative control (red line) and mean PE set to 0. BMH-21=positive control (dark blue line) and mean PE set to 100. All FDA-approved drugs tested=compounds (light blue line). Mean Z-prime value for the screen was 0.56 (range, 0.40 to 0.68).

(B) Distribution of the one nucleolus per nucleus normalized percent effect (NPE) for each of the 3,923 compounds tested in the pilot screen of FDA-approved compounds.

Threshold used to define hits was ≥3 standard deviations from the median NPE (red dashed line) or NPE ≥53.2.

(C) Percent viability relative to the one nucleolus per nucleus NPE for the 110 hits. Each dot represents a hit. Mean percent viability of the 110 hits was 10.9% relative to DMSO, set to 100% (range, 0.5 to 33.6).

(D) Representative images of the controls and top hits that caused a decrease in nucleolar number to one nucleolus per nucleus. DMSO=negative control and BMH-21=positive control. Hits represented include sanguinarine sulfate, pixantrone dimaleate, vindesine, pyrvinium pamoate, digitoxin, and benzethonium choloride.

Table 4-4. Compounds identified more than once in the screen for decreased nucleolar number. Drug name, the number (No.) of times the drug appeared in the hit list, and the range of the normalized percent effect (NPE) for the drug in the screen are indicated.

Drug name	No. of times in hit list	Mean NPE (Lowest NPE, Highest NPE)
Vinblastine (Velban)	5	106.0 (78.2, 125.7)
Mycophenolic acid (Mycophenolate mofetil; CellCept)	4	77.8 (63.8, 99.7)
Vinorelbine (Navelbine)	3	106.0 (91.7, 114.8)
Plicamycin (Mithracin)	3	86.2 (73.6, 100.9)
Vincristine (Oncovin)	3	112.7 (105.8, 122.5)
Podofilox (Condylox)	2	83.6 (81.0, 86.2)
Piroctone olamine (Octopirox; piroctone)	2	94.1 (94.0, 94.1)
Ouabain	2	98.1 (96.3, 99.8)
Colchicine	2	81.7 (75.3, 88.1)
Mitoxantrone hydrochloride (Mitoxantrone)	2	160.3 (131.9, 188.7)
Ciclopirox olamine (Ciclopirox)	2	84.6 (83.7, 85.5)
Albendazole	2	73.4 (70.4, 76.4)
Mebendazole (Vermox)	2	60.1 (55.0, 65.2)
Aclarubicin	2	107.7 (96.8, 118.6)
Proscillaridin (Caradrin)	2	107.7 (99.1, 116.3)

Digitoxin (Crystodigin)	2	107.5 (102.3, 112.7)
Mitomycin (Mitomycin C; Mutamycin)	2	90.4 (77.3, 103.5)
Vindesine sulfate (Eldesine)	2	117.3 (96.5, 138.1)
Topotecan hydrochloride (Topotecan)	2	123.5 (120.5, 126.4)

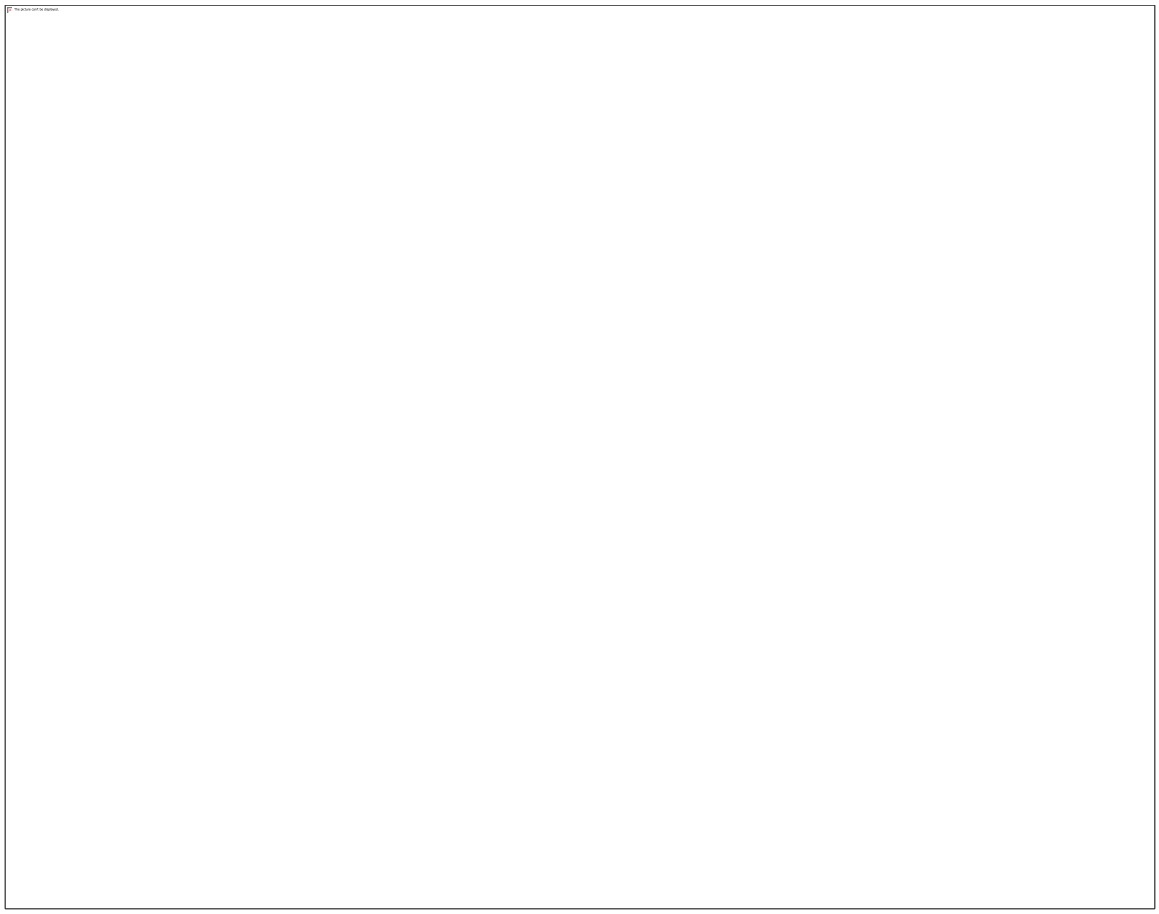

Figure 4-2. High-throughput screen of FDA-approved drugs revealed 30 compounds (0.8%) that caused an increase in nucleolar number.

(A) Frequency distribution of the one nucleolus phenotype percent effect (PE) of the negative and positive control treatments included on each screening plate. DMSO=negative control (red line) and mean PE set to 0. Mitomycin C=positive control (purple line) and mean PE set to 100. All FDA-approved drugs tested=compounds (light blue line). Mean Z-prime value for the screen was -0.56 (range, -1.05 to -0.20).

(B) Distribution of the normalized percent effect (NPE) for each of the 3,923 compounds tested in the pilot screen of FDA-approved compounds. Threshold used to define hits was ≥3 standard deviations from the median NPE (red dashed line) or NPE ≥108.3.

(C) Percent viability relative to the ≥5 nucleoli per nucleus NPE for the 30 hits. Each dot represents a hit. Mean percent viability of the 30 hits was 35.7% relative to DMSO, set to 100% (range, 0.8 to 99.2).

(D) Representative images of the controls and top hits yielding an increase in the percentage of nuclei with ≥5 nucleoli. DMSO=negative control and mitomycin C=positive control. Hits represented include melphalan, merimepodib, docetaxel, oxiconazole, butoconazole, and alvocidib.

Table 4-5. Comparison to other screens for small molecule inhibitors of ribosome biogenesis. Drug names are indicated. In parentheses are the number of overlapping hits compared to the total number of hits identified by the screening approach.

Low-throughput screen of chemotherapeutic drugs for inhibition of ribosome biogenesis (Burger et al., 2010) (7/20)	Virtual structure-based screen for RNAPI inhibitors (Tan and Awuah, 2019) (1/6)	Screen for ribosomal subunit export and pre-rRNA processing inhibitors (Awad et al., 2019) (7/128)
Cycloheximide	Cerivastatin sodium	Daunorubicin
Doxorubicin		Doxorubicin
Etoposide		Flubendazole
Melphalan		Idarubicin
Mitoxantrone		Lasalocid A
Mitomycin C		Mycophenolic acid
Vinblastine		Vindesine sulfate

Bioinformatic analysis of screen hits reveals known cancer therapeutics

Screening for changes in nucleolar number was successful in identifying compounds that regulate nucleolar number; but, was I successful in identifying drugs approved for use in cancer treatment? To address this question, I manually curated medical use and molecular target information for each of the 140 hits using KEGG DRUG Database, DrugBank Online and a review of relevant literature (Appendix V; Appendix VI). The analysis of drug hits by medical use revealed that when screening for regulators of nucleolar number, antineoplastic drugs were the most common type of drugs among the hits (Figure 4-3; Appendix V; Appendix VI). Also represented among top hits were several unexpected categories of drugs, including antiparasitic compounds, cardiovascular agents, antifungals, antiseptics, and antibiotics. Among the antiparasitc drugs, antihelmintics were the most common; among the cardiovascular agents, cardiac glycosides were the primary drugs identified. Interestingly, however, differences between decreased and increased nucleolar number among the drug medical uses identified were minimal, which suggests in part a possible shared mechanism by which these two phenotypes are generated. Taken together, screening for changes in nucleolar number was successful in identifying several antineoplastic drugs and may therefore be a viable approach for the discovery of novel antineoplastic compounds.

Classification of the molecular target for each hit also revealed significant overlap among the drugs identified by decreased versus increased nucleolar number. Common molecular targets among the drug hits include tubulin, DNA, topoisomerases and inosine-5'-monophosphate dehydrogenase (IMPDH; Figure 4-4; Appendix V; Appendix VI). Interestingly, a common mechanism underlying the targeting of DNA,

topoisomerases, and IMPHD is the inhibition of DNA and RNA synthesis and implies, not unexpectedly, the importance of these essential cellular functions in maintaining normal nucleolar numbers. Other notable drug targets among the hits include the ribosome, which supports a putative feedback mechanism between translation and ribosome biogenesis (Figure 4-4, A and B), and the Na^+/K^+ ATPase, which is the molecular target for cardiac glycosides, but has also been reported to be up-regulated in cancer [Figure 4-4, A-C (Khajah et al., 2018)]. Differences, among the two datasets however are also present, including most notably the identification of several drugs identified by increased nucleolar number that target ergosterol, a fungal cell wall lipid (Figure 4-4, B and D; Appendix V; Appendix VI). Intriguingly, however, ergosterol is also a provitamin in humans that is converted into vitamin D_2 upon UV exposure and suggests a putative link between vitamin D_2 and the nucleolus that has yet to be elucidated. Thus, analysis of the molecular targets among the drugs identified by screening for changes in nucleolar number again support common mechanisms underlying the generation of the two phenotypes, and further emphasize promising drug targets for the development of new cancer therapeutics.

In conclusion, I screened for compounds that regulate nucleolar number and identified several known antineoplastic drugs. Furthermore, I identified several common unexpected categories of drugs that will be interesting to explore in greater detail with regards to harboring antineoplastic potential. Additionally, I identified drugs with several common molecular targets that will be intriguing to explore with regards to putative functional roles in nucleolar biology. In all, these data suggest that screening FDA-approved compounds for changes in nucleolar number was a successful endeavor, and

one that supports expanding our search for novel cancer therapeutics using our approach with a larger library of small molecule compounds.

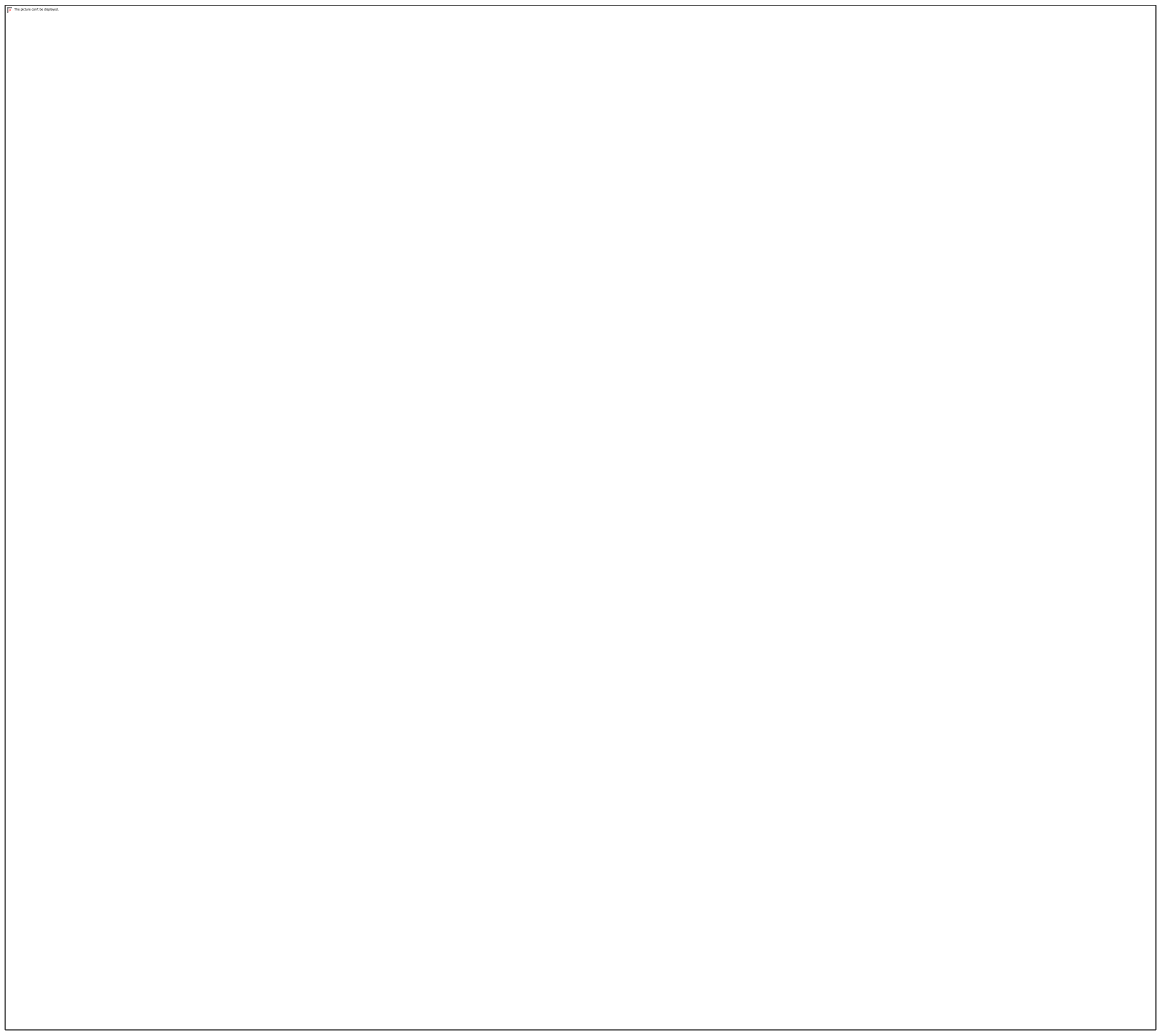

Figure 4-3. Antineoplastic drugs were the most frequently identified compounds among the FDA-approved drugs that regulate nucleolar number.

(A) Compounds that caused a decrease in nucleolar number classified by medical use. Of the 110 hits identified, 13 categories of drugs were defined. Antineoplastic drugs were the most common (n=52 hits). Cardiovascular agents include cardiac glycosides (n=10), statins (n=1), vasopressin receptor antagonists (n=1), and Ca^{+} channel blockers (n=1). Antiparasitics include anthelmintics (n=12) and antiprotozoals (n=3). 11 drugs were classified in more than one category.

(B) Compounds that caused an increase in nucleolar number classified by medical use. Of the 30 hits identified, 11 categories of drugs were defined. Antineoplastic drugs were the most common (n=11). Antiparasitics include broad-spectrum antiparasitic (n=2) and antihelmintics (n=1). Four drugs were classified in more than one category.

(C) Pie chart of top 4 categories of drugs that cause a decrease in nucleolar number by medical use. The most common categories of drugs identified were (1) antineoplastic drugs, (2) antiparasitics, (3) cardiovascular agents, and (4) antiseptics. Created, in part, with Biorender.com.

(D) Pie chart of top 4 categories of drugs that cause an increase in nucleolar number by medical use. The most common categories of drugs identified were (1) antineoplastic drugs, (2) antifungals, (3) antiparasitics, and (4) antiseptics. Created, in part, with Biorender.com.

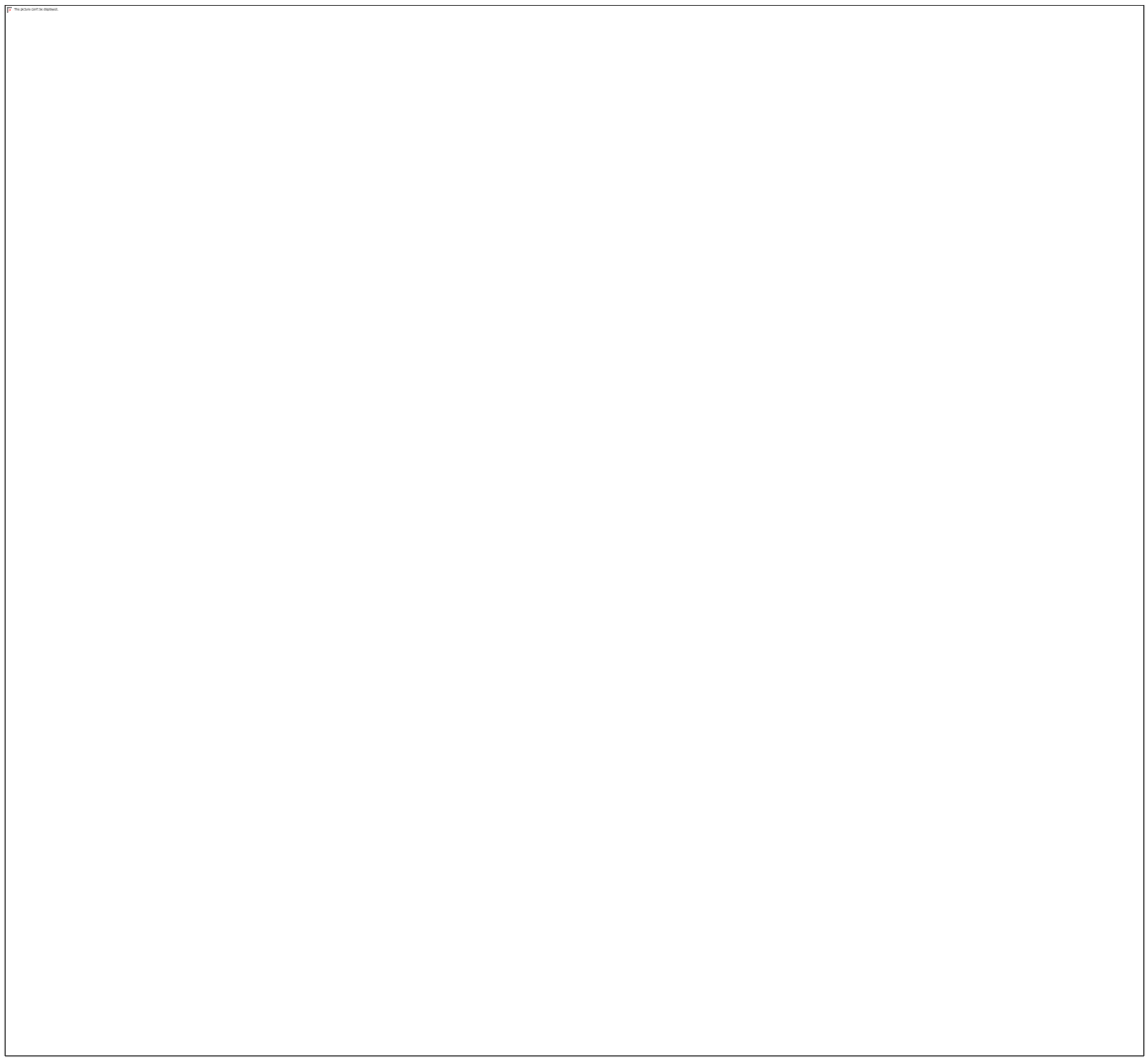

Figure 4-4. Several common molecular targets were identified among the FDA-approved drugs that regulate nucleolar number.

(A) Compounds that caused a decrease in nucleolar number classified by molecular target. Of the 110 hits identified, 24 different categories were defined. The most common molecular target among the hits was tubulin (n=32).

(B) Compounds that caused an increase in nucleolar number classified by molecular target. Of the 30 hits identified, 15 different categories were defined. The most common molecular target among the hits was ergosterol, a sterol found in fungal cell membranes and also precursor to vitamin D_2 (n=6).

(C) Pie chart of top 4 molecular targets that cause a decrease in nucleolar number. The most common molecular targets are (1) tubulin, (2) plasma membrane, (3) topoisomerase, and (4) Na^+/K^+ ATPase. Created, in part, with Biorender.com.

(D) Pie chart of top 4 molecular targets that cause an increase in nucleolar number. The most common categories of drugs identified were (1) ergosterol, (2) DNA, (3) tubulin, and (4) inosine-5'-monophosphate dehydrogenase (IMPDH). Created, in part, with Biorender.com.

Screen of synthetic library of drug-like small molecules identified 234 hits

With the objective of identifying new cancer therapeutics, I therefore expanded our search by screening a library of novel, synthetic, drug-like compounds to identify regulators of nucleolar number. First, however, given the poor Z-prime values obtained in the pilot screen for increased nucleolar number due to a low PE among some treatments, I selected 3 of the top hits to re-screen as new positive controls. The 3 hits included, oxiconazole, butoconazole, and melphalan, which all yielded a NPE ≥100 and were therefore promising candidates. Re-screening, however at several different concentrations for each compound, revealed that only melphalan yielded positive Z-prime values and a high signal to background (S/B; Table 4-6). Mitomycin C, however, was included in the experiment for comparison and yielded similar results. As a result, I decided to proceed with the original positive control, mitomycin C (250 nM), with which to expand our search for novel small molecule regulators of nucleolar number.

The high-throughput screen for novel small molecule regulators of nucleolar number revealed 202 compounds that decrease nucleolar number. I screened 25,246 compounds on 79 plates that contained a synthetic library of compounds enriched in sp^3 tetravalent carbons (3-D) and other physicochemical properties common among known bioactive, therapeutic compounds (Life Chemicals, Inc.). The library was also designed to be void in known pan-assay interference compounds (PAINS). Screening for compounds that cause a decrease in nucleolar number revealed 202 compounds. The mean S/B across all 79 screening plates was 3.17 (range, 1.96 to 5.60) and the mean Z-prime value was 0.53 (range, 0.21 to 0.74), suggesting good separation between the negative (DMSO) and positive control (BMH-21; Figure 4-5, A). As with the FDA-

approved pilot screen, hits were then identified based on a conservative threshold of ≥3 SD from the median NPE of all 25,246 compounds. As a result, compounds that yielded a one nucleolus per nucleus NPE ≥16.8 were considered a hit, yielding 202 hits with a mean percent viability of 68.1 (range, 6.2 to 354.7; Figure 4-5, B-D; Appendix VII). As with the pilot screen for decreased nucleolar number, this screen was robust and identified 234 novel small molecular regulators of nucleolar number with the potential to harbor antineoplastic activity.

The screen for novel small molecules that cause an increase in nucleolar number revealed 32 compounds. Again, however, Z-prime calculation of the screen controls revealed a less than robust screen. While the mean S/B across the 79 screening plates was strong, 2.38 (range, 1.15 to 3.46), the mean Z-prime value was -0.39 (range, -6.70 to 0.41) suggesting poor separation of the controls due to variability in PE of mitomycin C, at least on some assay plates (Figure 4-6, A). The majority of screening plates, however, yielded relatively consistent Z-prime values >0, except for a few of the early plates and a later batch of plates. I therefore decided again to proceed with caution in evaluating the results for increased nucleolar number. Hits were identified as those that yielded a NPE ≥3 SD from the median NPE of all 25,246 compounds. As a result, compounds that yielded a ≥5 nucleoli per nucleus NPE ≥139.9 were considered a hit, yielding 32 hits with a mean percent viability of 81.3 (range, 24.3 to 155.0; Figure 4-6, B-D; Appendix VII). While some of these hits may again be false positives due to the poor screening statistics, several may still be valuable novel regulators of nucleolar number and worth including in validation studies.

In conclusion, the screen of a synthetic library of drug-like compounds was effective in identifying 234 compounds that regulate nucleolar number. As observed in the pilot screen of FDA-approved drugs, the screen for decreased nucleolar number was more robust with favorable and reproducible Z-prime values, while the screen for increased nucleolar number was more variable. The one nucleolus per nucleus NPE was also more successful in the number of compounds it identified, uncovering 202 compounds. However, while the ≥5 nucleoli per nucleus NPE identified only 32, each compound yielded an NPE greater than the positive control (NPE≥100). Given the high percentage of antineoplastic compounds identified in the pilot screen by screening for regulators of nucleolar number, these results are promising candidates for the discovery of novel antineoplastic compounds and necessitate validation and further evaluation.

Table 4-6. Summary statistics of candidate positive controls for increased nucleolar number. Top hits from the pilot screen of FDA-approved drugs were re-screened at three different concentrations. Signal-to-background (S/B), Z-prime values, and percent viability were calculated to evaluate suitability as a new control and compared to statistics from the current control, mitomycin C (in bold).

Candidate	Concentration (μM)	S/B	Z-prime	Percent viability (relative to DMSO)
Mitomycin C	**0.25**	**3.9**	**0.26**	**35.8**
Melphalan	20	4.3	0.17	16.8
Melphalan	10	4.7	0.14	20.9
Melphalan	5	2.7	-0.26	35.4
Oxiconazole	20	1.6	-1.63	62.1
Oxiconazole	10	1.7	-0.82	84.6
Oxiconazole	5	1.4	-1.74	100.6
Butoconazole	10	1.8	-1.05	65.2
Butoconazole	5	1.4	-2.08	98.7
Butoconazole	2.5	1.5	-1.78	106.2

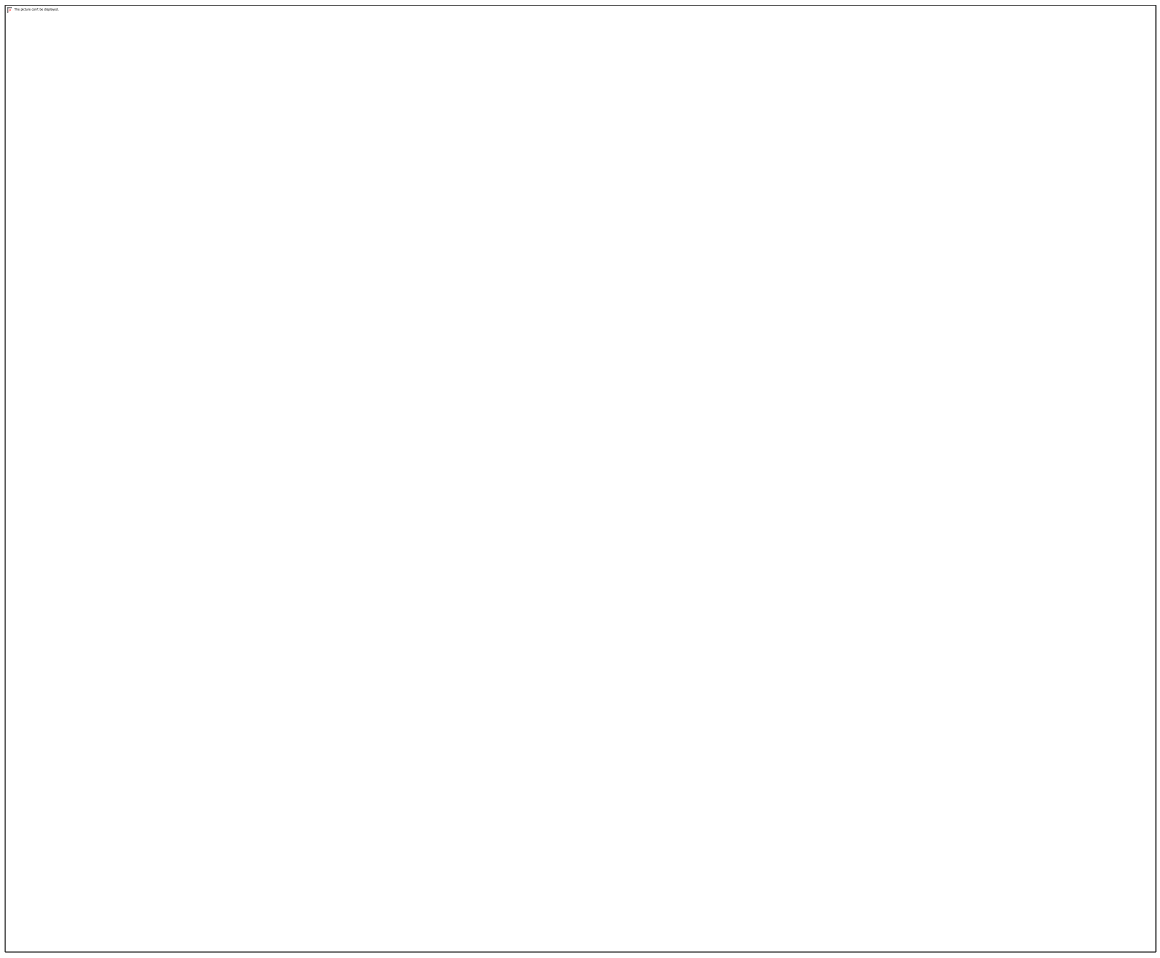

Figure 4-5. High-throughput screen of a synthetic library of drug-like compounds identified 202 hits that decrease nucleolar number.

(A) Z-prime values across all 79 screening plates. The mean Z-prime value was 0.53 (range, 0.21 to 0.74). A Z-prime >0 suggests separation between the positive and negative controls and ≥0.5 is a robust screening assay (black dashed line).

(B) Distribution of the normalized percent effect (NPE) for each of the 25,246 compounds. Threshold used to define hits was ≥3 standard deviations from the median NPE (red dashed line) or NPE ≥16.8. Screen hits are compounds (black dots) above the red dashed line.

(C) Percent viability relative to the one nucleolus per nucleus NPE. Each dot represents a hit. Mean percent viability of the hits was 68.1% relative to DMSO (range, 6.2 to 354.7). (D) Representative images of the controls and top hits yielding an increase in the percentage of cells with one nucleolus per nucleus. DMSO=negative control and BMH-21=positive control. Top hits are represented.

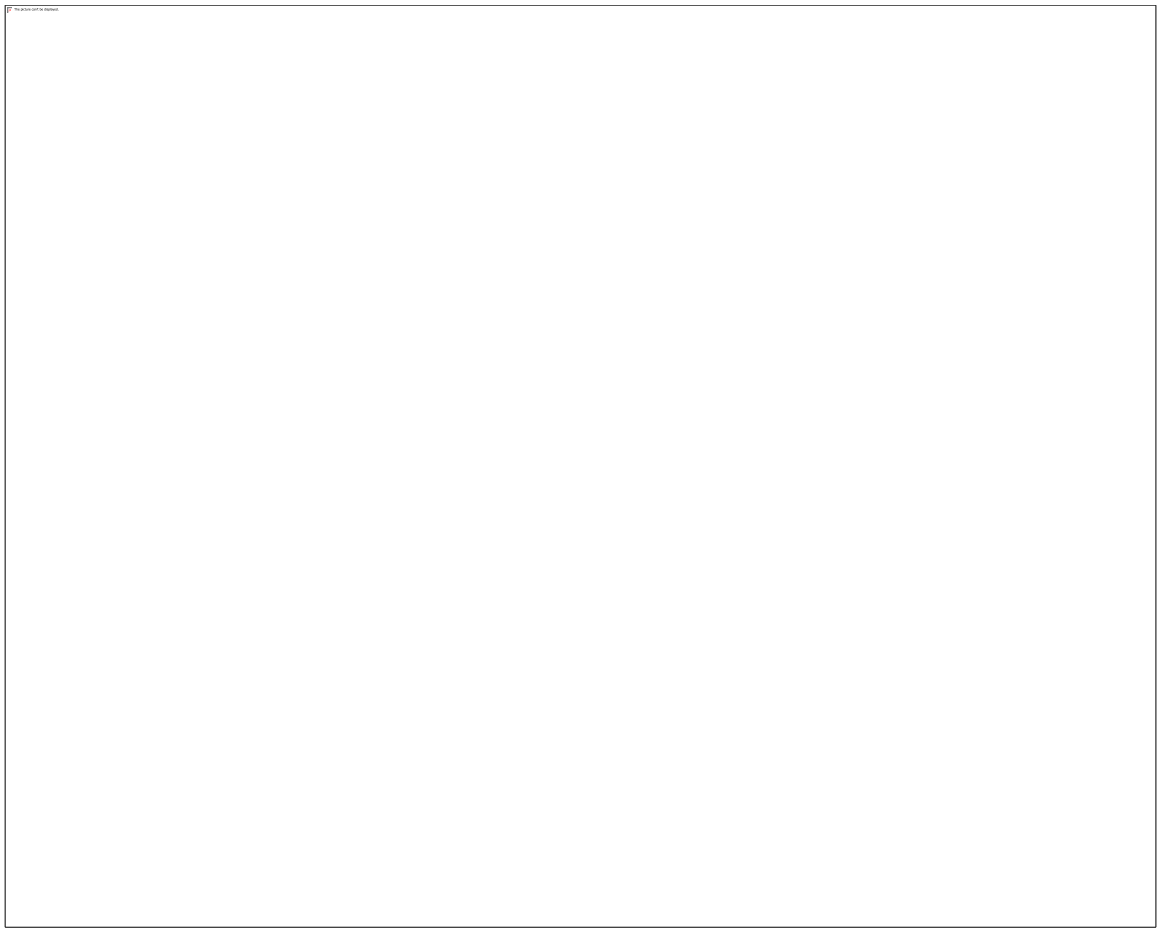

Figure 4-6. High-throughput screen of a synthetic library of drug-like compounds identified 32 hits that increase nucleolar number.

(A) Z-prime values across all 79 screening plates. The mean Z-prime value was -0.39 (range, -6.70 to 0.41). A Z-prime >0 suggests separation between the positive and negative controls and ≥0.5 is a robust screening assay (black dashed line).

(B) Distribution of the normalized percent effect (NPE) for each of the 25,246 compounds. Threshold used to define hits was ≥3 standard deviations from the median NPE (red dashed line) or NPE ≥139.9. Screen hits are compounds (black dots) above the red dashed line.

(C) Percent viability relative to the ≥5 nucleoli per nucleus NPE. Each dot represents a hit. Mean percent viability of the hits was 81.3% relative to DMSO (range, 24.3 to 155.0).

(D) Representative images of the controls and top hits yielding an increase in the percentage of cells with ≥5 nucleoli per nucleus. DMSO=negative control and mitomycin C=positive control. Top hits are represented.

Re-screening revealed 185 high confidence hits

The Baserga lab's unique screening approach identified several hundred compounds required to maintain typical numbers of nucleoli in cells. Furthermore, analysis of the FDA-approved drug hits revealed several antineoplastic compounds. Together, these data suggest that the hits identified in the screen of the synthetic, drug-like library are promising novel antineoplastic drug candidates. To identify a promising subset of compounds to investigate for antineoplastic potential, I validated each hit and its ability to yield the initially observed effect on nucleolar number. To validate the hits, I re-screened each hit from both the FDA-approved drug libraries and the synthetic drug-like compound library. Re-screening was performed in duplicate and hits were identified based on an average of the negative, DMSO, control wells on the 3 screening plates. The threshold was thus designated as ≥3 SD from the median percent effect (PE) of the negative control (Table 4-7). This change was necessary given that the population of compounds tested are now enriched for compounds known to regulate nucleolar number and therefore setting a threshold based on the median of the screened population of compounds would exclude those with milder, yet still potentially significant effect. Hits were considered validated if they yielded the same phenotype in at least 1 of the 2 replicates.

Of the FDA-approved drug hits, I re-screened 130 compounds. One-hundred and four (104) were compounds that decreased nucleolar number, 26 were compounds that increased nucleolar number, and 10 were compounds discarded prior to re-screening based on a manual review of the images to confirm the quality of the images and presence of the expected phenotype. Of the 120 hits re-screened, 105 were identified as

compounds that yielded the one nucleolus per nucleus phenotype. Interestingly, however, 12 of these compounds were originally designated as hits that caused an increase in nucleolar number. Thus, excluding those, 93 of 104 hits that decreased nucleolar number validated (89%), 84 of which were identified in both replicates (Table 4-8; Appendix VIII). With regard to the hits that caused an increase in nucleolar number, 27 were identified as yielding an increase in nuclei with ≥5 nucleoli. Of these, however, 13 were originally designated as hits that decrease nucleolar number, and therefore 14 of the 26 compounds re-screened validated (54%), of which 11 were identified in both replicates (Table 4-8; Appendix VIII). In all, of the 130 FDA-approved compounds re-screened, 107 showed reproducible activity with a consistent phenotype suggesting a strong approach for identifying novel compounds with antineoplastic potential.

Of the synthetic, drug-like hits, I re-screened 233 compounds. 183 were compounds that decreased nucleolar number, 50 were compounds that increased nucleolar number, and 1 was discarded based on a manual review of the images. Of the 183 hits re-screened that yielded a decrease in nucleolar number, 157 were identified as compounds that yielded the one nucleolus per nucleus phenotype, 11 of which were originally designated as hits that yielded an increase nucleolar number. Excluding those hits that switched designation, 147 hits validated (80%), 92 of which were identified in both replicates (Table 4-8; Appendix VIII). With regards to the hits that increased nucleolar number, the reproducibility of these compounds was poor. Strikingly, of the 50 hits re-screened, only 8 yielded an increase in the percentage of nuclei with ≥5 nucleoli, and all 8 were originally designated as hits that caused a decrease in nucleolar number. As a result, no hits from the initial screen that were designated to increase nucleolar

number validated (Table 4-8). In reviewing data from the original screen, all but 1 of the hits that caused an increase in nucleolar number came from the same 2 assay plates. The Z-prime values for these two plates were, -1.53 and -6.7, which suggests that the positive control (100 PE) was not significantly different from the negative control (0 PE). Because compounds are normalized to the controls screened on the same plate, this could cause some compounds on plates with poor Z-prime values to have exaggerated NPE values relative to compounds on plates with good Z-prime values and lead to false positives. This may likely explain the lack of reproducibility among hits that increased nucleolar number and suggests that this dataset should be re-analyzed following the removal of plates with poor Z-prime values in order to identify true positive hits. In all, re-screening the synthetic, drug-like library of compounds resulted in the identification of 147 novel compounds that have a reproducible effect nucleolar number.

Finally, in addition to validation by identifying hits that yield reproducible effects on nucleolar number, I also considered viability in order to identify a high confidence subset of hits to investigate for putative antineoplastic potential. In this analysis, hits were discarded if viability was <10% between the two replicates. The rationale for discarding hits with low viability is to ensure an adequate population of cells with which to calculate the PE on nucleolar number. Furthermore, our objective is to identify drugs that effect cancer cell viability more than normal cell viability and since MCF10A cells are not derived from cancer, a viability filter seems appropriate. Using this threshold, among the 107 validated hits identified in the re-screening of the FDA-approved drugs, 59 were discarded due to low viability (Table 4-8; Appendix VIII). This left 48 high confidence hits, and of those, 39 decreased nucleolar number and 9 increased nucleolar number.

Among the 147 validated hits identified in the re-screening of the synthetic, drug-like compounds, 10 were discarded due to low viability (Table 4-8; Appendix VIII). This left 137 high confidence hits, and of those, all 137 decreased nucleolar number. In all, by re-screening hits and applying reproducibility and viability filters I identified 185 high confidence compounds that regulate nucleolar number and that may harbor antineoplastic potential.

Table 4-7. Designated thresholds to identify hits in the validation re-screening assays. Two replicates were performed, each with their own set of thresholds. Thresholds were set at the median of the DMSO percent effect (PE) for each phenotype +3 standard deviations (SD). Hits with a percent effect ≥ the designated threshold were considered a validated hit. DMSO=negative control.

Replicate	DMSO one nucleolus per nucleus PE (median + 3SD)	DMSO ≥5 nucleoli per nucleus PE (median + 3SD)
1	14.0	26.6
2	9.1	52.8

Table 4-8. Number of high confidence hits identified by re-screening all hits in duplicate and applying reproducibility and viability filters. Compounds were considered high confidence hits if they yielded the same phenotype in at least 1 of the 2 replicates ("validated"). Hits were also included if the mean viability of the 2 replicates was >10%.

Screen	Phenotype (1/≥5)	No. of hits re-screened	No. of hits validated	No. of hits validated in both replicates	No. of hits with mean viability <10%	Total no. of high confidence hits
FDA-approved drugs	1	104	93	84	54	39
FDA-approved drugs	≥5	26	14	11	5	9
Synthetic drug-like compounds	1	183	147	92	10	137
Synthetic drug-like compounds	≥5	50	0	0	0	0

Cluster analysis reveals diverse structures among the high confidence hits

High-throughput screening for regulators of nucleolar number identified 185 high confidence compounds, 137 of which are novel, synthetic, drug-like compounds with no known medical use or molecular target. Due to the large number of compounds identified, to help select compounds for further evaluation, I decided to perform a chemical structure cluster analysis to determine whether there were any structural similarities shared among the hits. Using the DataWarrior software [OSIRIS (Sander et al., 2015)], I performed the Cluster Compounds analysis to identify structural clusters among the 137 high confidence hits from the synthetic, drug-like compounds library. Compounds were analyzed based on the Simplified Molecular Input Line Entry System (SMILES) code structure, and the number of clusters present in the dataset were identified.

To determine whether screening for changes in nucleolar number identified compounds with high structural similarity, I performed the cluster analysis based on a threshold of ≥80% similarity. This initial analysis of the 137 high confidence hits from the synthetic drug-like library returned 98 clusters, suggesting few compounds with highly similar structural features (Table 4-9). While initially striking given the shared effect on nucleolar number for each compound, it is common in order to enhance discovery for curated compound libraries to be designed to limit compounds with a high degree of structural similarity [≥85 similarity; (Martin et al., 2002)]. As a result, I repeated the cluster analysis with two additional thresholds, ≥65% and ≥50% similarity. Clustering based on a ≥65% similarity revealed 47 clusters, 20 of which included just one compound; and, at a threshold of ≥50% similarity, 11 clusters were revealed, 3 of which

included just a single compound. Furthermore, at the latter threshold, one cluster included 75 compounds or nearly 55% of the dataset. Taken together, there is little similarity among the high confidence compounds identified in the synthetic drug-like compound screen, thus further analysis of these clusters is necessary to help identify candidate compounds for exploring antineoplastic potential.

In an attempt to gain additional information on the 137 high confidence compounds identified by screening the synthetic drug-like library, I also evaluated the high confidence compounds identified in the screen of FDA-approved drugs. Interestingly, structure cluster analysis alone on the 48 high confidence FDA-approved drugs revealed similar results. At a similarity threshold of ≥80%, 40 clusters were identified, suggesting very little structural similarity among the FDA-approved drugs hits that regulate nucleolar number (Table 4-9). Decreasing the threshold to ≥50% similarity, only reduced the number of clusters to 23, with 15 including just a single drug. Finally, I decided to evaluate the synthetic, drug-like hits together with the FDA-approved drug hits. Because more about the mechanisms underlying the FDA-approved drugs are known, any clusters containing both an FDA-approved drug and a synthetic, drug-like compound could be informative. In this analysis of the 185 total high confidence compounds, 138 clusters were identified at a ≥80% similarity threshold, 82 were identified at a ≥65% similarity threshold, and 31 were identified at ≥50% similarity threshold (Table 4-9; Appendix VIII). Among the 31 clusters including drugs with ≥50% similarity, 5 clusters contained both FDA-approved drug hits and the synthetic drug-like hits. Interesting clusters from this analysis are cluster 3 and cluster 11. Cluster 3 is the largest with 73 synthetic, drug-like compounds and 7 FDA-approved drugs, including

antineoplastic mitotic inhibitors and antifungal metal ion chelators. Cluster 11 contained 4 compounds, 3 synthetic compounds and the FDA-approved translation inhibitor, cycloheximide. In all, analyzing the FDA-approved drugs together with the synthetic, drug-like compounds revealed limited structural similarities between the two sets of compounds, and further reinforced that the synthetic, drug-like library contains diverse and novel compounds that may lead to the discovery of novel cancer therapeutics.

Table 4-9. Number of compound clusters identified among the high confidence hits using different structure similarity thresholds. Cluster analysis was performed in DataWarrior software based the Simplified Molecular Input Line Entry System (SMILES) code-derived structure.

Screen	No. of high confidence compounds analyzed	No. of clusters (≥80% similarity)	No. of clusters (≥65% similarity)	No. of clusters (≥50% similarity)
FDA-approved drugs	48	40	35	23
Synthetic drug-like compounds	137	98	47	11
Combined	185	138	82	31

DISCUSSION

To identify putative new cancer therapeutics, I performed two high-throughput screens for small molecules that regulate nucleolar number in MCF10A cells. In a pilot screen of nearly 4,000 FDA-approved drugs, I identified 140 compounds that impact nucleolar number, the majority of which decreased the percentage of nuclei with 2-3 nucleoli and increased the percentage of nuclei with just a single nucleolus. Bioinformatic analysis of these drugs revealed that several are antineoplastic agents used in the treatment of cancer, suggesting that regulators of nucleolar number are promising targets for cancer therapeutics. I therefore expanded the search for regulators of nucleolar number by screening a curated collection of approximately 25,000 synthetic drug-like compounds and uncovered 234 novel small molecules that alter nucleolar number. Re-screening of both drug libraries to test for reproducibility and viability ≥10% led to the identification of 185 high confidence compounds, several of which may harbor antineoplastic activity. This screening campaign was thus successful as it revealed several small molecular compounds that regulate nucleolar number and that have putative drug development potential.

Antineoplastic compounds were the most frequently identified compounds in the screen of FDA-approved drugs, even when filtering from the analysis the compounds that were included more than once in screened libraries. Some of the more common molecular targets for these drugs included tubulin and DNA. The mechanism underlying targeting tubulin in cancer therapeutics lies in the stabilization of microtubules and impairing mitosis in actively dividing cells or neoplasms (Mukhtar et al., 2014; Zhou and Giannakakou, 2005). These data suggest a strong interdependence between microtubule

dynamics and nucleolar biology, that may be related to the dissolution and reformation of nucleoli that occurs during mitosis (Hernandez-Verdun, 2011). The targeting of DNA on the other hand included compounds that are either intercalators or crosslinking agents, both leading to impaired replication and RNA synthesis. The preclinical cancer therapeutic, BMH-21, that specifically targets RNAPI transcription is also a DNA intercalator and was the positive control for increased nucleolar number in these screens. While structure analyses clustered few novel compounds with drugs known to function through interactions with tubulin or DNA, this does not rule out the possible identification of novel classes of tubulin and DNA-targeting drugs. Thus, screening for changes in nucleolar number identified several antineoplastic drugs, including modulators of tubulin dynamics and DNA replication, and further validates the approach of screening novel compounds for effects on the nucleolus in order to identify novel cancer therapeutics.

While the structure analysis clustered many of the FDA-approved drug hits together, the synthetic, drug-like hits often formed distinct clusters. While it is possible that the synthetic drug-like hits may represent novel classes of compounds that target the same molecular targets revealed by the FDA-approved drug hits, it is also likely that these compounds target different proteins and ones that specifically regulate nucleolar function. Prior screening for changes in nucleolar number using a genome-wide siRNA approach identified several hundred proteins required for maintaining typical nucleolar numbers [(Farley-Barnes et al., 2018); Chapter 2-3]. Follow up biochemical studies revealed that depletion of both hits that decrease and increase nucleolar number, caused defects not only in protein synthesis, but also in RNAPI transcription or pre-rRNA

processing (and in some cases, both). It is, however, exciting to speculate that the targeting of tubulin and/or other molecular targets revealed by the bioinformatic analysis, like ergosterol and the Na+/K+ ATPase may also regulate ribosome biogenesis. In fact, there is a literature on the potential of repositioning cardiac glycosides as cancer therapeutics (Newman et al., 2008; Prassas and Diamandis, 2008). Furthermore, the recent discovery that the cardiovascular drug and HMG-CoA inhibitor, cerivastatin sodium (which was also a hit in our screen), inhibits RNAPI (Tan and Awuah, 2019), acts as independent validation. Additional validation includes the prevalence of the vinca alkaloid cancer drugs among the screen hits [vincristine, vinblastine, vinorelbine, (Johnson et al., 1963; Martino et al., 2018), and literature proposing antihelmintics, like mebendazole, as putative cancer therapies although further research on clinical efficacy and safety are required (Laudisi et al., 2020; Mezzatesta et al., 2020). In all, these data suggest that while some of the novel compounds identified in this screen may be targeting tubulin, DNA or topoisomerases, it is also possible that these compounds target proteins that regulate ribosome biogenesis, which have not yet been fully explored as therapeutic targets.

Finally, the screen for small molecule regulators of nucleolar number has revealed confounding results regarding the putative mechanisms underlying increased versus decreased nucleolar number. The Baserga lab has often considered the two phenomena as produced by distinct processes. This understanding is supported by the non-overlapping subset of proteins uncovered in our prior screens using a genome-wide siRNA approach for decreased and increased nucleolar number, respectively [(Farley-Barnes et al., 2018); Chapter 2]. In this study, however, in re-screening to validate reproducibility of the hits

in regulating nucleolar number, 23 compounds were identified as switching from either a compound that decreases nucleolar number to one that increases nucleolar number, or vice versa. This switching phenomenon was even evident in our initial screening to identify positive controls for the screens. For example, BMH-21, at 1 μM caused an increase in the one nucleolus per nucleus PE, whereas at lower concentrations resulted in an increase in the ≥5 nucleoli per nucleus PE (Appendix IV). Mitomycin C, as well, caused an increase in the ≥5 nucleoli per nucleus PE at low concentrations, but at higher concentrations caused an increase in the one nucleolus per nucleus PE (Appendix IV; Table 4-2; Table 4-3). In fact, although mitomycin C was the positive control for the screen for increased nucleolar number, it was also a hit (screened at 10 μM) among the FDA-approved drugs that caused a decrease in nucleolar number (Appendix V). Finally, the clustering analysis of the high confidence compounds based on structural similarities revealed that both subsets of hits can be found in the same clusters (e.g. cluster 2). Taken together, these data suggest that while there are some identifiable differences between the two phenotypes and >80% yielded the same phenotype in subsequent replicate experiments, changes in nucleolar number may be more dynamic and may represent different stages of nucleolar disruption by impacts on nucleolar function.

In conclusion, this high-throughput screening campaign to uncover small molecule regulators of nucleolar number was effective in identifying several hundred compounds that either increase or decrease nucleolar number. Several of these compounds are FDA-approved as cancer therapeutics and suggests that the novel drug-like compounds also identified may too harbor antineoplastic potential. Furthermore, it is known that the assay reports changes in nucleolar number that predict changes in

nucleolar function [(Farley-Barnes et al., 2018); Chapter 2-3], and several cancer therapeutics are reported to have secondary effects on nucleolar activity (Burger et al., 2010; Quin et al., 2014); thus, it is probable that we have identified new compounds that regulate ribosome biogenesis that will be important to test in future studies. Furthermore, this screen has also identified several unexpected drug targets that not only may be promising novel targets for drug discovery programs, but further may lend insight into mechanisms underlying the regulation of nucleolar number and activity. Thus, this screen not only broadens our understanding of what governs changes in nucleolar number, but also revealed several compounds that hold potential as next generation cancer therapeutics.

MATERIALS AND METHODS

Cell culture

As described in Chapter 2, the human breast epithelial cell line, MCF10A (ATCC, CRL-10317), was 2D subcultured in DMEM/F-12 medium (Gibco, 1130-032) supplemented with 5% horse serum (Gibco, 16050), 10 μg/mL insulin (Sigma, I1882), 0.5 μg/mL hydrocortisone (Sigma, H0135), 100 ng/mL cholera toxin (Sigma, C8052), and 20 ng/mL epidermal growth factor (Peprotech, AF-100-15).

High-content screening

The high-content small molecule screening was performed as reported in (Farley-Barnes et al., 2018) with the Yale Center for Molecular Discovery. Cells were imaged on

an IN Cell Analyzer 2200 (Cytiva), which is a widefield, multicolor, fluorescence microscope. 9 fields of view (20X; 665.63 μm x 665.63 μm) were acquired per well and high throughput image analysis was performed using CellProfiler (Carpenter et al., 2006; McQuin et al., 2018) to segment nucleoli based on fibrillarin staining (72B9; (Reimer et al., 1987)) and nuclei based on Hoechst 33342 staining.

Positive control identification

To identify positive controls to use in a high-throughput screen for small molecule regulators of nucleolar number, we tested 25 unique compounds with different mechanisms of action (Table 4-1). All compounds were dissolved in DMSO and tested at eight different concentrations, 20.0 μM, 6.67 μM, 2.22 μM, 741 nM, 247 nM, 82.3 nM, 27.4 nM, 9.14 nM (3-fold dilutions), three times points (24, 48, and 72 hrs), and two cell-seeding densities (1,000 and 2,000 cells/well) in 384-well plates. MCF10A cells were seeded in 30 uL growth medium 24 hrs prior to adding the different compounds or DMSO control (0.1%, final concentration). 30 nL of compounds were dispensed at 1000X by an Echo 550 Acoustic Liquid Handler (Labcyte, Inc.). Following compound addition, plates were incubated at 37° C and 5% CO_2. At 24, 48, or 72 hrs, the plates were then fixed, permeabilized, stained and imaged as described in (Farley-Barnes et al., 2018). For each compound, concentration, time point and seeding density, 3 replicates were performed and 9 fields of view imaged (20X). Select candidates were re-screened at several different concentrations, 16 replicates each (9 fields of view), and Z' statistics were calculated relative to 64 replicates of DMSO (9 fields of view; Table 4-2; Table 4-3). These candidates included BMH-21 (8.8 μM, 4.4 μM, 2.2 μM, 1.5 μM, 1 μM, 750

nM, and 375 nM) and CX-5461 (30 μM, 20 μM, and 10 μM) for the one nucleolus phenotype, and mitomycin C (14 μM, 7 μM, 3.5 μM, 500 nM, 250 nM, and 125 nM) and topotecan (18 nM, 9 nM, 4.5 nM and 2.3 nM) for the ≥5 nucleoli phenotype.

High-throughput FDA drug screen

FDA-approved compounds were screened in a high-throughput assay for small molecule regulators of nucleolar number. Three libraries comprising a total of 3,923 drugs were screened. The libraries included the MicroSource Pharmakon 1600, Enzo 640 FDA-approved drug, and the Yale Center for Molecular Discovery curated "Tested in Humans" collection. Compounds were screened in MCF10A cells seeded at a cell density of 2,000 cells per well in 13 x 384-well plates. Cells were incubated with 10 μM of each compound dissolved in 0.1% DMSO for 48 hrs, and then fixed and stained to detect nuclei and nucleoli as described in (Farley-Barnes et al., 2018). Nucleolar number per nucleus was quantified using the same CellProfiler pipeline developed in (Farley-Barnes et al., 2018), and a normalized percent effect (NPE) from an average of 9 fields of view (20X) was calculated relative to the average of the 12 negative (PE=0) and 12 positive (PE=100) control replicates included on each screening plate. The negative control was 0.1% DMSO, and the positive controls were BMH-21 (1 μM) for the one nucleolus per nucleus phenotype and mitomycin C (0.25 μM) for the ≥5 nucleoli per nucleus phenotype.

High-throughput synthetic, drug-like screen

Synthetic, drug-like compounds were screened in the same high-throughput assay as performed for the FDA-approved drug pilot screen. The compounds screened were from an Fsp^3-enriched screening library curated by Life Chemicals, Inc. Included in the library were 25,246 small molecules enriched in sp^3 tetravalent carbons (3-D) and other physicochemical properties common among known bioactive, therapeutic compounds, including molecular weight <450 Da and ClogP values <4 (Lipinski, 2000, 2004; Lovering et al., 2009). The library was also curated to limit common pan-assay interference compounds (PAINS).

Three (3) top hits from the FDA-approved pilot screen for increased nucleolar number were re-screened to test for a new positive control following the inconsistent Z-prime values attained in the pilot screen. The three hits included oxiconazole (SML1474, Sigma-Aldrich), butoconazole (SML1663, Sigma-Aldrich), and melphalan (M2011, Sigma-Aldrich), and were tested at three different concentrations (Table 4-6). Screening statistics were compared to mitomycin C and only melphalan yielded comparable results. As a result, mitomycin C was kept as the positive control for increased nucleolar number.

Bioinformatic analysis

The bioinformatic analysis of the FDA-approved pilot screen hits was performed by manual curation of the medical use and molecular target from the KEGG DRUG Database (https://www.genome.jp/kegg/drug/), DrugBank Online (https://go.drugbank.com/), and a review of relevant literature. Compounds with more

than one medical use or molecular target were classified as both, and led to the total number classified exceeding the total number of screen hits.

Cluster Compounds analysis

The Cluster Compounds analysis was performed in the open-source software, DataWarrior [OSIRIS; http://www.openmolecules.org/datawarrior/; (Sander et al., 2015)]. The analysis was performed based on the Simplified Molecular Input Line Entry System (SMILES) code structure produced by DataWarrior and compared to database of 512 predefined structure fragments. Compound clusters were evaluated multiple times using different *Tanimoto* similarity thresholds, 0.8, 0.65, and 0.5 (Bajusz et al., 2015) on each set of screen results separately and combined (Table 4-9).

Chapter 5

Perspectives and future directions

INTRODUCTION

High-throughput screening for changes in nucleolar number has revealed several novel discoveries in the regulation of nucleolar form and function in higher eukaryotes. Here, I asked whether novel factors governing ribosome biogenesis could be identified by investigating regulators of nucleolar number in the human breast epithelial cell line, MCF10A. What I discovered was that, indeed, identifying factors required to maintain typical nucleolar number is a viable approach for identifying factors required for maintaining typical nucleolar function. In Chapter 1, I provided background on the nucleolus, its primary function in ribosome biogenesis, and its association with a panoply of diseases. In Chapter 2, I identified 113 proteins that when depleted cause an increase in nucleolar number that were enriched in cell cycle related proteins, including ones required specifically for faithful progression through S and G2/M phase. In Chapter 3, I discovered that a subset of the proteins identified were also overwhelmingly required for the regulation of RNAPI transcription and protein synthesis. In Chapter 4, based on these discoveries and prior results from our lab (Farley-Barnes et al., 2018), I applied our screening platform to cancer drug discovery and identified several small molecule regulators of nucleolar number. Together, the data presented in this thesis broaden our understanding of the regulation of nucleolar number and provide a foundation for defining novel mechanisms and proteins required to maintain nucleolar form and function.

Several novel discoveries have thus been made, however several questions still remain. While it is clear that nucleolar number artificially increased by siRNA depletion overwhelmingly predicts defects in RNAPI transcription and protein synthesis, the

mechanisms that underly the increase in nucleolar number remain incompletely understood. Other questions stemming from this research include: (1) How do DNA replication, recombination and repair factors contribute to maintaining typical nucleolar form and function?; (2) How do mitosis factors contribute to maintaining typical nucleolar form and function?; and, (3) Are small molecule regulators of nucleolar number effective cancer therapies? In this chapter, I will elaborate on these questions, suggest testable models, and present possible future directions.

Increased nucleolar number reflects changes in RNAPI transcription

siRNA screening for increased nucleolar number has revealed several proteins required for cell cycle progression and RNAPI transcription. These results, however, were based on a functional analysis of only a subset of the 113 high confidence hits. While my initial bioinformatic analysis of the screen hits did not necessarily suggest factors required for ribosome biogenesis or RNAPI transcriptional regulation (Chapter 2), I questioned whether there were other known transcription factors among the screen hits that might suggest novel transcriptional regulators of RNAPI. Thus, using the PANTHER classification system (v16.0; (Thomas et al., 2003)), I identified the screen hits by protein class and performed an overrepresentation analysis to determine whether any of the protein classes were enriched. Although 40 hits could not be defined using this classification system ("undefined"), in this analysis only 1 protein class was significantly enriched among the hits. DNA metabolism protein (PC00009) was enriched 6-fold among the hits (Binomial test with Bonferroni correction for multiple testing; $p<0.05$), and is a sub-class within nucleic acid metabolism protein (PC00171), which was among

the top represented protein classes (Figure 5-1, A; Table 5-1). The discovery of proteins associated with nucleic acid metabolism is not unexpected given that ribosomes are comprised mostly of RNA that are transcribed from DNA. What is striking, however, is that proteins associated with DNA metabolism were not only enriched, but also more abundant relative to proteins associated with RNA metabolism (Figure 5-1, B; Table 5-1). The screen hits associated with DNA metabolism are primarily associated with DNA replication, recombination, and repair, which is consistent with prior bioinformatic analysis (Chapter 2). Furthermore, among these hits, RFC1 and ATAD5 were also tested for functional roles in ribosome biogenesis and identified as repressors of RNAPI transcription (Chapter 3). Thus, while these results were unexpected, together these data support the intriguing connection between DNA-associated processes and nucleolar function.

Proteins associated with RNA metabolism were also identified among the screen hits. Of the hits associated with nucleic acid metabolism, only 4 were associated with RNA metabolism, and they were all unique (Table 5-1). TAF1D is a known RNAPI transcription cofactor, whereas SMG5 is associated with non-sense mediated decay and telomerase function. FAM98A is a regulator of the arginine methyltransferase, PRMT1, and I also identified it as a regulator of RNAPI transcription in my functional analysis (Chapter 3). Finally, GTF2IRD1 may function as a positive transcriptional regulator with the tumor suppressor, retinoblastoma protein, but intriguingly has also been identified in the 7q11.23 deletion associated with Williams-Beuren syndrome (Franke et al., 1999). Williams-Beuren syndrome is a congenital disorder that manifests with craniofacial dysmorphology and cognitive delays that are consistent with features of those with

ribosomopathies (Farley-Barnes* and Ogawa* et al., 2019; Franke et al., 1999). Williams-Beuren syndrome has also previously been suggested to be a putative ribosomopathy based on homology of WBSCR20 and WBSCR22 in the 7q11.23 deletion to yeast proteins, Nol1 and Bud23, respectively (Doll and Grzeschik, 2001; Sondalle and Baserga, 2014). Nol1 is a nucleolar protein and Bud23 is a methyltransferase required for SSU maturation (Black et al., 2020). GTF2IRD1-null mice, however, also show features consistent with William-Beuren syndrome (Tassabehji et al., 2005), and it is intriguing to speculate that as a hit identified in this screen GTF2IRD1 may also contribute to the pathophysiology of the syndrome through a role in ribosome biogenesis. Thus, while proteins associated specifically with RNA metabolism were few, they highlight a range of functions that may be linked to the function of the nucleolus.

Remarkably, also among the top represented protein classes were transcriptional regulators. In the PANTHER protein class analysis, 12 proteins were classified as gene-specific transcription regulators [(PC00264); Figure 5-1, A). Of these, the majority were DNA-binding transcription factors, rather than transcription cofactors (Figure 5-1, C). Manual review of the screen hits also revealed 2 additional "undefined" proteins that are known or probable regulators of transcription (Table 5-2). Included among these proteins are 2 nucleolar proteins based on my analysis in Chapter 2, GZF1 and ZNF678. ZFN678 is a ubiquitously expressed zinc finger protein that has not been reported in the literature (Thul et al., 2017). GZF1, on the other hand, is a zinc finger protein that is also expressed in all tissues and has recently been associated with a form of Larsen syndrome (Patel et al., 2017; Thul et al., 2017). Larsen syndrome is a congenital disorder caused by several genes including FLNB and is associated with joint dislocations and an abnormal facial

appearance, including cleft palate and hearing loss (Patel et al., 2017; Stanley et al., 1988; Zeng et al., 2021). Again, craniofacial dysmorphology is a common clinical feature of the ribosomopathies, as is hearing loss in some patients (Farley-Barnes* and Ogawa* et al., 2019). Together, these data are again intriguing in that, as a hit identified in this screen, GZF1 may regulate RNAPI transcription and contribute to the pathophysiology of the disease.

Several other intriguing transcription regulators were identified among the screen hits. Included among these are putative tumor suppressors, including EBF3 and RBBP1. EBF3, or early B-cell factor, is required not only for B-cell differentiation, but has also been reported to be important for bone development and neurogenesis (Chao et al., 2017; Seike et al., 2018; Sleven et al., 2017). RBBP1, on the other hand, is reported as a putative tumor suppressor through its interaction with the retinoblastoma protein (pRB). pRB is required for cell cycle progression and has been reported to also regulate RNAPI transcription (Giacinti and Giordano, 2006; Voit et al., 1997), suggesting a possible role for RBBP1 in the regulation of RNAPI through pRB. NFYB, on the other hand, was another identified transcription factor among the screen hits; it functions in a trimeric complex that directly regulates c-Myc (Izumi et al., 2001). The myc-family of transcription factors are also reported regulators of ribosome biogenesis and thus NFYB may be a regulator of ribosome biogenesis through its interaction with myc (van Riggelen et al., 2010). Additionally, NFYB depletion has also been reported to inhibit cell cycle progression through G2/M phase and stabilize p53 independent of DNA damage (Benatti et al., 2008). These data suggest activation of the nucleolar stress response, which is concomitant with inhibition of RNAP1, and suggest another possible indirect mechanism

through which NFYB may regulate nucleolar function. Finally, ENY2 was also identified among the transcription factors and is a known RNAPII transcription co-activator through its association with the SAGA complex and others (García-Oliver et al., 2012; Kopytova et al., 2010; Vijayalingam et al., 2016). Interestingly, ENY2 was also a protein that I tested for a role in ribosome biogenesis and identified that depletion caused a significant decrease in not only RNAPI transcription but also protein synthesis. Taken together, these results suggest that although I tested only a subset of screen hits for roles in ribosome biogenesis, given the identification of several transcription factors and cofactors, it is possible there are several more novel regulators of RNAPI transcription among the screen hits waiting to be defined.

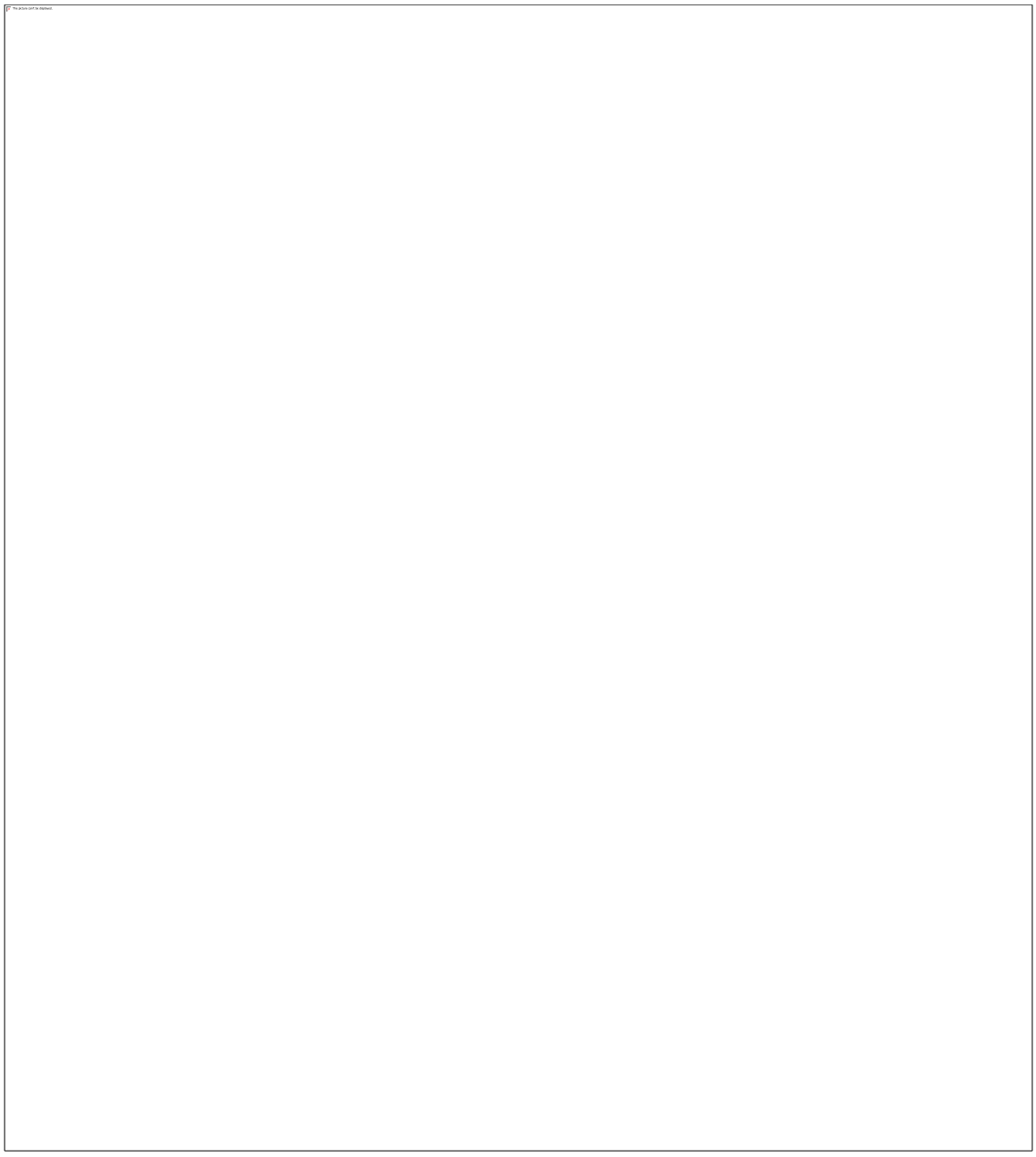

Figure 5-1. Screen hit classification by protein class reveals several proteins involved in nucleic acid metabolism and transcriptional regulation.

(A) Bar graph of the PANTHER protein classifications for the screen hits. 40 hits were undefined in the PANTHER classification system.

(B) Eleven hits (~10%) were classified as proteins associated with nucleic acid metabolism. PANTHER sub-classification revealed proteins associated with both DNA (PC00009) and RNA metabolism (PC00031).

(C) Twelve hits (~11%) were classified as proteins associated with gene-specific transcriptional regulation. PANTHER sub-classification revealed both DNA-binding transcription factors (PC00218) and transcription cofactors (PC00217).

Table 5-1. Screen hits identified as nucleic acid metabolism proteins (PC00171) using the PANTHER classification system by protein class. Sub-classification [DNA metabolism (PC00009) or RNA metabolism (PC00031)] and protein descriptions are included. Descriptions are summarized from GeneCards (Stelzer et al., 2016), and the literature.

Screen hit (HGNC)	Gene name	Nucleic acid metabolism protein sub-class	Description
RFC1	Replication factor C subunit 1	DNA metabolism	Large subunit of the DNA replication factor C complex; PCNA clamp loader
MCM6	Minichromosome maintenance complex component 6	DNA metabolism	Minichromosome maintenance complex subunit; complex is a key component of the pre-replication complex
XRCC5	X-ray repair cross complementing 5	DNA metabolism	Ku protein (80 kDa) that binds DNA in non-homologous end joining DNA repair
LIG3	DNA ligase 3	DNA metabolism	DNA ligase in base-excision DNA repair

ATAD5	ATPase family AAA domain containing 5	DNA metabolism	Large subunit of an alternate DNA replication factor C complex; PCNA clamp unloader
TOPBP1	DNA topoisomerase II binding protein 1	DNA metabolism	Interacts with topoisomerase and supports DNA double strand break repair; aids in rescue of stalled replication forks
GEN1	GEN1 Holliday junction 5’ flap endonuclease	DNA metabolism	Required for Holliday junction resolution in DNA repair by homologous recombination
SMG5	SMG5 nonsense mediated mRNA decay factor	RNA metabolism	Required for nonsense-mediated mRNA decay; also necessary for telomerase reverse transcriptase activity
GTF2IRD1	GTF2I repeat domain containing 1	RNA metabolism	May function as a positive transcriptional regulator with retinoblastoma protein; plays a role in craniofacial and cognitive development, associated with Williams-Beuren syndrome
TAF1D	TATA-box binding protein	RNA metabolism	RNAPI transcription-associated factor containing the TATA-binding protein; member of the SL1 complex

	associated factor, RNAPI subunit D		
FAM98A	Family with sequence similarity 98 member A	RNA metabolism	Regulator of arginine methyltransferase, PRMT1, and contains a putative RNA-binding domain

Table 5-2. Screen hits identified as gene-specific transcription regulators (PC00264) using the PANTHER classification system by protein class. Sub-classification [DNA-binding transcription factor (PC00218) or transcription co-factor (PC00217)] and protein descriptions are included. Two "Undefined" proteins that were not included in the PANTHER classification, but were included based on a manual review of the screen hits. Descriptions are summarized from GeneCards (Stelzer et al., 2016), and the literature.

Screen hit (HGNC)	Gene name	Gene-specific transcriptional regulator sub-class	Description
EBF3	Early B-cell factor	DNA-binding transcription factor	Required for B-cell differentiation, bone development and neurogenesis, and may function as a tumor suppressor
NFYB	Nuclear transcription factor Y beta	DNA-binding transcription factor	Recognizes CCAAT motifs in a trimeric complex; complex regulates MYC and also interacts with p53
SMAD5	SMAD family member 5	DNA-binding transcription factor	Inhibits proliferation of hematopoietic progenitor cells through TGF-beta signaling; activated by BMP1 kinase
ZNF219	Zinc finger protein 219	DNA-binding transcription factor	Krüppel-like zinc finger protein; Repressor of HMGN1 expression

ZNF678	Zinc finger protein 678	DNA-binding transcription factor	Data deficient; mainly localized to cytosol and mitochondria, but also nucleoli (Thul et al., 2017)
LCORL	Ligand dependent nuclear receptor corepressor-like	DNA-binding transcription factor	May function in spermatogenesis; associated with measures of height (Carty et al., 2012)
ENY2	Enhancer of yellow 2 homolog	DNA-binding transcription factor	Transcriptional co-activator through association with the SAGA complex and others
IRF2BP1	Interferon regulatory factor 2 binding protein 1	DNA-binding transcription factor	Transcriptional corepressor in a IRF-2 dependent manner; may also have E3 ligase activity
GZF1	GDNF-inducible zinc finger protein 1	DNA-binding transcription factor	Transcriptional repressor that binds the GZF1 responsive element; associated with joint laxity, short stature and myopia (Patel et al., 2017)

NR0B2	Nuclear receptor subfamily 0 group B member 2	DNA-binding transcription factor	Orphan nuclear receptor; inhibits estrogen receptor function
RBBP8	Retinoblastoma binding protein 8	Transcription cofactor	Leukemia and tumor suppressor that interacts with the retinoblastoma protein
LDB1	LIM domain binding 1	Transcription cofactor	Binds LIM domain in LIM domain-containing transcription factors; acts with LMO2 in red blood cell development
KRBA1	KRAB-A domain containing 1	Undefined	Data deficient; Krüppel-associated box proteins are transcriptional repressors
TAF1D	TATA box binding protein-associated factor RNAPI D (41 kDa)	Undefined	RNAPI transcription-associated factor containing the TATA-binding protein; member of the SL1 complex

An interaction network of the high confidence screen hits also revealed several intriguing proteins that were not selected as part of my functional analysis. An interaction network was generated in STRINGdb, using a medium confidence threshold and MCL clustering (inflation parameter=2; Figure 5-2). This analysis revealed 12 distinct clusters of proteins representing 44 of the 113 hits. As expected, the largest clusters were mitosis and DNA replication, recombination, and repair factors, as determined from my bioinformatic analysis in Chapter 2. However, in addition to these proteins, other small protein clusters stood out. MAN1A1 and PMM2 are interacting proteins associated with mannose metabolism and were also uncovered in screens identifying regulators of nucleolar size (Neumuller et al., 2013). PMM2/Sec53 was identified in *S. cerevisiae* and MAN1A1/alpha-Man-I was identified in *D. melanogaster*, together supporting a putative novel role for glycoprotein biosynthesis in the regulation of nucleolar form and function. Additionally, the interacting proteins SKP1 and CUL1 are also intriguing. These two proteins are both members of the Skp1-Cul1-Fbox protein (SCF) E3 ubiquitin ligase complex required for cell cycle progression from late G1 through anaphase (Nakayama and Nakayama, 2006). Although no SCF-associated Fbox proteins were identified among the screen hits, the association with progression through S and G2/M phase are consistent with the cell cycle defects observed when screen hits were depleted. Finally, a cluster of 3 interacting proteins, SMG5, WRAP53, and ZNF219, is also interesting in that SMG5 and WRAP53 are both associated with telomerase activity. In fact, WRAP53 is an essential component of the telomerase enzyme. Furthermore, depletion of WRAP53 led to a significant decrease in both RNAPI transcription and protein synthesis. A link between telomeres and the nucleolus is tantalizing given the relatively close physical

proximity between the telomeres and the rDNA arrays on the short arms of the acrocentric chromosomes. While ZNF219 has not been reported to be associated with telomerase function its interaction with this cluster of proteins suggests perhaps an associated role that links telomerase function to nucleolar function. In all, analyzing the screen hits as an interaction network highlights clusters of proteins that may otherwise have been overlooked and suggests intriguingly cellular functions that may integral to the regulation of ribosome biogenesis.

In conclusion, several intriguing proteins were identified as important for the maintenance of typical nucleolar numbers. While the majority of these hits were not tested in the screen validation assay, of the 20 hits that were tested, 19 or 95% validated. That being said, prior to follow up on any of these hits, the appropriate validation should be performed to rule out potential off-target effects that can be common with siRNA-mediated knockdown. Once validated, however, screen hits beyond the initial subset tested in Chapter 3 hold significant promise in revealing proteins and novel mechanisms required for the nucleolar function of ribosome biogenesis.

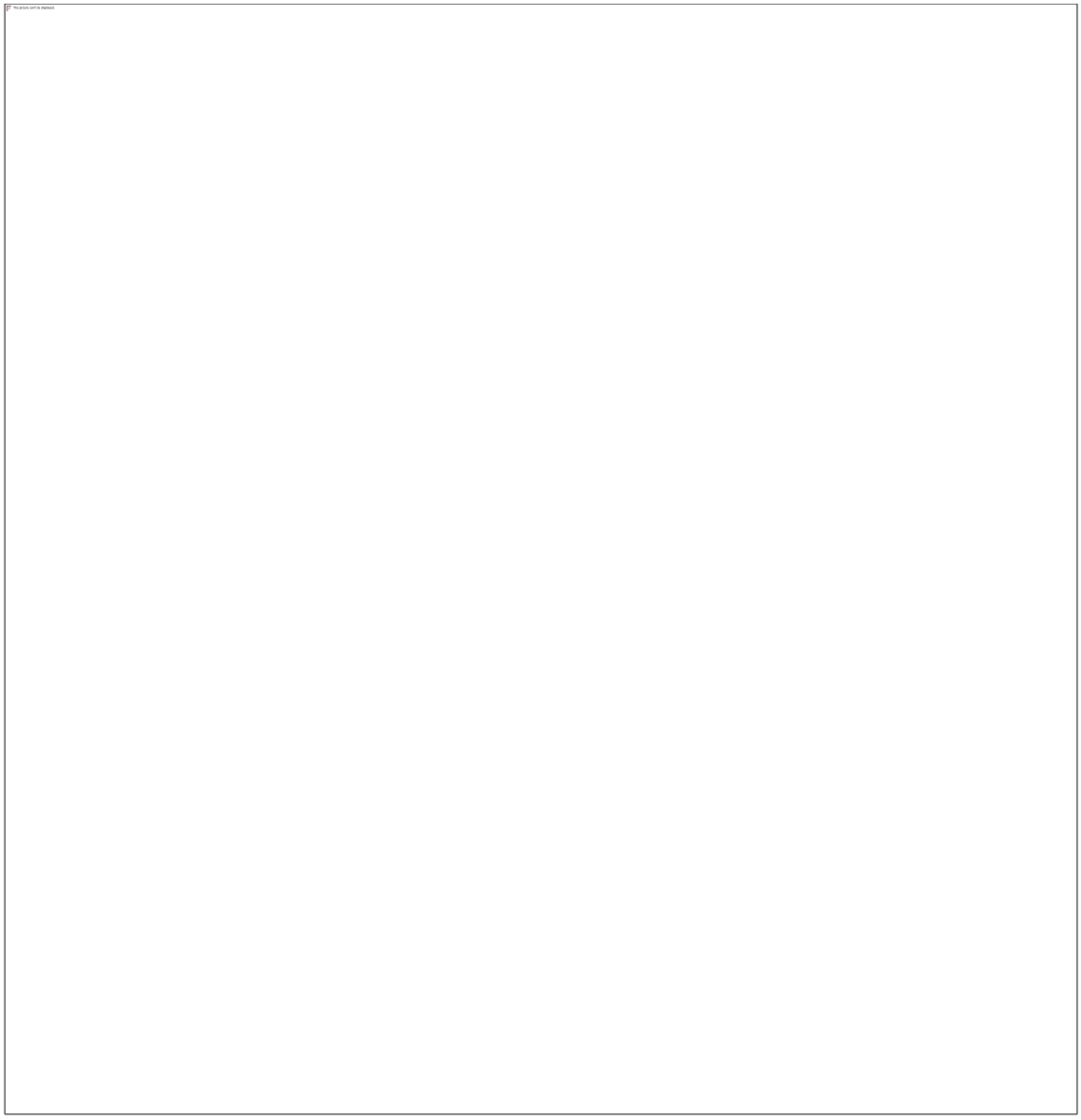

Figure 5-2. Interaction network of high confidence screen hits that, when depleted, cause an increase in nucleolar number. Interaction network was generated in STRINGdb, using a medium confidence threshold and MCL clustering (inflation parameter=2) revealing 12 clusters. Screen hits that did not interact with other screen hits are not shown. Mitosis

(red circle) and DNA replication, recombination, & repair (yellow circle) clusters are highlighted.

What mechanism underlies the increase in nucleolar number?

Screening for increased nucleolar number has revealed several proteins required for cell cycle progression and RNAPI transcription, yet the mechanisms underlying the change in number remains unclear. I now know that several screen hits, but not all, are required for S and G2/M phase progression (Figure 5-3; Table 5-3). I also know that the increased number of nucleoli observed is largely driven by cells in G2/M phase of the cell cycle and cells with ≥5 nucleoli exhibit significantly larger nuclei. Furthermore, of a subset of hits tested, the majority regulate RNAPI transcription, and consequently global protein synthesis (Table 5-3). Yet, how failures in cell cycle progression and RNAPI transcription regulate nucleolar number remains unclear. Two leading models emerge based on the discoveries described herein, and will be described in the following two sections.

Figure 5-3. Model illustrating our current understanding of increased nucleolar number based on discoveries reported in this thesis. Observed increases in nucleolar number are linked to RNAPI transcription and the cell cycle. Depletion of several proteins required for S and G2/M phase progression resulted in an increase in the percentage of nuclei with ≥5 nucleoli (solid-line rectangle). The increase is largely driven by cells in G2/M phase of the cell cycle (dashed-line rectangle). Consistent with the latter, nuclear volume is significantly increased in nuclei with ≥5 nucleoli. Blue dashed circles=nuclei; Pink solid circles=nucleoli.

Table 5-3. Expanded summary of discoveries on the subset of screen hits that cause an increase in nucleolar number. Depleted hits were tested for defects in RNAPI transcription, pre-rRNA processing, global protein synthesis, p53 stabilization, and cell cycle defects inferred by accumulation of nuclei in a particular phase. Inc=Increased; Dec=Decreased; Y=Yes; N=No; Dash ("-")=No significant change or no defect detected.

Screen hit (HGNC)	RNAPI transcription (Inc/Dec)	Pre-rRNA processing defect (Y/N)	Global protein synthesis (Inc/Dec)	p53 stabiliz-ation (Y/N)	Cell cycle defect
siATAD5	Inc	-	Dec	-	-
siCDCA8	-	-	Dec	-	>4N
siENY2	Dec	-	Dec	-	S; >4N
siFAM98A	Dec	-	-	-	S
siH1-10	Dec	-	Dec	-	-
siINCENP	Dec	-	Dec	-	G2/M; >4N
siINKA1	-	-	Dec	-	>4N
siKIF11	Dec	-	Dec	-	G2/M
siMDN1	Dec	Y	Dec	-	-
siRACGAP1	Dec	-	Dec	Y	>4N
siRFC1	Inc	-	Dec	Y	S
siSTK24	-	-	Dec	-	S
siTPX2	Dec	-	Dec	-	G2/M; >4N
siCCN4	Dec	-	Dec	-	-
siWRAP53	Dec	-	Dec	-	S

What mechanism underlies the increased nucleolar number observed when DNA replication, recombination, and repair factors are depleted?

Proteins required for DNA replication, recombination, and repair, were among some of the most common proteins identified in the screen for increased nucleolar number. Furthermore, depletion of a subset of hits resulted in failures in S phase progression (Chapter 2). The mechanism that underlies the connection between these processes and nucleolar number remain unknown; however, based on results obtained upon depletion of DNA replication and repair proteins in functional assays (Chapter 3), a possible model has emerged. Depletion of RFC1 and ATAD5 both resulted in a significant increase in RNAPI transcription; however, depletion of these proteins was also identified as causing a concomitant decrease in protein synthesis. This suggested the possible model that screen hits associated with DNA replication and repair are important for maintaining genome stability at the replication fork (Figure 5-4). DNA replication at highly transcribed loci can cause conflict and DNA double strand breaks. Thus, maintaining genome stability during DNA replication and repair is important because instability, particularly at the rDNA loci, has been associated with increased rates of recombination, rDNA copy loss, and cancer (Lindstrom et al., 2018; Stults et al., 2009; Xu et al., 2017a). Protective mechanisms, however, have evolved to deal with replication stress (Lindstrom et al., 2018). For instance, the RNAPI transcription termination factor 1 (TTF-1) and a replisome component, TIMELESS (TIM), have been reported to regulate replication fork activity during DNA replication (Akamatsu and Kobayashi, 2015). Thus, I hypothesize that screen hits may encompass another protective mechanism to maintain

genome stability during DNA replication through dynamic regulation of RNAPI at the replication fork.

The proteins identified as screen hits have been localized to the replication fork and nascent chromatin. A recent proteomic analysis using 5-ethynyl-2′-deoxyuridine (5-EdU) labeling and enrichment followed by quantitative mass spectrometry, identified proteins associated with nascent chromatin and the replication fork (Wessel et al., 2019). Comparing the proteins identified in this experiment to the screen hits revealed that 9 screen hits are present at the replication fork (Table 5-4). These data would support a putative role for screen hits in the regulation of RNAPI during DNA replication. Among these hits were RFC1 and ATAD5, further supporting the hypothesis that these proteins may be important for the repression of RNAPI transcription during DNA replication to limit conflict. Furthermore, of the proteins enriched at the replication fork, 148 localize to the nucleolus based on identification in at least one of the three datasets used in Chapter 2 [Appendix IX; (Ahmad et al., 2009; Jarboui et al., 2011; Leung et al., 2006; Thul et al., 2017)]. Interestingly, of these hits, several have previously been reported to regulate RNAPI transcription, including BLM, FANCI, ATM and ATR. ATM and ATR are kinases that regulate the DNA damage response, which includes the transient inhibition of RNAPI during DNA repair (Kruhlak et al., 2007). BLM and FANCI, on the other hand, are reported to decrease RNAPI transcription when depleted. Together, these data suggest not only the localization of screen hits at the replication fork, but also proteins required for the regulation of RNAPI.

DNA repair is important for maintaining genome stability during DNA replication, especially at highly transcribed loci like the rDNA. The existence of a

mechanism to transiently silence RNAPI transcription in response to DNA damage validates this importance. An ATM- and ATR- mediated mechanism has been described that results in the activation and recruitment of proteins required not only to silence RNAPI, but to repair the DNA damage (Ciccia et al., 2014; Korsholm et al., 2019; Kruhlak et al., 2007; Larsen and Stucki, 2016; Mooser et al., 2020). As such, several substrates of ATM and ATR have been defined, and several others have been predicted. In one study aimed at defining all the substrates of ATM and ATR in response to DNA damage identified ~700 putative proteins (Matsuoka et al., 2007). I therefore asked whether any of the screen hits were also identified among the putative ATM and ATR substrates in response to DNA damage. Interestingly, 10 screen hits were identified and included among these were RFC1 and ATAD5 (Table 5-4). TOPBP1 was also identified and has already been reported as important for mediating the transcriptional silencing of RNAPI upon DNA damage (Mooser et al., 2020). Finally, KIF11 was another hit identified as a putative ATM or ATR substrate. KIF11 is primarily known for its role in spindle assembly during mitosis (Blangy et al., 1995); however, I have also discovered that depletion of KIF11 leads to a decrease in RNAPI transcription, which begs the question, is KIF11 required for the regulation of RNAPI in response to DNA damage rather than in a mitosis-specific role? These data thus suggest that a subset of screen hits may regulate RNAPI transcription during DNA replication through the ATM- and ATR-mediated response to DNA damage.

Moving forward, it will be important to establish whether DNA damage and replication stress at the rDNA loci might be the cause for the increased numbers of nucleoli that we observe. Furthermore, it will be interesting to ascertain whether other

screen hits also regulate RNAPI transcription and if it is in response to DNA damage during replication. Finally, to link the defects in RNAPI transcription to increased nucleolar numbers, it will be critical to further define nucleoli from these cells. Outstanding questions pertaining to this objective include: (1) Are these nucleoli functional nucleoli with a defined tripartite substructure? And (2), are these nucleoli mature nucleoli that contain multiple NORs or is there just a single NOR per nucleolus? The latter might suggest the disassembly of nucleoli in response to a particular stressor, like DNA damage, or a defect in S phase that manifests in mitosis as a failure in reassembly and discussed in more detail in the next section. Taken together, the increased number of nucleoli that we observe upon depletion of screen hits remains incomplete, but several lines of evidence suggest the phenotype reflects changes in RNAPI transcription and perhaps proteins required for maintaining genome stability at the rDNA loci during replication.

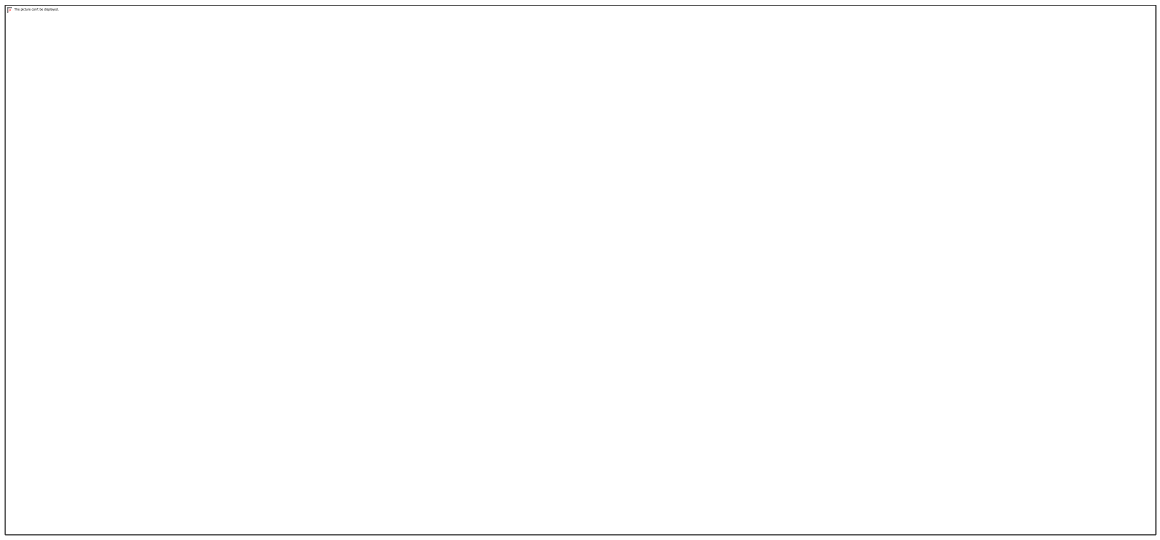

Figure 5-4. Screen hits may be required for maintaining genome stability at the replication fork. Due to the high rate of transcription among the rDNA genes, transcription by RNAPI presents a potential conflict. One hypothesis for the increase in nucleolar number observed upon depletion of screen hits is that the screen hits are required for dynamic regulation of RNAPI during replication to prevent conflict. In the absence of this regulation, the rDNA loci would exhibit genome instability and nucleoli would disassemble and could appear as an increase in nucleolar number.

Table 5-4. Screen hits identified at the replication fork and as substrates of ATM and ATR kinases.

Screen hits at replication fork and nascent chromatin (Wessel et al., 2019)	Screen hits phosphorylated by ATM/ATR in response to DNA damage (Matsuoka et al., 2007)
ATAD5	CASP8AP2
CUL1	GTF2IRD1
LDB1	KIF11
MCM6	MCM6
MDN1	RBBP8
PMM2	RFC1
RFC1	RIMS3
SKP1	STK24
XRCC5	TOPBP1
	TPX2

What mechanism underlies the increased nucleolar number observed when mitosis factors are depleted?

Proteins required for mitosis were also among the most common proteins identified in the screen for increased nucleolar number. Furthermore, depletion of a subset of hits resulted in failures in G2/M phase progression (Chapter 2). The mechanism, however, that underlies the connection between mitosis and increased nucleolar number remains unknown. Yet, based on results obtained from depletion of mitosis proteins in functional assays (Chapter 3), a possible model has emerged. Depletion of KIF11, RACGAP1, TPX2, and INCENP all resulted in a significant decrease in RNAPI transcription and concomitant decrease in protein synthesis. This suggested the possible model that screen hits associated with mitosis are important for the re-initiation of RNAPI transcription following metaphase (Figure 5-5). Nucleoli are highly dynamic organelles during mitosis that not only require the coordinated disassembly and relocalization of pre-rRNA and ribosome biogenesis factors, but also require reassembly upon mitotic exit (Gautier et al., 1992; Hernandez-Verdun, 2011; Savino et al., 2001). Furthermore, in early G1, nascent nucleoli fuse to form mature nucleoli (Hernandez-Verdun, 2011), which might be a consequence of LLPS (Lafontaine et al., 2020), although convincing evidence is still lacking. Failure of nucleoli to fuse upon mitotic exit due to defects during mitosis could lead to the increased nucleolar number observed.

Beyond the functional assays reported in this thesis, currently there is little additional evidence to support a hypothesis for lack of nucleolar fusion upon mitotic exit. Not only are the screen hits not enriched for proteins associated with LLPS, but screen

hits are also not associated with proteins identified as localizing to the chromosomes during mitosis. Proteins with intrinsically disordered regions (IDRs) are thought to be key drivers of LLPS (Lafontaine et al., 2020); yet, in an analysis of proteins in the DisProt database of proteins with IDRs (Hatos et al., 2020) only 4 hits were identified (HYPK, MICA, SMG5, and XRCC5). Additionally, in the recent survey identifying nucleolar proteins associated with the mitotic perichromosomal compartment, 65 proteins were identified and 36 were not previously known to localize to chromosomes (Stenström et al., 2020). A comparison of the screen hits with proteins that localize to mitotic chromosomes reveal 0 overlapping proteins. Interestingly, this study also found that proteins that localize to the perichromosomal compartment are enriched in proteins with intrinsically disordered domains (IDRs). These data are consistent with the fact that few proteins with IDRs were identified among the screen hits. Thus, the proteins identified in this screen may represent a unique subset of proteins that are required for nucleolar form and function.

Moving forward, it will be important to understand whether failure in the re-initiation of transcription during mitosis leads the increased numbers of nucleoli that we observe. The identification of several mitosis-associated hits that when depleted lead to decreased RNAPI transcription supports this putative link. Furthermore, it will be important to ascertain whether the increased nucleolar numbers in fact represent nascent nucleoli or mature nucleoli. A similar set of experiments as proposed in the prior section can answer this question and include determining whether the nucleoli observed contain the tripartite substructure consistent with mature functional nucleoli, and whether a single or multiple NORs are present. Again, if the nucleoli contain only a single NOR, then

these data would support failure in nascent nucleolar fusion. Taken together, the mechanism underlying the increased nucleolar numbers that we observe in cells depleted of screen hits remains incomplete; however, discoveries described herein suggest that the regulation of RNAPI transcription in G2/M phase may be an important contributing factor.

Figure 5-5. Screen hits may be required for the re-initiation of RNAPI transcription during mitosis. In every mitosis, the nucleolus disassembles in late prophase and reassembles in telophase. In prophase, pre-rRNA and processing factors relocate to the chromosomal periphery, also called the perichromosomal compartment. Activation of CDK1-cyclin B inhibits RNAPI transcription by metaphase (red). Inhibition of CDK1-cyclin B by PP1 phosphatases re-initiates RNAPI transcription by telophase (green). In telophase, nucleolar proteins in the perichromosomal compartment condense into prenucleolar bodies (PNB) from which ribosome biogenesis factors are recruited to the competent nucleolar organizer regions (NORs) and, with early processing factors and pre-rRNA, promote nascent nucleolar formation. In early G1, nascent nucleoli fuse to from mature nucleoli. One hypothesis for the increase in nucleolar number observed upon depletion of screen hits is that screen hits are required for re-initiation of transcription during mitosis and when disrupted, results in the failure of nascent nucleoli to mature and fuse. Failure to fuse upon mitotic exit could appear as an increase in nucleolar number.

FC=fibrillar center (green); DFC=dense fibrillar component; GC=granular component. Created with BioRender.com.

Targeting the nucleolus for cancer therapy

The nucleolus holds promise as a target for the development of novel cancer therapeutics. Not only has the nucleolus been associated with cancer for over two hundred years, but an analysis of common cancer therapies has revealed that many impact nucleolar form and function. The screen I performed of FDA-approved drugs for regulators of nucleolar number revealed several drugs used in the treatment of cancer. These results suggest that screening for changes in nucleolar number is an effective strategy for identifying novel cancer therapies. As a result, I expanded the screen to test ~25,000 novel, synthetic compounds which uncovered an additional 234 compounds that regulate nucleolar number. While we know that changes in nucleolar number reflect changes in nucleolar function, this needs to be tested in order to identify a subset of lead compounds with antineoplastic potential.

RNAPI is a promising target for the development of novel cancer therapeutics. Several FDA-approved drugs target RNAPI through non-specific mechanisms, which include drugs like AMD, oxaliplatin, doxorubicin and camptothecin (Ferreira et al., 2020). Furthermore, in the past decade, specific RNAPI inhibitors have been developed that not only show promising preclinical efficacy but have also had positive results in Phase I trials for breast cancer and hematological malignancies. Indeed, the large subunit of RNAPI, RPA194/POLR1A, is highly expressed among a range of cancers and is a prognostic marker specifically in liver, ovarian, and thyroid cancer (Uhlen et al., 2017). Survival analysis based on expression of RPA194/PORL1A, has revealed that patients with tumors that exhibit high RPA194/POLR1A expression had a lower survival

probability (Uhlen et al., 2017). Thus, identifying novel compounds that effectively target RNAPI would be a good strategy for the treatment of cancer. Given that changes in nucleolar number have been successful in identifying novel regulators of RNAPI, moving forward, a secondary screen testing specifically for regulators of RNAPI transcription from among the 185 high confidence compounds would be a good strategy moving forward.

Pre-rRNA processing may also be a promising target for the development of novel cancer therapeutics. While fewer FDA-approved drugs have been demonstrated to regulate pre-rRNA processing, there are still several that have been used in the treatment of cancer, including 5-fluorouracil, flavopiridol, roscovitine, and bortezomib (Burger et al., 2010). These data suggest, that while drugs targeting pre-rRNA processing are not as common, they still may be viable in the development of a novel cancer therapeutic. We know from prior studies that regulators of nucleolar number can also reflect changes in pre-rRNA processing; however, this observation was restricted primarily to proteins that when depleted cause a decrease in nucleolar number. Furthermore, northern blots are the best way to determine impact on pre-rRNA processing and therefore it would be difficult to perform a high-throughput secondary assay to determine whether the screen hits are regulators of pre-rRNA processing. Thus, a more low-throughput survey of a subset of the novel synthetic compounds that cause a decrease in nucleolar number might be the best approach to identify regulators of pre-rRNA processing. Cluster analysis was performed to identify compounds with structural similarities, and based on a threshold of 50% similarity, 11 clusters were revealed among the novel synthetic compounds (Chapter 4). Thus, testing a single compound from each cluster for pre-rRNA processing defects

might be the best approach. Taken together, while identifying regulators of RNAPI transcription may be a highly effective strategy, targeting pre-rRNA may also hold promise for the discovery of novel and effective cancer therapies.

In conclusion, the nucleolus is a fascinating nuclear domain that is integral to a multitude of cellular functions. Screening for changes in nucleolar number has only further highlighted the centrality of the nucleolus by uncovering several novel proteins and small molecules that are associated with a wide range of cellular processes. Furthermore, probing changes in nucleolar number has uncovered novel regulators of nucleolar function, and has led to intriguing hypotheses for the role of these diverse proteins in maintaining typical nucleolar form. Moving forward, however, it will be critical to further validate screen hits through rescue experiments due the off-target effects common among siRNA depletion methods like the siGENOME pools used here. Furthermore, it will be important to develop the model used to study changes in nucleolar number, perhaps through live cell imaging to observe changes in nucleolar number in real time. Overall, the discoveries described herein broaden our understanding of nucleolar biology in higher eukaryotes and provide a foundation for the development of novel and more effective therapeutics for the treatment of cancer.

REFERENCES

Ahmad, Y., Boisvert, F.M., Gregor, P., Cobley, A., and Lamond, A.I. (2009). NOPdb: Nucleolar Proteome Database--2008 update. Nucleic Acids Res *37*, D181-184.

Ajore, R., Raiser, D., McConkey, M., Jöud, M., Boidol, B., Mar, B., Saksena, G., Weinstock, D.M., Armstrong, S., Ellis, S.R., *et al.* (2017). Deletion of ribosomal protein genes is a common vulnerability in human cancer, especially in concert with TP53 mutations. EMBO Mol Med *9*, 498-507.

Akamatsu, Y., and Kobayashi, T. (2015). The Human RNA Polymerase I Transcription Terminator Complex Acts as a Replication Fork Barrier That Coordinates the Progress of Replication with rRNA Transcription Activity. Molecular and Cellular Biology *35*, 1871-1881.

Alberti, S., Gladfelter, A., and Mittag, T. (2019). Considerations and Challenges in Studying Liquid-Liquid Phase Separation and Biomolecular Condensates. Cell *176*, 419-434.

Allen, M.A., Andrysik, Z., Dengler, V.L., Mellert, H.S., Guarnieri, A., Freeman, J.A., Sullivan, K.D., Galbraith, M.D., Luo, X., Kraus, W.L., *et al.* (2014). Global analysis of p53-regulated transcription identifies its direct targets and unexpected regulatory mechanisms. Elife *3*, e02200.

Anastassova-Kristeva, M. (1977). The nucleolar cycle in man. Journal of Cell Science *25*, 103-110.

Andersen, J.S., Lam, Y.W., Leung, A.K., Ong, S.E., Lyon, C.E., Lamond, A.I., and Mann, M. (2005). Nucleolar proteome dynamics. Nature *433*, 77-83.

Andersen, J.S., Lyon, C.E., Fox, A.H., Leung, A.K., Lam, Y.W., Steen, H., Mann, M., and Lamond, A.I. (2002). Directed proteomic analysis of the human nucleolus. Curr Biol *12*, 1-11.

Antoniali, G., Lirussi, L., Poletto, M., and Tell, G. (2014). Emerging roles of the nucleolus in regulating the DNA damage response: the noncanonical DNA repair enzyme APE1/Ref-1 as a paradigmatical example. Antioxid Redox Signal *20*, 621-639.

Aspesi, A., and Ellis, S.R. (2019). Rare ribosomopathies: insights into mechanisms of cancer. Nature Reviews Cancer *19*, 228-238.

Aubert, M., O'Donohue, M.F., Lebaron, S., and Gleizes, P.E. (2018). Pre-Ribosomal RNA Processing in Human Cells: From Mechanisms to Congenital Diseases. Biomolecules *8*.

Awad, D., Prattes, M., Kofler, L., Rössler, I., Loibl, M., Pertl, M., Zisser, G., Wolinski, H., Pertschy, B., and Bergler, H. (2019). Inhibiting eukaryotic ribosome biogenesis. BMC Biology *17*, 46.

Badertscher, L., Wild, T., Montellese, C., Alexander, L.T., Bammert, L., Sarazova, M., Stebler, M., Csucs, G., Mayer, T.U., Zamboni, N., *et al.* (2015). Genome-wide RNAi Screening Identifies Protein Modules Required for 40S Subunit Synthesis in Human Cells. Cell Rep *13*, 2879-2891.

Bajusz, D., Rácz, A., and Héberger, K. (2015). Why is Tanimoto index an appropriate choice for fingerprint-based similarity calculations? Journal of Cheminformatics *7*, 20.

Balakrishnan, R., Park, J., Karra, K., Hitz, B.C., Binkley, G., Hong, E.L., Sullivan, J., Micklem, G., and Cherry, J.M. (2012). YeastMine--an integrated data warehouse for Saccharomyces cerevisiae data as a multipurpose tool-kit. Database (Oxford) *2012*, bar062.

Bartoli, K.M., Jakovljevic, J., Woolford, J.L., Jr., and Saunders, W.S. (2011). Kinesin molecular motor Eg5 functions during polypeptide synthesis. Mol Biol Cell *22*, 3420-3430.

Bassler, J., and Hurt, E. (2019). Eukaryotic Ribosome Assembly. Annu Rev Biochem *88*, 281-306.

Bassler, J., Kallas, M., Pertschy, B., Ulbrich, C., Thoms, M., and Hurt, E. (2010). The AAA-ATPase Rea1 drives removal of biogenesis factors during multiple stages of 60S ribosome assembly. Mol Cell *38*, 712-721.

Beckerman, R., and Prives, C. (2010). Transcriptional regulation by p53. Cold Spring Harb Perspect Biol *2*, a000935.

Benatti, P., Basile, V., Merico, D., Fantoni, L.I., Tagliafico, E., and Imbriano, C. (2008). A balance between NF-Y and p53 governs the pro- and anti-apoptotic transcriptional response. Nucleic Acids Res *36*, 1415-1428.

Bersaglieri, C., and Santoro, R. (2019). Genome Organization in and around the Nucleolus. Cells *8*.

Birnstiel, M.L., Chipchase, M.I.H., and Hyde, B.B. (1963). The nucleolus, a source of ribosomes. Biochimica et Biophysica Acta (BBA) - Specialized Section on Nucleic Acids and Related Subjects *76*, 454-462.

Black, J.J., Sardana, R., Elmir, E.W., and Johnson, A.W. (2020). Bud23 promotes the final disassembly of the small subunit Processome in Saccharomyces cerevisiae. PLOS Genetics *16*, e1009215.

Blander, G., Zalle, N., Daniely, Y., Taplick, J., Gray, M.D., and Oren, M. (2002). DNA damage-induced translocation of the Werner helicase is regulated by acetylation. J Biol Chem *277*, 50934-50940.

Blangy, A., Lane, H.A., d'Herin, P., Harper, M., Kress, M., and Nigg, E.A. (1995). Phosphorylation by p34cdc2 regulates spindle association of human Eg5, a kinesin-related motor essential for bipolar spindle formation in vivo. Cell *83*, 1159-1169.

Boisvert, F.M., Lam, Y.W., Lamont, D., and Lamond, A.I. (2010). A quantitative proteomics analysis of subcellular proteome localization and changes induced by DNA damage. Mol Cell Proteomics *9*, 457-470.

Boisvert, F.M., van Koningsbruggen, S., Navascues, J., and Lamond, A.I. (2007). The multifunctional nucleolus. Nat Rev Mol Cell Biol *8*, 574-585.

Bolze, A., Mahlaoui, N., Byun, M., Turner, B., Trede, N., Ellis, S.R., Abhyankar, A., Itan, Y., Patin, E., Brebner, S., *et al.* (2013). Ribosomal protein SA haploinsufficiency in humans with isolated congenital asplenia. Science *340*, 976-978.

Boutelle, A.M., and Attardi, L.D. (2021). p53 and Tumor Suppression: It Takes a Network. Trends in Cell Biology.

Bowen, M.E., and Attardi, L.D. (2019). The role of p53 in developmental syndromes. Journal of Molecular Cell Biology *11*, 200-211.

Bowman, M., Oldridge, M., Archer, C., O'Rourke, A., McParland, J., Brekelmans, R., Seller, A., and Lester, T. (2012). Gross deletions in TCOF1 are a cause of Treacher–Collins–Franceschetti syndrome. European Journal of Human Genetics *20*, 769-777.

Bradsher, J., Auriol, J., Proietti de Santis, L., Iben, S., Vonesch, J.L., Grummt, I., and Egly, J.M. (2002). CSB is a component of RNA pol I transcription. Mol Cell *10*, 819-829.

Brangwynne, C.P., Mitchison, T.J., and Hyman, A.A. (2011). Active liquid-like behavior of nucleoli determines their size and shape in Xenopus laevis oocytes. Proc Natl Acad Sci U S A *108*, 4334-4339.

Brighenti, E., Trere, D., and Derenzini, M. (2015). Targeted cancer therapy with ribosome biogenesis inhibitors: a real possibility? Oncotarget *6*, 38617-38627.

Brinkley , B.R. (1965). The find structure of the nucleolus in mitotic divisions of Chinese hamster cells in vitro. Journal of Cell Biology *27*, 411-422.

Brown, D.D., and Gurdon, J.B. (1964). Absence of ribosomal RNA synthesis in the anucleolate mutant of *Xenopus laevis*. Proceedings of the National Academy of Sciences *51*, 139-146.

Bruno, P.M., Lu, M., Dennis, K.A., Inam, H., Moore, C.J., Sheehe, J., Elledge, S.J., Hemann, M.T., and Pritchard, J.R. (2020). The primary mechanism of cytotoxicity of the chemotherapeutic agent CX-5461 is topoisomerase II poisoning. Proc Natl Acad Sci U S A *117*, 4053-4060.

Buchwalter, A., and Hetzer, M.W. (2017). Nucleolar expansion and elevated protein translation in premature aging. Nature communications *8*, 328.

Burger, K., and Eick, D. (2013). Functional ribosome biogenesis is a prerequisite for p53 destabilization: impact of chemotherapy on nucleolar functions and RNA metabolism. Biol Chem *394*, 1133-1143.

Burger, K., Muhl, B., Harasim, T., Rohrmoser, M., Malamoussi, A., Orban, M., Kellner, M., Gruber-Eber, A., Kremmer, E., Holzel, M., *et al.* (2010). Chemotherapeutic drugs inhibit ribosome biogenesis at various levels. J Biol Chem *285*, 12416-12425.

Burger, K., Muhl, B., Rohrmoser, M., Coordes, B., Heidemann, M., Kellner, M., Gruber-Eber, A., Heissmeyer, V., Strasser, K., and Eick, D. (2013). Cyclin-dependent kinase 9 links RNA polymerase II transcription to processing of ribosomal RNA. J Biol Chem *288*, 21173-21183.

Bursac, S., Prodan, Y., Pullen, N., Bartek, J., and Volarevic, S. (2020). Dysregulated Ribosome Biogenesis Reveals Therapeutic Liabilities in Cancer. Trends Cancer.

Calkins, A.S., Iglehart, J.D., and Lazaro, J.B. (2013). DNA damage-induced inhibition of rRNA synthesis by DNA-PK and PARP-1. Nucleic Acids Res *41*, 7378-7386.

Calo, E., Flynn, R.A., Martin, L., Spitale, R.C., Chang, H.Y., and Wysocka, J. (2015). RNA helicase DDX21 coordinates transcription and ribosomal RNA processing. Nature *518*, 249-253.

Calo, E., Gu, B., Bowen, M.E., Aryan, F., Zalc, A., Liang, J., Flynn, R.A., Swigut, T., Chang, H.Y., Attardi, L.D., *et al.* (2018). Tissue-selective effects of nucleolar stress and rDNA damage in developmental disorders. Nature *554*, 112-117.

Calviño, F.R., Kharde, S., Ori, A., Hendricks, A., Wild, K., Kressler, D., Bange, G., Hurt, E., Beck, M., and Sinning, I. (2015). Symportin 1 chaperones 5S RNP assembly

during ribosome biogenesis by occupying an essential rRNA-binding site. Nature Communications *6*, 6510.
Cantwell, H., and Nurse, P. (2019). Unravelling nuclear size control. Curr Genet *65*, 1281-1285.
Caragine, C.M., Haley, S.C., and Zidovska, A. (2018). Surface Fluctuations and Coalescence of Nucleolar Droplets in the Human Cell Nucleus. Phys Rev Lett *121*, 148101.
Caragine, C.M., Haley, S.C., and Zidovska, A. (2019). Nucleolar dynamics and interactions with nucleoplasm in living cells. Elife *8*.
Carpenter, A.E., Jones, T.R., Lamprecht, M.R., Clarke, C., Kang, I.H., Friman, O., Guertin, D.A., Chang, J.H., Lindquist, R.A., Moffat, J., *et al.* (2006). CellProfiler: image analysis software for identifying and quantifying cell phenotypes. Genome Biol *7*, R100.
Carty, C.L., Johnson, N.A., Hutter, C.M., Reiner, A.P., Peters, U., Tang, H., and Kooperberg, C. (2012). Genome-wide association study of body height in African Americans: the Women's Health Initiative SNP Health Association Resource (SHARe). Hum Mol Genet *21*, 711-720.
Chan, G.K., Kleinheinz, T.L., Peterson, D., and Moffat, J.G. (2013). A simple high-content cell cycle assay reveals frequent discrepancies between cell number and ATP and MTS proliferation assays. PLoS One *8*, e63583.
Chan, K.L., Palmai-Pallag, T., Ying, S., and Hickson, I.D. (2009). Replication stress induces sister-chromatid bridging at fragile site loci in mitosis. Nat Cell Biol *11*, 753-760.
Chao, H.-T., Davids, M., Burke, E., Pappas, J.G., Rosenfeld, J.A., McCarty, A.J., Davis, T., Wolfe, L., Toro, C., Tifft, C., *et al.* (2017). A Syndromic Neurodevelopmental Disorder Caused by De Novo Variants in EBF3. The American Journal of Human Genetics *100*, 128-137.
Chipchase, M.I.H., and Birnstiel, M.L. (1963). On the nature of nucleolar RNA. Proceedings of the National Academy of Sciences *50*, 1101-1107.
Ciccia, A., Huang, J.W., Izhar, L., Sowa, M.E., Harper, J.W., and Elledge, S.J. (2014). Treacher Collins syndrome TCOF1 protein cooperates with NBS1 in the DNA damage response. Proc Natl Acad Sci U S A *111*, 18631-18636.
Colis, L., Peltonen, K., Sirajuddin, P., Liu, H., Sanders, S., Ernst, G., Barrow, J.C., and Laiho, M. (2014). DNA intercalator BMH-21 inhibits RNA polymerase I independent of DNA damage response. Oncotarget *5*, 4361-4369.
Conconi, A., Widmer, R.M., Koller, T., and Sogo, J.M. (1989). Two different chromatin structures coexist in ribosomal RNA genes throughout the cell cycle. Cell *57*, 753-761.
Dai, M.S., and Lu, H. (2004). Inhibition of MDM2-mediated p53 ubiquitination and degradation by ribosomal protein L5. J Biol Chem *279*, 44475-44482.
Dameshek, W. (1967). Editorial: Riddle: What Do Aplastic Anemia, Paroxysmal Nocturnal Hemoglobinuria (PNH) and "Hypoplastic" Leukemia Have in Common? Blood *30*, 251-254.
Daniloski, Z., Bisht, K.K., McStay, B., and Smith, S. (2019). Resolution of human ribosomal DNA occurs in anaphase, dependent on tankyrase 1, condensin II, and topoisomerase IIalpha. Genes Dev *33*, 276-281.

Danilova, N., and Gazda, H.T. (2015). Ribosomopathies: how a common root can cause a tree of pathologies. Dis Model Mech *8*, 1013-1026.
Dauwerse, J.G., Dixon, J., Seland, S., Ruivenkamp, C.A., van Haeringen, A., Hoefsloot, L.H., Peters, D.J., Boers, A.C., Daumer-Haas, C., Maiwald, R., *et al.* (2011). Mutations in genes encoding subunits of RNA polymerases I and III cause Treacher Collins syndrome. Nat Genet *43*, 20-22.
de Groot, C.O., Hsia, J.E., Anzola, J.V., Motamedi, A., Yoon, M., Wong, Y.L., Jenkins, D., Lee, H.J., Martinez, M.B., Davis, R.L., *et al.* (2015). A Cell Biologist's Field Guide to Aurora Kinase Inhibitors. Front Oncol *5*, 285.
Derenzini, M., Montanaro, L., and Trere, D. (2009). What the nucleolus says to a tumour pathologist. Histopathology *54*, 753-762.
Ding, Q., Markesbery, W.R., Cecarini, V., and Keller, J.N. (2006). Decreased RNA, and increased RNA oxidation, in ribosomes from early Alzheimer's disease. Neurochem Res *31*, 705-710.
Ding, Q., Markesbery, W.R., Chen, Q., Li, F., and Keller, J.N. (2005). Ribosome dysfunction is an early event in Alzheimer's disease. J Neurosci *25*, 9171-9175.
Doll, A., and Grzeschik, K.H. (2001). Characterization of two novel genes, WBSCR20 and WBSCR22, deleted in Williams-Beuren syndrome. Cytogenet Cell Genet *95*, 20-27.
Donmez-Altuntas, H., Akalin, H., Karaman, Y., Demirtas, H., Imamoglu, N., and Ozkul, Y. (2005). Evaluation of the nucleolar organizer regions in Alzheimer's disease. Gerontology *51*, 297-301.
Dousset, T., Wang, C., Verheggen, C., Chen, D., Hernandez-Verdun, D., and Huang, S. (2000). Initiation of Nucleolar Assembly Is Independent of RNA Polymerase I Transcription. Molecular Biology of the Cell *11*, 2705-2717.
Draptchinskaia, N., Gustavsson, P., Andersson, B., Pettersson, M., Willig, T.N., Dianzani, I., Ball, S., Tchernia, G., Klar, J., Matsson, H., *et al.* (1999). The gene encoding ribosomal protein S19 is mutated in Diamond-Blackfan anaemia. Nat Genet *21*, 169-175.
Drygin, D., Lin, A., Bliesath, J., Ho, C.B., O'Brien, S.E., Proffitt, C., Omori, M., Haddach, M., Schwaebe, M.K., Siddiqui-Jain, A., *et al.* (2011). Targeting RNA polymerase I with an oral small molecule CX-5461 inhibits ribosomal RNA synthesis and solid tumor growth. Cancer Res *71*, 1418-1430.
Drygin, D., Rice, W.G., and Grummt, I. (2010). The RNA Polymerase I Transcription Machinery: An Emerging Target for the Treatment of Cancer. Annual Review of Pharmacology and Toxicology *50*, 131-156.
Drygin, D., Siddiqui-Jain, A., O'Brien, S., Schwaebe, M., Lin, A., Bliesath, J., Ho, C.B., Proffitt, C., Trent, K., Whitten, J.P., *et al.* (2009). Anticancer Activity of CX-3543: A Direct Inhibitor of rRNA Biogenesis. Cancer Research *69*, 7653-7661.
Drygin, D., Whitten, J., Rice, W., O'Brien, S., Schwaebe, M., Lin, A., Ho, C., and Trent, K. (2008). Quarfloxin (CX-3543) disrupts the Nucleolin/ rDNA quadruplex complexes, inhibits the elongation by RNA Polymerase I and exhibits potent antitumor activity in models of cancer. Cancer Research *68*, 3301-3301.
Ebersberger, I., Simm, S., Leisegang, M.S., Schmitzberger, P., Mirus, O., von Haeseler, A., Bohnsack, M.T., and Schleiff, E. (2014). The evolution of the ribosome biogenesis pathway from a yeast perspective. Nucleic Acids Res *42*, 1509-1523.

Edvardson, S., Nicolae, C.M., Agrawal, P.B., Mignot, C., Payne, K., Prasad, A.N., Prasad, C., Sadler, L., Nava, C., Mullen, T.E., *et al.* (2017). Heterozygous De Novo UBTF Gain-of-Function Variant Is Associated with Neurodegeneration in Childhood. Am J Hum Genet *101*, 267-273.

Ellis, S.R., and Gleizes, P.-E. (2011). Diamond Blackfan Anemia: Ribosomal Proteins Going Rogue. Seminars in Hematology *48*, 89-96.

Etchegaray, J.-P., and Mostoslavsky, R. (2018). A sirtuin's role in preventing senescence by protecting ribosomal DNA. Journal of Biological Chemistry *293*, 11251-11252.

Evsyukov, V., Domanskyi, A., Bierhoff, H., Gispert, S., Mustafa, R., Schlaudraff, F., Liss, B., and Parlato, R. (2017). Genetic mutations linked to Parkinson's disease differentially control nucleolar activity in pre-symptomatic mouse models. Disease Models & Mechanisms *10*, 633-643.

Farley-Barnes, K.I., McCann, K.L., Ogawa, L.M., Merkel, J., Surovtseva, Y.V., and Baserga, S.J. (2018). Diverse Regulators of Human Ribosome Biogenesis Discovered by Changes in Nucleolar Number. Cell Rep *22*, 1923-1934.

Farley-Barnes, K.I., Ogawa, L.M., and Baserga, S.J. (2019). Ribosomopathies: Old Concepts, New Controversies. Trends Genet *35*, 754-767.

Farley, K.I., Surovtseva, Y., Merkel, J., and Baserga, S.J. (2015). Determinants of mammalian nucleolar architecture. Chromosoma *124*, 323-331.

Feric, M., Vaidya, N., Harmon, T.S., Mitrea, D.M., Zhu, L., Richardson, T.M., Kriwacki, R.W., Pappu, R.V., and Brangwynne, C.P. (2016). Coexisting Liquid Phases Underlie Nucleolar Subcompartments. Cell *165*, 1686-1697.

Ferreira, R., Schneekloth, J.S., Panov, K.I., Hannan, K.M., and Hannan, R.D. (2020). Targeting the RNA Polymerase I Transcription for Cancer Therapy Comes of Age. Cells *9*, 266.

Floutsakou, I., Agrawal, S., Nguyen, T.T., Seoighe, C., Ganley, A.R., and McStay, B. (2013). The shared genomic architecture of human nucleolar organizer regions. Genome Res *23*, 2003-2012.

Franchitto, A. (2013). Genome instability at common fragile sites: searching for the cause of their instability. Biomed Res Int *2013*, 730714.

Franek, M., Kovarikova, A., Bartova, E., and Kozubek, S. (2016). Nucleolar Reorganization Upon Site-Specific Double-Strand Break Induction: DNA Repair and Epigenetics of Ribosomal Genes. J Histochem Cytochem.

Franke, Y., Peoples, R.J., and Francke, U. (1999). Identification of GTF2IRD1, a putative transcription factor within the Williams-Beuren syndrome deletion at 7q11.23. Cytogenet Cell Genet *86*, 296-304.

Frankowski, K.J., Wang, C., Patnaik, S., Schoenen, F.J., Southall, N., Li, D., Teper, Y., Sun, W., Kandela, I., Hu, D., *et al.* (2018). Metarrestin, a perinucleolar compartment inhibitor, effectively suppresses metastasis. Sci Transl Med *10*.

Freed, E.F., Prieto, J.L., McCann, K.L., McStay, B., and Baserga, S.J. (2012). NOL11, implicated in the pathogenesis of North American Indian childhood cirrhosis, is required for pre-rRNA transcription and processing. PLoS Genet *8*, e1002892.

Fu, X., Xu, L., Qi, L., Tian, H., Yi, D., Yu, Y., Liu, S., Li, S., Xu, Y., and Wang, C. (2017). BMH-21 inhibits viability and induces apoptosis by p53-dependent

nucleolar stress responses in SKOV3 ovarian cancer cells. Oncol Rep *38*, 859-865.

Fujimura, A., Hayashi, Y., Kato, K., Kogure, Y., Kameyama, M., Shimamoto, H., Daitoku, H., Fukamizu, A., Hirota, T., and Kimura, K. (2020). Identification of a novel nucleolar protein complex required for mitotic chromosome segregation through centromeric accumulation of Aurora B. Nucleic Acids Res *48*, 6583-6596.

Fumagalli, S., Di Cara, A., Neb-Gulati, A., Natt, F., Schwemberger, S., Hall, J., Babcock, G.F., Bernardi, R., Pandolfi, P.P., and Thomas, G. (2009). Absence of nucleolar disruption after impairment of 40S ribosome biogenesis reveals an rpL11-translation-dependent mechanism of p53 induction. Nat Cell Biol *11*, 501-508.

Galani, K., Nissan, T.A., Petfalski, E., Tollervey, D., and Hurt, E. (2004). Rea1, a dynein-related nuclear AAA-ATPase, is involved in late rRNA processing and nuclear export of 60 S subunits. J Biol Chem *279*, 55411-55418.

Gallagher, J.E., Dunbar, D.A., Granneman, S., Mitchell, B.M., Osheim, Y., Beyer, A.L., and Baserga, S.J. (2004). RNA polymerase I transcription and pre-rRNA processing are linked by specific SSU processome components. Genes Dev *18*, 2506-2517.

Ganley, A.R., and Kobayashi, T. (2014). Ribosomal DNA and cellular senescence: new evidence supporting the connection between rDNA and aging. FEMS Yeast Res *14*, 49-59.

García-Oliver, E., García-Molinero, V., and Rodríguez-Navarro, S. (2012). mRNA export and gene expression: The SAGA–TREX-2 connection. Biochimica et Biophysica Acta (BBA) - Gene Regulatory Mechanisms *1819*, 555-565.

Gassmann, R., Carvalho, A., Henzing, A.J., Ruchaud, S., Hudson, D.F., Honda, R., Nigg, E.A., Gerloff, D.L., and Earnshaw, W.C. (2004). Borealin: a novel chromosomal passenger required for stability of the bipolar mitotic spindle. J Cell Biol *166*, 179-191.

Gautier, T., Robert-Nicoud, M., Guilly, M.N., and Hernandez-Verdun, D. (1992). Relocation of nucleolar proteins around chromosomes at mitosis. A study by confocal laser scanning microscopy. J Cell Sci *102 (Pt 4)*, 729-737.

Gemble, S., Buhagiar-Labarchede, G., Onclercq-Delic, R., Fontaine, G., Lambert, S., and Amor-Gueret, M. (2020). Topoisomerase IIalpha prevents ultrafine anaphase bridges by two mechanisms. Open Biol *10*, 190259.

Genuth, N.R., and Barna, M. (2018). The Discovery of Ribosome Heterogeneity and Its Implications for Gene Regulation and Organismal Life. Molecular Cell *71*, 364-374.

Ghoshal, K., Majumder, S., Datta, J., Motiwala, T., Bai, S., Sharma, S.M., Frankel, W., and Jacob, S.T. (2004). Role of human ribosomal RNA (rRNA) promoter methylation and of methyl-CpG-binding protein MBD2 in the suppression of rRNA gene expression. J Biol Chem *279*, 6783-6793.

Giacinti, C., and Giordano, A. (2006). RB and cell cycle progression. Oncogene *25*, 5220-5227.

Gibbons, J.G., Branco, A.T., Godinho, S.A., Yu, S., and Lemos, B. (2015). Concerted copy number variation balances ribosomal DNA dosage in human and mouse genomes. Proceedings of the National Academy of Sciences *112*, 2485-2490.

Gomes, C.J., Harman, M.W., Centuori, S.M., Wolgemuth, C.W., and Martinez, J.D. (2018). Measuring DNA content in live cells by fluorescence microscopy. Cell Div *13*, 6.

Gonzales, B., Henning, D., So, R.B., Dixon, J., Dixon, M.J., and Valdez, B.C. (2005). The Treacher Collins syndrome (TCOF1) gene product is involved in pre-rRNA methylation. Hum Mol Genet *14*, 2035-2043.

Gonzalez, I.L., and Sylvester, J.E. (1995). Complete sequence of the 43-kb human ribosomal DNA repeat: analysis of the intergenic spacer. Genomics *27*, 320-328.

Gorski, J.J., Pathak, S., Panov, K., Kasciukovic, T., Panova, T., Russell, J., and Zomerdijk, J.C. (2007). A novel TBP-associated factor of SL1 functions in RNA polymerase I transcription. EMBO J *26*, 1560-1568.

Gottlieb, S., and Esposito, R.E. (1989). A new role for a yeast transcriptional silencer gene, SIR2, in regulation of recombination in ribosomal DNA. Cell *56*, 771-776.

Grierson, P.M., Lillard, K., Behbehani, G.K., Combs, K.A., Bhattacharyya, S., Acharya, S., and Groden, J. (2012). BLM helicase facilitates RNA polymerase I-mediated ribosomal RNA transcription. Hum Mol Genet *21*, 1172-1183.

Griffin, J.N., Sondalle, S.B., Del Viso, F., Baserga, S.J., and Khokha, M.K. (2015). The ribosome biogenesis factor Nol11 is required for optimal rDNA transcription and craniofacial development in Xenopus. PLoS Genet *11*, e1005018.

Grob, A., Colleran, C., and McStay, B. (2014). Construction of synthetic nucleoli in human cells reveals how a major functional nuclear domain is formed and propagated through cell division. Genes Dev *28*, 220-230.

Guarente, L. (1997). Link between aging and the nucleolus. Genes Dev *11*, 2449-2455.

Gustafsdottir, S.M., Ljosa, V., Sokolnicki, K.L., Anthony Wilson, J., Walpita, D., Kemp, M.M., Petri Seiler, K., Carrel, H.A., Golub, T.R., Schreiber, S.L., *et al.* (2013). Multiplex cytological profiling assay to measure diverse cellular states. PLoS One *8*, e80999.

Haddach, M., Schwaebe, M.K., Michaux, J., Nagasawa, J., O'Brien, S.E., Whitten, J.P., Pierre, F., Kerdoncuff, P., Darjania, L., Stansfield, R., *et al.* (2012). Discovery of CX-5461, the First Direct and Selective Inhibitor of RNA Polymerase I, for Cancer Therapeutics. ACS Med Chem Lett *3*, 602-606.

Hagner, P.R., Schneider, A., and Gartenhaus, R.B. (2010). Targeting the translational machinery as a novel treatment strategy for hematologic malignancies. Blood *115*, 2127-2135.

Hannan, K.M., Sanij, E., Rothblum, L.I., Hannan, R.D., and Pearson, R.B. (2013). Dysregulation of RNA polymerase I transcription during disease. Biochim Biophys Acta *1829*, 342-360.

Hannan, K.M., Soo, P., Wong, M.S., Lee, J.K., Hein, N., Evers, M., Wysoke, K.D., Williams, T.D., Montellese, C., Smith, L.K., *et al.* (2021). Nuclear stabilisation of p53 requires a functional nucleolar surveillance pathway. bioRxiv, 2021.2001.2021.427535.

Harding, S.M., Boiarsky, J.A., and Greenberg, R.A. (2015). ATM Dependent Silencing Links Nucleolar Chromatin Reorganization to DNA Damage Recognition. Cell Rep *13*, 251-259.

Hart, T., Komori, H.K., LaMere, S., Podshivalova, K., and Salomon, D.R. (2013). Finding the active genes in deep RNA-seq gene expression studies. BMC Genomics *14*, 778.

Hatos, A., Hajdu-Soltesz, B., Monzon, A.M., Palopoli, N., Alvarez, L., Aykac-Fas, B., Bassot, C., Benitez, G.I., Bevilacqua, M., Chasapi, A., *et al.* (2020). DisProt: intrinsic protein disorder annotation in 2020. Nucleic Acids Res *48*, D269-D276.

Hayashi, Y., Kato, K., and Kimura, K. (2017). The hierarchical structure of the perichromosomal layer comprises Ki67, ribosomal RNAs, and nucleolar proteins. Biochem Biophys Res Commun *493*, 1043-1049.

Heix, J., Vente, A., Voit, R., Budde, A., Michaelidis, T.M., and Grummt, I. (1998). Mitotic silencing of human rRNA synthesis: inactivation of the promoter selectivity factor SL1 by cdc2/cyclin B-mediated phosphorylation. EMBO J *17*, 7373-7381.

Hekselman, I., and Yeger-Lotem, E. (2020). Mechanisms of tissue and cell-type specificity in heritable traits and diseases. Nature Reviews Genetics *21*, 137-150.

Henderson, A.S., Warburton, D., and Atwood, K.C. (1972). Location of ribosomal DNA in the human chromosome complement. Proc Natl Acad Sci U S A *69*, 3394-3398.

Henras, A.K., Plisson-Chastang, C., O'Donohue, M.F., Chakraborty, A., and Gleizes, P.E. (2015). An overview of pre-ribosomal RNA processing in eukaryotes. Wiley Interdiscip Rev RNA *6*, 225-242.

Hernandez-Ortega, K., Garcia-Esparcia, P., Gil, L., Lucas, J.J., and Ferrer, I. (2016). Altered Machinery of Protein Synthesis in Alzheimer's: From the Nucleolus to the Ribosome. Brain Pathol *26*, 593-605.

Hernandez-Verdun, D. (2011). Assembly and disassembly of the nucleolus during the cell cycle. Nucleus *2*, 189-194.

Herrmann, D., and Parlato, R. (2018). C9orf72-associated neurodegeneration in ALS-FTD: breaking new ground in ribosomal RNA and nucleolar dysfunction. Cell Tissue Res *373*, 351-360.

Hetman, M., and Pietrzak, M. (2012). Emerging roles of the neuronal nucleolus. Trends Neurosci *35*, 305-314.

Hilton, J., Gelmon, K., Cescon, D., Tinker, A., Jonker, D., Goodwin, R., Laurie, S., Hansen, A., Aparicio, S., Soong, J., *et al.* (2020). Abstract PD4-02: Canadian cancer trials group trial IND.231: A phase 1 trial evaluating CX-5461, a novel first-in-class G-quadruplex stabilizer in patients with advanced solid tumors enriched for DNA-repair deficiencies. Cancer Research *80*, PD4-02-PD04-02.

Honda, K., Smith, M.A., Zhu, X., Baus, D., Merrick, W.C., Tartakoff, A.M., Hattier, T., Harris, P.L., Siedlak, S.L., Fujioka, H., *et al.* (2005). Ribosomal RNA in Alzheimer disease is oxidized by bound redox-active iron. J Biol Chem *280*, 20978-20986.

Hyman, A.A., Weber, C.A., and Jülicher, F. (2014). Liquid-Liquid Phase Separation in Biology. Annual Review of Cell and Developmental Biology *30*, 39-58.

Ide, S., Miyazaki, T., Maki, H., and Kobayashi, T. (2010). Abundance of ribosomal RNA gene copies maintains genome integrity. Science *327*, 693-696.

Ishimura, R., Nagy, G., Dotu, I., Zhou, H., Yang, X.L., Schimmel, P., Senju, S., Nishimura, Y., Chuang, J.H., and Ackerman, S.L. (2014). RNA function.

Ribosome stalling induced by mutation of a CNS-specific tRNA causes neurodegeneration. Science *345*, 455-459.
Izumi, H., Molander, C., Penn, L.Z., Ishisaki, A., Kohno, K., and Funa, K. (2001). Mechanism for the transcriptional repression by c-Myc on PDGF beta-receptor. J Cell Sci *114*, 1533-1544.
James, A., Wang, Y., Raje, H., Rosby, R., and DiMario, P. (2014). Nucleolar stress with and without p53. Nucleus *5*, 402-426.
Jarboui, M.A., Bidoia, C., Woods, E., Roe, B., Wynne, K., Elia, G., Hall, W.W., and Gautier, V.W. (2012). Nucleolar protein trafficking in response to HIV-1 Tat: rewiring the nucleolus. PLoS One *7*, e48702.
Jarboui, M.A., Wynne, K., Elia, G., Hall, W.W., and Gautier, V.W. (2011). Proteomic profiling of the human T-cell nucleolus. Mol Immunol *49*, 441-452.
Johnson, I.S., Armstrong, J.G., Gorman, M., and Burnett, J.P. (1963). The Vinca Alkaloids: A New Class of Oncolytic Agents. Cancer Research *23*, 1390-1427.
Jones, N.C., Lynn, M.L., Gaudenz, K., Sakai, D., Aoto, K., Rey, J.P., Glynn, E.F., Ellington, L., Du, C., Dixon, J., *et al.* (2008). Prevention of the neurocristopathy Treacher Collins syndrome through inhibition of p53 function. Nat Med *14*, 125-133.
Jorgensen, P., Edgington, N.P., Schneider, B.L., Rupes, I., Tyers, M., and Futcher, B. (2007). The size of the nucleus increases as yeast cells grow. Mol Biol Cell *18*, 3523-3532.
Kandoth, C., McLellan, M.D., Vandin, F., Ye, K., Niu, B., Lu, C., Xie, M., Zhang, Q., McMichael, J.F., Wyczalkowski, M.A., *et al.* (2013). Mutational landscape and significance across 12 major cancer types. Nature *502*, 333-339.
Karikkineth, A.C., Scheibye-Knudsen, M., Fivenson, E., Croteau, D.L., and Bohr, V.A. (2017). Cockayne syndrome: Clinical features, model systems and pathways. Ageing Res Rev *33*, 3-17.
Kelleher, A.R., Kimball, S.R., Dennis, M.D., Schilder, R.J., and Jefferson, L.S. (2013). The mTORC1 signaling repressors REDD1/2 are rapidly induced and activation of p70S6K1 by leucine is defective in skeletal muscle of an immobilized rat hindlimb. Am J Physiol Endocrinol Metab *304*, E229-236.
Khajah, M.A., Mathew, P.M., and Luqmani, Y.A. (2018). Na+/K+ ATPase activity promotes invasion of endocrine resistant breast cancer cells. PLoS One *13*, e0193779.
Khajuria, R.K., Munschauer, M., Ulirsch, J.C., Fiorini, C., Ludwig, L.S., McFarland, S.K., Abdulhay, N.J., Specht, H., Keshishian, H., Mani, D.R., *et al.* (2018). Ribosome Levels Selectively Regulate Translation and Lineage Commitment in Human Hematopoiesis. Cell *173*, 90-103.e119.
Khot, A., Brajanovski, N., Cameron, D.P., Hein, N., Maclachlan, K.H., Sanij, E., Lim, J., Soong, J., Link, E., Blombery, P., *et al.* (2019). First-in-Human RNA Polymerase I Transcription Inhibitor CX-5461 in Patients with Advanced Hematologic Cancers: Results of a Phase I Dose-Escalation Study. Cancer Discov *9*, 1036-1049.
Kim, S., Balakrishnan, S.K., and Gross, D.S. (2011). p53 Interacts with RNA polymerase II through its core domain and impairs Pol II processivity in vivo. PLoS One *6*, e22183.

Kinsella, R.J., Kahari, A., Haider, S., Zamora, J., Proctor, G., Spudich, G., Almeida-King, J., Staines, D., Derwent, P., Kerhornou, A., *et al.* (2011). Ensembl BioMarts: a hub for data retrieval across taxonomic space. Database (Oxford) *2011*, bar030.

Kiss, T. (2002). Small nucleolar RNAs: an abundant group of noncoding RNAs with diverse cellular functions. Cell *109*, 145-148.

Kobayashi, T., Heck, D.J., Nomura, M., and Horiuchi, T. (1998). Expansion and contraction of ribosomal DNA repeats in Saccharomyces cerevisiae: requirement of replication fork blocking (Fob1) protein and the role of RNA polymerase I. Genes Dev *12*, 3821-3830.

Kontomanolis, E.N., Kalagasidou, S., Pouliliou, S., Anthoulaki, X., Georgiou, N., Papamanolis, V., and Fasoulakis, Z.N. (2018). The Notch Pathway in Breast Cancer Progression. ScientificWorldJournal *2018*, 2415489.

Kopytova, D.V., Orlova, A.V., Krasnov, A.N., Gurskiy, D.Y., Nikolenko, J.V., Nabirochkina, E.N., Shidlovskii, Y.V., and Georgieva, S.G. (2010). Multifunctional factor ENY2 is associated with the THO complex and promotes its recruitment onto nascent mRNA. Genes & Development *24*, 86-96.

Korsholm, L.M., Gál, Z., Lin, L., Quevedo, O., Ahmad, D.A., Dulina, E., Luo, Y., Bartek, J., and Larsen, D.H. (2019). Double-strand breaks in ribosomal RNA genes activate a distinct signaling and chromatin response to facilitate nucleolar restructuring and repair. Nucleic Acids Research *47*, 8019-8035.

Kruhlak, M., Crouch, E.E., Orlov, M., Montano, C., Gorski, S.A., Nussenzweig, A., Misteli, T., Phair, R.D., and Casellas, R. (2007). The ATM repair pathway inhibits RNA polymerase I transcription in response to chromosome breaks. Nature *447*, 730-734.

Kuhn, A., Vente, A., Dorée, M., and Grummt, I. (1998). Mitotic phosphorylation of the TBP-containing factor SL1 represses ribosomal gene transcription. J Mol Biol *284*, 1-5.

Lafontaine, D.L.J., Riback, J.A., Bascetin, R., and Brangwynne, C.P. (2020). The nucleolus as a multiphase liquid condensate. Nat Rev Mol Cell Biol.

Langstrom, N.S., Anderson, J.P., Lindroos, H.G., Winblad, B., and Wallace, W.C. (1989). Alzheimer's disease-associated reduction of polysomal mRNA translation. Brain Res Mol Brain Res *5*, 259-269.

Larsen, D.H., Hari, F., Clapperton, J.A., Gwerder, M., Gutsche, K., Altmeyer, M., Jungmichel, S., Toledo, L.I., Fink, D., Rask, M.B., *et al.* (2014). The NBS1-Treacle complex controls ribosomal RNA transcription in response to DNA damage. Nat Cell Biol *16*, 792-803.

Larsen, D.H., and Stucki, M. (2016). Nucleolar responses to DNA double-strand breaks. Nucleic Acids Res *44*, 538-544.

Laudisi, F., Marônek, M., Di Grazia, A., Monteleone, G., and Stolfi, C. (2020). Repositioning of Anthelmintic Drugs for the Treatment of Cancers of the Digestive System. International Journal of Molecular Sciences *21*, 4957.

Lebedev, A., Scharffetter-Kochanek, K., and Iben, S. (2008). Truncated Cockayne Syndrome B Protein Represses Elongation by RNA Polymerase I. Journal of Molecular Biology *382*, 266-274.

Lee, S.Y., Lee, H., Kim, E.S., Park, S., Lee, J., and Ahn, B. (2015). WRN translocation from nucleolus to nucleoplasm is regulated by SIRT1 and required for DNA repair and the development of chemoresistance. Mutat Res *774*, 40-48.

Leung, A.K., Trinkle-Mulcahy, L., Lam, Y.W., Andersen, J.S., Mann, M., and Lamond, A.I. (2006). NOPdb: Nucleolar Proteome Database. Nucleic Acids Res *34*, D218-220.

Li, P., Gao, S., Wang, L., Yu, F., Li, J., Wang, C., Li, J., and Wong, J. (2013a). ABH2 couples regulation of ribosomal DNA transcription with DNA alkylation repair. Cell Rep *4*, 817-829.

Li, Z., Zhu, Y., Zhai, Y., M, R.C., Bao, Y., White, T.E., and Glavy, J.S. (2013b). Werner complex deficiency in cells disrupts the Nuclear Pore Complex and the distribution of lamin B1. Biochim Biophys Acta *1833*, 3338-3345.

Lindsley, R.C., Saber, W., Mar, B.G., Redd, R., Wang, T., Haagenson, M.D., Grauman, P.V., Hu, Z.-H., Spellman, S.R., Lee, S.J., *et al.* (2017). Prognostic Mutations in Myelodysplastic Syndrome after Stem-Cell Transplantation. New England Journal of Medicine *376*, 536-547.

Lindstrom, M.S., Jurada, D., Bursac, S., Orsolic, I., Bartek, J., and Volarevic, S. (2018). Nucleolus as an emerging hub in maintenance of genome stability and cancer pathogenesis. Oncogene *37*, 2351-2366.

Lipinski, C.A. (2000). Drug-like properties and the causes of poor solubility and poor permeability. J Pharmacol Toxicol Methods *44*, 235-249.

Lipinski, C.A. (2004). Lead- and drug-like compounds: the rule-of-five revolution. Drug Discov Today Technol *1*, 337-341.

Lirussi, L., Antoniali, G., Vascotto, C., D'Ambrosio, C., Poletto, M., Romanello, M., Marasco, D., Leone, M., Quadrifoglio, F., Bhakat, K.K., *et al.* (2012). Nucleolar accumulation of APE1 depends on charged lysine residues that undergo acetylation upon genotoxic stress and modulate its BER activity in cells. Mol Biol Cell *23*, 4079-4096.

Liu, Q., Wang, J., Miki, D., Xia, R., Yu, W., He, J., Zheng, Z., Zhu, J.K., and Gong, Z. (2010). DNA replication factor C1 mediates genomic stability and transcriptional gene silencing in Arabidopsis. Plant Cell *22*, 2336-2352.

Lodish, H.F. (1974). Model for the regulation of mRNA translation applied to haemoglobin synthesis. Nature *251*, 385-388.

Lohrum, M.A., Ludwig, R.L., Kubbutat, M.H., Hanlon, M., and Vousden, K.H. (2003). Regulation of HDM2 activity by the ribosomal protein L11. Cancer Cell *3*, 577-587.

Lovering, F., Bikker, J., and Humblet, C. (2009). Escape from flatland: increasing saturation as an approach to improving clinical success. J Med Chem *52*, 6752-6756.

Low, J.Y., Sirajuddin, P., Moubarek, M., Agarwal, S., Rege, A., Guner, G., Liu, H., Yang, Z., De Marzo, A.M., Bieberich, C., *et al.* (2019). Effective targeting of RNA polymerase I in treatment-resistant prostate cancer. Prostate *79*, 1837-1851.

Ludwig, L.S., Gazda, H.T., Eng, J.C., Eichhorn, S.W., Thiru, P., Ghazvinian, R., George, T.I., Gotlib, J.R., Beggs, A.H., Sieff, C.A., *et al.* (2014). Altered translation of GATA1 in Diamond-Blackfan anemia. Nature Medicine *20*, 748-753.

Lutomska, A., Lebedev, A., Scharffetter-Kochanek, K., and Iben, S. (2008). The transcriptional response to distinct growth factors is impaired in Werner syndrome cells. Exp Gerontol *43*, 820-826.
Maeshima, K., Iino, H., Hihara, S., and Imamoto, N. (2011). Nuclear size, nuclear pore number and cell cycle. Nucleus *2*, 113-118.
Mais, C., Wright, J.E., Prieto, J.L., Raggett, S.L., and McStay, B. (2005). UBF-binding site arrays form pseudo-NORs and sequester the RNA polymerase I transcription machinery. Genes Dev *19*, 50-64.
Malina, A., Mills, J.R., and Pelletier, J. (2012). Emerging therapeutics targeting mRNA translation. Cold Spring Harb Perspect Biol *4*, a012377.
Mangan, H., and McStay, B. (2021). Human nucleoli comprise multiple constrained territories, tethered to individual chromosomes. Genes Dev.
Mann, D.M., Marcyniuk, B., Yates, P.O., Neary, D., and Snowden, J.S. (1988). The progression of the pathological changes of Alzheimer's disease in frontal and temporal neocortex examined both at biopsy and at autopsy. Neuropathol Appl Neurobiol *14*, 177-195.
Mantovani, F., Collavin, L., and Del Sal, G. (2019). Mutant p53 as a guardian of the cancer cell. Cell Death Differ *26*, 199-212.
Martin, Y.C., Kofron, J.L., and Traphagen, L.M. (2002). Do structurally similar molecules have similar biological activity? J Med Chem *45*, 4350-4358.
Martino, E., Casamassima, G., Castiglione, S., Cellupica, E., Pantalone, S., Papagni, F., Rui, M., Siciliano, A.M., and Collina, S. (2018). Vinca alkaloids and analogues as anti-cancer agents: Looking back, peering ahead. Bioorg Med Chem Lett *28*, 2816-2826.
Matsuoka, S., Ballif, B.A., Smogorzewska, A., McDonald, E.R., 3rd, Hurov, K.E., Luo, J., Bakalarski, C.E., Zhao, Z., Solimini, N., Lerenthal, Y., *et al.* (2007). ATM and ATR substrate analysis reveals extensive protein networks responsive to DNA damage. Science *316*, 1160-1166.
Mayer, C., and Grummt, I. (2006). Ribosome biogenesis and cell growth: mTOR coordinates transcription by all three classes of nuclear RNA polymerases. Oncogene *25*, 6384-6391.
McClintock, B. (1934). The relation of a particular chromosomal element to the development of the nucleoli in Zea mays. Zeitschrift für Zellforschung und Mikroskopische Anatomie *21*, 294-326.
McQuin, C., Goodman, A., Chernyshev, V., Kamentsky, L., Cimini, B.A., Karhohs, K.W., Doan, M., Ding, L., Rafelski, S.M., Thirstrup, D., *et al.* (2018). CellProfiler 3.0: Next-generation image processing for biology. PLoS Biol *16*, e2005970.
McStay, B., and Grummt, I. (2008). The epigenetics of rRNA genes: from molecular to chromosome biology. Annu Rev Cell Dev Biol *24*, 131-157.
McSwiggen, D.T., Mir, M., Darzacq, X., and Tjian, R. (2019). Evaluating phase separation in live cells: diagnosis, caveats, and functional consequences. Genes Dev *33*, 1619-1634.
Mélèse, T., and Xue, Z. (1995). The nucleolus: an organelle formed by the act of building a ribosome. Curr Opin Cell Biol *7*, 319-324.

Melnikov, S.V., Söll, D., Steitz, T.A., and Polikanov, Y.S. (2016). Insights into RNA binding by the anticancer drug cisplatin from the crystal structure of cisplatin-modified ribosome. Nucleic Acids Research *44*, 4978-4987.

Merlo, G.R., Basolo, F., Fiore, L., Duboc, L., and Hynes, N.E. (1995). p53-dependent and p53-independent activation of apoptosis in mammary epithelial cells reveals a survival function of EGF and insulin. J Cell Biol *128*, 1185-1196.

Mezzatesta, C., Abduli, L., Guinot, A., Eckert, C., Schewe, D., Zaliova, M., Vinti, L., Marovca, B., Tsai, Y.-C., Jenni, S., *et al.* (2020). Repurposing anthelmintic agents to eradicate resistant leukemia. Blood Cancer Journal *10*, 72.

Mi, H., Huang, X., Muruganujan, A., Tang, H., Mills, C., Kang, D., and Thomas, P.D. (2017). PANTHER version 11: expanded annotation data from Gene Ontology and Reactome pathways, and data analysis tool enhancements. Nucleic Acids Res *45*, D183-D189.

Miller, W.T. (2012). Tyrosine kinase signaling and the emergence of multicellularity. Biochim Biophys Acta *1823*, 1053-1057.

Mills, E.W., and Green, R. (2017). Ribosomopathies: There's strength in numbers. Science *358*, eaan2755.

Montanaro, L., Trere, D., and Derenzini, M. (2008). Nucleolus, ribosomes, and cancer. Am J Pathol *173*, 301-310.

Montgomery Jr., T.S.H. (1898). Comparative cytological studies, with especial regard to the morphology of the nucleolus. Journal of Morphology *15*, 265-582.

Moore, H.M., Bai, B., Boisvert, F.M., Latonen, L., Rantanen, V., Simpson, J.C., Pepperkok, R., Lamond, A.I., and Laiho, M. (2011). Quantitative proteomics and dynamic imaging of the nucleolus reveal distinct responses to UV and ionizing radiation. Mol Cell Proteomics *10*, M111 009241.

Mooser, C., Symeonidou, I.E., Leimbacher, P.A., Ribeiro, A., Shorrocks, A.K., Jungmichel, S., Larsen, S.C., Knechtle, K., Jasrotia, A., Zurbriggen, D., *et al.* (2020). Treacle controls the nucleolar response to rDNA breaks via TOPBP1 recruitment and ATR activation. Nat Commun *11*, 123.

Mukherjee, S., Sinha, D., Bhattacharya, S., Srinivasan, K., Abdisalaam, S., and Asaithamby, A. (2018). Werner Syndrome Protein and DNA Replication. International journal of molecular sciences *19*.

Mukhtar, E., Adhami, V.M., and Mukhtar, H. (2014). Targeting microtubules by natural agents for cancer therapy. Mol Cancer Ther *13*, 275-284.

Murayama, A., Ohmori, K., Fujimura, A., Minami, H., Yasuzawa-Tanaka, K., Kuroda, T., Oie, S., Daitoku, H., Okuwaki, M., Nagata, K., *et al.* (2008). Epigenetic control of rDNA loci in response to intracellular energy status. Cell *133*, 627-639.

Muro, E., Gébrane-Younís, J., Jobart-Malfait, A., Louvet, E., Roussel, P., and Hernandez-Verdun, D. (2010). The traffic of proteins between nucleolar organizer regions and prenucleolar bodies governs the assembly of the nucleolus at exit of mitosis. Nucleus *1*, 202-211.

Nakayama, K.I., and Nakayama, K. (2006). Ubiquitin ligases: cell-cycle control and cancer. Nat Rev Cancer *6*, 369-381.

Narla, A., and Ebert, B.L. (2010). Ribosomopathies: human disorders of ribosome dysfunction. Blood *115*, 3196-3205.

Nelson, J.O., Watase, G.J., Warsinger-Pepe, N., and Yamashita, Y.M. (2019). Mechanisms of rDNA Copy Number Maintenance. Trends in Genetics *35*, 734-742.

Neumann, F.R., and Nurse, P. (2007). Nuclear size control in fission yeast. J Cell Biol *179*, 593-600.

Neumuller, R.A., Gross, T., Samsonova, A.A., Vinayagam, A., Buckner, M., Founk, K., Hu, Y., Sharifpoor, S., Rosebrock, A.P., Andrews, B., *et al.* (2013). Conserved regulators of nucleolar size revealed by global phenotypic analyses. Sci Signal *6*, ra70.

Newman, R.A., Yang, P., Pawlus, A.D., and Block, K.I. (2008). Cardiac glycosides as novel cancer therapeutic agents. Mol Interv *8*, 36-49.

Nousbeck, J., Spiegel, R., Ishida-Yamamoto, A., Indelman, M., Shani-Adir, A., Adir, N., Lipkin, E., Bercovici, S., Geiger, D., van Steensel, M.A., *et al.* (2008). Alopecia, neurological defects, and endocrinopathy syndrome caused by decreased expression of RBM28, a nucleolar protein associated with ribosome biogenesis. Am J Hum Genet *82*, 1114-1121.

Novac, O., Guenier, A.S., and Pelletier, J. (2004). Inhibitors of protein synthesis identified by a high throughput multiplexed translation screen. Nucleic Acids Res *32*, 902-915.

Ogawa, L.M., and Baserga, S.J. (2017). Crosstalk between the nucleolus and the DNA damage response. Mol Biosyst *13*, 443-455.

Ogawa, L.M., Buhagiar, A.F., Abriola, L., Leland, B.A., Surovtseva, Y.V., and Baserga, S.J. (2021). Increased numbers of nucleoli in a genome-wide RNAi screen reveal proteins that link the cell cycle to RNA polymerase I transcription. Mol Biol Cell, mbcE20100670.

Okur, M.N., Lee, J.H., Osmani, W., Kimura, R., Demarest, T.G., Croteau, D.L., and Bohr, V.A. (2020). Cockayne syndrome group A and B proteins function in rRNA transcription through nucleolin regulation. Nucleic Acids Res *48*, 2473-2485.

Palade , G.E. (1955). A small particulate component of the cytoplasm. The Journal of Biophysical and Biochemical Cytology *1*, 59-68.

Paolini, N.A., Attwood, M., Sondalle, S.B., Vieira, C., van Adrichem, A.M., di Summa, F.M., O'Donohue, M.F., Gleizes, P.E., Rachuri, S., Briggs, J.W., *et al.* (2017). A Ribosomopathy Reveals Decoding Defective Ribosomes Driving Human Dysmorphism. Am J Hum Genet *100*, 506-522.

Papadopoulos, K.P., Northfelt, D.W., Hufnagel, D.M., Ricart, A.D., Griffin, P.P., Oslund, M.D., Hoff, D.D.V., Rice, W.G., Lim, J.K., and Marschke, R.F. (2007). Phase I clinical trial of CX-3543, a protein-rDNA quadruplex inhibitor. Journal of Clinical Oncology *25*, 3585-3585.

Paredes, S., Angulo-Ibanez, M., Tasselli, L., Carlson, S.M., Zheng, W., Li, T.-M., and Chua, K.F. (2018). The epigenetic regulator SIRT7 guards against mammalian cellular senescence induced by ribosomal DNA instability. Journal of Biological Chemistry *293*, 11242-11250.

Parks, M.M., Kurylo, C.M., Dass, R.A., Bojmar, L., Lyden, D., Vincent, C.T., and Blanchard, S.C. (2018). Variant ribosomal RNA alleles are conserved and exhibit tissue-specific expression. Sci Adv *4*, eaao0665.

Parlato, R., and Bierhoff, H. (2015). Role of nucleolar dysfunction in neurodegenerative disorders: a game of genes? AIMS Molecular Science *2*, 211-224.
Parlato, R., and Kreiner, G. (2013). Nucleolar activity in neurodegenerative diseases: a missing piece of the puzzle? J Mol Med (Berl) *91*, 541-547.
Parlato, R., and Liss, B. (2014). How Parkinson's disease meets nucleolar stress. Biochim Biophys Acta *1842*, 791-797.
Patel, N., Shamseldin, H.E., Sakati, N., Khan, A.O., Softa, A., Al-Fadhli, F.M., Hashem, M., Abdulwahab, F.M., Alshidi, T., Alomar, R., *et al.* (2017). GZF1 Mutations Expand the Genetic Heterogeneity of Larsen Syndrome. Am J Hum Genet *100*, 831-836.
Pederson, T. (1998). The plurifunctional nucleolus. Nucleic Acids Res *26*, 3871-3876.
Pederson, T. (2011). The nucleolus. Cold Spring Harb Perspect Biol *3*.
Pelletier, G., Stefanovsky, V.Y., Faubladier, M., Hirschler-Laszkiewicz, I., Savard, J., Rothblum, L.I., Cote, J., and Moss, T. (2000). Competitive recruitment of CBP and Rb-HDAC regulates UBF acetylation and ribosomal transcription. Mol Cell *6*, 1059-1066.
Pelletier, J., Thomas, G., and Volarević, S. (2018). Ribosome biogenesis in cancer: new players and therapeutic avenues. Nature Reviews Cancer *18*, 51-63.
Peltonen, K., Colis, L., Liu, H., Trivedi, R., Moubarek, M.S., Moore, H.M., Bai, B., Rudek, M.A., Bieberich, C.J., and Laiho, M. (2014). A targeting modality for destruction of RNA polymerase I that possesses anticancer activity. Cancer Cell *25*, 77-90.
Peng, A., and Weber, S.C. (2019). Evidence for and against Liquid-Liquid Phase Separation in the Nucleus. Noncoding RNA *5*.
Penzo, M., Montanaro, L., Trere, D., and Derenzini, M. (2019). The Ribosome Biogenesis-Cancer Connection. Cells *8*.
Pfister, A.S., and Kuhl, M. (2018). Of Wnts and Ribosomes. Prog Mol Biol Transl Sci *153*, 131-155.
Phillips, D.M., and Phillips, S.G. (1973). Repopulation of postmitotic nucleoli by preformed RNA. II. Ultrastructure. J Cell Biol *58*, 54-63.
Phillips, S.G. (1972). Repopulation of the postmitotic nucleolus by preformed RNA. J Cell Biol *53*, 611-623.
Pianese, G. (1896). Beitrag zur Histologie und Aetiologie des Carcinoms : histologische und experimentelle Untersuchungen (G. Fischer).
Pietrzak, M., Rempala, G., Nelson, P.T., Zheng, J.J., and Hetman, M. (2011). Epigenetic silencing of nucleolar rRNA genes in Alzheimer's disease. PLoS One *6*, e22585.
Pisarev, A.V., Skabkin, M.A., Pisareva, V.P., Skabkina, O.V., Rakotondrafara, A.M., Hentze, M.W., Hellen, C.U., and Pestova, T.V. (2010). The role of ABCE1 in eukaryotic posttermination ribosomal recycling. Mol Cell *37*, 196-210.
Potapova, T.A., and Gerton, J.L. (2019). Ribosomal DNA and the nucleolus in the context of genome organization. Chromosome Res *27*, 109-127.
Prassas, I., and Diamandis, E.P. (2008). Novel therapeutic applications of cardiac glycosides. Nature Reviews Drug Discovery *7*, 926-935.
Pressato, B., Valli, R., Marletta, C., Mare, L., Montalbano, G., Curto, F.L., Pasquali, F., and Maserati, E. (2015). Cytogenetic Monitoring in Shwachman-Diamond

Syndrome: A Note on Clonal Progression and a Practical Warning. Journal of Pediatric Hematology/Oncology *37*.
Prieto, J.L., and McStay, B. (2007). Recruitment of factors linking transcription and processing of pre-rRNA to NOR chromatin is UBF-dependent and occurs independent of transcription in human cells. Genes Dev *21*, 2041-2054.
Quin, J.E., Devlin, J.R., Cameron, D., Hannan, K.M., Pearson, R.B., and Hannan, R.D. (2014). Targeting the nucleolus for cancer intervention. Biochim Biophys Acta *1842*, 802-816.
Raaijmakers, J.A., and Medema, R.H. (2014). Function and regulation of dynein in mitotic chromosome segregation. Chromosoma *123*, 407-422.
Raška, I., Shaw, P.J., and Cmarko, D. (2006). New Insights into Nucleolar Architecture and Activity. In International Review of Cytology, K.W. Jeon, ed. (Academic Press), pp. 177-235.
Rawlinson, S.M., Zhao, T., Rozario, A.M., Rootes, C.L., McMillan, P.J., Purcell, A.W., Woon, A., Marsh, G.A., Lieu, K.G., Wang, L.F., *et al.* (2018). Viral regulation of host cell biology by hijacking of the nucleolar DNA-damage response. Nat Commun *9*, 3057.
Reimer, G., Pollard, K.M., Penning, C.A., Ochs, R.L., Lischwe, M.A., Busch, H., and Tan, E.M. (1987). Monoclonal autoantibody from a (New Zealand black x New Zealand white)F1 mouse and some human scleroderma sera target an Mr 34,000 nucleolar protein of the U3 RNP particle. Arthritis Rheum *30*, 793-800.
Reynolds, R.C., Montgomery, P.O., and Hughes, B. (1964). Nucleolar "Caps" Produced by Actinomycin D. Cancer Res *24*, 1269-1277.
Reynolds, R.C., Montgomery, P.O.B., and Karney, D.H. (1963). Nucleolar “Caps”—a Morphologic Entity Produced by the Carcinogen 4-Nitroquinoline N-Oxide. Cancer Research *23*, 535-538.
Rieker, C., Engblom, D., Kreiner, G., Domanskyi, A., Schober, A., Stotz, S., Neumann, M., Yuan, X., Grummt, I., Schutz, G., *et al.* (2011). Nucleolar disruption in dopaminergic neurons leads to oxidative damage and parkinsonism through repression of mammalian target of rapamycin signaling. The Journal of neuroscience : the official journal of the Society for Neuroscience *31*, 453-460.
Rinon, A., Molchadsky, A., Nathan, E., Yovel, G., Rotter, V., Sarig, R., and Tzahor, E. (2011). p53 coordinates cranial neural crest cell growth and epithelial-mesenchymal transition/delamination processes. Development *138*, 1827-1838.
Ritossa, F.M., and Spiegelman, S. (1965). Localization of DNA complementary to ribosomal RNA in the nucleolus organizer region of *Drosophila melanogaster* Proceedings of the National Academy of Sciences *53*, 737-745.
Roukos, V., Pegoraro, G., Voss, T.C., and Misteli, T. (2015). Cell cycle staging of individual cells by fluorescence microscopy. Nat Protoc *10*, 334-348.
Roukos, V., Voss, T.C., Schmidt, C.K., Lee, S., Wangsa, D., and Misteli, T. (2013). Spatial dynamics of chromosome translocations in living cells. Science *341*, 660-664.
Roussel, P., André, C., Comai, L., and Hernandez-Verdun, D. (1996). The rDNA transcription machinery is assembled during mitosis in active NORs and absent in inactive NORs. J Cell Biol *133*, 235-246.

Rubbi, C.P., and Milner, J. (2003). Disruption of the nucleolus mediates stabilization of p53 in response to DNA damage and other stresses. EMBO J *22*, 6068-6077.
Ruggero, D. (2012). Revisiting the nucleolus: from marker to dynamic integrator of cancer signaling. Sci Signal *5*, pe38.
Ruggero, D. (2013). Translational control in cancer etiology. Cold Spring Harb Perspect Biol *5*.
Ruggero, D., and Pandolfi, P.P. (2003). Does the ribosome translate cancer? Nat Rev Cancer *3*, 179-192.
Ruggero, D., and Shimamura, A. (2014). Marrow failure: a window into ribosome biology. Blood *124*, 2784-2792.
Russo, A., and Russo, G. (2017). Ribosomal Proteins Control or Bypass p53 during Nucleolar Stress. Int J Mol Sci *18*.
Salim, D., Bradford, W.D., Freeland, A., Cady, G., Wang, J., Pruitt, S.C., and Gerton, J.L. (2017). DNA replication stress restricts ribosomal DNA copy number. PLOS Genetics *13*, e1007006.
Sampath, S.C., Ohi, R., Leismann, O., Salic, A., Pozniakovski, A., and Funabiki, H. (2004). The chromosomal passenger complex is required for chromatin-induced microtubule stabilization and spindle assembly. Cell *118*, 187-202.
Sanchez, E., Laplace-Builhé, B., Mau-Them, F.T., Richard, E., Goldenberg, A., Toler, T.L., Guignard, T., Gatinois, V., Vincent, M., Blanchet, C., *et al.* (2020). POLR1B and neural crest cell anomalies in Treacher Collins syndrome type 4. Genetics in Medicine *22*, 547-556.
Sander, T., Freyss, J., von Korff, M., and Rufener, C. (2015). DataWarrior: an open-source program for chemistry aware data visualization and analysis. J Chem Inf Model *55*, 460-473.
Sanij, E., Hannan, K.M., Xuan, J., Yan, S., Ahern, J.E., Trigos, A.S., Brajanovski, N., Son, J., Chan, K.T., Kondrashova, O., *et al.* (2020). CX-5461 activates the DNA damage response and demonstrates therapeutic efficacy in high-grade serous ovarian cancer. Nature Communications *11*, 2641.
Sanij, E., and Hannan, R.D. (2009). The role of UBF in regulating the structure and dynamics of transcriptionally active rDNA chromatin. Epigenetics *4*, 374-382.
Savino, T.M., Gebrane-Younes, J., De Mey, J., Sibarita, J.B., and Hernandez-Verdun, D. (2001). Nucleolar assembly of the rRNA processing machinery in living cells. J Cell Biol *153*, 1097-1110.
Scherl, A., Coute, Y., Deon, C., Calle, A., Kindbeiter, K., Sanchez, J.C., Greco, A., Hochstrasser, D., and Diaz, J.J. (2002). Functional proteomic analysis of human nucleolus. Mol Biol Cell *13*, 4100-4109.
Schmickel, R.D. (1973). Quantitation of Human Ribosomal DNA: Hybridization of Human DNA with Ribosomal RNA for Quantitation and Fractionation. Pediatric Research *7*, 5-12.
Scull, C.E., Zhang, Y., Tower, N., Rasmussen, L., Padmalayam, I., Hunter, R., Zhai, L., Bostwick, R., and Schneider, D.A. (2019). Discovery of novel inhibitors of ribosome biogenesis by innovative high throughput screening strategies. Biochemical Journal *476*, 2209-2219.
Seike, M., Omatsu, Y., Watanabe, H., Kondoh, G., and Nagasawa, T. (2018). Stem cell niche-specific Ebf3 maintains the bone marrow cavity. Genes & Development.

Sen Gupta, A., and Sengupta, K. (2017). Lamin B2 Modulates Nucleolar Morphology, Dynamics, and Function. Molecular and cellular biology *37*.
Shi, Z., Fujii, K., Kovary, K.M., Genuth, N.R., Röst, H.L., Teruel, M.N., and Barna, M. (2017). Heterogeneous Ribosomes Preferentially Translate Distinct Subpools of mRNAs Genome-wide. Mol Cell *67*, 71-83 e77.
Shiratori, M., Suzuki, T., Itoh, C., Goto, M., Furuichi, Y., and Matsumoto, T. (2002). WRN helicase accelerates the transcription of ribosomal RNA as a component of an RNA polymerase I-associated complex. Oncogene *21*, 2447-2454.
Sia, P.I., Wood, J.P., Chidlow, G., Sharma, S., Craig, J., and Casson, R.J. (2016). Role of the nucleolus in neurodegenerative diseases with particular reference to the retina: a review. Clin Exp Ophthalmol *44*, 188-195.
Sigoillot, F.D., and King, R.W. (2011). Vigilance and validation: Keys to success in RNAi screening. ACS Chem Biol *6*, 47-60.
Silvera, D., Formenti, S.C., and Schneider, R.J. (2010). Translational control in cancer. Nature Reviews Cancer *10*, 254-266.
Sinclair, D.A., and Guarente, L. (1997). Extrachromosomal rDNA circles--a cause of aging in yeast. Cell *91*, 1033-1042.
Sirri , V., Hernandez-Verdun , D.l., and Roussel , P. (2002). Cyclin-dependent kinases govern formation and maintenance of the nucleolus. Journal of Cell Biology *156*, 969-981.
Sirri, V., Roussel, P., and Hernandez-Verdun, D. (2000). In Vivo Release of Mitotic Silencing of Ribosomal Gene Transcription Does Not Give Rise to Precursor Ribosomal RNA Processing. Journal of Cell Biology *148*, 259-270.
Sleven, H., Welsh, S.J., Yu, J., Churchill, M.E.A., Wright, C.F., Henderson, A., Horvath, R., Rankin, J., Vogt, J., Magee, A., *et al.* (2017). De Novo Mutations in EBF3 Cause a Neurodevelopmental Syndrome. The American Journal of Human Genetics *100*, 138-150.
Sloan, K.E., Mattijssen, S., Lebaron, S., Tollervey, D., Pruijn, G.J., and Watkins, N.J. (2013). Both endonucleolytic and exonucleolytic cleavage mediate ITS1 removal during human ribosomal RNA processing. J Cell Biol *200*, 577-588.
Smith, J.S., Caputo, E., and Boeke, J.D. (1999). A genetic screen for ribosomal DNA silencing defects identifies multiple DNA replication and chromatin-modulating factors. Mol Cell Biol *19*, 3184-3197.
Snodgrass, R.G., Collier, A.C., Coon, A.E., and Pritsos, C.A. (2010). Mitomycin C inhibits ribosomal RNA: a novel cytotoxic mechanism for bioreductive drugs. J Biol Chem *285*, 19068-19075.
Sokka, M., Rilla, K., Miinalainen, I., Pospiech, H., and Syvaoja, J.E. (2015). High levels of TopBP1 induce ATR-dependent shut-down of rRNA transcription and nucleolar segregation. Nucleic Acids Res *43*, 4975-4989.
Sondalle, S.B., and Baserga, S.J. (2014). Human diseases of the SSU processome. Biochim Biophys Acta *1842*, 758-764.
Splendore, A., Silva, E.O., Alonso, L.G., Richieri-Costa, A., Alonso, N., Rosa, A., Carakushanky, G., Cavalcanti, D.P., Brunoni, D., and Passos-Bueno, M.R. (2000). High mutation detection rate in TCOF1 among Treacher Collins syndrome patients reveals clustering of mutations and 16 novel pathogenic changes. Hum Mutat *16*, 315-322.

Stacchiotti, A., Favero, G., and Rezzani, R. (2018). Resveratrol and SIRT1 Activators for the Treatment of Aging and Age-Related Diseases.
Stanley, C.S., Thelin, J.W., and Miles, J.H. (1988). Mixed hearing loss in Larsen Syndrome. Clinical Genetics *33*, 395-398.
Stelzer, G., Rosen, N., Plaschkes, I., Zimmerman, S., Twik, M., Fishilevich, S., Stein, T.I., Nudel, R., Lieder, I., Mazor, Y., *et al.* (2016). The GeneCards Suite: From Gene Data Mining to Disease Genome Sequence Analyses. Current Protocols in Bioinformatics *54*, 1.30.31-31.30.33.
Stenström, L., Mahdessian, D., Gnann, C., Cesnik, A.J., Ouyang, W., Leonetti, M.D., Uhlén, M., Cuylen-Haering, S., Thul, P.J., and Lundberg, E. (2020). Mapping the nucleolar proteome reveals a spatiotemporal organization related to intrinsic protein disorder. Molecular Systems Biology *16*, e9469.
Stults, D.M., Killen, M.W., Pierce, H.H., and Pierce, A.J. (2008). Genomic architecture and inheritance of human ribosomal RNA gene clusters. Genome Res *18*, 13-18.
Stults, D.M., Killen, M.W., Williamson, E.P., Hourigan, J.S., Vargas, H.D., Arnold, S.M., Moscow, J.A., and Pierce, A.J. (2009). Human rRNA gene clusters are recombinational hotspots in cancer. Cancer Res *69*, 9096-9104.
Sudmant, P.H., Lee, H., Dominguez, D., Heiman, M., and Burge, C.B. (2018). Widespread Accumulation of Ribosome-Associated Isolated 3' UTRs in Neuronal Cell Populations of the Aging Brain. Cell Rep *25*, 2447-2456 e2444.
Sugihara, R., and Yasuzumi, G. (1970). The fine structure of nuclei as revealed by electron microscopy. Zeitschrift für Zellforschung und Mikroskopische Anatomie *107*, 466-478.
Sulima, S.O., Kampen, K.R., and De Keersmaecker, K. (2019). Cancer Biogenesis in Ribosomopathies. Cells *8*.
Sullivan, G.J., Bridger, J.M., Cuthbert, A.P., Newbold, R.F., Bickmore, W.A., and McStay, B. (2001). Human acrocentric chromosomes with transcriptionally silent nucleolar organizer regions associate with nucleoli. EMBO J *20*, 2867-2874.
Tafforeau, L., Zorbas, C., Langhendries, J.L., Mullineux, S.T., Stamatopoulou, V., Mullier, R., Wacheul, L., and Lafontaine, D.L. (2013). The complexity of human ribosome biogenesis revealed by systematic nucleolar screening of Pre-rRNA processing factors. Mol Cell *51*, 539-551.
Tan, X., and Awuah, S.G. (2019). A cell-based screening system for RNA polymerase I inhibitors. Medchemcomm *10*, 1765-1774.
Tassabehji, M., Hammond, P., Karmiloff-Smith, A., Thompson, P., Thorgeirsson, S.S., Durkin, M.E., Popescu, N.C., Hutton, T., Metcalfe, K., Rucka, A., *et al.* (2005). GTF2IRD1 in craniofacial development of humans and mice. Science *310*, 1184-1187.
Teber, O.A., Gillessen-Kaesbach, G., Fischer, S., Böhringer, S., Albrecht, B., Albert, A., Arslan-Kirchner, M., Haan, E., Hagedorn-Greiwe, M., Hammans, C., *et al.* (2004). Genotyping in 46 patients with tentative diagnosis of Treacher Collins syndrome revealed unexpected phenotypic variation. Eur J Hum Genet *12*, 879-890.
Tee, A.R. (2018). The Target of Rapamycin and Mechanisms of Cell Growth. Int J Mol Sci *19*.

Thomas, P.D., Campbell, M.J., Kejariwal, A., Mi, H., Karlak, B., Daverman, R., Diemer, K., Muruganujan, A., and Narechania, A. (2003). PANTHER: a library of protein families and subfamilies indexed by function. Genome Res *13*, 2129-2141.

Thul, P.J., Akesson, L., Wiking, M., Mahdessian, D., Geladaki, A., Ait Blal, H., Alm, T., Asplund, A., Bjork, L., Breckels, L.M., *et al.* (2017). A subcellular map of the human proteome. Science *356*.

Thul, P.J., and Lindskog, C. (2018). The human protein atlas: A spatial map of the human proteome. Protein Sci *27*, 233-244.

Tiku, V., and Antebi, A. (2018). Nucleolar Function in Lifespan Regulation. Trends Cell Biol *28*, 662-672.

Tiku, V., Jain, C., Raz, Y., Nakamura, S., Heestand, B., Liu, W., Spath, M., Suchiman, H.E.D., Muller, R.U., Slagboom, P.E., *et al.* (2017). Small nucleoli are a cellular hallmark of longevity. Nat Commun *8*, 16083.

Trainor, P.A., and Merrill, A.E. (2014). Ribosome biogenesis in skeletal development and the pathogenesis of skeletal disorders. Biochimica et Biophysica Acta (BBA) - Molecular Basis of Disease *1842*, 769-778.

Turi, Z., Lacey, M., Mistrik, M., and Moudry, P. (2019). Impaired ribosome biogenesis: mechanisms and relevance to cancer and aging. Aging (Albany NY) *11*, 2512-2540.

Uehara, R., Tsukada, Y., Kamasaki, T., Poser, I., Yoda, K., Gerlich, D.W., and Goshima, G. (2013). Aurora B and Kif2A control microtubule length for assembly of a functional central spindle during anaphase. J Cell Biol *202*, 623-636.

Uhlen, M., Zhang, C., Lee, S., Sjöstedt, E., Fagerberg, L., Bidkhori, G., Benfeitas, R., Arif, M., Liu, Z., Edfors, F., *et al.* (2017). A pathology atlas of the human cancer transcriptome. Science *357*, eaan2507.

Valdez, B.C., Henning, D., So, R.B., Dixon, J., and Dixon, M.J. (2004). The Treacher Collins syndrome (TCOF1) gene product is involved in ribosomal DNA gene transcription by interacting with upstream binding factor. Proc Natl Acad Sci U S A *101*, 10709-10714.

van Riggelen, J., Yetil, A., and Felsher, D.W. (2010). MYC as a regulator of ribosome biogenesis and protein synthesis. Nat Rev Cancer *10*, 301-309.

van Sluis, M., and McStay, B. (2015). A localized nucleolar DNA damage response facilitates recruitment of the homology-directed repair machinery independent of cell cycle stage. Genes Dev *29*, 1151-1163.

van Sluis, M., van Vuuren, C., Mangan, H., and McStay, B. (2020). NORs on human acrocentric chromosome p-arms are active by default and can associate with nucleoli independently of rDNA. Proc Natl Acad Sci U S A *117*, 10368-10377.

van Sluis, M., van Vuuren, C., and McStay, B. (2016). The Relationship Between Human Nucleolar Organizer Regions and Nucleoli, Probed by 3D-ImmunoFISH. In The Nucleolus: Methods and Protocols, A. Németh, ed. (New York, NY: Springer New York), pp. 3-14.

Verstraeten, V.L., Peckham, L.A., Olive, M., Capell, B.C., Collins, F.S., Nabel, E.G., Young, S.G., Fong, L.G., and Lammerding, J. (2011). Protein farnesylation inhibitors cause donut-shaped cell nuclei attributable to a centrosome separation defect. Proc Natl Acad Sci U S A *108*, 4997-5002.

Vesela, E., Chroma, K., Turi, Z., and Mistrik, M. (2017). Common Chemical Inductors of Replication Stress: Focus on Cell-Based Studies. Biomolecules *7*.
Vijayalingam, S., Subramanian, T., Zhao, L.-j., and Chinnadurai, G. (2016). The Cellular Protein Complex Associated with a Transforming Region of E1A Contains c-MYC. Journal of Virology *90*, 1070-1079.
Visintin, R., and Amon, A. (2000). The nucleolus: the magician's hat for cell cycle tricks. Curr Opin Cell Biol *12*, 372-377.
Voit, R., Schafer, K., and Grummt, I. (1997). Mechanism of repression of RNA polymerase I transcription by the retinoblastoma protein. Mol Cell Biol *17*, 4230-4237.
Walters, H.E., and Cox, L.S. (2018). mTORC Inhibitors as Broad-Spectrum Therapeutics for Age-Related Diseases. Int J Mol Sci *19*.
Wang, M., Anikin, L., and Pestov, D.G. (2014). Two orthogonal cleavages separate subunit RNAs in mouse ribosome biogenesis. Nucleic Acids Res *42*, 11180-11191.
Wang, M., and Lemos, B. (2019). Ribosomal DNA harbors an evolutionarily conserved clock of biological aging. Genome Res *29*, 325-333.
Warmerdam, D.O., van den Berg, J., and Medema, R.H. (2016). Breaks in the 45S rDNA Lead to Recombination-Mediated Loss of Repeats. Cell Rep *14*, 2519-2527.
Warmerdam, D.O., and Wolthuis, R.M.F. (2019). Keeping ribosomal DNA intact: a repeating challenge. Chromosome Res *27*, 57-72.
Warner, J.R., Vilardell, J., and Sohn, J.H. (2001). Economics of ribosome biosynthesis. Cold Spring Harb Symp Quant Biol *66*, 567-574.
Warren, A.J. (2018). Molecular basis of the human ribosomopathy Shwachman-Diamond syndrome. Adv Biol Regul *67*, 109-127.
Watt, K.E.N., Neben, C.L., Hall, S., Merrill, A.E., and Trainor, P.A. (2018). tp53-dependent and independent signaling underlies the pathogenesis and possible prevention of Acrofacial Dysostosis–Cincinnati type. Human Molecular Genetics *27*, 2628-2643.
Watt, K.E.N., and Trainor, P.A. (2014). Chapter 17 - Neurocristopathies: The Etiology and Pathogenesis of Disorders Arising from Defects in Neural Crest Cell Development. In Neural Crest Cells, P.A. Trainor, ed. (Boston: Academic Press), pp. 361-394.
Weaver, K.N., Watt, Kristin E.N., Hufnagel, Robert B., Navajas Acedo, J., Linscott, Luke L., Sund, Kristen L., Bender, Patricia L., König, R., Lourenco, Charles M., Hehr, U., *et al.* (2015). Acrofacial Dysostosis, Cincinnati Type, a Mandibulofacial Dysostosis Syndrome with Limb Anomalies, Is Caused by POLR1A Dysfunction. The American Journal of Human Genetics *96*, 765-774.
Weiss, W.A., Taylor, S.S., and Shokat, K.M. (2007). Recognizing and exploiting differences between RNAi and small-molecule inhibitors. Nat Chem Biol *3*, 739-744.
Wessel, S.R., Mohni, K.N., Luzwick, J.W., Dungrawala, H., and Cortez, D. (2019). Functional Analysis of the Replication Fork Proteome Identifies BET Proteins as PCNA Regulators. Cell Reports *28*, 3497-3509.e3494.
Wild, T., Horvath, P., Wyler, E., Widmann, B., Badertscher, L., Zemp, I., Kozak, K., Csucs, G., Lund, E., and Kutay, U. (2010). A protein inventory of human

ribosome biogenesis reveals an essential function of exportin 5 in 60S subunit export. PLoS Biol *8*, e1000522.
Woolford, J.L., Jr., and Baserga, S.J. (2013). Ribosome biogenesis in the yeast Saccharomyces cerevisiae. Genetics *195*, 643-681.
Xu, B., Li, H., Perry, J.M., Singh, V.P., Unruh, J., Yu, Z., Zakari, M., McDowell, W., Li, L., and Gerton, J.L. (2017a). Ribosomal DNA copy number loss and sequence variation in cancer. PLOS Genetics *13*, e1006771.
Xu, H., Di Antonio, M., McKinney, S., Mathew, V., Ho, B., O'Neil, N.J., Santos, N.D., Silvester, J., Wei, V., Garcia, J., *et al.* (2017b). CX-5461 is a DNA G-quadruplex stabilizer with selective lethality in BRCA1/2 deficient tumours. Nature Communications *8*, 14432.
Yao, R.-W., Xu, G., Wang, Y., Shan, L., Luan, P.-F., Wang, Y., Wu, M., Yang, L.-Z., Xing, Y.-H., Yang, L., *et al.* (2019). Nascent Pre-rRNA Sorting via Phase Separation Drives the Assembly of Dense Fibrillar Components in the Human Nucleolus. Molecular Cell *76*, 767-783.e711.
Yin, T., Lallena, M.J., Kreklau, E.L., Fales, K.R., Carballares, S., Torrres, R., Wishart, G.N., Ajamie, R.T., Cronier, D.M., Iversen, P.W., *et al.* (2014). A novel CDK9 inhibitor shows potent antitumor efficacy in preclinical hematologic tumor models. Mol Cancer Ther *13*, 1442-1456.
Young, D.J., Guydosh, N.R., Zhang, F., Hinnebusch, A.G., and Green, R. (2015). Rli1/ABCE1 Recycles Terminating Ribosomes and Controls Translation Reinitiation in 3'UTRs In Vivo. Cell *162*, 872-884.
Zeng, L., Li, Z., Pan, L., Li, H., Wu, J., Yuan, X., Li, Z., Liang, D., and Wu, L. (2021). Novel GZF1 pathogenic variants identified in two Chinese patients with Larsen syndrome. Clinical Genetics *99*, 281-285.
Zhai, W., and Comai, L. (2000). Repression of RNA polymerase I transcription by the tumor suppressor p53. Mol Cell Biol *20*, 5930-5938.
Zhou, J., and Giannakakou, P. (2005). Targeting microtubules for cancer chemotherapy. Curr Med Chem Anticancer Agents *5*, 65-71.
Zhou, Y., Schmitz, K.-M., Mayer, C., Yuan, X., Akhtar, A., and Grummt, I. (2009). Reversible acetylation of the chromatin remodelling complex NoRC is required for non-coding RNA-dependent silencing. Nature Cell Biology *11*, 1010-1016.

Appendix I

166 DNA repair proteins localize to the nucleolus. Three nucleolar proteomes were analyzed for the presence of DNA repair proteins based on Gene Ontology (GO) Consortium categorization (GO: 0006281). The “Combined” column is the 166 total unique DNA repair proteins identified. HGNC symbols are shown. Proteins in bold were identified in more than one proteome.

NOPDB [n=136; (Ahmad et al., 2009; Leung et al., 2006)]	Gautier [n=38; (Jarboui et al., 2011)]	Human Protein Atlas [n=40; (Thul et al., 2017; Thul and Lindskog, 2018)	Combined (n=166)
ACTL6A	APEX1	APEX2	ACTL6A
APEX1	AQR	APTX	**APEX1**
APTX	BAZ1B	CDC5L	APEX2
AQR	BRCA2	CHAF1A	**APTX**
ASF1A	CDC5L	CSNK1D	**AQR**
ATM	CHD1L	DCLRE1A	ASF1A
ATR	DDB1	DTL	ATM
ATRIP	DDX1	FANCD2	ATR
ATRX	DEK	FANCG	ATRIP
BAZ1B	EXO1	FEN1	ATRX
BCCIP	FANCI	HMGA1	**BAZ1B**
BLM	FEN1	HMGA2	BCCIP
CDK1	HMGA1	HMGB2	BLM
CDK2	HMGB1	INO80C	BRCA2
CDK7	HMGB2	INO80E	**CDC5L**
CDK9	HUWE1	KDM2A	CDK1
CHAF1A	KDM2A	KDM4A	CDK2
COPS2	NONO	MAD2L2	CDK7

COPS3	PARP1	MEIOB	CDK9
COPS7B	PCNA	MUS81	**CHAF1A**
COPS8	PRKDC	NPM1	CHD1L
CSNK1D	RAD21	NUDT16	COPS2
CSNK1E	RAD50	PARP2	COPS3
CUL4A	RBM14	PNKP	COPS7B
CUL4B	RFC1	POLR2F	COPS8
DDB1	RFC2	POLR2K	**CSNK1D**
DDX1	RFC4	PRMT6	CSNK1E
DEK	RFC5	RAD51	CUL4A
ERCC2	RPA1	RNF111	CUL4B
ERCC3	SETX	RPAIN	DCLRE1A
FANCD2	SFPQ	SETMAR	**DDB1**
FANCI	SMC1A	SFR1	**DDX1**
FEN1	SMC3	SMARCA5	**DEK**
GTF2H1	SSRP1	SUMO1	DTL
GTF2H2	SUMO3	SUPT16H	ERCC2
GTF2H2C	TERF2	UBE2N	ERCC3
GTF2H4	TRRAP	UBE2T	EXO1
H2AFX	UHRF1	USP28	**FANCD2**
HIST1H4A		WDR33	FANCG
HIST3H2A		YY1	**FANCI**
HIST3H3			**FEN1**

HLTF			GTF2H1
HMGA1			GTF2H2
HMGA2			GTF2H2C
HMGB1			GTF2H4
HMGB2			H2AFX
HSPA1A			HIST1H4A
HUS1B			HIST3H2A
HUWE1			HIST3H3
INTS3			HLTF
ISG15			**HMGA1**
KDM1A			**HMGA2**
KDM2A			**HMGB1**
KIN			**HMGB2**
KPNA2			HSPA1A
LIG1			HUS1B
LIG3			**HUWE1**
MC1R			INO80C
MDC1			INO80E
MLH1			INTS3
MMS19			ISG15
MNAT1			KDM1A
MORF4L1			**KDM2A**
MRE11A			KDM4A

MSH2			KIN
MSH6			KPNA2
MUTYH			LIG1
NONO			LIG3
NPM1			MAD2L2
NSMCE1			MC1R
NSMCE4A			MDC1
OTUB1			MEIOB
PARG			MLH1
PARP1			MMS19
PCNA			MNAT1
PNKP			MORF4L1
POLR2E			MRE11A
POLR2H			MSH2
POLR2K			MSH6
POLR2L			MUS81
PPIE			MUTYH
PPP4C			**NONO**
PRKDC			**NPM1**
PRPF19			NSMCE1
PSMD14			NSMCE4A
PSME4			NUDT16
RAD21			OTUB1

RAD50			PARG
RAD51AP1			**PARP1**
RBM14			PARP2
RBX1			**PCNA**
RECQL			**PNKP**
RFC1			POLR2E
RFC2			POLR2F
RFC3			POLR2H
RFC4			**POLR2K**
RFC5			POLR2L
RIF1			PPIE
RPA3			PPP4C
RPS27A			**PRKDC**
RPS27L			PRMT6
RPS3			PRPF19
RUVBL1			PSMD14
RUVBL2			PSME4
SFPQ			**RAD21**
SMARCA5			**RAD50**
SMC1A			RAD51
SMC3			RAD51AP1
SMC5			**RBM14**
SMC6			RBX1

SSRP1			RECQL
SUMO1			**RFC1**
SUMO2			**RFC2**
SUMO3			RFC3
SUPT16H			**RFC4**
TCEA1			**RFC5**
TOPBP1			RIF1
TRIM28			RNF111
TRIP12			RPA1
TRRAP			RPA3
UBA52			RPAIN
UBB			RPS27A
UBC			RPS27L
UBE2D3			RPS3
UBE2I			RUVBL1
UBE2N			RUVBL2
UBE2V2			SETMAR
UBR5			SETX
USP28			**SFPQ**
USP7			SFR1
VCP			**SMARCA5**
WHSC1			**SMC1A**
WRN			**SMC3**

XRCC1			SMC5
XRCC5			SMC6
XRCC6			**SSRP1**
			SUMO1
			SUMO2
			SUMO3
			SUPT16H
			TCEA1
			TERF2
			TOPBP1
			TRIM28
			TRIP12
			TRRAP
			UBA52
			UBB
			UBC
			UBE2D3
			UBE2I
			UBE2N
			UBE2T
			UBE2V2
			UBR5
			UHRF1

			USP28
			USP7
			VCP
			WDR33
			WHSC1
			WRN
			XRCC1
			XRCC5
			XRCC6
			YY1

Appendix II

The 113 high confidence screen hits that, when depleted, caused an increase in the percentage of nuclei with ≥5 nucleoli. Yeast ortholog, ≥5 nucleoli per nucleus normalized percent effect (NPE), percent viability, and nucleolar localization are indicated. The positive control, KIF11, was the top hit.

Screen hit (HGNC)	Yeast ortholog	≥5 nucleoli per nucleus NPE	Percent viability	Nucleolar (Y/N)
KIF11	Cin8/Kip1	68.75	19.00	N
CDCA8	Nbl1	66.59	12.91	Y
ASIC1		65.17	5.21	N
CMPK2	Cdc8	64.91	17.38	N
WBP11		64.64	12.61	Y
KRT222		61.43	30.53	N
MICA		60.63	28.23	N
ATAD5	Elg1	59.75	27.67	N
RAP2C		57.83	38.96	N
SKP1	Skp1	57.64	13.00	Y
TPX2		53.84	5.99	Y
CIAO2B		47.53	26.97	N
PRRT2		47.35	21.61	N
RFFL		47.17	8.70	N
C11orf63		47.03	11.05	N
ZER1		46.73	43.72	N
MAN1A1	Mnl2	46.40	35.63	N
MFSD4		46.29	15.22	N
INCENP	Sli15	45.64	18.92	Y
SHC3		45.32	21.55	N
ENY2	Sus1	41.93	6.02	N
CUL1	Cdc53	41.61	36.50	Y
SHROOM2		40.79	16.04	N
CTF1		40.36	8.66	N
MDN1	Rea1	39.82	29.07	Y
ZDHHC17	Akr1/2	39.45	53.42	N
CDCA5		39.33	9.55	N
CASP8AP2		39.14	13.82	Y
HYPK		38.87	15.80	N
INKA1		38.64	14.41	N
NAT2		38.52	27.49	N
IRF2BP1		37.62	38.21	N

PMM2	Sec53	37.35	23.22	N
GLYATL2		36.68	28.51	N
TTC22		36.12	21.61	N
XRCC5	Yku80	35.61	42.14	Y
CYP4V2		35.61	58.17	N
RRM1	Rnr1/3	35.33	9.46	N
FAM221A		34.73	49.23	N
ECHDC2		34.49	22.43	N
RBBP8		33.82	21.42	N
CCDC81		33.78	22.74	N
KRBA1		32.89	29.14	N
PRUNE		32.76	19.24	N
SCRN3		32.28	63.05	N
AGR2		31.52	25.80	N
SMG5	Ebs1/Est1	31.03	27.66	N
LAPTM5		30.61	32.18	N
DBNDD1		30.51	10.27	N
RFC1		30.18	46.61	Y
IFT88		30.16	57.16	N
C9orf142		29.86	29.73	N
SGOL1		29.67	16.63	N
EBF3		29.63	36.33	N
MCM6	Mcm6	29.60	54.59	Y
OSBP2	Hes1/Kes1	29.58	14.65	N
PRAM1		29.56	14.07	N
GCNT2		29.56	34.99	N
ZNF219		29.31	45.34	N
LDB1		29.25	50.16	N
FAM58A		29.22	22.15	N
LIG3		29.07	40.91	Y
SNX21		29.02	25.45	N
GLTP		28.95	20.74	N
GZF1		28.93	47.20	Y
MAP4K5		28.92	27.53	N
SLC26A7		28.77	61.21	N

TARS2	Mst1	28.66	36.20	N
ABCE1	Rli1	28.57	25.65	Y
LCORL		28.28	21.07	N
TYMP		28.06	72.51	N
MRPL52		27.86	36.04	N
RIMS3	Tcb3	27.82	10.82	Y
WBSCR27		27.79	33.22	N
H1-10	Hho1	27.78	31.61	Y
ZNF678		27.75	19.58	Y
RACGAP1	Bem2/Rga1/2/Rgd1	27.62	15.60	N
STK24	Kic1/Pbs2	27.53	13.92	Y
SLC2A12	Stl1	27.49	71.34	N
NGRN	Rrg9	27.47	25.68	N
LUC7L	Luc7	27.15	25.86	N
YIPF7	Yip1	27.11	5.29	N
WRAP53	Swt21	27.10	9.48	N
DYNC1H1	Dyn1	26.87	19.67	Y
GEN1		26.82	51.87	N
NR0B2		26.79	37.50	N
ANKEF1		26.73	22.43	Y
KTN1		26.70	14.57	N
FGD4	Cdc24/Rom1/2	26.65	28.85	N
MIA		26.64	39.43	N
CCN4		26.52	46.48	N
GOLGA8EP		26.48	20.11	N
TOPBP1	Dpb11	26.37	10.58	Y
SMAP2	Glo3/Gts1	26.24	33.90	N
OXNAD1	Aim33/Pga3	26.16	60.29	N
HSD11B2		26.09	21.32	N
MARCH9	Ssm4	26.06	68.46	N
TM2D1		26.04	19.78	N
PCOLCE2		26.02	19.56	N
CAMK2N1		25.99	26.33	N
RAPH1		25.95	6.16	N
MPV17L2	Mpv17	25.65	13.92	N

FAM98A		25.60	10.13	N
SUV39H1		25.56	32.30	N
TAF1D		25.54	27.66	Y
NFYB	Hap3	25.50	41.60	N
MASTL	Pkh3/Rim15	25.41	32.46	N
GTF2IRD1		25.38	24.82	N
SCN2B		25.29	15.56	N
MLL3		25.28	73.70	N
DDAH1		25.27	55.36	Y
NLRC5	Gip3/Her1	25.12	46.44	N
SMAD5		25.00	61.84	N

Appendix III

Cell cycle analysis of screen hits selected for validation by oligonucleotide deconvolution. Each siRNA in the pool of 4 was tested independently (n=3). Controls, siRISC-free and the siKIF11 pool, were also assayed (n=48). The column with the number (No.) of cells is the total sum of nuclei analyzed in all replicates and is number of cells used to generate the cumulative histograms in Figure 2-5. Significance is listed in parentheses below the mean ± SD and was determined by unpaired t-tests relative to siRISC-free and a False Discovery Rate approach using the two-stage step-up method of Benjamini, Krieger and Yekutieli (n=3 or 48; $q<0.01$=*; $q<0.001$=**; $q<0.0001$=***; ns=not significant). A column that includes the ≥5 nucleoli per nucleus normalized percent effect (NPE) is also included. NPE in black=validated; NPE in red=not validated.

Screen Hit (siRNA HGNC, -last 2 digits of product number)	**No. of cells (sum)**	**% G0/G1 (mean ± SD)**	**% S (mean ± SD)**	**% G2/M (mean ± SD)**	**% >4N (mean ± SD)**	**≥5 nucleoli per nucleus NPE**
siRISC-free	498,155	48.3 ± 2.0	10.2 ± 1.1	20.3 ± 0.8	2.7 ± 0.5	0
siKIF11 (pool)	93,027	12.2 ± 1.2 (q<0.0001)	7.5 ± 0.8 (q<0.0001)	60.6 ± 1.7 (q<0.0001)	12.1 ± 1.1 (q<0.0001)	100
siKIF11 -05	3426	16.5 ± 1.9 (q<0.0001)	9.1 ± 1.2 (ns)	56.1 ± 2.5 (q<0.0001)	7.2 ± 1.8 (q<0.0001)	89.98
siKIF11 -06	6816	15.8 ± 1.0 (q<0.0001)	8.7 ± 0.3 (q<0.01)	56.7 ± 0.8 (q<0.0001)	9.9 ± 0.3 (q<0.0001)	118.62
siKIF11 -07	2154	23.8 ± 4.5 (q<0.0001)	10.8 ± 2.1 (ns)	42.1 ± 1.6 (q<0.0001)	6.9 ± 2.4 (q<0.0001)	74.75

siKIF11 -08	2721	20.6 ± 2.3 (q<0.0001)	10.5 ± 1.0 (ns)	50.7 ± 3.5 (q<0.0001)	7.3 ± 0.4 (q<0.0001)	116.70
siABCE1 -01	12653	30.6 ± 0.7 (q<0.0001)	20.0 ± 0.3 (q<0.0001)	33.6 ± 1.0 (q<0.0001)	8.3 ± 0.6 (q<0.0001)	50.71
siABCE1 -02	22023	42.7 ± 1.0 (q<0.0001)	15.4 ± 0.7 (q<0.0001)	25.9 ± 0.6 (q<0.0001)	5.8 ± 0.3 (q<0.0001)	22.63
siABCE1 -04	19958	49.9 ± 1.5 (ns)	23.3 ± 0.4 (q<0.0001)	15.9 ± 0.9 (q<0.0001)	1.8 ± 0.2 (q<0.01)	26.31
siABCE1 -17	21264	50.2 ± 2.9 (ns)	12.9 ± 0.8 (q<0.0001)	21.7 ± 1.6 (q<0.001)	1.9 ± 0.2 (q<0.01)	9.86
siATAD5 -01	11302	32.3 ± 14.3 (q<0.0001)	32.3 ± 11.6 (q<0.0001)	24.1 ± 1.6 (q<0.0001)	3.9 ± 2.4 (q<0.01)	55.60

siATAD5 -02	17992	49.9 ± 3.5 (ns)	19.4 ± 2.0 (q<0.0001)	22.3 ± 1.2 (q<0.0001)	1.5 ± 0.4 (q<0.001)	16.49
siATAD5 -03	21010	45.1 ± 1.9 (q<0.01)	17.2 ± 0.9 (q<0.0001)	25.7 ± 1.1 (q<0.0001)	2.7 ± 0.2 (ns)	25.01
siATAD5 -04	14337	37.0 ± 5.6 (q<0.0001)	19.8 ± 3.9 (q<0.0001)	27.8 ± 2.2 (q<0.0001)	4.1 ± 0.5 (q<0.0001)	22.60
siCCN4 -01	24641	45.9 ± 0.9 (q<0.01)	20.3 ± 1.8 (q<0.0001)	15.4 ± 0.4 (q<0.0001)	2.6 ± 0.2 (ns)	17.85
siCCN4 -02	4868	40.6 ± 4.3 (q<0.0001)	14.6 ± 2.0 (q<0.0001)	30.8 ± 3.3 (q<0.0001)	2.5 ± 0.6 (ns)	18.51
siCCN4 -03	7630	44.5 ± 1.7 (q<0.01)	13.7 ± 1.0 (q<0.0001)	27.8 ± 0.3 (q<0.0001)	2.0 ± 0.4 (ns)	23.89
siCCN4 -17	12550	35.7 ± 2.2	24.5 ± 1.1	28.1 ± 0.3	3.3 ± 0.5	42.10

		(q<0.0001)	(q<0.0001)	(q<0.0001)	(ns)	
siCDCA8 -01	6261	10.6 ± 0.4 (q<0.0001)	7.9 ± 0.8 (q<0.001)	26.6 ± 0.6 (q<0.0001)	43.2 ± 0.5 (q<0.0001)	82.17
siCDCA8 -02	5595	10.4 ± 0.7 (q<0.0001)	8.7 ± 0.3 (ns)	23.8 ± 1.1 (q<0.0001)	45.2 ± 1.5 (q<0.0001)	60.19
siCDCA8 -03	5073	30.5 ± 1.0 (q<0.0001)	14.6 ± 0.9 (q<0.0001)	27.0 ± 0.8 (q<0.0001)	13.6 ± 1.3 (q<0.0001)	23.40
siCDCA8 -04	8186	23.7 ± 0.4 (q<0.0001)	12.0 ± 0.8 (q<0.01)	28.7 ± 0.5 (q<0.0001)	20.4 ± 0.1 (q<0.0001)	44.40
siCIAO2B -01	16932	42.3 ± 2.1 (q<0.0001)	32.0 ± 4.2 (q<0.0001)	16.3 ± 0.8 (q<0.0001)	1.7 ± 0.0 (q<0.001)	24.41
siCIAO2B -03	14686	38.2 ± 1.6	32.7 ± 1.7	17.1 ± 0.7	2.1 ± 0.2 (ns)	7.62

		(q<0.0001)	(q<0.0001)	(q<0.0001)		
siCIAO2B -04	19264	41.6 ± 1.5 (q<0.0001)	24.0 ± 1.8 (q<0.0001)	21.9 ± 0.8 (q<0.001)	4.8 ± 0.2 (q<0.0001)	15.48
siCIAO2B -18	14660	41.3 ± 3.7 (q<0.0001)	37.7 ± 3.5 (q<0.0001)	10.1 ± 0.3 (q<0.0001)	0.9 ± 0.1 (q<0.0001)	26.18
siDYNC1H1 -01	15255	32.0 ± 0.3 (q<0.0001)	25.3 ± 0.9 (q<0.0001)	33.1 ± 1.0 (q<0.0001)	4.0 ± 0.7 (q<0.001)	22.40
siDYNC1H1 -02	16855	33.3 ± 0.2 (q<0.0001)	21.1 ± 0.8 (q<0.0001)	26.3 ± 0.2 (q<0.0001)	7.1 ± 0.6 (q<0.0001)	24.91
siDYNC1H1 -03	10371	23.0 ± 0.7 (q<0.0001)	22.4 ± 1.1 (q<0.0001)	39.2 ± 0.1 (q<0.0001)	6.9 ± 0.4 (q<0.0001)	79.29
siDYNC1H1 -04	21012	37.7 ± 1.3	18.7 ± 1.3	23.3 ± 0.5	7.0 ± 0.3	9.05

		(q<0.0001)	(q<0.0001)	(q<0.0001)	(q<0.0001)	
siENY2 -01	18169	39.6 ± 0.7 (q<0.0001)	25.0 ± 0.8 (q<0.0001)	19.3 ± 0.3 (q<0.01)	5.3 ± 0.1 (q<0.0001)	15.62
siENY2 -02	10196	43.1 ± 1.4 (q<0.0001)	15.5 ± 0.7 (q<0.0001)	26.4 ± 1.3 (q<0.0001)	7.0 ± 0.9 (q<0.0001)	29.06
siENY2 -03	21547	35.8 ± 0.5 (q<0.0001)	24.5 ± 0.9 (q<0.0001)	21.2 ± 0.9 (ns)	5.7 ± 0.7 (q<0.0001)	24.64
siENY2 -04	14896	43.8 ± 1.6 (q<0.0001)	28.6 ± 0.9 (q<0.0001)	16.5 ± 0.4 (q<0.0001)	2.1 ± 0.5 (ns)	16.54
siFAM98A -01	7481	38.5 ± 1.5 (q<0.0001)	24.4 ± 1.0 (q<0.0001)	23.8 ± 0.5 (q<0.0001)	3.1 ± 0.4 (ns)	23.43
siFAM98A -02	9898	31.0 ± 3.6	32.0 ± 1.7	23.9 ± 1.2	5.1 ± 0.6	30.61

		(q<0.0001)	(q<0.0001)	(q<0.0001)	(q<0.0001)	
siFAM98A -03	31999	47.9 ± 0.8 (ns)	11.2 ± 0.6 (ns)	20.0 ± 0.4 (ns)	3.6 ± 0.2 (q<0.0001)	-1.10
siFAM98A -04	12092	33.1 ± 3.6 (q<0.0001)	35.2 ± 3.1 (q<0.0001)	18.8 ± 0.7 (q<0.001)	4.1 ± 0.4 (q<0.0001)	37.85
siH1-10 -01	19495	40.2 ± 7.0 (q<0.0001)	17.5 ± 5.7 (q<0.0001)	27.4 ± 1.0 (q<0.0001)	5.4 ± 0.3 (q<0.0001)	19.98
siH1-10 -02	3095	26.7 ± 1.4 (q<0.0001)	10.9 ± 1.3 (ns)	37.6 ± 4.7 (q<0.0001)	5.7 ± 0.4 (q<0.0001)	38.30
siH1-10 -03	20063	54.2 ± 0.6 (q<0.0001)	10.3 ± 1.4 (ns)	19.8 ± 0.7 (ns)	2.1 ± 0.2 (ns)	16.89
siH1-10 -04	5378	64.3 ± 5.4	16.2 ± 5.3	9.0 ± 0.6	1.5 ± 0.5 (q<0.001)	10.30

		(q<0.0001)	(q<0.0001)	(q<0.0001)		
siINCENP -01	5191	14.1 ± 0.5 (q<0.0001)	9.3 ± 1.0 (ns)	29.6 ± 0.7 (q<0.0001)	28.0 ± 2.1 (q<0.0001)	63.31
siINCENP -02	6073	13.1 ± 1.2 (q<0.0001)	7.9 ± 0.3 (q<0.001)	43.1 ± 2.0 (q<0.0001)	25.7 ± 0.9 (q<0.0001)	107.86
siINCENP -03	5151	14.6 ± 1.9 (q<0.0001)	9.5 ± 0.3 (ns)	42.4 ± 2.7 (q<0.0001)	19.4 ± 0.9 (q<0.0001)	84.39
siINCENP -04	7989	19.9 ± 0.6 (q<0.0001)	9.1 ± 0.3 (ns)	38.4 ± 0.4 (q<0.0001)	20.0 ± 1.7 (q<0.0001)	65.05
siINKA1 -01	8245	24.3 ± 0.6 (q<0.0001)	13.0 ± 1.4 (q<0.0001)	50.4 ± 0.5 (q<0.0001)	5.7 ± 0.2 (q<0.0001)	81.39
siINKA1 -02	18874	33.1 ± 0.5	15.1 ± 0.7	28.0 ± 1.2	10.6 ± 0.9	12.47

		(q<0.0001)	(q<0.0001)	(q<0.0001)	(q<0.0001)	
siINKA1 -03	20994	56.5 ± 1.3 (q<0.0001)	21.2 ± 1.2 (q<0.0001)	14.5 ± 0.1 (q<0.0001)	1.3 ± 0.2 (q<0.0001)	17.64
siINKA1 -04	7543	30.0 ± 3.2 (q<0.0001)	16.8 ± 2.7 (q<0.0001)	38.3 ± 1.2 (q<0.0001)	6.9 ± 0.2 (q<0.0001)	31.55
siKTN1 -17	15844	43.6 ± 1.3 (q<0.0001)	26.6 ± 1.7 (q<0.0001)	16.9 ± 0.8 (q<0.0001)	3.5 ± 0.4 (q<0.01)	41.87
siKTN1 -18	2762	22.7 ± 2.1 (q<0.0001)	10.0 ± 0.7 (ns)	47.8 ± 1.8 (q<0.0001)	4.2 ± 0.7 (q<0.0001)	44.02
siKTN1 -19	29473	55.4 ± 2.1 (q<0.0001)	10.9 ± 0.7 (ns)	19.2 ± 0.9 (ns)	2.7 ± 0.3 (ns)	4.61
siKTN1 -20	22507	46.0 ± 0.4 (ns)	18.1 ± 0.2	22.4 ± 0.6	3.9 ± 0.2 (q<0.001)	16.93

			(q<0.0001)	(q<0.0001)		
siLUC7L -01	1855	30.5 ± 2.8 (q<0.0001)	11.6 ± 1.4 (q<0.01)	34.1 ± 3.0 (q<0.0001)	6.2 ± 2.2 (q<0.0001)	36.19
siLUC7L -02	9450	39.6 ± 2.7 (q<0.0001)	30.3 ± 3.8 (q<0.0001)	15.7 ± 0.2 (q<0.0001)	2.4 ± 0.6 (ns)	6.67
siLUC7L -03	24023	51.5 ± 0.7 (q<0.01)	25.4 ± 1.1 (q<0.0001)	14.2 ± 0.6 (q<0.0001)	1.6 ± 0.2 (q<0.001)	7.84
siLUC7L -04	15445	38.4 ± 1.5 (q<0.0001)	28.5 ± 2.5 (q<0.0001)	21.1 ± 0.7 (q<0.01)	2.2 ± 0.0 (ns)	22.01
siMDN1 -03	22383	61.8 ± 4.5 (q<0.0001)	17.6 ± 4.3 (ns)	11.6 ± 0.5 (q<0.0001)	1.5 ± 0.2 (q<0.001)	16.23
siMDN1 -17	10682	64.0 ± 0.2	10.7 ± 0.9 (ns)	16.0 ± 0.3	1.4 ± 0.1	10.86

		(q<0.0001)		(q<0.0001)	(q<0.0001)	
siMDN1 -18	18302	52.2 ± 0.9 (q<0.001)	24.3 ± 3.0 (q<0.0001)	14.6 ± 0.6 (q<0.0001)	1.4 ± 0.2 (q<0.001)	8.92
siMDN1 -19	16924	51.6 ± 1.8 (q<0.01)	15.7 ± 1.3 (q<0.0001)	18.9 ± 1.2 (q<0.001)	2.1 ± 0.2 (ns)	28.03
siRACGAP1 -01	10345	28.6 ± 1.8 (q<0.0001)	19.5 ± 1.6 (q<0.0001)	31.1 ± 0.8 (q<0.0001)	10.7 ± 0.9 (q<0.0001)	51.56
siRACGAP1 -02	14099	33.4 ± 1.3 (q<0.0001)	15.0 ± 0.3 (q<0.0001)	27.8 ± 0.6 (q<0.0001)	9.0 ± 1.3 (q<0.0001)	34.13
siRACGAP1 -03	9246	20.7 ± 2.0 (q<0.0001)	14.2 ± 0.6 (q<0.0001)	37.3 ± 1.6 (q<0.0001)	17.2 ± 1.5 (q<0.0001)	66.49
siRACGAP1 -04	6630	15.1 ± 1.7	15.7 ± 1.0	34.3 ± 0.7	23.8 ± 2.4	58.42

		(q<0.0001)	(q<0.0001)	(q<0.0001)	(q<0.0001)	
siRFC1 -01	22242	36.7 ± 1.0 (q<0.0001)	21.5 ± 1.7 (q<0.0001)	28.7 ± 0.9 (q<0.0001)	5.1 ± 0.2 (q<0.0001)	12.31
siRFC1 -02	18739	35.2 ± 2.3 (q<0.0001)	24.5 ± 0.3 (q<0.0001)	27.6 ± 0.9 (q<0.0001)	3.7 ± 0.4 (q<0.01)	15.79
siRFC1 -03	18566	38.5 ± 2.1 (q<0.0001)	24.6 ± 1.4 (q<0.0001)	26.9 ± 0.6 (q<0.0001)	2.6 ± 0.2 (ns)	20.99
siRFC1 -04	32219	46.9 ± 0.6 (ns)	10.8 ± 1.0 (ns)	21.8 ± 0.2 (q<0.001)	4.5 ± 0.1 (q<0.0001)	0.60
siSTK24 -05	13758	41.3 ± 2.1 (q<0.0001)	34.8 ± 1.9 (q<0.0001)	15.0 ± 0.6 (q<0.0001)	2.0 ± 0.3 (q<0.01)	7.04
siSTK24 -21	30865	52.6 ± 2.3	11.5 ± 1.7 (ns)	19.3 ± 0.4 (q<0.01)	2.8 ± 0.2 (ns)	1.81

		(q<0.0001)				
siSTK24 -22	15617	37.4 ± 3.9 (q<0.0001)	25.7 ± 2.9 (q<0.0001)	23.6 ± 0.6 (q<0.0001)	3.6 ± 0.4 (q<0.01)	17.66
siSTK24 -23	11330	43.4 ± 3.4 (q<0.0001)	37.5 ± 2.9 (q<0.0001)	12.0 ± 0.8 (q<0.0001)	1.4 ± 0.1 (q<0.0001)	29.89
siTPX2 -01	3189	18.7 ± 2.6 (q<0.0001)	12.4 ± 2.2 (q<0.001)	49.8 ± 2.8 (q<0.0001)	9.0 ± 0.3 (q<0.0001)	38.82
siTPX2 -02	6023	16.5 ± 1.3 (q<0.0001)	10.6 ± 1.1 (ns)	50.9 ± 0.6 (q<0.0001)	6.7 ± 0.7 (q<0.0001)	102.59
siTPX2 -03	10750	47.2 ± 3.5 (ns)	22.9 ± 2.6 (q<0.0001)	15.9 ± 0.4 (q<0.0001)	2.8 ± 0.4 (ns)	39.05
siTPX2 -04	7667	34.5 ± 2.3	18.3 ± 0.6 (ns)	26.0 ± 1.3	6.1 ± 0.9	31.55

		(q<0.0001)		(q<0.0001)	(q<0.0001)	
siWRAP53 -19	31592	49.2 ± 1.4 (ns)	12.6 ± 1.0 (q<0.001)	21.4 ± 0.9 (q<0.01)	4.2 ± 0.4 (q<0.0001)	2.90
siWRAP53 -20	17584	38.1 ± 1.9 (q<0.0001)	33.2 ± 0.6 (q<0.0001)	16.5 ± 1.4 (q<0.0001)	2.4 ± 0.3 (ns)	28.11
siWRAP53 -21	18888	41.2 ± 0.6 (q<0.0001)	26.9 ± 0.5 (q<0.0001)	20.9 ± 0.7 (ns)	3.3 ± 0.3 (ns)	18.45
siWRAP53 -22	17244	41.0 ± 1.0 (q<0.0001)	29.8 ± 0.9 (q<0.0001)	18.6 ± 0.2 (q<0.001)	2.4 ± 0.2 (ns)	38.53
siXRCC5 -01	24899	50.9 ± 2.0 (q<0.01)	21.5 ± 1.4 (q<0.0001)	18.8 ± 0.5 (q<0.01)	1.9 ± 0.3 (q<0.01)	8.08
siXRCC5 -02	25424	49.4 ± 1.2 (ns)	13.2 ± 0.8	23.2 ± 1.0	3.3 ± 0.3 (ns)	6.89

			(q<0.0001)	(q<0.0001)		
siXRCC5 -03	24903	48.2 ± 2.0 (ns)	15.0 ± 0.7 (q<0.0001)	25.8 ± 0.8 (q<0.0001)	2.2 ± 0.4 (ns)	-1.50
siXRCC5 -04	31137	53.9 ± 0.8 (ns)	10.2 ± 0.3 (ns)	19.3 ± 0.2 (q<0.01)	2.7 ± 0.2 (ns)	-2.68

Effect on nucleolar number of 25 candidate compounds screened in positive control search for a high-throughput screen. 25 compounds were tested at 8 different concentrations. Mean percent effect (PE) from 3 replicates relative to DMSO (0.1%; DMSO=100 PE), seeded at 2,000 cells per well and incubated for 48 hrs, are shown for each phenotype. Percent viability relative to DMSO (0.1%) is also shown for each condition.

Appendix IV

Effect on nucleolar number of 25 candidate compounds screened in positive control search for a high-throughput screen. 25 compounds were tested at 8 different concentrations. Mean percent effect (PE) from 3 replicates relative to DMSO (0.1%; DMSO=100 PE), seeded at 2,000 cells per well and incubated for 48 hrs, are shown for each phenotype. Percent viability relative to DMSO (0.1%) is also shown for each condition.

Drug name	Concentr-ation (μM)	One nucleolus per nucleus PE (mean ± SD)	≥5 nucleoli per nucleus PE (mean ± SD)	Percent viability (mean ± SD)
5-Fluorouracil	20	106.7 ± 46.8	139.1 ± 103.5	20.2 ± 13.1
5-Fluorouracil	6.7	81.3 ± 12.7	292.7 ± 55.5	27.4 ± 0.8
5-Fluorouracil	2.2	80.3 ± 15.1	251.2 ± 19	29.1 ± 1.8
5-Fluorouracil	0.7	74 ± 6.5	219.7 ± 30.3	27 ± 8.5
5-Fluorouracil	0.2	73.1 ± 9.7	283.9 ± 7.3	41.3 ± 3.1
5-Fluorouracil	0.08	68.7 ± 8.1	222.5 ± 41.7	89.5 ± 2.5
5-Fluorouracil	0.03	77.4 ± 5.4	178.2 ± 28	109.3 ± 8.2
5-Fluorouracil	0.009	78 ± 7.7	177.3 ± 4.4	116.2 ± 6.4
Actinomycin D	20	13.5 ± 6.5	9.2 ± 8.3	3.4 ± 0.7
Actinomycin D	6.7	19.6 ± 12.4	69.3 ± 78.2	3.6 ± 2.3
Actinomycin D	2.2	18 ± 5.5	70.5 ± 96	2.5 ± 0.8
Actinomycin D	0.7	18 ± 9	32.7 ± 26.9	2.8 ± 0.8
Actinomycin D	0.2	22.1 ± 7.6	22.4 ± 19.7	4.2 ± 0.8
Actinomycin D	0.08	29.8 ± 5.6	156.2 ± 119	1.9 ± 0.4
Actinomycin D	0.03	48.9 ± 23.3	58.9 ± 62.6	2.3 ± 1.1
Actinomycin D	0.009	17.2 ± 13.8	10 ± 13.6	5.4 ± 2.6
Amperozide	20	86.2 ± 3.3	54.4 ± 10.5	66.1 ± 8.6
Amperozide	6.7	86.6 ± 7.6	86.1 ± 11.8	82 ± 5.5
Amperozide	2.2	87 ± 3.7	139.4 ± 4.4	86.1 ± 0.9
Amperozide	0.7	91.6 ± 4.6	106.2 ± 25.1	73.1 ± 1.6

Amperozide	0.2	70.5 ± 7.1	83.8 ± 8.4	77.8 ± 10.1
Amperozide	0.08	85.8 ± 4.9	124.2 ± 21.8	70 ± 1.5
Amperozide	0.03	92.7 ± 10.5	101.8 ± 21.6	77 ± 3.6
Amperozide	0.009	103.8 ± 4.8	100.5 ± 23.1	68.6 ± 2.9
BMH-21	20	26.8 ± 22.3	31 ± 23	5 ± 0.2
BMH-21	6.7	215.2 ± 135.6	40 ± 24.3	7.6 ± 3.5
BMH-21	2.2	331.1 ± 22.1	5.1 ± 1.1	15.8 ± 0.5
BMH-21	0.7	314.5 ± 34	7.6 ± 1.9	17.2 ± 3.2
BMH-21	0.2	89.6 ± 9.6	111.7 ± 46.2	50.8 ± 3
BMH-21	0.08	73.9 ± 7.1	155.2 ± 25	114.8 ± 17.1
BMH-21	0.03	76.5 ± 12.1	169.1 ± 12	120.1 ± 7.4
BMH-21	0.009	59.8 ± 15.4	153.9 ± 26.5	103.1 ± 19.2
C646	20	102.6 ± 11.5	127.4 ± 30.3	44.7 ± 23.8
C646	6.7	96.2 ± 22.8	107 ± 12.3	83.6 ± 6.2
C646	2.2	92.8 ± 22.1	104.1 ± 37.6	89.8 ± 5.8
C646	0.7	91.9 ± 10.1	115.2 ± 20.5	96.7 ± 9.5
C646	0.2	89.4 ± 3.5	124.2 ± 30	90.1 ± 1.6
C646	0.08	82.7 ± 9.3	99.4 ± 17	93.5 ± 4.3
C646	0.03	92.4 ± 2.5	123 ± 4.3	87.2 ± 10.8
C646	0.009	87.4 ± 15	108 ± 23.1	83.6 ± 5.1
CDK9 Inhibitor	20	70.2 ± 3.2	342.4 ± 16	47.5 ± 4.5
CDK9 Inhibitor	6.7	78.1 ± 13.5	179.1 ± 1.9	89.4 ± 10.2
CDK9 Inhibitor	2.2	88 ± 7.6	151.4 ± 15.4	94 ± 14.6

CDK9 Inhibitor	0.7	75.8 ± 24.2	133.1 ± 38.7	97.6 ± 11.4
CDK9 Inhibitor	0.2	63.4 ± 48.5	96 ± 75.7	62.6 ± 52.1
CDK9 Inhibitor	0.08	73.9 ± 13.2	122.5 ± 11.4	96.4 ± 9.7
CDK9 Inhibitor	0.03	61.3 ± 19.8	78.6 ± 57.4	61.2 ± 49.2
CDK9 Inhibitor	0.009	81.5 ± 21	119.7 ± 31.8	90.1 ± 13.4
Cisplatin	20	77.2 ± 15.2	281.8 ± 47.1	23.9 ± 2.9
Cisplatin	6.7	53.6 ± 29.9	157.9 ± 71	40 ± 9.1
Cisplatin	2.2	92.7 ± 10.6	162.4 ± 15.1	69.1 ± 10.2
Cisplatin	0.7	116.4 ± 7.3	96.6 ± 16.3	101.4 ± 0.2
Cisplatin	0.2	75.7 ± 7.6	108.1 ± 5.4	95.3 ± 3.1
Cisplatin	0.08	77.3 ± 23.4	94.5 ± 34	97.5 ± 6
Cisplatin	0.03	108.8 ± 7.1	100.3 ± 14.7	81.9 ± 12.1
Cisplatin	0.009	100 ± 22.5	67.7 ± 53.5	57.7 ± 44.5
CX-5461	20	173.9 ± 6.4	91.2 ± 13	26.8 ± 2.6
CX-5461	6.7	133 ± 3.3	115 ± 14.2	26.2 ± 4.5
CX-5461	2.2	107.1 ± 11.8	164.5 ± 10.7	33.2 ± 7.9
CX-5461	0.7	92.2 ± 29.1	131.7 ± 42.5	25.5 ± 18.8
CX-5461	0.2	100.5 ± 5.5	182.1 ± 5.6	36.4 ± 11
CX-5461	0.08	75.9 ± 6.1	193.1 ± 29.9	60.7 ± 7.5
CX-5461	0.03	67.1 ± 13	186.2 ± 28.4	86.5 ± 4.2
CX-5461	0.009	79.1 ± 1.2	183.9 ± 22	113.3 ± 8.6
Doxorubicin	20	99.5 ± 19.1	36.3 ± 51.5	7.9 ± 1
Doxorubicin	6.7	91.5 ± 21.3	37.2 ± 32.5	10.1 ± 1

Doxorubicin	2.2	91.2 ± 9.8	2.6 ± 2.7	9.8 ± 0.6
Doxorubicin	0.7	235.8 ± 58.8	42.3 ± 28.4	2.3 ± 1.2
Doxorubicin	0.2	300 ± 35.1	8.6 ± 7.6	7.6 ± 2.5
Doxorubicin	0.08	232.9 ± 28.3	22.9 ± 1.4	7.3 ± 1.5
Doxorubicin	0.03	121.6 ± 5.6	162.7 ± 46.6	10.4 ± 1.7
Doxorubicin	0.009	71.7 ± 25.5	88.3 ± 30	38.5 ± 5.4
Etoposide	20	173.7 ± 21.4	125.6 ± 20.2	14.7 ± 1.6
Etoposide	6.7	111.2 ± 15.5	275 ± 43.2	15.1 ± 0.8
Etoposide	2.2	88.1 ± 7	415.8 ± 36.8	15.9 ± 1.7
Etoposide	0.7	95.5 ± 4.3	365.2 ± 36.4	21.7 ± 2.3
Etoposide	0.2	89.1 ± 10.4	258.6 ± 26.5	46.3 ± 4.1
Etoposide	0.08	82.7 ± 23	185.1 ± 43.3	73.6 ± 5.3
Etoposide	0.03	85.7 ± 14.6	179.5 ± 19.4	96.6 ± 4.6
Etoposide	0.009	91.4 ± 10.2	138.6 ± 2.3	110.6 ± 12
Fenbendazole	20	143.1 ± 20.2	251.4 ± 45.7	4.8 ± 0.8
Fenbendazole	6.7	136.5 ± 12.7	185.8 ± 114.7	5 ± 0.4
Fenbendazole	2.2	113.2 ± 16.8	261.2 ± 35.4	5.2 ± 2.8
Fenbendazole	0.7	161.8 ± 17.4	138.2 ± 9.3	13.4 ± 1.8
Fenbendazole	0.2	89.7 ± 11.7	107 ± 5.7	86.4 ± 5.1
Fenbendazole	0.08	73.8 ± 22.9	85.8 ± 51.8	64 ± 49.8
Fenbendazole	0.03	89.2 ± 4.8	112.1 ± 19.7	85.2 ± 7.8
Fenbendazole	0.009	98.6 ± 18.5	94.4 ± 19.6	77.6 ± 6
Flavopiridol	20	133.5 ± 39	215.7 ± 50.6	1.9 ± 0.6

Flavopiridol	6.7	125.3 ± 83.7	130 ± 65.6	2.2 ± 0.9
Flavopiridol	2.2	163.9 ± 44.5	104.7 ± 59.7	1.6 ± 0.9
Flavopiridol	0.7	87.1 ± 44.6	163 ± 115.8	1.4 ± 1
Flavopiridol	0.2	114.6 ± 74.2	88.7 ± 67	3.8 ± 1.6
Flavopiridol	0.08	97.5 ± 6.2	241.7 ± 80.6	7.9 ± 1.2
Flavopiridol	0.03	73.1 ± 8.9	194.3 ± 56.1	73.7 ± 4.7
Flavopiridol	0.009	79.3 ± 9.7	127.3 ± 13.1	93.5 ± 3.9
Hesperadin	20	230.3 ± 11.8	55.2 ± 25.1	3.2 ± 0.9
Hesperadin	6.7	211.3 ± 17.4	92.2 ± 29.1	9.4 ± 1
Hesperadin	2.2	200.4 ± 2.9	130.9 ± 16.4	10 ± 0.5
Hesperadin	0.7	152.1 ± 29.9	192.5 ± 45.4	10.4 ± 1.5
Hesperadin	0.2	120 ± 3.7	374 ± 37.6	12.4 ± 1.8
Hesperadin	0.08	96.9 ± 4.9	459.7 ± 38	16.1 ± 3.4
Hesperadin	0.03	73.3 ± 10.3	242.2 ± 52.5	44.3 ± 5.9
Hesperadin	0.009	90.5 ± 4.2	154.4 ± 28.4	89.9 ± 9.5
Ispinesib	20	6 ± 1.7	2 ± 3.5	5.8 ± 0.9
Ispinesib	6.7	201.6 ± 19.3	121.6 ± 24.2	3.2 ± 0.7
Ispinesib	2.2	93.4 ± 16.4	332.8 ± 51.2	3.7 ± 0.4
Ispinesib	0.7	94.6 ± 10.1	296.5 ± 58.2	3.6 ± 0.9
Ispinesib	0.2	105.7 ± 22.5	266.9 ± 80.4	4.7 ± 1.7
Ispinesib	0.08	114 ± 18.8	316.7 ± 12	4.1 ± 0.8
Ispinesib	0.03	83.5 ± 43.4	152 ± 130.3	5 ± 1.4
Ispinesib	0.009	79.7 ± 41.9	197.9 ± 159.6	6.6 ± 0.7

IWP-2	20	77.9 ± 31.9	71.6 ± 44.7	48.3 ± 35
IWP-2	6.7	89.6 ± 14.4	96.9 ± 13.8	80.9 ± 2.8
IWP-2	2.2	80 ± 20	91.3 ± 21.6	72.5 ± 10
IWP-2	0.7	104.2 ± 9.6	85 ± 7	75.8 ± 1.1
IWP-2	0.2	87.5 ± 22.3	85 ± 30.8	53.8 ± 41.6
IWP-2	0.08	99.6 ± 9.1	89.4 ± 5.9	76.7 ± 3.6
IWP-2	0.03	97.3 ± 11.7	85.8 ± 16	54.3 ± 15.1
IWP-2	0.009	109.3 ± 11.6	74.2 ± 27	57.1 ± 18.9
LY411575	20	70.9 ± 4.2	121.7 ± 26.9	79.6 ± 3.8
LY411575	6.7	85.6 ± 10	123.7 ± 16.2	78.1 ± 5
LY411575	2.2	86.4 ± 7.9	139.1 ± 10.5	85.1 ± 1.8
LY411575	0.7	84.1 ± 2	143.8 ± 18.1	93.5 ± 6.8
LY411575	0.2	79.6 ± 7.2	127.1 ± 19.8	85.4 ± 2.6
LY411575	0.08	83.7 ± 13.6	136.9 ± 5.3	90.1 ± 1.8
LY411575	0.03	67.8 ± 18.3	112.3 ± 28.2	85.1 ± 6.3
LY411575	0.009	68.7 ± 18.3	124.9 ± 29.8	90.6 ± 6.8
Metarrestin	20	201.9 ± 35	12 ± 3.4	26.5 ± 3.3
Metarrestin	6.7	86.2 ± 26.9	46.4 ± 14	48.2 ± 36.1
Metarrestin	2.2	87.6 ± 4.6	83.9 ± 10.4	76.6 ± 5.8
Metarrestin	0.7	101 ± 7.9	74.5 ± 3.5	74 ± 20.8
Metarrestin	0.2	95.3 ± 3.7	125.8 ± 10.3	79.4 ± 6
Metarrestin	0.08	91.2 ± 3.4	105 ± 12.8	77.5 ± 9.9
Metarrestin	0.03	85.4 ± 22.9	66.8 ± 42.7	54.5 ± 40.2

Metarrestin	0.009	97.2 ± 19.4	72.4 ± 4.4	69.4 ± 1.8
Metformin	20	121.5 ± 8.5	78.3 ± 27.7	66.2 ± 51.4
Metformin	6.7	111.9 ± 8	99.6 ± 5.1	85.7 ± 10.7
Metformin	2.2	104.1 ± 9.5	108 ± 11.4	92.5 ± 3.9
Metformin	0.7	93.4 ± 12.9	115.1 ± 16.3	98.2 ± 7.9
Metformin	0.2	82.1 ± 14.5	98.3 ± 24.2	95.5 ± 6.5
Metformin	0.08	85.1 ± 6.4	136.6 ± 12.3	87.8 ± 19.5
Metformin	0.03	67.1 ± 29.4	95.2 ± 59.2	60.4 ± 46
Metformin	0.009	80.9 ± 13.5	135.9 ± 22.8	96 ± 0.6
Mitomycin C	20	237 ± 135.9	18.2 ± 16.2	1 ± 0.3
Mitomycin C	6.7	213.3 ± 142	13.1 ± 6.6	9.6 ± 2.8
Mitomycin C	2.2	155 ± 95.8	36.7 ± 14.4	10.4 ± 5.4
Mitomycin C	0.7	117.4 ± 5	219.2 ± 20.8	18 ± 1
Mitomycin C	0.2	78.4 ± 15.9	346 ± 65.7	26 ± 3.8
Mitomycin C	0.08	78.7 ± 11.1	297.5 ± 51.7	42.1 ± 8.6
Mitomycin C	0.03	77 ± 2.9	236.7 ± 11.7	67.7 ± 8.3
Mitomycin C	0.009	76.5 ± 8.9	180.2 ± 30.5	85.5 ± 2.2
Paclitaxel	20	123.7 ± 18.8	372 ± 49.3	3.2 ± 0.2
Paclitaxel	6.7	112.5 ± 65	171.7 ± 161.3	4.1 ± 3.5
Paclitaxel	2.2	121.5 ± 11.2	359.4 ± 60.8	2 ± 0.3
Paclitaxel	0.7	154.6 ± 4.7	306.7 ± 24	2.2 ± 0.5
Paclitaxel	0.2	90.1 ± 22.4	268.4 ± 55.3	1.8 ± 0.4
Paclitaxel	0.08	143.4 ± 6.3	227 ± 40.5	2.3 ± 1

Paclitaxel	0.03	113.2 ± 35.3	374.5 ± 88.2	2.3 ± 0.1
Paclitaxel	0.009	152.6 ± 15.9	250 ± 60.9	7.9 ± 1.4
SBE 13	20	54.6 ± 37.4	100.7 ± 73.9	69.7 ± 55.8
SBE 13	6.7	81 ± 7	163.5 ± 22.7	108 ± 2.9
SBE 13	2.2	79.6 ± 14.7	157.7 ± 13.4	106.3 ± 5.3
SBE 13	0.7	78.5 ± 9.6	160.3 ± 12.8	109.2 ± 1
SBE 13	0.2	82.8 ± 8.2	151.7 ± 10.5	105.2 ± 5.2
SBE 13	0.08	43.3 ± 28.9	47.6 ± 78.7	39 ± 56.9
SBE 13	0.03	78.8 ± 18.6	122.4 ± 21.3	84.7 ± 24.7
SBE 13	0.009	90.3 ± 4.1	114.8 ± 26.1	97.1 ± 8
Temsirolimus	20	116 ± 14.5	81 ± 24	25.5 ± 1.9
Temsirolimus	6.7	62 ± 9.9	159.6 ± 34.3	54.4 ± 4.6
Temsirolimus	2.2	77.4 ± 8.2	181 ± 9	54.4 ± 3.9
Temsirolimus	0.7	69.1 ± 8.2	213.4 ± 11.4	52.5 ± 3.8
Temsirolimus	0.2	57.6 ± 1.6	181.5 ± 53.6	43.1 ± 23.2
Temsirolimus	0.08	67.7 ± 3.1	198.5 ± 21.8	55.1 ± 6.6
Temsirolimus	0.03	65 ± 14.6	199 ± 31.9	58.1 ± 1.9
Temsirolimus	0.009	63 ± 7.6	206.3 ± 37.5	65.3 ± 2.6
Topotecan	20	263.1 ± 42.7	10.2 ± 17.7	1.2 ± 0.6
Topotecan	6.7	351.9 ± 31.8	3.4 ± 5.9	3.1 ± 0.3
Topotecan	2.2	247.9 ± 41.4	52.3 ± 10.7	8.1 ± 1.2
Topotecan	0.7	214.6 ± 24.3	69.3 ± 10.4	8.3 ± 1.5
Topotecan	0.2	156.7 ± 25.4	101 ± 9	11 ± 0.8

Topotecan	0.08	129.3 ± 27.1	150.6 ± 26.2	12.2 ± 1.1
Topotecan	0.03	95.5 ± 16.1	223.4 ± 41.2	12.8 ± 0.5
Topotecan	0.009	87.9 ± 11.2	302.7 ± 37.4	17.6 ± 1.6
Trichostatin A	20	148.7 ± 37.2	10.3 ± 8	7.4 ± 1.5
Trichostatin A	6.7	136.6 ± 34.2	5.6 ± 1.7	7.4 ± 0.6
Trichostatin A	2.2	186.6 ± 86	26.7 ± 10.5	3.8 ± 3
Trichostatin A	0.7	187.9 ± 4	49.8 ± 11.2	9.4 ± 0.6
Trichostatin A	0.2	88.6 ± 7.5	129.9 ± 30	48.3 ± 3.1
Trichostatin A	0.08	96.7 ± 7.2	133.7 ± 33.5	56.1 ± 4.5
Trichostatin A	0.03	95.4 ± 5.3	126.5 ± 15.2	66.6 ± 3.5
Trichostatin A	0.009	99.4 ± 21.7	91 ± 26.7	67.7 ± 3.8
XAV939	20	92.4 ± 3.9	107.6 ± 28	78.7 ± 9.3
XAV939	6.7	64 ± 6.5	101.3 ± 14.3	80.6 ± 2.6
XAV939	2.2	80.7 ± 8.8	136.4 ± 21.2	83.2 ± 8.9
XAV939	0.7	74.4 ± 9.7	139.7 ± 21	89 ± 11.4
XAV939	0.2	78.8 ± 11.9	144 ± 12.8	84.1 ± 9.9
XAV939	0.08	81.5 ± 5.7	141 ± 6.1	100.4 ± 5
XAV939	0.03	79.1 ± 11.2	137.4 ± 29.5	91.6 ± 10.1
XAV939	0.009	83.6 ± 6	138.2 ± 22.1	96.1 ± 6.2

Appendix V

The 110 FDA-approved drugs that caused a decrease in nucleolar number. Drug name, Chemical Abstracts Service (CAS) registry number, the one nucleolus normalized percent effect (NPE), percent (%) viability relative DMSO, medical use, and molecular target are indicated.

Drug Name	CAS No.	NPE	% Viab-ility	Medical use	Molecular target
Viadent (Sanguinarine sulfate)	5578-73-4	235.4	1.3	Antibacterial	Plasma membrane
Cetrimonium bromide	57-09-0	208.9	1.1	Antiseptic	Plasma membrane
Mitoxantrone	65271-80-9	188.7	5.9	Antineoplastic	Topo-isomerase
Rubitecan	91421-42-0	146.6	8.4	Antineoplastic	Topo-isomerase
Pixantrone dimaleate	144675-97-8	142.3	11.7	Antineoplastic	Topo-isomerase
GVS (gentian violet)	548-62-9	139.2	4.2	Antiseptic	Unknown
Vindesine sulfate	59917-39-4	138.1	6.6	Antineoplastic	Tubulin
Mitoxantrone hydrochloride	70476-82-3	131.9	5.9	Antineoplastic	Topo-isomerase
Lanoxin (digoxin)	20830-75-5	126.4	3.8	Cardiovascular agent	Na^+/K^+ ATPase
Topotecan hydrochloride	119413-54-6	126.4	7.9	Antineoplastic	Topo-isomerase

Vinblastine	865-21-4	125.7	6.3	Antineoplastic	Tubulin
Lanatoside C	17575-22-3	125.6	3.8	Cardiovascular agent	Na^+/K^+ ATPase
Ispinesib	336113-53-2	122.7	1.6	Antineoplastic	Kinesin (KIF11)
Vincristine sulfate	2068-78-2	122.5	7.1	Antineoplastic	Tubulin
Povan (pyrvinium pamoate)	3546-41-6	121.1	14.3	Antiparasitic	Unknown
Deslanoside	17598-65-1	120.5	2.7	Cardiovascular agent	Na^+/K^+ ATPase
Topotecan	123948-87-8	120.5	13.0	Antineoplastic	Topo-isomerase
Aclarubicin	57576-44-0	118.6	4.6	Antineoplastic	Topo-isomerase
Vinblastine sulfate	143-67-9	117.6	6.7	Antineoplastic	Tubulin
Proscillaridin	466-06-8	116.3	1.9	Cardiovascular agent	Na^+/K^+ ATPase
Cetylpyridinium chloride	6004-24-6	115.0	1.6	Antiseptic; Pharmaceutical preservative	Plasma membrane
Vinorelbine	71486-22-1	114.8	6.5	Antineoplastic	Tubulin
Crystodigin (digitoxin)	71-63-6	112.7	9.0	Cardiovascular agent	Na^+/K^+ ATPase

Velban (vinblastine sulfate)	143-67-9	111.5	7.5	Antineoplastic	Tubulin
Vinorelbine	71486-22-1	111.4	7.4	Antineoplastic	Tubulin
Vincristine	57-22-7	109.8	6.3	Antineoplastic	Tubulin
Acetyldigitoxin	1111-39-3	106.4	2.9	Cardiovascular agent	Na^+/K^+ ATPase
Oncovin (vincristine sulfate)	2068-78-2	105.8	6.3	Antineoplastic	Tubulin
Dacinostat	404951-53-7	104.7	6.1	Antineoplastic	Histone deacetylases
Vinleurosine	54081-68-4	104.4	8.2	Antineoplastic	Tubulin
Zinc omadine (pyrithione zinc)	13463-41-7	103.9	1.0	Antibacterial; Antifungal	Plasma membrane
Mutamycin (mitomycin)	50-07-7	103.5	15.7	Antineoplastic	DNA
Methyl-benzethonium chloride	1320-44-1	102.9	21.9	Antiseptic	Plasma membrane
Digitoxin	71-63-6	102.3	4.0	Cardiovascular agent	Na^+/K^+ ATPase
Plicamycin	18378-89-7	100.9	2.7	Antineoplastic	DNA
Maitansine	35846-53-8	100.5	6.8	Antineoplastic	Tubulin

Ouabain	11018-89-6	99.8	4.3	Cardiovascular agent	Na^+/K^+ ATPase
Mycophenolic acid	24280-93-1	99.7	20.4	Immuno-modulator	IMPDH
Caradrin (proscillaridin)	466-06-8	99.1	2.6	Cardiovascular agent	Na^+/K^+ ATPase
Miripirium	2748-88-1	99.0	18.2	Antiseptic	Plasma membrane
Dasatinib	863127-77-9	99.0	20.1	Antineoplastic	Tyrosine kinases
Podophyllin	900-55-9	97.3	6.2	Antiviral	Tubulin
Velban (vinblastine)	865-21-4	96.8	5.7	Antineoplastic	Tubulin
Aclarubicin	57576-44-0	96.8	1.0	Antineoplastic	Topo-isomerase
Puromycin dihydrochloride	58-58-2	96.7	13.7	Antibacterial; Antiparasitic	Ribosome
Eldesine (vindesine sulfate)	59917-39-4	96.5	6.2	Antineoplastic	Tubulin
Ouabain	11018-89-6	96.3	2.2	Cardiovascular agent	Na^+/K^+ ATPase
Octopirox (piroctone olamine)	68890-66-4	94.1	19.1	Antifungal	Unknown

Piroctone	50650-76-5	94.0	17.3	Antifungal	Unknown
Cerivastatin	145599-86-6	93.0	14.2	Cardiovascular agent	HMG-CoA reductase
Navelbine (vinorelbine)	71486-22-1	91.7	6.6	Antineoplastic	Tubulin
Soblidotin	149606-27-9	91.3	6.7	Antineoplastic	Tubulin
Emetine dihydrochloride	316-42-7	90.1	8.2	Antiparasitic	Ribosome
Vumon (teniposide)	29767-20-2	89.9	8.2	Antineoplastic	Topo-isomerase
Colchicine	64-86-8	88.1	8.9	Anti-inflammatory	Tubulin
Taltobulin	228266-40-8	87.3	7.0	Antineoplastic	Tubulin
Anthelvet (tetramizole hydrochloride)	5086-74-8	87.2	5.3	Antiparasitic; Antineoplastic; Immuno-modulator	Acetylcholine receptors
Benzethonium chloride	121-54-0	87.0	21.2	Antiseptic; Pharmaceutical preservative	Plasma membrane
Podofilox	518-28-5	86.2	7.0	Antineoplastic; Antiviral	Tubulin

Ciclopirox (ciclopirox olamine)	41621-49-2	85.5	18.0	Antifungal	Plasma membrane
Plicamycin	18378-89-7	84.0	2.3	Antineoplastic	DNA
Ciclopirox	29342-05-0	83.7	15.3	Antifungal	Plasma membrane
Azacitidine	320-67-2	83.0	10.8	Antineoplastic	DNA methyl-transferase
Pranidipine	99522-79-9	83.0	23.8	Cardiovascular agent	Ca^{+} channels
Mycophenolate mofetil	115007-34-6	82.9	20.5	Immuno-modulator	IMPDH
Vinformide	54022-49-0	82.6	6.8	Antineoplastic	Tubulin
Docusate sodium	577-11-7	81.6	2.5	Gastrointestinal agent	Unknown
Mepacrine	83-89-6	81.1	24.5	Antiparasitic	DNA
Condylox (podofilox)	518-28-5	81.0	6.3	Antiviral	Tubulin
Sertindole	106516-24-9	80.1	22.0	Antipsychotic	Dopamine receptor
Halofuginone	55837-20-2	79.1	0.5	Antiparasitic	tRNA synthetase

Alexidine hydrochloride	22573-93-9	78.4	25.4	Antiseptic	Plasma membrane
Vinblastine	865-21-4	78.2	5.8	Antineoplastic	Tubulin
Mitomycin C	50-07-7	77.3	21.4	Antineoplastic	DNA
Albendazole	54965-21-8	76.4	15.5	Antiparasitic	Fumarate reductase
Gemcitabine	95058-81-4	76.1	13.5	Antineoplastic	Ribonucleotide reductase
Colchicine	64-86-8	75.3	7.9	Anti-inflammatory	Tubulin
Roccal (benzalkonium chloride)	8001-54-5	74.9	22.4	Antiseptic; Pharmaceutical preservative	Plasma membrane
Mithracin (plicamycin)	18378-89-7	73.6	2.1	Antineoplastic	DNA
Hexachlorophene	70-30-4	73.1	20.9	Antiseptic	D-lactate dehydrogenase
BI-2536	755038-02-9	72.4	14.5	Antineoplastic	Polo-like kinase
Mozavaptan	137975-06-5	72.0	20.5	Cardiovascular agent	Arginine vasopressin receptor

Lestaurtinib	111358-88-4	71.6	6.7	Antineoplastic	Tyrosine kinases
Nocodazole	31430-18-9	71.4	8.1	Antineoplastic	Tubulin
Gramicidin	1405-97-6	70.7	24.7	Antibacterial	Plasma membrane
Albendazole	54965-21-8	70.4	19.4	Antiparasitic	Fumarate reductase
Edoxudine	15176-29-1	68.8	28.3	Antiviral	DNA polymerase
Idarubicin	58957-92-9	68.2	1.2	Antineoplastic	Topo-isomerase
Ixabepilone	219989-84-1	68.2	2.9	Antineoplastic	Tubulin
Clofarabine	123318-82-1	68.0	18.3	Antineoplastic	Ribonucleotide reductase
Cambendazole	26097-80-3	67.0	12.1	Antiparasitic	Fumarate reductase
Parbendazole	14255-87-9	65.4	5.7	Antiparasitic	Tubulin
Mebendazole	31431-39-7	65.2	6.0	Antiparasitic	Tubulin
Flubendazole	31430-15-6	64.5	14.2	Antiparasitic	Tubulin
CellCept (mycophenolate mofetil)	128794-94-5	63.9	20.4	Immuno-modulator	IMPDH

Mycophenolic acid	24280-93-1	63.8	20.9	Immuno-modulator	IMPDH
Riboprine	7724-76-7	62.3	16.4	Antineoplastic	Unknown
Daunorubicin	20830-81-3	62.2	1.4	Antineoplastic	Topo-isomerase
Lasalocid	25999-20-6	62.1	33.6	Antibacterial; Antiparasitic	Plasma membrane
Bryamycin (thiostrepton)	1393-48-2	61.3	23.8	Antibacterial	Ribosome
Gefitinib	184475-35-2	58.4	16.0	Antineoplastic	Tyrosine kinases
Fenbendazole	43210-67-9	58.1	14.1	Antiparasitic	Tubulin
Oxyphenbutazone	7081-38-1	57.8	3.8	Analgesic; Anti-inflammatory	Cyclo-oxygenase
Vorinostat	149647-78-9	57.7	16.9	Antineoplastic	Histone deacetylases
Oxibendazole	20559-55-1	55.5	32.4	Antiparasitic	Tubulin
Cosmegen (Dactinomycin)	50-76-0	55.4	1.3	Antineoplastic	DNA
Vermox (mebendazole)	31431-39-7	55.0	14.5	Antiparasitic	Tubulin
Niclofolan	10331-57-4	54.5	20.1	Antiparasitic	Unknown

Patupilone	152044-54-7	53.4	7.6	Antineoplastic	Tubulin
Cicloheximide (cycloheximide)	66-81-9	53.2	20.7	Antibacterial; Antifungal	Ribosome

Appendix VI

The 30 FDA-approved drugs that caused an increase in nucleolar number. Drug name, Chemical Abstracts Service (CAS) registry number, the ≥5 nucleoli normalized percent effect (NPE), percent (%) viability relative DMSO, medical use, and molecular targets are indicated.

Drug Name	CAS No.	NPE	% Viab-ility	Medical Use	Molecular Target
Monacrin (aminacrine)	90-45-9	364.3	16.5	Antiseptic	DNA
Melphalan	148-82-3	353.1	29.9	Antineoplastic	DNA
Merimepodib	198821-22-6	271.6	24.7	Antiparasitic; Antiviral	IMPDH
Docetaxel	114977-28-5	260.7	9.1	Antineoplastic	Tubulin
Acrisorcin	7527-91-5	236.6	18.6	Antifungal	DNA
Jevtana (cabazitaxel)	183133-96-2	235.3	8.4	Antineoplastic	Tubulin
Agrosan (phenylmercuric acetate)	62-38-4	201.4	2.1	Pharmaceutical preservative	Unknown
Taxol	33069-62-6	199.7	7.0	Antineoplastic	Tubulin
Fungizone (amphotericin B)	1397-89-3	183.6	6.2	Antifungal	Ergosterol
BI-831266	958227-46-8	174.4	28.7	Antineoplastic	Aurora B kinase
Taxotere (docetaxel)	148408-66-6	173.3	9.6	Antineoplastic	Tubulin

Alvocidib	131740-09-5	169.0	4.9	Antineoplastic	Cyclin-dependent kianses
Oxiconazole	64211-46-7	155.2	86.9	Antifungal	Ergosterol
CellCept (mycophenolate mofetil)	128794-94-5	145.0	18.9	Immuno-modulator	IMPDH
Chlormethine (mechlorethamine)	55-86-7	140.8	19.9	Antineoplastic	DNA
Butoconazole	64872-77-1	135.2	72.6	Antifungal	Ergosterol
Piperacillin	61477-96-1	134.2	99.2	Antibacterial	Penicillin binding protein
Vepesid (etoposide)	33419-42-0	133.3	32.3	Antineoplastic	Topo-isomerase
Thiomersal	54-64-8	132.7	1.0	Pharmaceutical preservative; Antiseptic	Unknown
Panflavin (acriflavinium hydrochloride)	8063-24-9	129.1	20.5	Antiseptic; Antiparasitic	DNA
Dalfopristin	112362-50-2	128.6	53.0	Antibacterial	Ribosome

Actosin (bucladesine)	362-74-3	126.6	44.3	Cardiovascular agent; Anti-ulcerative	Phospho-diesterase
Bortezomib	179324-69-7	125.9	0.8	Antineoplastic	Proteasome
Tegafur	17902-23-7	124.5	66.7	Antineoplastic	Thymidylate synthase
Sertaconazole	99592-32-2	124.2	90.0	Antifungal	Ergosterol
Mebendazole	31431-39-7	119.8	6.0	Antiparasitic	Tubulin
Tioconazole	65899-73-2	118.7	83.9	Antifungal	Ergosterol
Istaroxime	374559-48-5	117.5	34.3	Cardiovascular agent	Na^+/K^+ ATPase
Clobetasol propionate	25122-46-7	112.2	83.6	Anti-inflammatory	Gluco-corticoid recceptor
Oxiconazole	64211-46-7	110.3	90.0	Antifungal	Ergosterol

Appendix VII

The 234 synthetic, drug-like compounds that yielded either an increase or decrease in nucleolar number. Unique compound ID, the designated phenotype (one nucleolus per nucleus or ≥5 nucleoli per nucleus), the normalized percent effect (NPE) for each phenotype, and percent viability relative to DMSO (0.1%) are shown.

Compound ID	Pheno-type (1/≥5)	1 nucleolus per nucleus NPE	≥5 nucleoli per nucleus NPE	Percent viability
YU275173	1	82.1	-55.4	30.8
YU275624	1	79.5	-41.7	21.5
YU258006	1	78.8	-500.4	13.7
YU257337	1	74.0	-190.9	25.7
YU268831	1	73.0	-116.0	28.8
YU263255	1	68.4	-12.4	22.3
YU268218	1	67.4	-4.7	6.7
YU262883	1	62.1	-41.0	40.2
YU257828	1	61.1	-415.4	14.1
YU270835	1	61.1	18.7	6.3
YU271333	1	61.0	-40.2	36.2
YU258701	1	58.3	-114.4	7.2
YU256667	1	57.3	-61.7	10.0
YU256773	1	55.5	-189.4	30.1
YU270716	1	53.8	-22.4	22.2
YU256771	1	53.4	-91.2	8.1
YU265245	1	53.3	-45.3	19.9
YU269527	1	48.6	-170.4	215.2
YU275232	1	48.2	-29.5	56.2
YU256691	1	47.2	-213.2	17.8

YU280992	1	47.1	-14.4	28.7
YU263854	1	46.8	-62.1	20.8
YU275534	1	46.8	52.3	38.3
YU256776	1	46.5	-229.8	6.2
YU265474	1	46.4	-458.2	354.7
YU263078	1	44.5	-27.0	51.7
YU276852	1	44.5	-58.5	41.7
YU276881	1	43.6	-43.5	55.4
YU277406	1	42.8	-38.1	63.1
YU276803	1	40.8	-51.7	67.9
YU262873	1	40.3	-34.1	61.6
YU276687	1	39.5	-28.6	76.5
YU276750	1	39.1	-45.7	68.2
YU267724	1	38.4	-86.9	253.4
YU276831	1	38.1	-47.0	60.7
YU271407	1	37.8	-37.9	26.3
YU257883	1	37.8	-20.3	22.9
YU257642	1	37.7	-246.5	26.7
YU257875	1	37.4	-384.4	35.0
YU276844	1	37.3	-40.0	74.6
YU275974	1	37.0	-41.4	56.2
YU258712	1	36.9	-208.1	27.1
YU279797	1	36.0	-34.0	53.4

YU270641	1	35.9	-151.4	214.0
YU279821	1	35.9	-24.6	63.4
YU270819	1	35.0	-34.3	31.2
YU279801	1	34.9	-33.3	60.7
YU279798	1	34.5	-29.6	52.1
YU276816	1	34.3	-29.2	39.5
YU276861	1	34.2	-35.0	91.5
YU276806	1	33.8	-28.0	63.8
YU256505	1	33.6	-253.8	18.9
YU275610	1	33.1	-26.9	60.1
YU277605	1	33.0	-26.9	67.1
YU276867	1	32.9	-31.1	93.6
YU279851	1	32.6	-28.5	56.7
YU276814	1	32.4	-36.7	85.8
YU279858	1	32.3	-44.4	62.8
YU276856	1	32.2	-22.2	63.0
YU268641	1	31.8	-39.9	47.1
YU279803	1	31.7	-18.8	46.7
YU265485	1	31.3	-266.2	19.5
YU276596	1	31.2	-28.7	93.2
YU256775	1	31.1	-91.9	6.6
YU275397	1	31.0	-23.3	41.2
YU260066	1	30.9	-21.6	133.6

YU276691	1	30.7	-36.2	57.4
YU258900	1	30.5	-210.9	19.9
YU266928	1	30.2	-52.6	58.2
YU276870	1	30.0	-13.3	86.6
YU276846	1	29.5	-27.0	74.0
YU279785	1	29.2	-24.7	55.1
YU279802	1	28.9	-26.9	55.2
YU275603	1	28.8	-23.3	33.2
YU270104	1	28.7	-33.9	56.9
YU276888	1	28.2	-29.4	118.1
YU276865	1	28.2	-27.5	72.7
YU276810	1	27.6	-27.1	76.2
YU277549	1	27.6	-15.8	43.1
YU275618	1	27.0	-22.6	49.7
YU276862	1	26.8	-18.6	100.4
YU263845	1	26.8	-50.8	21.2
YU278496	1	26.6	-21.9	63.9
YU277450	1	26.3	-23.3	70.7
YU275602	1	26.0	-21.0	36.1
YU268869	1	25.8	-57.5	31.3
YU279792	1	25.8	-46.3	57.1
YU274699	1	25.8	-35.2	111.2
YU258859	1	25.7	-245.0	46.4

YU270744	1	25.4	-31.0	57.2
YU276833	1	25.4	-30.8	86.2
YU270748	1	25.3	-36.4	51.2
YU258715	1	25.3	-209.7	72.7
YU277932	1	25.1	-17.8	74.7
YU275374	1	24.8	-19.4	54.3
YU277614	1	24.8	-13.3	78.7
YU279789	1	24.8	-10.5	82.1
YU261429	1	24.6	-26.3	62.7
YU260850	1	24.5	-8.8	107.6
YU276808	1	24.3	-16.5	59.4
YU276595	1	24.2	-41.5	70.9
YU279799	1	24.2	-16.1	69.9
YU270752	1	24.1	-37.1	53.3
YU276618	1	23.8	-16.2	92.4
YU259823	1	23.8	-31.0	152.1
YU273348	1	23.6	-31.1	50.7
YU275607	1	23.5	-26.8	34.5
YU277613	1	23.1	-12.4	71.8
YU276837	1	22.9	-5.1	83.0
YU279819	1	22.6	-25.2	60.6
YU276738	1	22.6	-30.1	79.7
YU276901	1	22.5	2.0	94.0

YU279793	1	22.5	-37.3	39.4
YU275612	1	22.5	-31.3	53.2
YU275775	1	22.4	-17.9	71.3
YU275402	1	22.4	-23.6	70.0
YU276727	1	22.3	-24.8	64.9
YU276807	1	22.2	-41.7	73.2
YU275398	1	22.2	-30.5	64.8
YU275243	1	22.2	-16.3	78.4
YU260480	1	22.1	-17.0	56.1
YU276764	1	22.0	-31.0	118.4
YU268679	1	22.0	-36.1	69.0
YU272087	1	21.9	-37.7	50.7
YU276879	1	21.6	-40.8	116.0
YU276305	1	21.6	-26.4	67.6
YU275286	1	21.6	-19.6	79.5
YU276871	1	21.5	-40.3	96.2
YU277943	1	21.4	-17.3	86.3
YU274118	1	21.4	-20.0	41.2
YU260026	1	21.1	-15.6	123.2
YU278495	1	21.1	-12.0	64.0
YU275632	1	21.1	-27.8	42.9
YU276809	1	20.9	-37.9	93.7
YU263335	1	20.9	-14.9	55.8

YU276863	1	20.8	-25.1	111.0
YU276576	1	20.7	-16.5	37.9
YU271638	1	20.4	-38.7	54.2
YU271833	1	20.2	-27.6	58.0
YU276827	1	20.2	-28.8	114.5
YU278475	1	20.2	-24.6	71.7
YU274377	1	20.1	-19.3	121.0
YU276789	1	20.0	-29.5	120.5
YU258334	1	19.8	-132.3	52.9
YU276594	1	19.8	-25.4	60.2
YU276905	1	19.7	-26.0	104.8
YU273331	1	19.7	-26.0	40.1
YU276798	1	19.6	-27.8	112.0
YU279309	1	19.6	-24.7	101.4
YU268935	1	19.5	-129.5	68.3
YU276773	1	19.4	-23.2	119.4
YU275819	1	19.4	-26.7	60.5
YU259930	1	19.4	-10.5	110.6
YU276703	1	19.3	-14.4	102.0
YU273238	1	19.3	-29.2	40.1
YU275604	1	19.3	-18.1	39.2
YU268938	1	19.3	-151.8	57.0
YU275440	1	19.3	-16.9	54.8

YU275570	1	19.2	-18.3	70.0
YU279838	1	19.2	-11.5	93.0
YU261750	1	19.2	-14.6	64.7
YU266010	1	19.0	-55.5	68.1
YU275588	1	19.0	-20.5	59.5
YU276699	1	18.9	-23.3	87.7
YU261190	1	18.8	-9.3	70.2
YU277461	1	18.8	-17.2	52.1
YU275987	1	18.7	-23.4	71.2
YU275628	1	18.7	-18.1	79.2
YU278050	1	18.6	-10.9	83.1
YU276848	1	18.6	-16.6	94.8
YU276689	1	18.6	-14.3	95.8
YU275300	1	18.5	-15.5	71.2
YU276836	1	18.5	-32.0	111.8
YU275609	1	18.5	-15.8	55.7
YU263612	1	18.5	-10.2	65.7
YU276568	1	18.4	-11.0	152.2
YU276712	1	18.4	-0.9	116.9
YU273533	1	18.3	-114.7	51.2
YU273745	1	18.3	-13.7	70.1
YU275623	1	18.3	-18.2	38.7
YU272308	1	18.3	-39.8	45.1

YU276688	1	18.3	-9.1	95.1
YU276746	1	18.1	-17.8	79.2
YU260673	1	18.1	3.6	57.8
YU268759	1	17.9	-44.5	67.1
YU276740	1	17.8	-11.8	106.0
YU268672	1	17.8	-33.0	54.1
YU278492	1	17.8	-9.9	57.3
YU269499	1	17.8	-46.7	44.5
YU274537	1	17.7	-31.6	111.9
YU256863	1	17.7	-216.2	65.3
YU271635	1	17.4	-38.1	58.8
YU259866	1	17.3	-16.6	110.9
YU274162	1	17.3	-20.1	59.9
YU279413	1	17.2	-23.4	102.2
YU259962	1	17.1	-9.7	85.1
YU278301	1	17.1	-16.1	92.2
YU275406	1	17.1	-17.9	82.3
YU275611	1	17.0	-20.1	53.2
YU275294	1	17.0	-10.5	102.8
YU261389	1	16.9	-27.9	83.0
YU276885	1	16.8	-11.0	120.5
YU265558	≥5	-4.2	347.2	51.2
YU265327	≥5	-3.5	319.8	86.2

YU265551	≥5	-3.1	315.9	55.9
YU258014	≥5	0.3	302.1	30.8
YU265571	≥5	-4.7	297.5	64.2
YU265323	≥5	-1.5	264.8	108.5
YU258011	≥5	-2.2	259.1	28.1
YU265585	≥5	-2.0	254.2	93.9
YU265315	≥5	0.9	250.4	77.7
YU265601	≥5	-6.1	243.1	86.7
YU265296	≥5	-4.2	240.8	122.7
YU258019	≥5	-6.2	240.7	24.3
YU258017	≥5	-4.6	236.2	39.4
YU265799	≥5	-0.7	228.0	133.0
YU266442	≥5	-0.3	225.3	155.0
YU265306	≥5	1.1	218.5	60.7
YU258013	≥5	-1.0	217.8	39.0
YU265301	≥5	2.2	210.2	98.7
YU258012	≥5	-4.7	208.9	39.8
YU265307	≥5	-3.2	208.6	42.4
YU265319	≥5	-3.9	188.2	88.9
YU265310	≥5	-8.4	178.8	85.6
YU265595	≥5	-0.2	174.5	88.0
YU265311	≥5	-2.9	161.9	83.3
YU265579	≥5	-0.9	156.3	74.6

YU265560	≥5	-11.6	153.2	66.8
YU265484	≥5	1.0	152.0	120.9
YU265332	≥5	2.7	150.2	116.3
YU280559	≥5	-0.2	148.2	103.8
YU265475	≥5	3.2	146.5	115.2
YU265473	≥5	0.7	142.6	132.6
YU265303	≥5	1.1	140.9	88.4

Appendix VIII

The 185 high confidence compounds that regulate nucleolar number from both the FDA-approved drug screen and screen of synthetic, drug-like compounds. Drug name or unique compound ID, the designated phenotype in initial screen (one nucleolus per nucleus or ≥5 nucleoli per nucleus), percent effect for each phenotype relative to DMSO, and the mean percent viability relative to DMSO are shown. The designated cluster from the combined structure cluster analysis at ≥0.5 similarity are also shown.

Compound ID or drug name	Pheno-type (1/≥5)	1 nucleolus per nucleus PE (Rep1, Rep2)	≥5 nucleoli per nucleus PE (Rep1, Rep2)	Mean percent viability	Cluster No.
Chlormethine (mechlorethamine)	≥5	-17.4, 1.3	150.3, 97	17.9	1
Actosin (bucladesine)	≥5	-10.9, -5	124.5, 100.9	43.0	2
Tegafur	≥5	-12.5, -8.4	61.6, 98.1	51.3	2
Docetaxel	≥5	4.2, -1.4	116.4, -8.6	59.9	2
Ouabain	1	54.4, 1.5	-53.7, 7.2	55.4	2
Mitomycin C	1	40.7, -4.4	-55.4, 26.4	62.4	2
Gemcitabine	1	21.6, 3.8	-11.4, 3.7	57.8	2
Clofarabine	1	30.5, 22.9	-23, 16.7	14.7	2
Taxol	≥5	37.5, 7.9	54.1, -26.2	56.3	2
Mutamycin (mitomycin)	1	49.5, 107.9	-60.4, -97.8	11.6	2
Edoxudine	1	47.7, 47.7	13.3, -12.1	22.6	2
Vepesid (etoposide)	≥5	-13.1, 0.4	53.2, 89.2	32.4	2
Riboprine	1	22.5, 60.5	-22.6, -64.7	17.2	2
Lasalocid	1	46.6, 53.4	-64.4, -96	28.2	2
Vinorelbine	1	27.6, 50.4	-48.1, -91.8	25.8	3
Octopirox (piroctone olamine)	1	38.6, 94.1	-47.1, -94.9	15.9	3

Ciclopirox (ciclopirox olamine)	1	64.7, 86.4	-64.1, -92.4	22.2	3
BI-2536	1	-8.8, 14.8	44.8, -35.8	12.4	3
Ciclopirox	1	53.2, 95.2	-66.2, -96.9	19.7	3
Piroctone	1	60.3, 98.9	-58, -78.7	24.0	3
BI-831266	≥5	8.4, 22.5	334, 180.9	30.4	3
YU256773	1	22.8, 45.8	82.7, 34.9	12.9	3
YU256863	1	18, 8.9	-38.7, -128.9	61.3	3
YU257337	1	71.4, 96.9	-63, -175.4	21.7	3
YU257828	1	1.5, 67.3	2.6, -153.7	53.1	3
YU257875	1	0.6, 44.9	4.7, -129.4	76.7	3
YU257883	1	36.4, 57.8	-43.5, -115.1	21.2	3
YU258006	1	-5.1, 104.8	-3.8, -170.9	70.1	3
YU258712	1	52.8, 68	-47.8, -149.1	20.7	3
YU258715	1	17.8, 10.5	-39.3, -110.2	46.6	3
YU258859	1	12.8, 13	-45.5, -111.3	51.1	3
YU260480	1	9.3, 11.2	-25.5, -92.5	58.3	3
YU260673	1	8.4, 10.7	-32.9, -100.3	64.2	3
YU261429	1	10.7, 10.1	-38.3, -100.8	73.0	3
YU261750	1	14.5, 13.4	-31.2, -119.1	63.0	3
YU262873	1	30.1, 34.2	-38.6, -115	82.9	3
YU262883	1	58.8, 74.2	-54, -174.9	31.8	3
YU263335	1	16.1, 18.4	-31.2, -106.1	43.4	3

YU263845	1	42.2, 113.5	-61.1, -176.2	21.1	3
YU263912	1	12.3, 13.2	-30, -116.2	48.2	3
YU264306	1	15.5, 18.1	-26.1, -77.8	84.9	3
YU265142	1	12.3, 15	-43.8, -113.5	60.9	3
YU265245	1	62.3, 64.8	-42.4, -129.6	30.6	3
YU266010	1	20.9, 13.7	-32.9, -116.3	52.4	3
YU266138	1	2.8, 10.3	-9.8, -21.7	60.5	3
YU266595	1	16.4, 8.4	-12, -26.5	77.8	3
YU266868	1	17.4, 20.4	-31.9, -99.1	77.2	3
YU266926	1	14.9, 6.2	-35.7, -110.5	64.6	3
YU268257	1	15.3, 4.2	-34.2, -137.8	62.8	3
YU268641	1	17.1, 30.4	-27.2, -149.3	41.7	3
YU268672	1	25.7, 16.5	-52.1, -127.4	55.9	3
YU268679	1	14, 17.9	-36.2, -121.6	62.2	3
YU268680	1	18.4, 11.4	-43, -108	48.9	3
YU268831	1	70.3, 107.2	-56.4, -125.1	22.9	3
YU268869	1	43, 74.7	-56.5, -165.9	30.5	3
YU268935	1	20, 18.3	-35.4, -70.7	41.5	3
YU268938	1	15.6, 18.8	-36.8, -78.5	51.1	3
YU270716	1	55, 64.5	-41.4, -128.8	24.9	3
YU270744	1	18, 8	-45.1, -132.8	77.8	3
YU270748	1	17.8, 7.9	-39.4, -123	69.9	3
YU270751	1	22.3, 9.1	-36.4, -96	84.2	3

YU270819	1	23.9, 66.2	-55.9, -169.6	30.8	3
YU271407	1	34.3, 26.8	-33.3, -103.9	62.6	3
YU272087	1	13.6, 13.1	-47.6, -93	64.7	3
YU272289	1	13.4, 14.3	-36.6, -63.5	63.4	3
YU272308	1	38.8, 13.5	-46.5, -98.8	39.1	3
YU273466	1	23.6, 22.2	-42.6, -75.3	56.2	3
YU273533	1	10.6, 13.7	-20.3, -56	62.6	3
YU273668	1	-6.7, 18.8	-40.7, -82.8	52.8	3
YU273758	1	27, 19.6	-32.6, -69	62.4	3
YU274118	1	17.4, 15.8	-27.6, -68.4	57.0	3
YU275232	1	19.9, 14.6	-34.8, -60.6	61.8	3
YU275243	1	13.2, 11.2	-16.4, -53.6	88.0	3
YU275374	1	8.2, 14.4	-23.2, -91.9	52.6	3
YU275397	1	14.8, 10.1	-35.9, -73.3	57.3	3
YU275398	1	13.9, 10.9	-25.4, -63.9	63.1	3
YU275402	1	7, 15	-28.6, -59.6	75.9	3
YU275534	1	24.4, 36.8	76.7, 48.4	10.4	3
YU275602	1	36.1, 15.5	-49.9, -105.8	30.9	3
YU275603	1	21.5, 46.6	-42.4, -118.2	34.2	3
YU275607	1	12.6, 22.9	-37.4, -81.3	67.3	3
YU275610	1	16.3, 17.5	-34.6, -76.2	39.4	3
YU275612	1	12.3, 12.9	-34.9, -77.4	46.3	3
YU275618	1	8.9, 16.3	-33.7, -72	62.9	3

YU275624	1	51.2, 105.2	-56.4, -125.2	25.5	3
YU275632	1	0.7, 12.2	-39.5, -65.4	63.4	3
YU276576	1	8.4, 20.1	-36.1, -73	58.8	3
YU276595	1	13.6, 22.7	-33.7, -76	60.8	3
YU276618	1	18, 9.7	-21.6, -45	65.7	3
YU276691	1	14.3, 14.4	-29.4, -58.3	50.6	3
YU276750	1	23.8, 18.4	-35.7, -68.4	62.8	3
YU277549	1	5.5, 14.7	-31.1, -96.3	47.2	3
YU277605	1	16.3, 18.5	-23, -66.8	63.0	3
YU280408	1	18.5, 26.2	-30.3, -80.8	69.4	3
Monacrin (aminacrine)	≥5	27.8, 5.2	65.1, 243.1	16.9	4
Zinc omadine (pyrithione zinc)	1	14.3, 15.6	-31.3, 12.5	18.2	5
YU264477	1	0.5, 17.9	-44.7, -112.9	53.7	5
YU277406	1	12.2, 19.9	-42.5, -77	43.8	5
YU277450	1	7.6, 12.3	-35.2, -76.1	75.3	5
YU280992	1	63, 51.5	-3.3, -73.9	26.5	5
Albendazole	1	48.7, 52	-29.1, -53.9	15.5	6
YU256419	1	18.6, 8.9	-32.1, -84.2	64.6	7
YU266928	1	15.2, 17.9	-34.6, -108.5	61.4	7
YU268759	1	13.3, 13.5	-35.4, -88.2	77.2	7
YU269011	1	13, 14.2	-30.4, -91.7	78.0	7

YU269499	1	13.1, 11.9	-34.1, -85.1	33.4	7
YU270104	1	12.7, 15.2	-29.7, -92.3	68.0	7
YU270941	1	21.7, 11.3	-36.9, -103.6	72.2	7
YU275775	1	10.3, 12.5	-39.3, -58.5	78.8	7
Melphalan	≥5	-20.5, -11.6	243.3, 222.6	27.7	8
Vorinostat	1	22.8, 0.5	-30, -43.2	17.5	9
YU263612	1	16.4, 17.3	-39.3, -109.5	63.2	10
YU265745	1	9.9, 16.3	-37.1, -98.6	60.6	10
YU273238	1	14.3, 12.1	-33.5, -71.6	58.8	10
YU273331	1	22.7, 12.8	-29.7, -74.7	49.2	10
YU275173	1	56.4, 103	-53.6, -117	19.3	10
YU275974	1	17.9, 16.2	-24.6, -61	59.3	10
Cicloheximide (cycloheximide)	1	17.8, 42.4	-30, -71.5	22.5	11
YU268779	1	3.5, 15.3	-29, -73.4	57.2	11
YU273745	1	14.7, 11.2	-25.2, -52.4	78.0	11
YU278496	1	9.1, 15.4	-38.2, -60	55.8	11
Hexachlorophene	1	49.2, 71.9	-50.5, -87	13.1	12
YU258334	1	11.5, 21.1	-8.9, -67.7	46.6	13
Roccal (benzalkonium chloride)	1	51.6, 65.6	-56.1, -92.1	19.8	14

Cetrimonium bromide	1	5.4, 130.5	-7.1, -97.8	57.8	14
YU261190	1	17.4, 16.3	-34.7, -93.3	81.3	15
YU271333	1	44.1, 64.4	-55.6, -170.9	31.3	15
YU271635	1	13.2, 18.4	-33.7, -100.6	78.1	15
YU271638	1	10, 17.2	-43.9, -108.8	69.6	15
Miripirium	1	62.1, 66.5	-54.1, -88	18.5	16
Niclofolan	1	17.8, 25	-29.1, -75	56.3	17
Mycophenolic acid	1	85.3, 111.4	-45.4, -88.1	21.1	18
Mycophenolic acid	1	80.6, 0.4	-52.1, 8	56.6	18
Mycophenolate mofetil	1	80, 96.6	-44.6, -74.1	24.2	18
CellCept (mycophenolate mofetil)	1	90.6, 119.1	-64.8, -92.6	22.4	18
YU276687	1	17.3, 18.6	-30.7, -60	59.1	19
YU276803	1	22.2, 15.9	-31.5, -66.1	62.2	19
YU276806	1	16.1, 10.7	-32.3, -72.2	65.8	19
YU276814	1	23, 19.2	-32.8, -74.3	66.0	19
YU276816	1	1.8, 9.1	-28, -61.2	63.1	19
YU276831	1	13.1, 13.1	-34, -68.6	58.2	19
YU276833	1	18.4, 13.1	-23.3, -53.7	54.0	19
YU276844	1	13.9, 12	-35, -63.7	51.2	19

YU276846	1	17.7, 11.6	-26.9, -54.6	62.4	19
YU276852	1	15, 13.8	-31.2, -62.5	51.0	19
YU276856	1	4.5, 19.1	-32.8, -62.8	68.7	19
YU276862	1	16.7, 11.7	-28.3, -66.8	63.3	19
YU276865	1	31.6, 18.4	-38.4, -83.2	50.7	19
YU276867	1	10.8, 18.7	-34.5, -77.5	68.4	19
YU276870	1	15.6, 12.2	-46.3, -73.6	58.4	19
YU276881	1	20, 16.4	-38.6, -74.8	41.7	19
YU279785	1	18.5, 16.8	-29, -69.3	61.4	19
YU279789	1	18, 3	-22.8, -54.9	66.0	19
YU279792	1	11.4, 17.6	-28.3, -66.9	53.9	19
YU279793	1	7.2, 18.3	-38, -86.4	55.2	19
YU279797	1	23.7, 12.2	-37.5, -64.4	51.9	19
YU279798	1	17.6, 2.1	-46.2, -87.1	45.0	19
YU279799	1	18.8, 13.5	-32.9, -75.5	54.6	19
YU279801	1	20.7, 12.1	-31.1, -63.4	57.4	19
YU279802	1	16, 18.9	-34.9, -74.4	55.3	19
YU279803	1	20.7, 5.1	-36.3, -77.1	57.4	19
YU279821	1	2.4, 15.9	-16.4, -74.4	58.8	19
YU279851	1	15.3, 12.8	-31.5, -80.3	60.2	19
Mitoxantrone hydrochloride	1	76.8, 141	-48.3, -97.8	10.4	20

Pixantrone dimaleate	1	90.7, 149.1	-64, -96.3	12.9	20
YU271832	1	21.4, 19.6	-39.4, -109.6	42.3	21
YU271833	1	13.3, 18.1	-34.9, -106.7	65.1	21
Gefitinib	1	53.9, 78.1	-57.5, -88.3	25.8	22
Methylbenzetho-nium chloride	1	45.3, 37.7	-49.5, -92.8	27.5	22
YU256505	1	27.5, 69.1	-46.3, -163.6	20.4	22
Istaroxime	≥5	-6.6, -10.1	57.4, 6.8	70.9	23
YU256254	1	15, 8.7	-50, -119.5	49.8	24
YU257642	1	34.2, 45.1	-37.1, -133.9	23.7	24
YU258900	1	44.5, 32.4	-28.2, -119.4	17.7	24
YU273265	1	19.5, 10.6	-21.8, -58.8	58.0	24
YU273348	1	21.2, 10.8	-33.6, -58.7	71.7	24
YU279858	1	21.2, 20	-32.3, -84.7	56.5	24
Mepacrine	1	63.1, 117.2	-58.5, -97	26.3	25
Sertindole	1	35.6, 50.2	-56.5, -84.7	29.2	26
YU263078	1	31.1, 52.8	-54, -156.6	34.7	26
Cerivastatin	1	48.3, -5	-47.9, 6.6	52.1	29
Pranidipine	1	70.3, 78.7	-66.6, -97.8	25.0	30
Alexidine hydrochloride	1	46, 52	-50.7, -87.1	30.5	31

Povan (pyrvinium pamoate)	1	36.7, 84.8	-55.6, -89.1	13.1	32
Bryamycin (thiostrepton)	1	10.2, 16.1	-13, -37.5	80.5	33

Appendix IX

Nucleolar proteins enriched on nascent chromatin at the replication fork

Nucleolar proteins at the replication fork and nascent chromatin (HGNC)
ANLN
ANXA1
APEX2
APTX
AQR
ATM
ATR
ATRIP
BAZ1B
BLM
BOLA2
BUB3
BUD31
CAND1
CBX1
CBX3
CBX5
CDC73
CDK1
CDK2

CDK5
CDK6
CDK7
CDK9
CHD1
CHD4
CHD8
CLIC1
CLIC4
CUL1
CUL4A
CUL4B
DDB1
DDX23
DDX41
DDX42
DDX46
DHX15
DHX16
DNMT1
DTL
DUT
EP400

ERCC2
ERCC3
FANCG
FANCI
FEN1
FKBP5
FOXK1
GLRX3
GSTP1
GTF2I
HAT1
HDAC1
HDAC2
HLTF
JADE3
KDM1A
KDM3B
KIF2A
KIFC1
LARP7
MCM10
MCM2
MCM3

MCM4
MCM5
MCM6
MCM7
MDN1
MED20
MED23
MLH1
MORC2
MSH2
MSH6
MTBP
MUTYH
NACC2
NASP
NCOR2
NFIC
NOSIP
ORC4
ORC6
OTUB1
PARG
PARP1

PARP2
PCBP1
PCNA
PDS5A
PGK1
PNKP
PPID
PPIH
PRKDC
PSME3
RAD21
RAD50
RBBP4
RBBP7
RBM12
RBM27
RBM4
RFC1
RFC2
RFC3
RFC4
RFC5
RPP30

RREB1
SAE1
SART3
SBNO1
SCML2
SET
SF3B2
SIMC1
SKP1
SLFN5
SMC1A
SMC2
SMC3
SMC4
SMC5
SMC6
SMU1
SR140
SRP14
SSRP1
STAT1
SUMO2
TCEA1

TKT
TOP2A
TOP2B
TRRAP
UBA1
UBE2T
UBR5
WDR82
WIZ
XPO5
XRCC1
XRCC5
XRCC6